EVALUATION OF LIGHTWEIGHT GEOFOAM FOR MITIGATING BRIDGE APPROACH SLAB SETTLEMENTS

by

PINIT RUTTANAPORAMAKUL

Presented to the Faculty of the Graduate School of

The University of Texas at Arlington in Partial Fulfillment

of the Requirements

for the Degree of

DOCTOR OF PHILOSOPHY

THE UNIVERSITY OF TEXAS AT ARLINGTON

December 2014

Acknowledgements

I would like to gratefully and sincerely thank Dr. Anand J. Puppala, my supervising professor, for his valuable guidance and kindness given to me during my graduate studies at the University of Texas at Arlington. This research project would not have been possible without the support and advice from him. My deepest gratitude is also due to the members of my graduate committee, Dr. Laureano R. Hoyos, Dr. Xinbao Yu, Dr. Shih-Ho Chao, and Dr. Chien-Pai Han, for sharing their valuable time and thoughtful suggestions. I would also like to express my sincere thanks to Mr. Richard S. Williammee, Dr. Aravind Pedarla, and Dr. Thornchaya Wejrungsikul for their suggestions and support during my research.

Moreover, I would to thank the UTA staff, Ginny Bowers, Sara Ridenour, Ava Chapman, Paul Shover, and others, for their friendly nature and unconditional help during my studies, as well as the Texas Department of Transportation (TxDOT) for funding this research.

I would also like to express appreciation my friends and colleagues, Tejo V. Bheemasetti, Raju Acharya, Alejandro Pinobravo, Chatuphat Savigamin, Rathna Mothkuri, and others for helping me with the research. My special thanks to my friends, Janwit Kampoon and Ketwalee Kositkanawuth for their unconditional support during my stay in the United States.

Finally, I am extremely grateful for the love and support given by my mother, Pannipa Ruttanaporamakul; my father, Somnuk Ruttanaporamakul; and my sisters, Krittiya and Jutapon Ruttanaporamakul. In addition, the important person that I cannot forget to thank is my wife, Yajai Ruttanaporamakul, for her love, support and the most valuable gift given to me, my son (Trin Ruttanaporamakul).

November 19, 2014

Abstract

EVALUATION OF LIGHTWEIGHT GEOFOAM FOR MITIGATING BRIDGE APPROACH SLAB SETTLEMENTS

Pinit Ruttanaporamakul, PhD

The University of Texas at Arlington, 2014

Supervising Professor: Anand J. Puppala

The bump at the end of a bridge infrastructure is one of the frequent problems found in Texas and other states. Transportation agencies spend millions of dollars annually to repair the bump problem. The major cause of the problem is the settlement of backfill materials and foundation soils, as well as the erosion of backfill. Research was undertaken at the University of Texas at Arlington to study the embankment located on US 67 over SH 174 in Johnson County, Cleburne, Texas. The embankment was reconstructed, replacing the top of existing fill soil with lightweight EPS 22 geofoam blocks to reduce the loads imposed on the underlying subgrade and, consequently, to reduce the magnitude of settlement due to the consolidation phenomenon. The main objective of this research is to assess the effectiveness of using light backfill, in the form of EPS geofoam, to mitigate embankment settlements. Laboratory studies were conducted to study the basic properties, compressibility characteristics, and shear strength of the soils and EPS 22 geofoam. Field monitoring studies were also conducted at regular time intervals to study the performance of EPS geofoam under live traffic. Modeling studies were conducted in this research, using the PLAXIS program to predict the long term performance of the test section. The above mentioned studies are being

currently pursued to achieve the final objective which is to develop the design and construction guidelines for the future use on other geofoam-related construction.

Table of Contents

List of Illustrations

List of Tables

Chapter 1

Introduction

1.1 General

The differential settlement between the bridge structure and the approach embankment creates the formation of the bump at the end of the bridge, which is one of the most frustrating problems found on bridge infrastructures in several states, including Texas, in the USA. The existence of the bump causes an unsafe driving condition, rider discomfort, and increasing maintenance costs. According to Briaud et al. (1997), 30% of the bridges in Texas (i.e., 13,800 out of 46,000 bridges) had a the problem of the bump at the end of the bridge. Jones et al. (2008) and a survey carried out in Kentucky by Hopkins and Deen (1969) reported that about 80% of several hundred highway bridges had required maintenance action to remedy the problems caused by differential settlement between a bridge abutment and approach embankment. Another study provided by Seo (2003) cited that approximately USD $7 million is spent annually for the bump problem repairs in Texas.

Bridge approach slabs have been introduced to be used for reducing the effects of the bump at the end of the bridge. The slabs are normally constructed with reinforced concrete material by installing one end on the bridge abutment and the other end on the embankment soil. The bridge approach slabs, in general, provide smooth grade and safe transition of vehicles from bridge structures to the roadway and vice versa (Puppala et al., 2009; Hoppe, 1999). However, in many cases, the use of the slabs results in moving the bump from the end of the bridge to the end of the approach slab (Hoppe, 1999). The poor performance of approach slabs has been reported in many states, and maintenance of the bridges, including repair or replacement of the bridge approach slabs, is often

required. As an example, Chen and Chai (2011) reported that in 2004, around $8 million was spent on replacement or retrofit of bridge approach slabs in California.

For the past two decades, several researchers (Ardani, 1987; Tadros and Benak, 1989; Briaud et al., 1997; White et al., 2007; Puppala et al., 2009; Archeewa, 2010; Chen and Chai, 2011) have studied the problem of the bump at the end of the bridge and the distress in the bridge approach slabs in order to figure out the causes of bump and the techniques required to mitigate the problems. According to Archeewa (2010), the factors contributing to the problem can be broadly classified into four categories: 1) Material properties of foundation and embankment, 2) Design criteria for bridge foundation, abutment, and deck, 3) Construction supervision of the structures, and 4) Maintenance criteria. Puppala et al. (2009; 2012) provided the summary of mechanisms causing the formation of the bumps problem, which include 1) Consolidation settlement of foundation soil, 2) Poor compaction and consolidation of backfill material, 3) Poor drainage and soil erosion, 4) Types of bridge abutments, 5) Traffic volume, 6) Age of the approach slab, 7) Approach slab design, 8) Skewness of the bridge, and 9) Seasonal temperature variations.

Several techniques to mitigate the differential settlement and the bump problem have been studied and proposed in many literatures. The methods can be summarized based on the groups of treatments as followings: 1) improvement of foundation soil, 2) improvement of backfill material, 3) design of bridge foundation, 4) design of approach slab, and 5) provide effective drainage and erosion control methods (Archeewa, 2010 and Puppala et al., 2012).

This dissertation research has been a comprehensive attempt to address the use of a light weight expanded polystyrene (EPS) geofoam as embankment fill material to mitigate settlements of the fill and foundation subsoils. Though many applications of the

geofoam for settlement reductions have been reported, very few documented studies reported the use of geofoam for bridge approach settlement problems. The EPS geofoam, which is a super-lightweight block made of rigid cellular foamed polymeric material, has been used in geotechnical engineering applications as a soil substitute material for more than 30 years. The weight of the EPS geofoam is approximately 1% of the weight of soil and less than 10% of the weight of other lightweight fill alternatives. With this benefit, the EPS geofoam is expected to reduce the loads imposed on the underlying subgrade and, consequently, reduce the magnitude of settlement due to the consolidation phenomenon so that the differential settlement problem can be mitigated. Moreover, the use of the EPS geofoam also provides benefits to construction schedules, as construction of geofoam embankments can take considerably less time than the construction of natural embankments. Because of its light weight, the EPS geofoam is easy to handle and install.

The dissertation works primarily focused on characterization, application, and validation aspects, including laboratory tests, to find basic and engineering properties of soils, field instrumentation and field data collection to study the performance of geofoam embankment in real field conditions, numerical modeling, and validation studies that led to the development of the design method for geofoam embankment systems.

1.2 Problem Statement and Research Objectives

Currently, several technologies have been recommended for use in mitigating the problem of bridge approach slab settlements. TxDOT's Fort Worth district implemented the technology, using EPS geofoam as an embankment fill material in a 40 ft. high bridge situated on US 67 over SH 174 in Johnson County, Texas as a part of an on-going research study with the Texas Department of Transportation. The approach slab of this bridge had experienced more than 16 in. of settlement in the sixteen years since its

construction. To mitigate the undesirable settlements, several treatment methods, including hot mix overlays, grout injections, soil nailing and others, were attempted; however, they were not proven to be effective. One of the primary causes of the settlement is the self-weight of the 40-ft high embankment fill material which undergoes self-consolidation, inducing large stresses and related settlement to the underlying foundation subgrade. The lightweight and compact EPS geofoam material has, therefore, been recommended and used in the rehabilitation work. Considering this, the present research was designed to fully address this geofoam application to mitigate settlements experienced near bridge approach slabs.

There are three main objectives of this research. The first objective is to comprehensively evaluate the effectiveness of using EPS geofoam as the fill material to alleviate the differential settlements near a bridge approach slab in real field conditions. The second objective is to study the prediction of future settlement of a bridge embankment by formulating numerical models, using the geotechnical finite element software. The last objective is to develop the design and construction guidelines for possible future use on the EPS geofoam embankment projects. It is anticipated that the results of this study will help agencies in lowering the volume of their maintenance work, thereby reducing the annual cost of repairing the bridge embankments,

1.3 Research Tasks

In order to accomplish the research objectives mentioned above, the following tasks were performed:

1. Reviewed the available literatures on the causes of bridge approach settlement problems and the techniques employed to reduce the problem; especially, the use of EPS geofoam as the embankment fill material.

2. Designed and instrumented a large bridge embankment system with geofoam, collected field data, and monitored the performance of the geofoam-embedded embankment system through the installed instrumentation. Horizontal inclinometers and pressure cells were installed in the project site for monitoring the settlement and pressure response from the geofoam material. Field visits were conducted once a month, and monitoring field data has been collected during the visits.

3. Formulated a numerical model, using the geotechnical finite element software, PLAXIS, to study the settlement and pressure trends of the tested embankment section. The model was calibrated, using the field measurement settlement and pressure data, and was used to make predictions for future settlements.

4. Performed necessary laboratory tests on fill soil, foundation subgrade, and EPS geofoam material to obtain the properties necessary for the numerical modeling.

5. Analyzed the field-monitored data and compared it with the results received from the numerical model.

6. Developed design guidelines and construction recommendations for possible future use on other highway projects. The guidelines will be developed based on the available design standards, the data collected, and observations made in more than two-year period, along with the statistical and numerical analysis conducted on the test section.

Figure 1.1 presents the flowchart summarizing the tasks performed in this study.

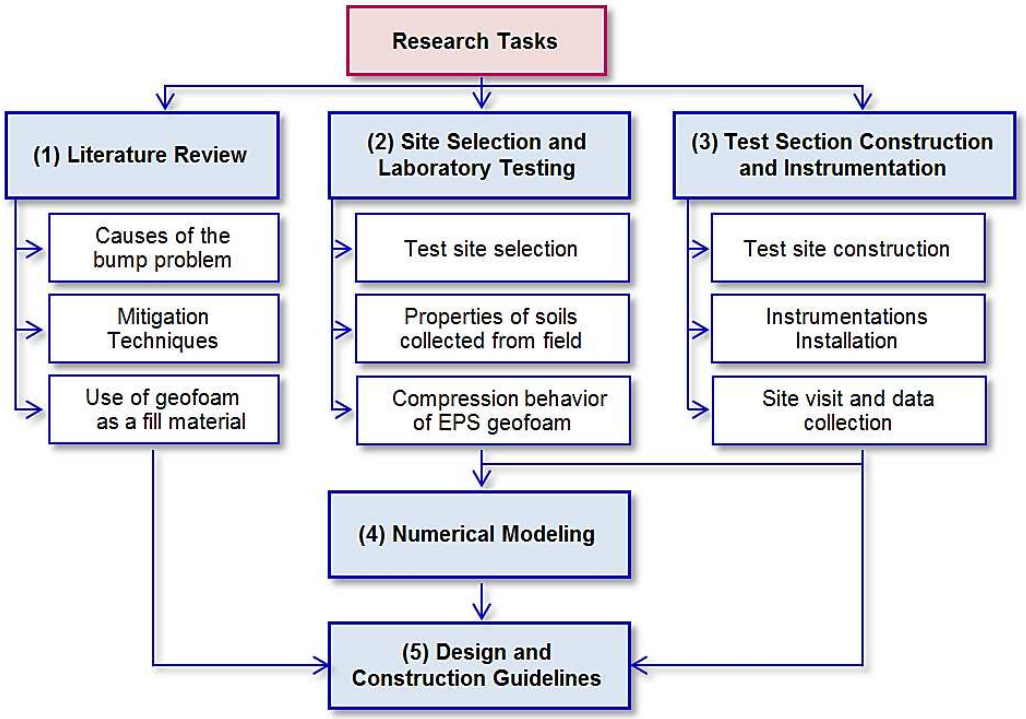

Figure 1.1 Flowchart of the research tasks

1.4 Dissertation Organization

This dissertation consists of eight chapters, including the Introduction (Chapter 1), Literature Review (Chapter 2), Laboratory Experimental Programs (Chapter 3), Construction and Instrumentation of EPS Geofoam Embankment Test Section (Chapter 4), Analysis of Field Monitored Data (Chapter 5), Numerical Modeling of Geofoam Embankment System (Chapter 6), Design Guidelines for EPS Geofoam Embankment (Chapter 7), and Summary, Conclusions and Recommendations (Chapter 8).

Chapter 1 presents the problem statements, research objectives, tasks involved to accomplish this research, and dissertation organization.

Chapter 2 presents details of the review from available literatures, addressing the problem of settlement in bridge approach slabs and embankments. The definition and

causes of the bump at the end of the bridge problem are provided, and the practicable techniques used to alleviate the settlement of the bridge approach are explained. Finally, the use of lightweight EPS geofoam material for mitigating the magnitude of bridge approach settlement is introduced.

Chapter 3 presents the laboratory tests conducted on the soil samples collected from the test site and the results obtained from the tests. The laboratory studies were carried out to determine the basic and engineering properties of the soils. The obtained results were used further as the input parameters in the numerical analysis. Moreover, the compression test was also conducted on EPS22 geofoam specimens to investigate their compression behaviors, comparing them with those specified in the ASTM standard.

Chapter 4 describes the construction practices of embedding the EPS geofoam in the embankment, along with the field instrumentation details used in the test field. In this chapter, the step-by-step procedures of the installation of the instruments, including horizontal inclinometer and earth pressure cells, are presented.

Chapter 5 presents the details of the data collected from the test embankment. The vertical displacement data, measured by using a horizontal inclinometer device, and the pressure response, recorded by the pressure cells equipment, are provided. The vertical displacement data was analyzed using the statistical method, and the hyperbolic model was used to predict the future settlement of the test embankment.

Chapter 6 presents the numerical analysis study performed in an attempt to understand the settlement behaviors of the EPS geofoam embankment. The laboratory test results obtained and explained in Chapter 3 were used as the input parameters in a finite element numerical model. The results from the FEM model were compared with the field monitored data provided in Chapter 5. The comparisons were performed to validate

the numerical model, which was used further to predict the vertical displacement that occurred under different conditions.

Chapter 7 provides the design guideline for possible future use on the EPS geofoam embankment projects. The guideline was summarized from three different standards, which are NCHRP 529, European standard, and Japanese standard, along with the results investigated from the test filed and obtained from the FEM models. Design charts involved are provided in the guideline.

Finally, in Chapter 8, the summary of the research, conclusions, and recommendations for future research are presented.

Chapter 2

Literature Review

2.1 Introduction

A literature review was conducted regarding issues pertaining to the problem of the differential settlement at the bridge approach. The comprehensive information collected from past literatures is presented in five sections. The first part of this chapter provides general information of the problem of the bump at the end of the bridge, including the definitions and the tolerance of the bump. In the second part, several possible factors causing the bump problem, including consolidation settlement of foundation soil, poor compaction and consolidation of backfill material, poor water drainage and soil erosion near the bridge abutments, types of bridge abutments, traffic volume passing over the bridge, age of the approach slab, design of the approach slab, skewness of the bridge, and seasonal temperature variations, are reviewed and briefly explained. The third part presents the mitigation techniques for the problem of bridge approach settlement. General information of the EPS geofoam such as the definition, types and manufacturing process, properties, applications, and advantages of using geofoam as the embankment fill material, is presented in the fourth section. The final section of the chapter is a summary.

2.2 The Bump at the End of the Bridge

The bump at the end of the bridge, or formally called bridge approach settlement, is defined as the difference in elevation of approach pavements and bridge decks, caused by unequal settlement of the embankment and bridge abutment (Helwany et al., 2007). Highway embankments are generally built on subgrade foundation soil; whereas, the bridge abutments are typically supported by deep foundation systems such as driven

piles, resting on a firm foundation material such as bedrock or very dense sand. For this reason, the total settlement of the bridge is usually much smaller than the total settlement of the adjacent embankment, and the noticeable bump can develop at both of the bridge ends (Archeewa, 2010).

The bump at the end of the bridge is one of the most frustrating problems found on bridges in Texas and other states in the USA. It causes drivers discomfort and is dangerous (Hopkins, 1969; Ardani, 1987). The problem also results in agencies spending millions of dollars on maintenance costs, and it can tarnish a transportation agency's public image (Briaud et al., 1997; Puppala et al., 2012). Approach slabs have been used by many state transportation agencies as a means of eliminating the effects of the bump at the end of the bridge problems. The functions of approach slabs are (1) to provide a smooth grade transition between the bridge and the roadway on approach embankment, (2) to keep the magnitude of differential settlement within a control limit, and (3) to provide a better seal against water percolation to prevent the erosion of backfill material (Briaud et al., 1997; Hoppe, 1999; Archeewa, 2010). However, Hoppe (1999) mentioned that based on a large number of cases, the use of approach slabs results only in moving the bump from the end of the bridge to the end of the approach slab connecting with the roadway. In such cases, the bump or approach settlement can be defined as the differential settlement of the approach slab with reference to the bridge abutment structure (Puppala et al., 2012).

Currently, the thresholds for the initiation of repair or maintenance of the bridge approach settlement problem have been studied by many researchers. For instance, Walkinshaw (1978) proposed that the differential settlement of 2.5 in. (63 mm) or greater, occurred on a bridge can be considered as the threshold for the bridge repair. Long et al. (1998) introduced a rating system on the basis of the differential settlement of the bridge

approach. In the rating system, the differential settlement of 1 in. (25 mm) is considered as a slight bump; whereas, the differential settlement of 2 in. (51 mm) and 3 in. (76 mm) or larger is regarded as a moderate and a significant bump requiring repair, respectively. The other way to describe the threshold for the bridge repair is expressing in term of the gradient of the bridge slab, which is the ratio of settlement and length of the slab. For example, Wahls (1990) concluded that the slope change of 1/200 of the approach slab length or less is acceptable from the standpoint of ride comfort. Long et al. (1998) suggested that the settlement gradient in the range 1/100 to 1/125 of the approach slab length will likely cause rider discomfort and should be considered as the threshold for initiating remedial measures. Jones et al. (2008) mentioned that the longitudinal angular distortion (differential settlement/span length) of 0.004 or 1/250 is likely to be tolerable for a continuous bridge.

Some researchers use the International Roughness Index (IRI) to present the riding quality of the traveling public. The IRI is the accumulations of waviness on a given segment length and is usually reported in the unit of in./ft. or mm/m (Puppala et al., 2012). Das et al. (1990) suggested that the IRI values at the bridge approach of 3.9 mm/m or less is considered as a very good riding quality. Whereas, the bridge approach that has an IRI value equal to 10 mm/m or greater indicates very poor riding quality. In Texas, the practice for repairs is different from district to district and these repairs are typically based on visual surveys and IRI values (Jayawickrama et al., 2005; James et al., 1991; Archeewa, 2010).

2.3 Factors causing the formation of the bump at the end of the bridge

As mentioned previously, the formation of the bump at the end of the bridge is a problem that reduces ride quality and increases significant maintenance costs. Moreover, the bump problem also tarnishes a transportation agency's public image. Although the

differential settlement at a bridge approach is commonly recognized, the factors causing the problem are difficult to identify (Hoppe, 1999). Puppala and Chittoori (2012) suggested that the primary sources of the bump problem can be broadly divided into four categories; (1) material properties of foundation and embankment; (2) design criteria for bridge foundation, abutment and deck; (3) construction supervision of the structures; and (4) maintenance criteria. However, not all the factors contribute to the formation of the bump concurrently.

From the past several years, many researchers have attempted to clarify the causes of the bump and to figure out the most effective techniques for reducing or eliminating the problem. Many factors are reported in the literatures, explaining the mechanisms causing the formation of bumps on the bridge transition. Hopkins and Deen (1969) conducted a survey of existing bridge approaches located in Kentucky in 1964 and 1968 to provide general information as to the prevalence of the problem of the bump at the end of the bridge. The researchers suggested the factors affecting differential settlement of the bridge approaches consisted of (1) type and compressibility of the soil and materials used in the embankment and foundation, (2) height of the embankment, (3) thickness of the compressible foundation soil layer, (4) lapse of time between completion of the embankment and construction of approach pavement, and (5) type of abutment. The observations were supported by the research studies performed by many researchers (Stewart, 1985; Ardani, 1987; Tadros and Benak, 1989; Kramer and Sajer, 1991; and Briaud et al., 1997).

A research study performed for California DOT (Caltrans) by Stewart (1985) indicated that the main causes of bridge approach slab settlement problem are the consolidation settlement of existing foundation soils and backfill materials. Whereas, Ardani (1987) proposed several contributing factors to the bump problem including (1)

time-dependent consolidation of foundation soil and the approach embankment, (2) poor drainage and soil erosion around the abutment, and (3) poor compaction of embankment fill adjacent to the abutment.

According to the field study conducted on 16 different embankment sites in Nebraska, Tadros and Benak (1989) concluded that the primary cause of the settlement of a bridge approach is the consolidation of the existing foundation soil, but not the settlement of the compacted embankment fill. Wahls (1990) attributed the settlement of bridge approach slabs to several factors, including foundation compression, embankment compression, poor compaction near the abutment, erosion of embankment at abutment face, improper drainage of embankment and abutment fill, approach slab design, and abutment and foundation type. The researcher also explained that the lateral creep of the foundation soil and the lateral movement of the abutment can be a potential cause of the problem.

Laguros et al. (1990) proposed the factors which affect the bridge approach settlement, including the age of approach slab, height of embankment, skewness of the bridge, and traffic volume. The researchers also observed that the flexibility of the approach pavements is the other factor that has a considerable influence on the settlement of the bridge approach. The greater differential settlement was observed in flexible pavements during initial stages following construction (short term performance). Whereas, for the long term period, similar performance was noticed in both flexible and rigid pavements.

A study performed by Mahmood (1990) indicated that the type of bridge abutment is the other factor contributing to the magnitude of the approach settlement problem. The spill-through abutment consists of a beam supporting the bridge seat, two or more columns supporting the beam, and a footing supporting the columns. Because of

the difficulty of properly compacting the embankment fill soil placed around the columns and under the abutment cap, an erosion problem is frequently encountered, resulting in accelerated approach embankment settlement.

Schaefer and Koch (1992) proposed in their study that weather change is the other cause contributing to the differential settlement between the bridge and approach slab. Soil movement behind the abutment occurs when the weather changes, which thereafter leads to void formation under the approach slab. This causes water infiltration under the slab and leads to erosion of backfill soil.

In 1997, Briaud et al. provided a useful diagram summarizing several possible factors which contribute to the formation of the bump at the end of the bridge, as presented in Figure 2.1. The author grouped the factors and ranked them in the order of their contribution to the bump problem. The top three causes of the approach problem consists of (1) settlement of fill material, (2) settlement of natural soil under the embankment, and (3) poor construction practices.

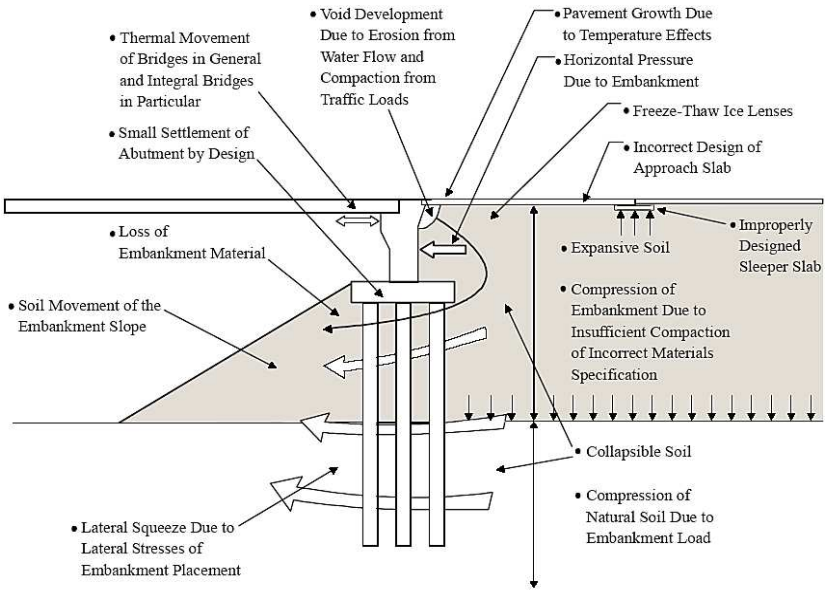

Figure 2.1 Different factors lead to the formation of bump problem (Briaud et at., 1997)

Seo (2003) performed a research study investigating the bump at the end of the bridge problem. Visual inspections of 18 bridge sites in Houston were conducted. An extensive program of laboratory and field tests was performed on the selected two bridge sites to investigate to main causes of the bump. Additionally, the effect of the repeated load from vehicles on the bump problem was studied by using a simulation device named Bridge to Embankments Simulator of Transition (BEST). The researcher listed the possible causes of the bump problem and the factors affecting the increasing in the bumps, including the compression of embankment soil and natural soil, poor compaction of embankment fill soil, strength of foundation soil, number of cycles of loading over the approach slab, velocity of vehicles, and weight of vehicles.

White et al. (2007) performed the study to evaluate the bridge approach problem in Iowa. A total of 74 bridge sites were inspected. Based on the field inspections results, the researchers concluded that the primary factors of the settlement problems of the bridge approach pavements are void development from backfill collapse, severe backfill erosion, poor soil compaction and construction practices, and poor surface and subsurface water management. The researchers also suggested that the consolidation settlement of the embankment fill and foundation soil is not necessarily the primary contributor to the approach settlement problem.

Based on the previous literatures, Puppala et al. (2012) summarized the major factors causing the approach bump problem as listed in following:

1. Consolidation settlement of foundation soil
2. Poor compaction and consolidation of backfill materials
3. Poor drainage system and soil erosion
4. Types of bridge abutment
5. Traffic volume

6. Age of the approach slab
7. Approach slab design
8. Skewness of the bridge
9. Seasonal temperature variations

The details of these factors are provided in the following subsections.

2.3.1 Consolidation Settlement of Foundation Soil

Consolidation settlement of the natural soil beneath an approach embankment is considered as the primary cause contributing to bridge approach settlements (Hopkins and Deen, 1969; Stewart, 1985; Ardani, 1987; Tadros and Benak, 1989; Wahls, 1990; Dupont and Allen, 2002; Seo, 2003; and Puppala et al., 2012). The settlement in foundation soil usually occurs as a result of the dynamic traffic loads applied on the pavement atop the embankment surface and the static load from the embankment weight itself (Dupont and Allen, 2002). Because of their time-dependent consolidation behavior, cohesive soils, such as soft and high plasticity clays, usually show the settlement problem more severely than non-cohesive soils (Archeewa, 2010).

In general, the soil settlement is classified into three broad categories, including (1) Elastic or immediate settlement, (2) Primary consolidation settlement, and (3) Secondary consolidation settlement.

2.3.1.1 Elastic or Immediate Settlement

An elastic settlement is caused by elastic deformation (short-term deformation) of soils, without any change in the moisture content (Das, 2010). This type of settlement is considered to be insignificant and does not contribute to the bump problem because it completely occurs during the embankment construction process (Hopkins and Deen, 1969; Stark et al., 2004; and Puppala et al., 2012).

2.3.1.2 Primary Consolidation Settlement

When saturated cohesive soil is subjected to a stress increase, the excess pore water pressure in the soil particles is generated and gradually dissipates over a long time period. The result of a volume change in the soil during the water dissipation process is called the primary consolidation settlement (Holtz and Kovacs, 1981 and Das, 2010). This type of settlement is regarded as the main factor contributing to the total settlement of natural soils (Archeewa, 2010).

2.3.1.3 Secondary Consolidation Settlement

The secondary consolidation settlement is the result of the plastic adjustment of soil fabrics observed after the dissipation of excess pore pressure, at the end of primary consolidation (Hopkins and Deen, 1969 and Das, 2010). This type of settlement can be as large as the primary consolidation if it occurs in very soft, highly plastic clay soils but, for the granular soils, it is negligible (Hopkins and Deen, 1969).

2.3.2 Poor Compaction and Consolidation of Backfill Materials

Inadequate fill compaction (i.e., relative compaction lower than 90 percent of standard Proctor result) is one of the most important contributing factors to the bridge approach settlement. The main problem found during the compaction process of bridge approach embankment is the difficulty in compacting around the columns and walls of bridge abutments. Hoppe (1999) reported in his survey that about 50 percent of 39 state DOTs have had difficulty in obtaining a specific degree of fill compaction in the area close to bridge abutments. It is a common practice that the bridge abutments are constructed prior to the embankment fill placement and compaction. This practice leads to the difficulty in the compaction of the area closest to the bridge because the equipment access to this area is restrictive or limited (Burke, 1987; Archeewa, 2010; and Puppala et

al., 2012). The poor compaction control causes low density and highly deformable embankment mass; consequently, resulting in the embankment settlement (Hopkins and Deen, 1969 and Lenke, 2006).

The other factor affecting the quality of embankment fill compaction is type of the soil used as embankment backfill material. Using low quality materials, such as locally available soft cohesive soil or expansive clay, as backfill can be the cause of severe bump problem (Archeewa, 2010). The clay backfill requires more compaction effort than granular soils, which is sometime difficult to attain in restrictive area (Helwany, 2007). Moreover, cohesive soils are generally more difficult to compact to their optimum moisture content and maximum density when compared to granular fill materials (Hopkins, 1973). Most highway agencies require only granular fill materials for a highway embankment project because it can be better compacted and reaches the maximum consolidation faster than cohesive soils (Wahls, 1990; Lenke, 2006; and Puppala et al., 2012). However, this material could impose more stresses on underlying foundation subgrades.

2.3.3 Poor Drainage and Soil Erosion

The surface and subsurface drainage systems are considered as a few of the major causes of bridge approach settlement (Wahls, 1990; Hope, 1999; White et al., 2005; Archeewa, 2010). Poor drainage systems cause an ineffectiveness of redirecting surface runoff (including the runoff from pavement) and infiltrated water behind abutments away from the bridge, resulting in constant erosion of backfill soil adjacent to the abutment. This leads to the development of voids and induces slope stability failures, causing the approach slab to settle (Hoppe, 1999; Mekkawy et al., 2005; White et al., 2007; and Mishra et al., 2010). Figure 2.2 provided by Hopkins and Deen (1969) presents the erosion of embankment fill caused by the ground water seepage. The loss of material

around the abutment results in erosion of subgrade material and, eventually, the settlement of the bridge approach slab.

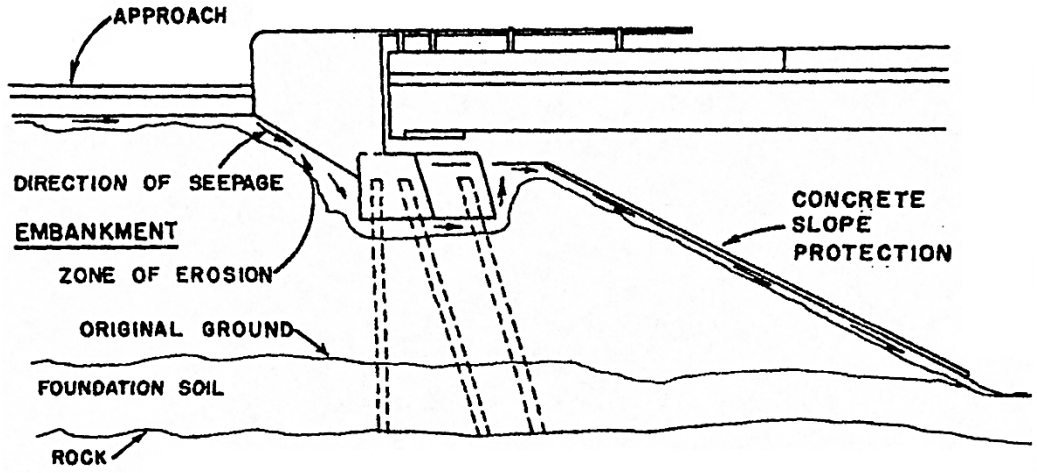

Figure 2.2 Direction of seepage and zone of erosion (Hopkins and Deen, 1969)

The causes of a dysfunctional drainage system can be incorrect construction practices, improper design methods, or both. Williammee (2008) suggested that an ineffective drainage system can occur when an incorrect placement, such as installing the outlet flow line higher than the inlet flow line of the drainage pipes in the concrete riprap in the newly constructed bridge, is performed.

Water leaking through the pavement joints or cracked pavement sections can significantly erode the embankment fill under the interface (Briaud et al., 1997; Dupont and Allen, 2002; White et al., 2005; and Jayawickrama et al., 2005). Figure 2.3 provided by Briaud et al. (1997) presents the comparison of improper and proper design practice for joints between the pavement and abutment wing wall. The improperly designed joint allows water draining from pavement to seep through the joint and erode the soil. The expansion joints used for transferring traffic loads and allowing pavement expansion, without damaging the abutment structure, should also prevent surface water from

infiltrating into the embankment (Wolde-Tinsae et al., 1987). The expansion joints with poor construction of joint sealants allow water to flow into the underlying fill materials. The leaked water can soften the embankment fill and wash out the fine particles from backfill material, causing erosion in the embankment mass and consequently, inducing void development under the bridge approach slab (Jayawickrama et al., 2005; White et al., 2005; and Mekkawy et al., 2005).

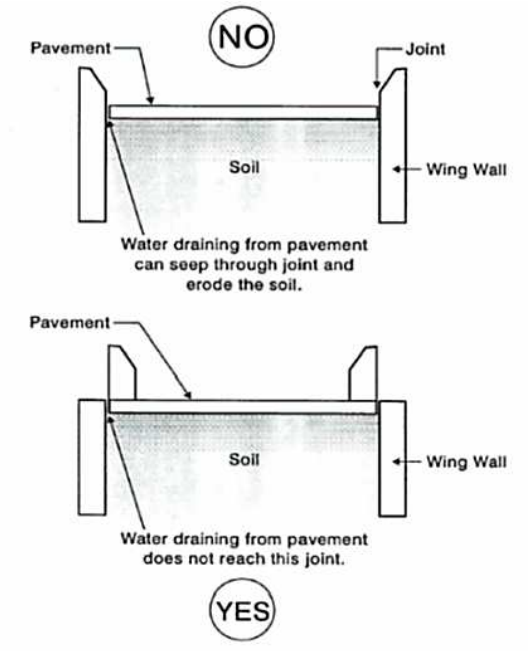

Figure 2.3 Comparison of improper and proper design practices for joints between pavement and abutment wing wall (Briaud et al., 1997)

Using erodible soils as the backfill material is the other factor increasing the potential for erosion of the embankment. The resistance to erosion of soils is dependent on their grain size distribution (Briaud et al., 1997). Figure 2.4, presenting the range of most erodible soils, indicates that a gradation band of material in the sand to silt size is improper for use as an embankment backfill unless an appropriate drainage system or erosion control system are provided (Briaud et al., 1997).

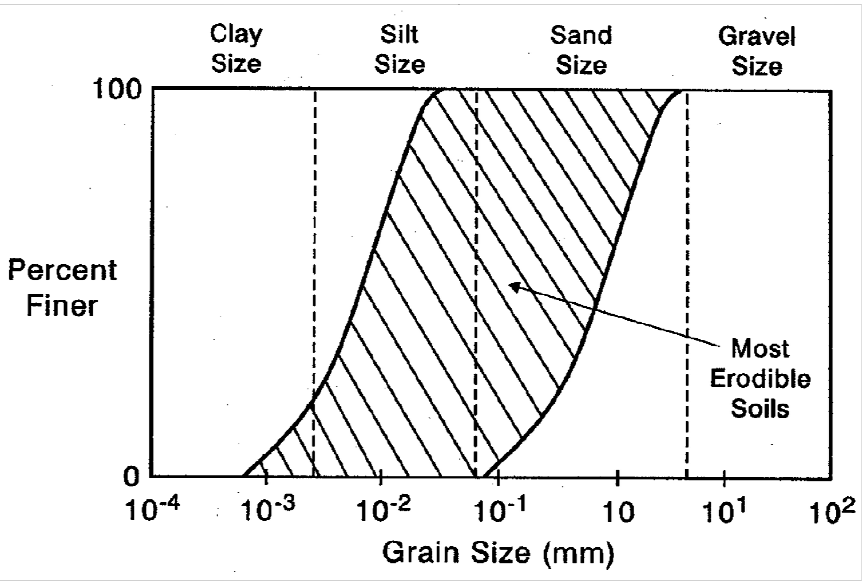

Figure 2.4 Range of most erodible soils (Briaud et al., 1997)

2.3.4 Types of Bridge Abutments

Abutments are the part, at the ends of the bridge structure, used to retain the embankment and to carry the vertical and horizontal loads from superstructures to the bridge foundations (WisDOT, 2014). Figure 2.5 presents the components of an abutment and its primary functions.

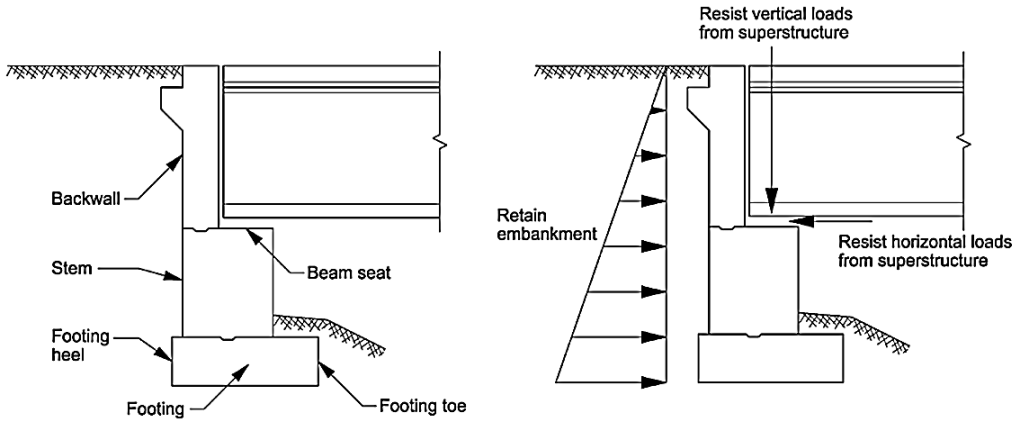

Figure 2.5 Abutment components and its primary function (WisDOT, 2014)

Bridge abutments can be classified into two major types, including integral (movable) and non-integral (conventional or stub) abutments (Greimann et al., 1987). The non-integral abutment is subdivided into three different types, which are closed or U-type, spill-through or cantilever, and stub or shelf abutments (Puppala et al., 2012). The details of each type of abutment and its effect on the bump problem are briefly explained in following.

2.3.4.1 Integral Abutments

Integral abutment bridges are designed to physically and structurally connect the superstructure (i.e., bridge deck slab) and abutment without any expansion joints in order to reduce the post-construction cost spent on the joints maintenance (Horvath, 2000 and Mistry, 2005). This abutment type is allowed to move laterally along with the bridge deck slab.

The approach slab system of an integral abutment bridge consists of the approach slab, sleeper slab, backfill soil, and foundation soil. The advantage of this type of abutment is that it is designed to carry both primary loads (i.e., dead and live loads) and secondary loads coming from creep, shrinkage, thermal gradients, and differential settlement (Archeewa, 2010 and Puppala et al., 2012).

For the integral abutments, the factor contributing to the bump problem is that this type of abutment introduces thermal-induced movements in the approach system, and lack of resilience could cause some permanent settlements. This movement consequently causes the aggravation in bump problem on the approach system (Schaefer and Koch, 1992; White et al., 2005; and Archeewa, 2010).

2.3.4.2 Closed Abutment or U-Type

A cross section of a closed abutment, or also called U-type abutment, is illustrated in Figure 2.6. The two side walls and front wall of the abutment are built on

spread footing below natural ground (TxDOT, 2001). For this type of abutment, the leaking of water through expansion joints can cause the erosion of embankment fill soil. In addition, the compaction of the embankment fill in this abutment is difficult because of the confined space near the abutment walls (TxDOT, 2001).

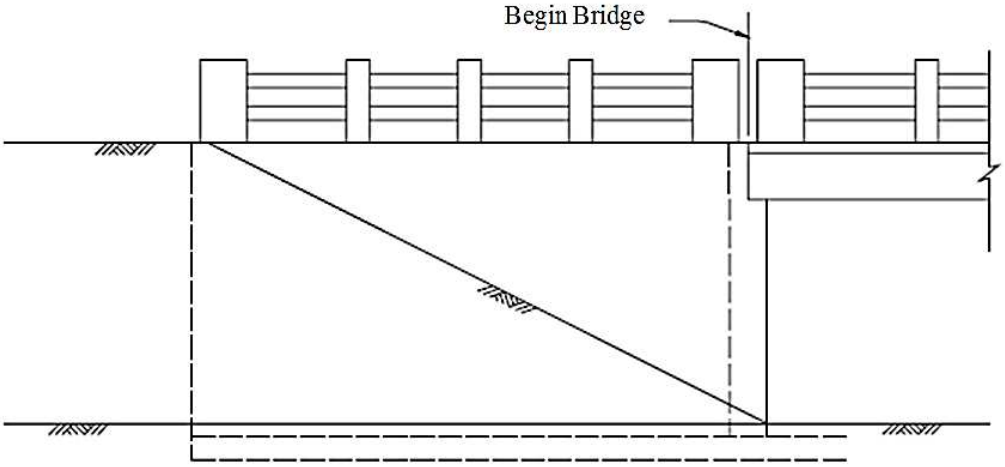

Figure 2.6 U-Type abutment (TxDOT, 2001)

2.3.4.3 Spill-through or Cantilever Abutment

The components of a spill-through abutment include a beam supporting the bridge seat, columns, and footing. Figure 2.7 presents the outward appearance of the spill-through abutment. The columns supporting the abutment beam are placed on spread footing below natural ground (TxDOT, 2001). The fill is built around the columns and allowed to spill through, on a reasonable slope, into the bridge opening. Similar to the U-type abutment, water infiltration through expansion joints may cause the erosion problem in backfill soil. In addition, the compaction of the backfill material between the columns and in the area close to abutment wall is very difficult. This can lead to the bump problem on the approach slab.

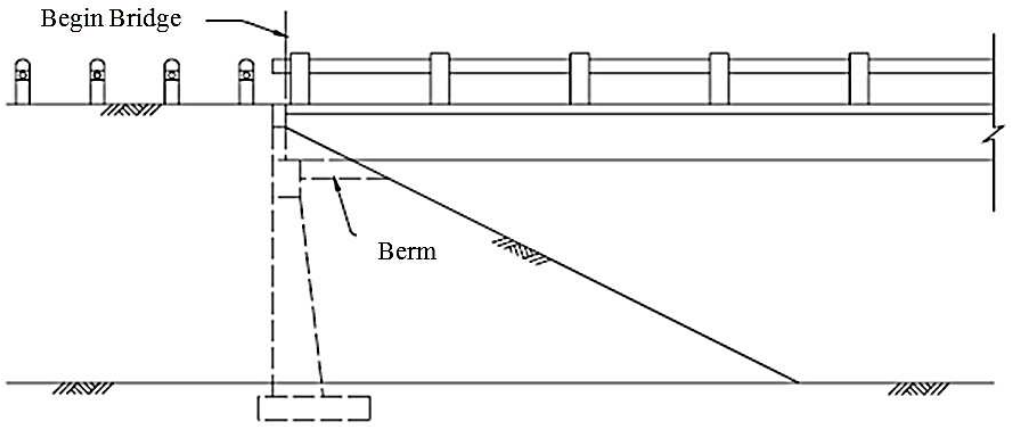

Figure 2.7 Spill-through (cantilever) abutment (TxDOT, 2001)

2.3.4.4 Stub or Shelf Abutment

This type of the abutment is mostly used in bridge construction projects in Texas. It is constructed, after the embankment fill soil is compacted, by driving piles or drilling shafts through the compacted fill and placing a cap and wing walls on top. With this construction procedure, the compaction of the backfill material is relatively easier than the U-type abutment. However, the compaction is still difficult for the soil behind the abutment (TxDOT, 2001). Figure 2.8 illustrates the simplified cross-section of a stub abutment.

From past experience, it has been found that the problem of the bump at the end of the bridge caused by fill settlement is particularly noticed on stub embankments (TxDOT, 2001).

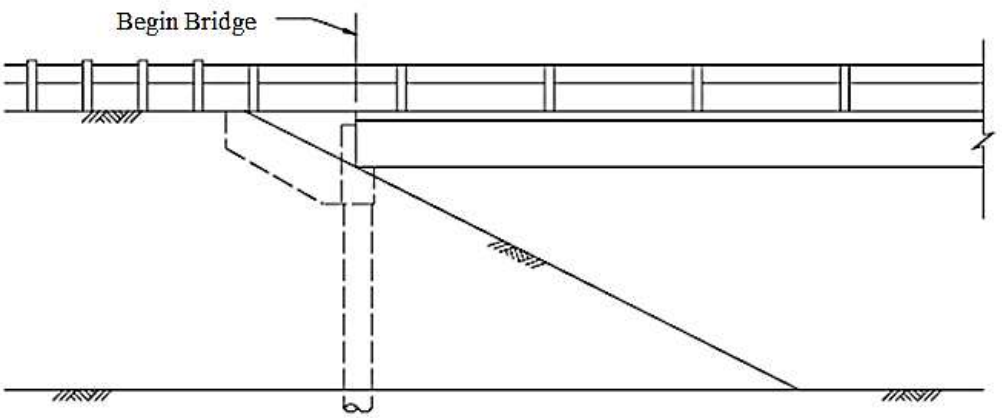

Figure 2.8 Stub or shelf abutment (TxDOT, 2001)

2.3.5 Traffic Volume

The effect of traffic volume on the bump at the end of the bridge has been studied in some research (Wong and Small, 1994; Ha et al., 2002; Bakeer et al., 2005; and Lenke, 2006). High volume traffic has been found as a compelling reason for using the approach slabs in a bridge construction (Archeewa, 2010 and Puppala et al., 2012). However, there is disagreement about the effect of traffic volume on the bump problem in some of previous literatures.

Ha et al. (2002) concluded from investigating results that the bump problem is more severe with high average daily traffic (ADT). Similarly, Lenke (2006) noted that the bump problem was found to increase with vehicle velocity, vehicle weight, and the volume of the average daily traffic. In contrast, Bakeer et al. (2005) concluded that the speed limit and traffic volume have no distinguishable impact on the performance of the approach slabs.

2.3.6 Age of the Approach Slab

The age of the approach slab affects the performance of other elements of the bridge structure, especially the expansion joints connecting to the slab. The expansion joint could negatively affect the backfill performance in terms of controlling settlements beneath the slab (Laguros et al., 1990 and Bakeer et al., 2005). In the concrete approach slab, the alkali-silica reactivity (ASR) is formed, inducing expansion stress in the surrounding area. The stress potentially leads to the expansion and distress in the approach slabs, approach joints, and vertical uplift of the slabs and pavement preceding the slabs (Lenke, 2006).

2.3.7 Approach Slab Design

In order to minimize effects of differential settlement between the bridge abutment and the embankment fill, the approach slab has been introduced to be used in the bridge construction. The other purposes of using the approach slab are to provide a smooth transition between the pavement and the bridge, to prevent voids that might occur under the slab, and to provide a better seal against water percolation and erosion of the backfill material (Burke, 1987; Archeewa, 2010).

Rough transitions can occasionally occur in bridge approach slab due to differential settlements between the abutment and roadway. The differential settlement is a result of the difference in the support systems of the bridge structure and approach embankment. The approach slabs are typically placed over an embankment supported by natural soil, whereas the bridge abutments are usually supported by pile foundations.

Briaud et al. (1997) suggested that the bridge approach slab with insufficient length can cause differential settlements at the bridge end. The studies proposed by Bakeer et al. (2005) reported that based on the IRI ratings, the 80 ft. (24 m) long slabs

performed the best, and no significant difference was found when compared to 100 ft. (30.5 m) long slabs.

The study, based on the performance of the approach slab in controlling the differential settlements performed by Dunn et al. (1983), showed that the rigidity of the slabs is also a contributing factor to the differential settlement. The comparison of the performance of various approach slabs in Wisconsin showed that 76% of the flexible approaches were rated as poor and 56% of non-reinforced approaches were rated as fair; whereas, the performance of 93% of reinforced concrete approaches was rated as good.

2.3.8 Skewness of the Bridge

Archeewa (2010) summarized that the skewness of the bridge affects overall performance and formation of approach settlement in the bridge. The skewed integral bridges tend to rotate under the influence of cyclic changes in earth pressure on the abutment (Hoppe and Gomez, 1996). The temperature-dependent volumetric change of concrete in the pile cap and abutment, and the rigid body translation and rotation of the abutment due to the longitudinal expansion or contraction of the superstructure for a skewed integral abutment bridge affect the change in position of the ends of an abutment. Abendroth et al. (2007) recommended that for the integral abutment bridge construction, the skewed integral abutments should be placed parallel to each other and ideally be of equal height. In addition, Nassif (2002) concluded that the skew angle of the approach slab and improper compaction in the soil area close to the abutments affect the higher rates of settlement at the bridge ends.

2.3.9 Seasonal Temperature Variations

The seasonal temperature changes result in cyclic horizontal displacement on the abutment, especially for the integral abutment, and back fill soil. This can create soil displacement behind the abutment, resulting in void development under the approach slab (White et al., 2005). The water infiltrating the void can accelerate an erosion and loss of backfill material under the approach slab. Figure 2.9 presents the expansion-contraction movements of the bridge, with the seasonal temperature changes resulting in the formation of voids beneath the approach slab.

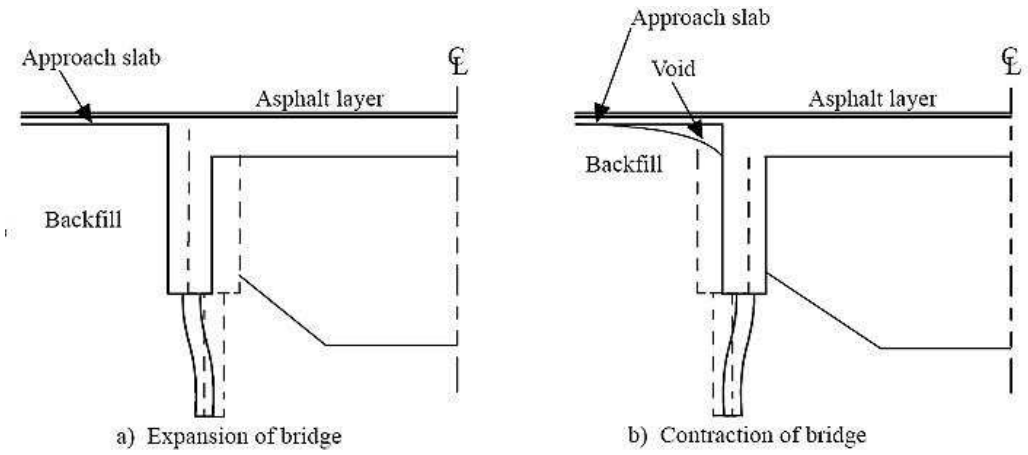

Figure 2.9 Movements of bridge structure induced by temperature change (Arsoy et al., 1999)

The phenomenon of thermally-induced displacements on a bridge abutment is illustrated in Figure 2.10. During winter, the contraction of concrete in the bridge structure causes the abutment to move outward from the retained earth; while, in summer, the abutment moves inward to the retained soil due to the thermal expansion of the bridge structure. These horizontal displacements are observed to be greater at the top of abutment, and the problem is aggravated when the superstructure is constructed primarily of concrete (Arsoy et al., 1999 and Horvath, 2005).

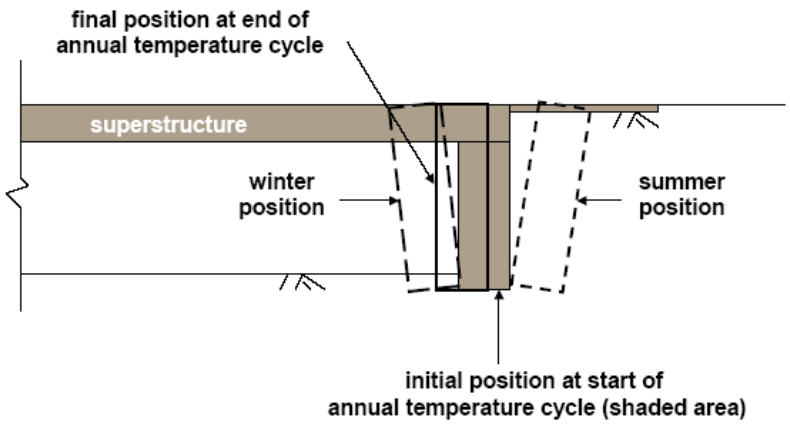

Figure 2.10 Thermal-induced displacements on an abutment (Horvath, 2005)

In addition, the climatic change, or also called seasonal temperature change, can also cause certain irreversible damage to the pavement and bridge approach slabs in terms of ice lenses due to frost action. Moreover, very low temperatures can cause the water under the slabs, either from precipitation or from other sources such as ground water, in both liquid and vapor forms, to freeze, causing a frost heave problem in the pavements (Puppala et al., 2012).

Based on the above sections, it can be noticed that there are several factors that can cause the bump at the ends of the bridge or differential settlement problems. The effects of those factors on the bump problem can be in either an individual mechanism or in a combination mechanism. In this study, the effects of the first three factors are focused on, which are (1) consolidation settlement of foundation soil, (2) poor compaction and consolidation of backfill materials, and (3) poor drainage and soil erosion. Various treatment or repair techniques involving mitigating the effects on the bump problem are provided in the following section.

2.4 Mitigation Techniques for Bridge Approach Settlement Problem

In this section, several techniques adopted for reducing the differential settlement problem between the bridge structure and approach slabs are briefly summarized. These techniques are grouped into four categories including (1) improvement of foundation soil, (2) improvement of approach embankment backfill materials, (3) water management and erosion control methods, and (4) use of lightweight materials.

2.4.1 Improvement of Foundation Soil

As discussed in the previous section, consolidation settlement of foundation soil is one of the most important factors causing the bridge approach settlements. When an approach embankment is constructed on cohesive soils such as normally consolidated clay, the large settlements, either from the primary and/or secondary consolidation settlement, can occur in the soils. However, the differential settlement between the bridge structure and the roadway embankment can be neglected if the foundation soil is a granular soil, such as sand, gravel, and rock. This is because the granular soils do not undergo long-term settlements. The settlements in the foundation soil lead to the settlement of the embankment mass and consequently, result in the formation of the bump or approach settlement problems (Wahls, 1990 and Archeewa, 2010).

Several ground improvement techniques have been proposed and attempted to be used to enhance the properties and mitigate the consolidation settlements in foundation soils (Wahls, 1990; Dupont and Allen, 2002; White et al., 2005; Abu-Hejleh et al., 2006; Hsi, 2008; Archeewa, 2010; and Puppala et al., 2012). The selection of the proper technique for a particular project is mainly based on the type of the foundation soil. Secondary factors to be considered are the degree of saturation, ground water table location, and permeability (Archeewa, 2010). For example, when the soil is cohesionless

soil, the techniques such as surcharge or preloading, dynamic compaction, compaction piles, soil reinforcement, and geopier are proposed. On the other hand, if the soil is cohesive soil, excavation and re-compaction, preloading, installation of wick drains, dynamic compaction, stone columns, lime treatment columns and grouting are preferred (Wahls, 1990 and Abu-Hejleh et al., 2006). Puppala et al. (2012) provided simplistic tables summarizing the groups of ground improvement techniques based on the soil type and their mechanisms, as presented in Table 2.1 and 2.2.

Table 2.1 Summary of Ground Improvement Methods Based on Soil Type (Puppala et al., 2012)

Technique	Cohesionless soils	Cohesive soils
Excavation and Replacement	✗	✔
Preloading w or w/o Surcharge	✔	✔
Dynamic Compaction	✔	✔
Grouting	✔	✔
Wick Drains	✗	✔
Compaction Piles	✔	✗
Gravel Columns	✔	✗
Lime Treatment	✗	✔
Stone Columns	✗	✔
Soil Reinforcement	✔	✔
Geopier	✔	✔

Table 2.2 Summary of Ground Improvement Methods Based on the Function (Puppala et al., 2012)

<table>
<tr><th colspan="3">Embankment Soft Foundation Soil Improvement Techniques</th></tr>
<tr><th>Mechanical</th><th>Hydraulic</th><th>Reinforcement</th></tr>
<tr><td rowspan="4">Excavation and replacement

Preloading and surcharge

Dynamic compaction</td><td rowspan="4">Sand drains

Prefabricated drains

Surcharge loading</td><td>Columns
Stone and Lime Columns
Geopiers
Concrete Injected Columns
Deep Soil Mixing Columns</td></tr>
<tr><td>Deep foundations
In-situ: Compacted piles
CFA piles
Driven piles: Timber and Concrete piles</td></tr>
<tr><td>Geosynthetics
Geotextiles/Geogrids
Geocells</td></tr>
</table>

The combination techniques are sometimes performed in a particular field condition; for example, the preloading technique can be used along with the installation of wick drain in order to faster consolidation settlement in soft foundation soils.

Some of the ground improvement techniques and available literature information with respect to approach settlement problems are briefly explained in the following sections.

2.4.1.1 Excavation and Replacement

This technique is selected when the top part of the proposed foundation soils are weak and vulnerable to excessive consolidation (Wahls, 1990; Hoppe, 1999; Luna et al., 2004; White et al., 2005; Archeewa, 2010; and Puppala et al., 2012). The excavation of undesirable top soil is performed in the range of 10-ft to 30-ft depths from the existing soil surface and then, filled back with the selected fill soil from borrowed sites (Dupont and

Allen, 2002). However, this technique is presently less favorable because of the difficulty involving maintaining uniform replacement and the expense involved in the complete removal and land-filling of undesirable soil. The excavation and replacement technique may be considered as the most economical solution only if the soil areas are underlain by shallow bedrock or firm ground (Tadros and Benak, 1989).

2.4.1.2 Preloading and Surcharge

Preloading, or also called the pre compression technique, is reported as one of the effective methods to control the settlement in foundation soil. This method is relatively inexpensive and effective in improving poor foundation soils (Bowles, 1988; Dupont and Allen, 2002; and Puppala et al., 2012). The two major objectives of this technique consist of (1) minimizing the post-construction settlement of the foundation soils and (2) improving the shear strength of the soils by increasing the density and decreasing the moisture content and void ratio of the soils.

Cotton et al. (1987) explained the preloading technique in an embankment construction as a process in which the weight of embankment is considered as the load inducing the consolidation settlement in the foundation soil. The process has to be completed before the actual pavement is constructed. Thus, in several construction cases, the schedule is deferred up to a year. Because of the lengthy construction period that could result in significant problems in construction schedules and increase total project costs, many highway agencies do not prefer this technique (Hsi, 2007 and Archeewa, 2010).

In order to accelerate the process of consolidation settlement, a temporary surcharge load is sometime applied on top of the embankment (Bowles, 1988; Hsi, 2007; Tjie-Liong et al., 2013). The applied surcharge load has to be superior to the normal load (i.e., the weight of the embankment). For the case of embankment construction, the

height of the desired extra load has to be limited by the embankment slope stability; therefore, a berm is sometime constructed to eliminate the limitation. The process of berm construction, excessive fill placement, and its removal cause an increase in the overall project cost and construction time (Bowles, 1988). The other way to accelerate the consolidation settlement in foundation soil is to use the pre-compression technique along with vertical drain method. The detail of vertical drains will be explained later.

2.4.1.3 Dynamic Compaction

Dynamic compaction technique is best suited for loose granular deposits in medium-to-soft clays (Archeewa, 2010). The concept of this technique is to improve the mechanical properties of soils by transmitting the high energy impacts from dropped tamper to the loose soils, which are initially compressible and have low bearing capacity (Slocombe, 2004 and Hamidi et al., 2011). During the compaction, a heavy tamper is repeatedly dropped in free fall from a designed level onto the ground surface. With this technique, densification of the soils is achieved (Lukas, 1986). The weight of the tamper mass is most often in the range of 8 to 25 tons; however, lighter or heavier weights are occasionally used. The drop heights in the range of 30 to 65 ft. are usually used (Hamidi et al., 2011).

Lukas (1986) provided a diagram, as presented in Figure 2.11, characterizing and grouping the soils into three different zones based on their properties (i.e., grain size and plasticity index) and suitability for dynamic compaction technique. As can be seen from the figure, the soils in zone I (i.e., pervious soils) are suitable for the dynamic compaction technique. Zone II (semi-pervious) soils need a longer time to allow the pore pressure induced by the dropped weight to dissipate and to obtain the required level of improvement. The soils grouped in zone III are not suited for being improved by the dynamic compaction technique and alternate improvement methods should be selected.

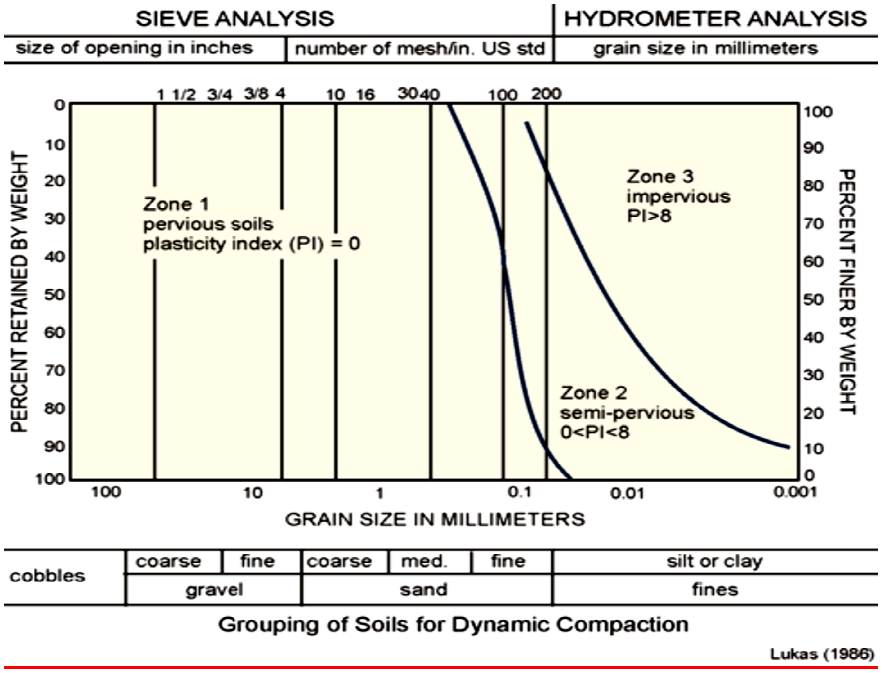

Zone 1: Best
Zone 3: Worst (consider alternate methods)
Zone 2: Must apply multiple phases to allow for pore pressure dissipation

Figure 2.11 Grouping of soils for dynamic compaction (Lukas, 1986)

The effective depth of dynamic compaction can be as deep as 40 ft. but it is usually ineffective for saturated impervious soils, such as peats and clayey soils (Wahls 1990; Puppala, 2012). This technique is not suitable for small areas of improvement such as highway embankments (Hausmann, 1990). According to the available literatures, the application of this method to highway-related projects is less than it is to other applications, such as sanitary landfills, dams, and air fields (Lukas, 1995).

2.4.1.4 Vertical Drains

The ground improvement technique of vertical drains deals with the hydraulic properties of the soils. This technique is used to accelerate the consolidation settlement expected to occur in the soft clay soils by shortening the drainage path to dissipate the

excess pore water pressure (Nicholson and Jardine, 1982; Puppala et al., 2012). The vertical drains can be classified into two major types: sand drains and prefabricated drains. However, the use of sand drains has recently been replaced by prefabricated vertical drains because of the ease and low cost of their installation (Archeewa, 2010 and Puppala et al., 2012).

The prefabricated vertical drains (PVDs), also called wick drains, are the band-shaped products consisting of a geotextile filter material surrounding a plastic core. The size of PVDs is typically 3.94 in (100 mm) wide by 0.24 to 0.32 in (6 to 8 mm) in thickness (Rixner et al, 1986). The example of a PVD cross section is shown in Figure 2.12. Bergado et al. (1996) provided the configurations of different types of the PVDs available in the market, as presented in Figure 2.13.

Figure 2.12 Isometric view of the prefabricated vertical drains
(http://www.tencate.com/apac/geosynthetics/product/infrastructure/tencate-polyfelt-alidrain-pvd.aspx)

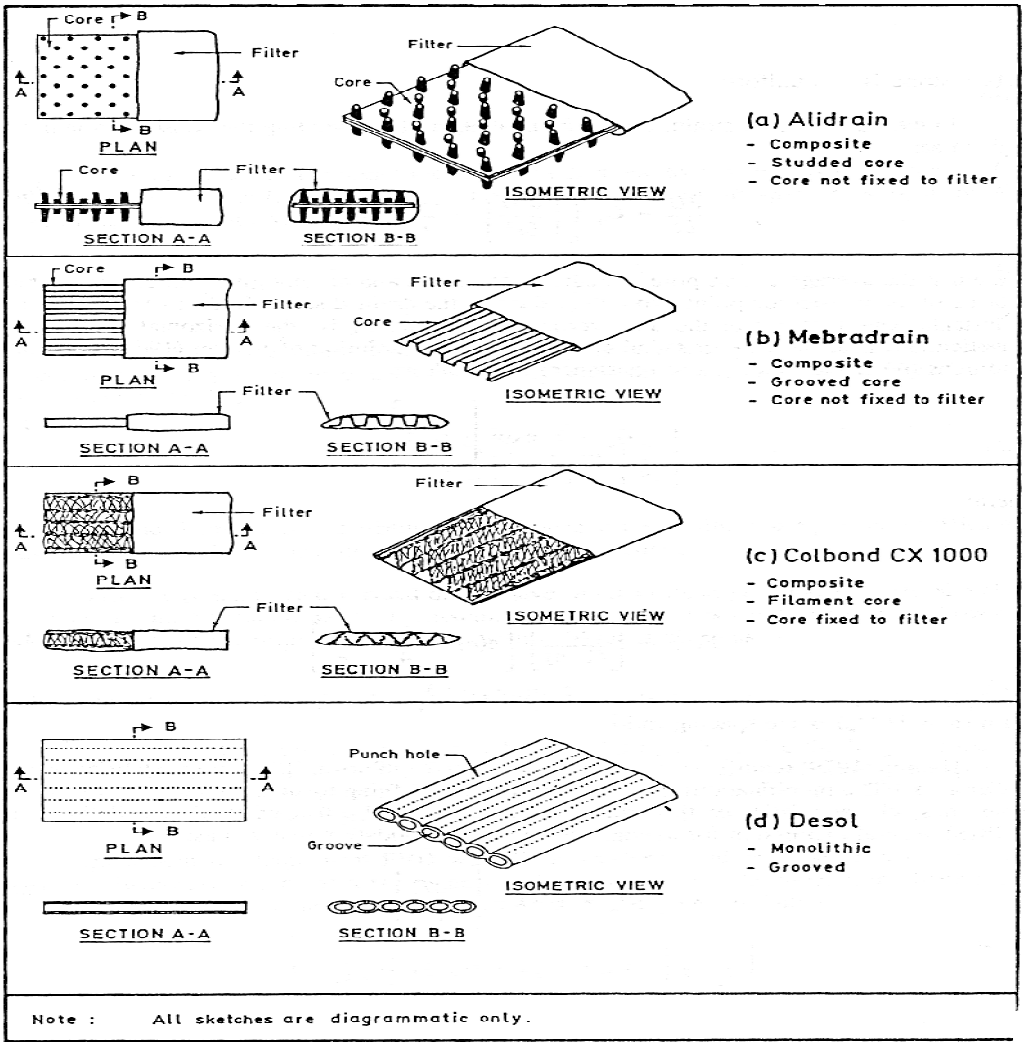

Figure 2.13 Configurations of different types of prefabricated vertical drains (Bergado et al., 1996)

As mentioned previously, the vertical drains technique is generally used together with preloading or surcharge to accelerate the process of consolidation settlement in the foundation soils (Rixner et al., 1986; Bergado et al., 1996; Stapelfeldt, 2006; Puppala et al., 2012). Figure 2.14 presents the process of installation and water drainage principle of the vertical drains with surcharge load system.

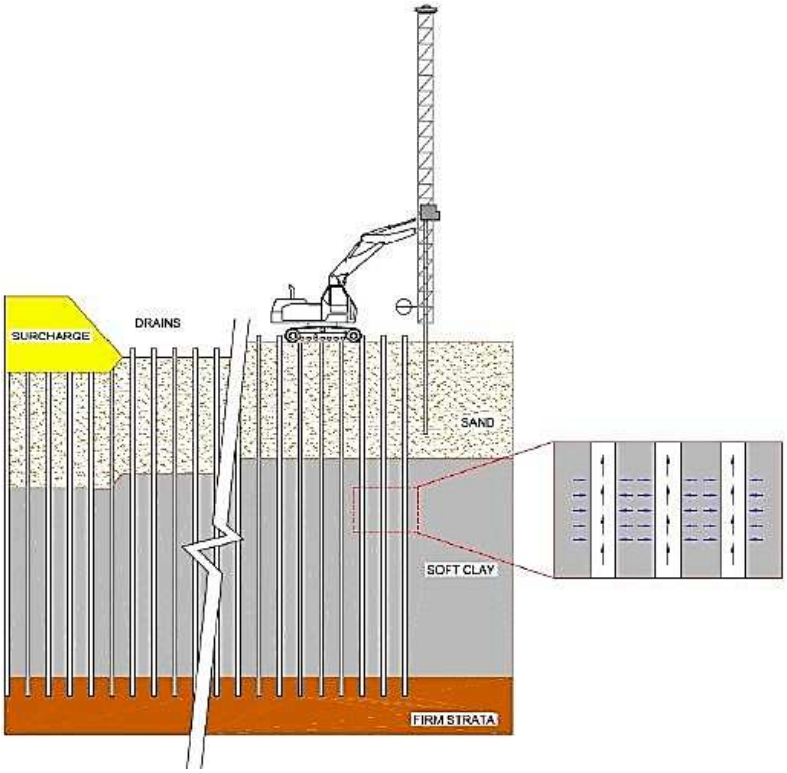

Figure 2.14 Vertical drain installation and water drainage principle
(http://www.groundimprovement.ch/Ground_Improvement_Solutions/Vertical_Drains.html)

2.4.1.5 Stone Columns

The stone columns technique is best suited for soft-to-moderately firm cohesive soils and very loose silty sands (Barksdale and Bachus, 1983; Archeewa, 2010; and Puppala et al., 2012). The main functions of this technique are to improve the load-bearing capacity of weak foundation soils, to provide long-term stability to the embankment; and to control settlements under the highway embankments (Munoz and Mattox, 1977; Goughnour and Bayuk, 1979; Barksdale and Bachus, 1983; Michell and Huber, 1985; Cooper and Rose, 1999; Serridge and Synac, 2007; Archeewa, 2010). Moreover, as the secondary function, the stone columns also provide the shortest drainage path to the excess pore water in the soils (Hausmann, 1990).

Stone columns are partially replaced in the native weak soils. The total cross section area of the columns is usually about 15 to 35 percent of the soil area, and the columns usually penetrate the entire depth of the weak soil layer (Barksdale and Bachus, 1983). The diagram of the construction stages of a stone column is illustrated in Figure 2.15. The method to construct the stone columns is vibro-replacement, with either wet top feed process or dry bottom feed process. For the wet top feed process, a high pressure water jet is used by the probe to create the hole, and stones are fed from the top of the probe; whereas, for the dry bottom feed process, air is used to advance the hole, and stones are fed from the bottom of the probe.

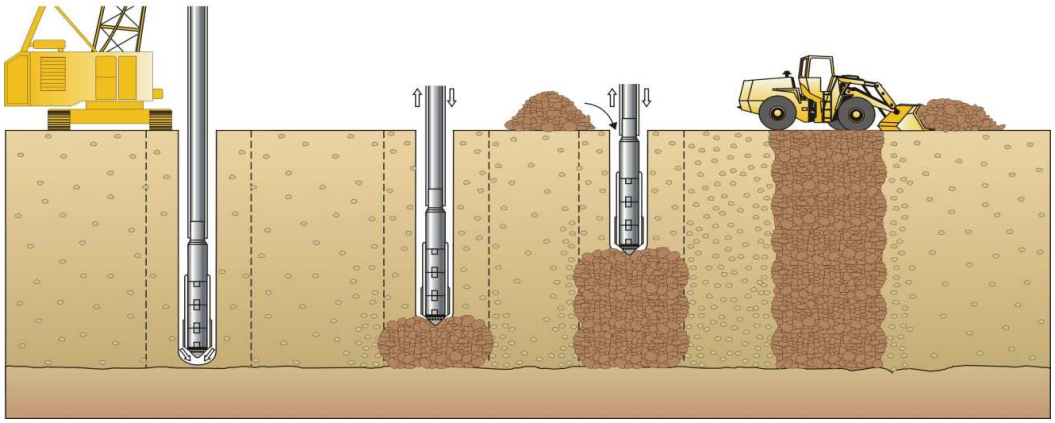

Figure 2.15 Construction stages of stone columns

(Hayward Baker; http://www.haywardbaker.com/services/vibro_replacement.htm)

Previous literatures indicate that the application of the stone columns technique is widely accepted and used in many European countries and many states in the US. (Munoz and Mattox, 1977; Goughnour and Bayuk, 1979; Barksdale and Bachus, 1983; and Serridge and Synac, 2007).

2.4.1.6 Geopiers

The concept of the geopiers technique is to improve the stiffness against compressibility of soils between the piers. The short aggregate piers can be constructed by drilling the soft ground and pushing the selected aggregate vertically into the gravity. These short piers also allow radial drainage of excess pore water pressure generated in the soft soil, and, consequently, accelerate the time-dependent consolidation process of the foundation soil (Lien and Fox, 2001; Puppala et al., 2012).

The details of geopiers design and construction are well explained by many researchers (Lawton and Fox, 1994; Minks et al, 2001; White and Suleiman, 2004). The schematic of the geopier construction sequence is illustrated in Figure 2.16. As can be seen from the figure, the steps involved in constructing a geopier consist of drilling a cavity in the soft ground, placing stones at bottom of the cavity and ramming the stones to form the bottom bulb, densifying stones in lifts to form an undulated-shaft; and finally, preloading on top of the geopier element.

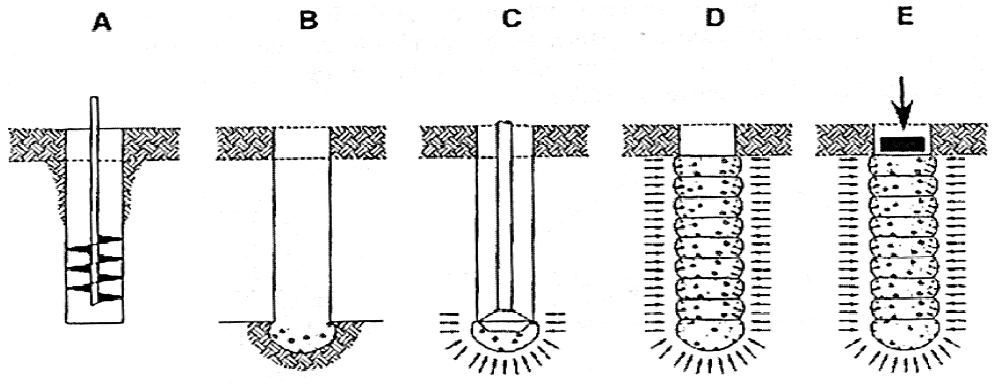

A. Drill cavity.
B. Place stone at bottom of cavity.
C. Ram stone to form bottom bulb.
D. Densify stone in lifts to form undulated-shaft.
E. Preload top of *Geopier* element.

Figure 2.16 Geopier construction sequence (Lien and Fox, 2001)

The application of the geopier technique has been adopted in transportation-related projects, such as roadway embankments and retaining walls, to mitigate the settlement that is expected to occur on these structures. The typical geopier system supporting the highway embankment is illustrated in Figure 2.17.

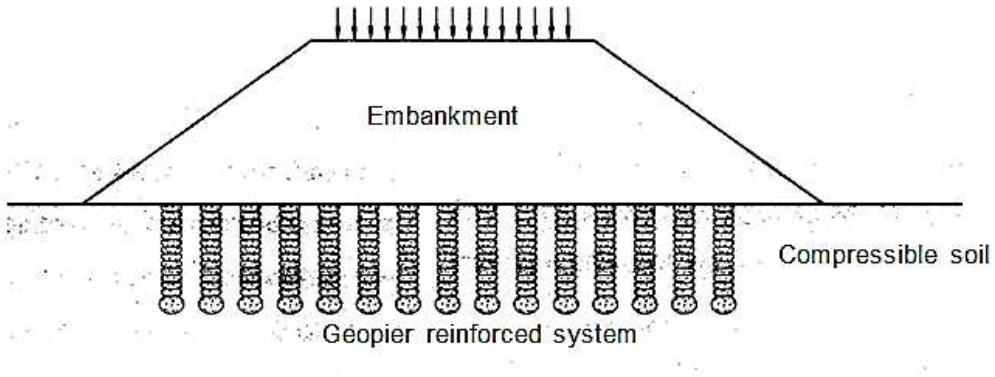

Figure 2.17 Typical geopier system supporting an embankment (Lien and Fox, 2001)

White et al. (2002) performed the test to compare the performance of the geopier system and stone columns to support highway embankments in Des Moines, Iowa. The settlements that occurred during and after the embankments construction were measured by using the settlement plates. The results showed that the settlement of the soil improved by stone columns was three times higher than the settlement of the soil improved by the geopier system.

2.4.1.7 Deep Soil Mixing (DSM) Column

Deep soil mixing (DSM) is the ground improvement technique involving the auger mixing of soils with the binders such as cement, lime, fly ash, or a combination of any two compounds, forming in-place soil-binder columns (Barron et al., 2006; Puppala et al., 2008; Archeewa, 2010). Figure 2.18 presents a typical DSM operation and resulting columns in the field. In this technique, the quality of soils is improved by in situ

stabilization of soft soil, or by in situ fixation of contaminated ground (Porbaha, 1998). The main purposes of improvement are to increase strength, to control deformation, to reduce permeability of the loose or compressible soils, or to clean a contaminated site.

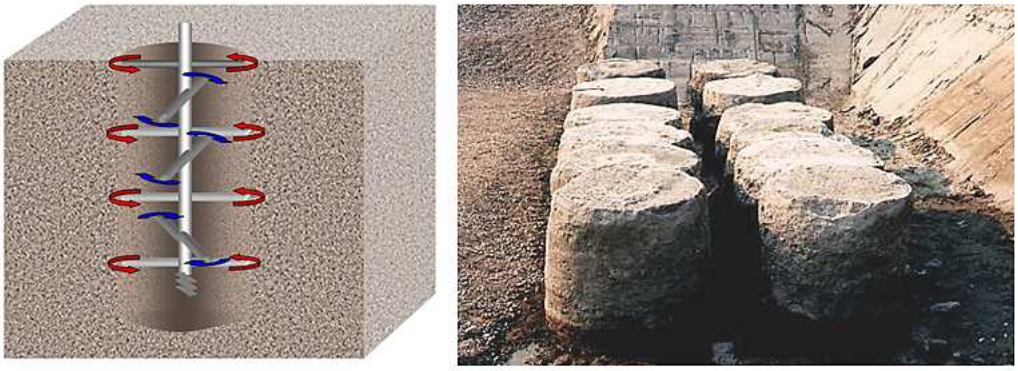

Figure 2.18 Deep soil mixing (DSM) operation and extruded DSM columns (Archeewa, 2010)

The selection of the binder used in the field is based on the requirements of the project. For instance, in the case of structures built on loose sandy soils, reclaimed soil, or peats and soft clays, the strength of the soils is the main consideration. Thus, the use of deep cement mixing is preferred (Puppala et al., 2008). Cement stabilization can provide a substantial increase in strength in a short time frame. This technique has been proven to be effective on soft clays, peats, mixed soils, and loose sandy soils (Rathmayer, 1996; Porbaha, 1998; Lin and Wong, 1999; Porbaha, 2000; Bruce, 2001; Burke, 2001; and Puppala et al., 2008). If the soil compressibility properties need to be enhanced to reduce undesirable settlements, lime or combinations of lime with cement, are typically used in the DSM treatments (Puppala, 2003).

The DSM columns technology has been used by various state highway agencies; for example, Caltrans, Utah DOT, and Minnesota DOT in cooperation with the National Deep Mixing (NDM) Program, a research collaboration of the FHWA with

10 state DOTs (Archeewa, 2010 and Puppala et al., 2012). Many case studies have been reported for the use of DSM columns to mitigate the settlement of highway embankments. Recently, Puppala et al. (2008) conducted the TxDOT research project 0-5179 for evaluating the performance of DSM columns in mitigating the pavement roughness in expansive soils. The results from two instrumented sites indicated that the DSM is a promising technique for mitigating the pavement roughness problem. The other case is the TxDOT research project 0-6022 conducted by Puppala et al. (2012) to investigate the use of DSM treatment in improving weak foundation soil underneath the bridge approach embankment. A new bridge on I-30 in Arlington, Texas, which was constructed on a weak foundation soil, was stabilized with the deep soil-cement mixing columns technique. The field performance data collected with a two-year timeframe showed that the DSM method was effective in improving the performance of the embankment system so that there was less settlement.

2.4.1.8 Driven Piles and Geosynthetic Reinforcement

For this technique, the driven piles, either timber piles or precast concrete piles, are installed adjacent to the abutment and under the embankment in order to avoid the impact of embankment settlement on the abutment piles (Hsi, 2007). The function of the driven piles is to transfer the loads of embankment onto the stiffer layers beneath, and as a result, negligible settlements can be expected on the embankment surface.

However, in the conventional piled embankment construction, very close spacing between the piles results in higher construction costs. By introducing a layer of geosynthetic reinforcement (i.e., geotextile or geogrid) at the base of the embankment, the cost of the construction can be brought down and the stability of the embankment structure is increased (Liu et al., 2007). Maddison et al. (1996) reported that the use of a geosynthetic layer laid at the base of an embankment constructed over highly

compressible peats and clays, along with a series of vibro-concrete columns, has been proven to be the most effective technique for increasing the stability of the embankment and reducing long term settlements. The example of the cross section of the embankment with the system of geogrid and driven piles is presented in Figure 2.19.

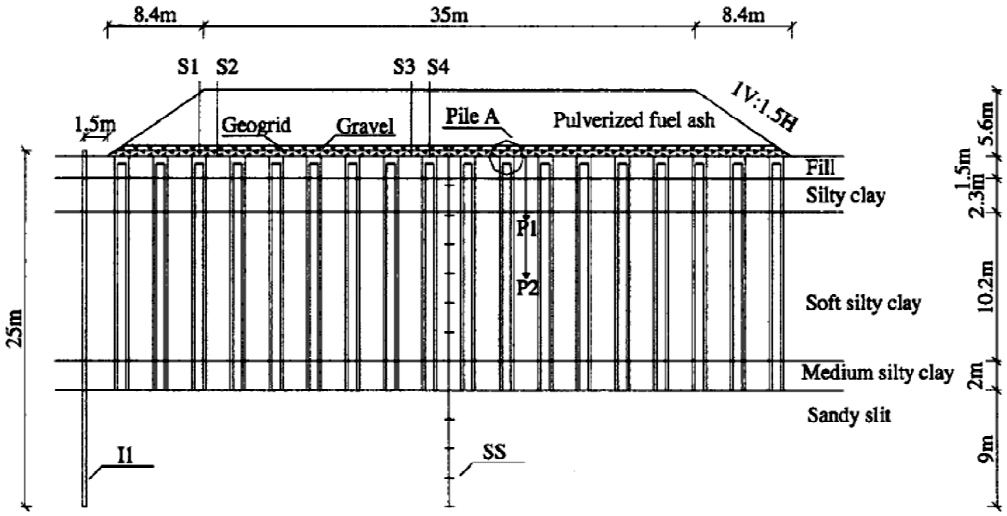

Figure 2.19 Cross section of embankment with basal geogrid and columns (Liu et al., 2007)

Recently, the new technology developed in geosynthetic reinforcement is using geocells to enhance the confinement to the foundation soils. Geocells are produced to have strongest structure shape with a three dimensional honeycomb configuration. The geocells are designed to provide lateral confinement to the soil against lateral spreading due to high structural loads, resulting in increasing of the load-carrying capacity of the foundation soil (Bush et al., 1990; Rowe et al., 1995; and Krishnaswany et al., 2000; Archeewa, 2010). The case studies and conclusions provided in literatures indicate that the application of geocells is effective for strengthening and increasing the load bearing capacity of foundation soils and reducing the settlement that has occurred in the soils

(Bush et al., 1990; Cowland and Wong, 1993; Rowe et al., 1995; Lin and Wong, 1999; and Krishnaswany et al., 2000). The typical cross section of a geocell foundation mattress supporting an embankment is presented in Figure 2.20.

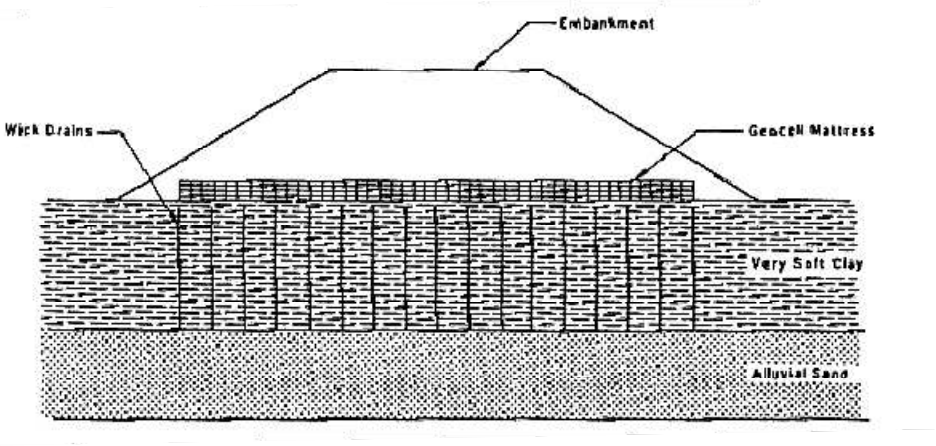

Figure 2.20 Geocell foundation mattress supporting an embankment
(Cowland and Wong, 1993)

2.4.2 Improvement of Approach Embankment Backfill Material

A bridge approach embankment is defined as the fill under the bridge abutment, which extends 100 ft. beyond the abutment wall (WSDOT, 2014). Two functions of the approach embankment are to support the highway pavement system and to connect the main road with bridge deck (Puppala et al., 2012).

In most of the approach embankment constructions, the materials from nearby roadway excavations or a convenient borrow pit close to the site are used, compacted with conventional compaction procedures. The serviceability of the embankment, including slope stability, settlement, consolidation, or bearing capacity, is dependent on the geotechnical properties of these fill materials and the compaction process. The standards for design and construction considerations, both in the quality of the materials

and the compaction specifications, have to be specified to limit the settlement magnitude to a small acceptable degree (Wahls, 1990; Archeewa, 2010; and Puppala et al., 2012).

White et al. (2005) suggested the desirable properties of the materials for embankment construction, including: (1) easily compactable; (2) unchangeable with time; (3) insensitive to moisture; (4) provides good drainage; (5) resistant to erosion; and (6) resistant to shear failure. NYSDOT (2002) defined the suitable materials for embankment construction as any inorganic soil, blasted or broken rock, and similar materials of natural or man-made origin. On the other hand, any material containing vegetable or organic matter, such as muck, peat, organic silt, topsoil, or sod was designated as an unsuitable material.

Hoppe (1999) surveyed various DOTs on the embankment material specifications. The results indicated that about 50 percent of the state agencies use stricter material specifications for a bridge approach fill than for a regular highway embankment fill. Based on the survey results, the common requirements for the backfill materials include (1) limitation of the percentage of fine particles in the fill material in order to reduce the material plasticity and (2) enhancement of the fill drainage properties by a requisite of pervious granular material. Dupont and Allen (2002) noted that the most successful method for constructing the approach embankment is to use high quality backfill materials. The researchers suggested that a coarse granular material with high internal friction is best suited to be used as an embankment backfill material.

According to the previous literatures (Wahls, 1990; FHWA, 2000; Dupont and Allen, 2002 Seo, 2003; White et al., 2005), some of the requirements for the properties of embankment fill materials can be summarized as listed in following:

(1) The fill materials should have a plasticity index (PI) less than 15 (Wahls, 1990 and Seo, 2003), and the percent passing No. 200 sieve can be varied from 5 to 20 percent (Wahls, 1990; FHWA, 2000; and Seo, 2003).

(2) The density requirements for the backfill materials can be divided into two parts. First, for the roadway embankment, the recommended compaction density is 90 to 95 percent of the maximum dry density from the AASHTO T-99 test method. Second, the compaction density for the bridge approach embankment is recommended to be 95 to 100 percent of the maximum dry density obtained from the AASHTO T-99 test standard (Wahls, 1990). Seo, (2003) and White et al. (2005) suggested that the other way to control the compaction density of the embankment fill is to compact the embankment fill to 95 percent of the modified Proctor density.

In the following subsections, the techniques to improve embankment fill materials, such as using mechanically stabilized earth (MSE) wall, geosynthetic reinforcement, and flowable fill, are briefly explained.

2.4.2.1 Mechanically Stabilized Earth (MSE) Wall

Mechanically stabilized earth (MSE) walls are the earthen retaining structures constructed by placing a number of reinforcement layers and compacting the fill soil behind a facing element to form a composite material which acts integrally to restrain lateral forces (Tarawneh and Siddiqi, 2014). This technology has been rapidly developed and widely used since the 1970s (Wahls, 1990). The use of MSE walls in embankment construction is cost effective and requires less site preparation. Moreover, it is technically more feasible when compared with a conventional concrete retaining wall (Elias et al., 2001; Tarawneh and Siddiqi, 2014). Figure 2.21 presents the layout of the typical MSE wall system supporting a bridge abutment foundation.

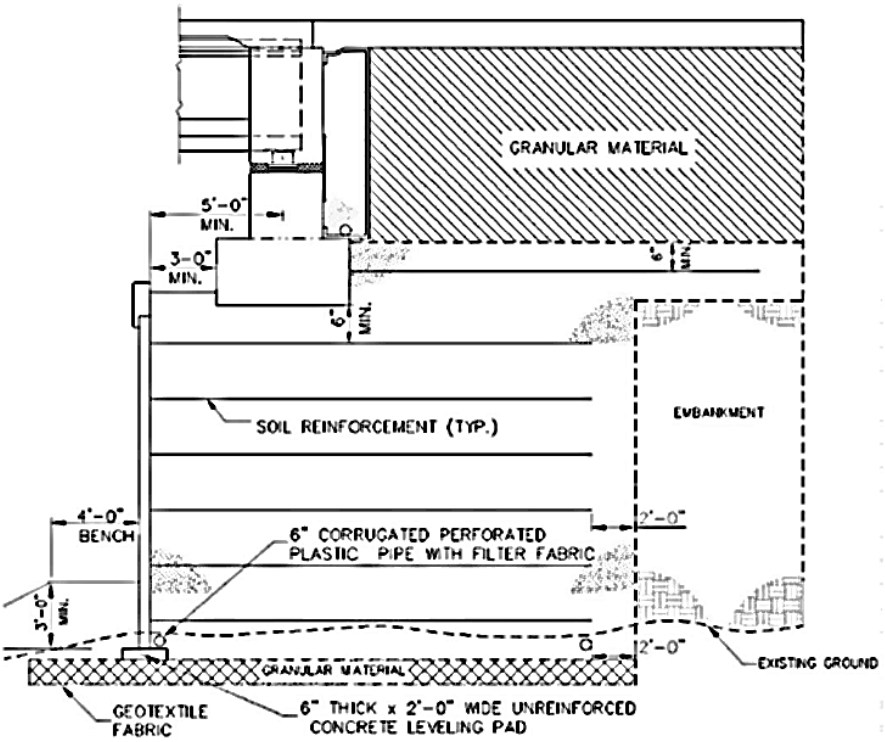

Figure 2.21 MSE wall system supporting bridge abutment (Tarawneh and Siddiqi, 2014)

The performance of a MSE wall is dependent on properties of the backfill materials used. MSE walls require high-quality backfill for durability, good drainage, constructability, and good soil reinforcement interaction. Using soil with high fine content as backfill can cause excessive wall movement or even failure because of its poor drainage behavior (Tarawneh and Siddiqi, 2014).

Lenke (2006) conducted a study to investigate the performance of bridge abutments supported by MSE wall systems. The study results indicated that the bridge abutment-MSE wall system tended to have approach slab settlement less often than other types of bridge abutment systems. This is because the MSE walls have excellent lateral constrains provided by the facing walls, and the tie back straps in the MSE system can provide additional stability to the embankment.

Another advantage of the MSE walls is that they reduce the time-dependent post-construction settlement in very soft clay foundations (White et al., 2005). Moreover, the use of a MSE wall system with a geosynthetic-reinforced backfill and a compressible material between the abutment and the backfill can tolerate a larger recoverable cyclic movement, as noted by Wahls (1990) and Horvath (1991). However, based on the studies performed by Chen et al. (2007) and Yenigalla (2011), the loss of backfill sand from the facing wall can cause the void development under the bridge approach slab and, consequently, cause the bump problem at the end of the bridge structure.

2.4.2.2 Geosynthetic-Reinforced Soils (GRS)

The geosynthetic-reinforced soil (GRS) system has been used widely in the construction of infrastructures, especially in transportation systems. It is primarily used to support the self-weight of backfill soil, roadway structures, and traffic loads. The use of GRS abutments to support bridge structures is a comparatively new application of this technique. The soil reinforced with geosynthetic is used to directly support both the bridge structure and approaching roadway, as presented in Figure 2.22. The use of GRS systems provides the potential to minimize the bump at the end of the bridge caused by differential settlements between the bridge abutment and approaching slabs (Abu-Hejleh et al., 2001; Puppala et al., 2012).

Wu et al. (2003) stated that the GRS system become a more viable alternative than other conventional bridge abutments. This technique provides many advantages, such as being more ductile, more flexible, more adaptable to use of low-quality backfill, easier to construct, more economical, and lower requirements for over-excavation. Moreover, the survey results performed by Edgar et al. (1989) showed that during five years of service, no maintenance activity was requested for the 90 approach slabs supported by geosynthetic-reinforced embankment. However, Abu-Hejleh et al. (2001)

recommended that the foundation soil supporting GRS bridge abutment must be firm enough to restrain the settlement that occurred after construction.

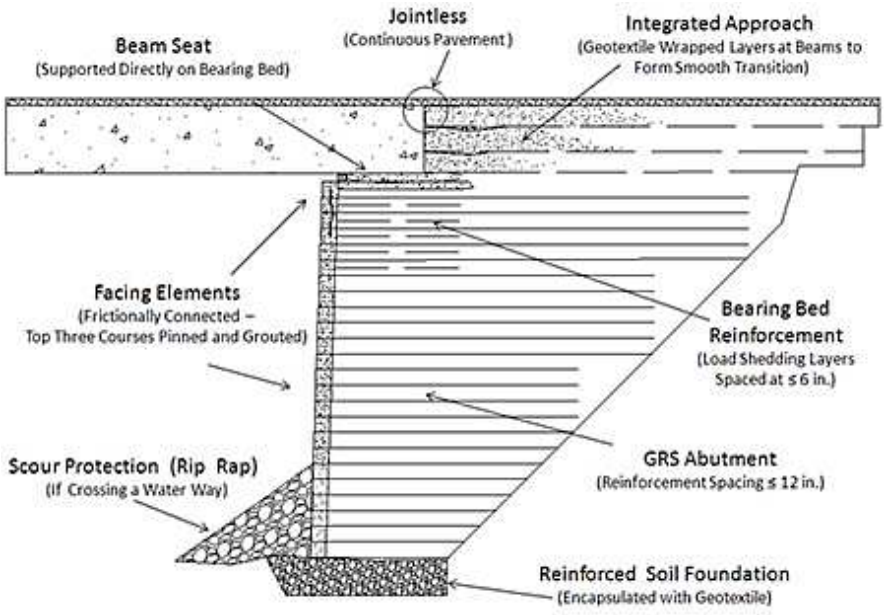

Figure 2.22 Typical GRS-integrated bridge system cross section (Adams et al., 2011)

2.4.2.3 Flowable Fill

According to ACI 229R-99 (2005), flowable fill is one of the several terms currently used to describe the controlled low-strength material (CLSM), a self-compacted, cementitious material used primarily as an alternative to compacted fill. The flowable fill works well in preventing erosion of the backfill and in improving constructability of the fill behind the walls and around the corners (Puppala et al., 2012). Using flowable fill as a backfill material behind the abutment wall can reduce the possibility of approach settlements caused by the compression of the backfill itself, and, consequently, reduce the problem of a bump at the end of the bridge (Snethen and Benson, 1998; Wilson, 1999; Abu-Hejleh et al., 2006; Archeewa, 2010). Another advantage of the flowable fill is that its ability to self-level allows the material to fill voids without the need of compaction.

According to the Colorado DOT specifications, the maximum lift thickness for flowable fill material is 3 ft. (0.91 m), and a placement of additional layers is not permitted until the flowable fill has lost sufficient moisture. The CDOT specifications do not specify any need for vibration in the compaction process. The materials required for the flowable fill specified in CDOT specifications are listed in Table 2.3 (Abu-Hejleh et al., 2006).

Table 2.3 CDOT Material Requirements for Flowable Fill Backfill

Ingredient	Lbs./C.Y.
Cement	50
Water	325 (or as needed)
Coarse Aggregate (AASHTO No.57 OR 67)	1700
Fine Aggregate (AASHTO M6)	1845

The flowable fill technique is considered an expensive construction practice; however, it is still a practical alternative in certain field and construction scenarios where the use of such practice justifies the higher costs (Abu-Hejleh et al., 2006).

2.4.3 Effective Drainage and Erosion Control Method

An efficient drainage system is required in the design of bridge approaches (Wahls, 1990; Hoppe, 1999; Abu-Hejleh et al., 2006; White et al., 2007). As stated previously in the section 2.3.3, an insufficient drainage system and poor expansion joint seal cause water infiltration into the underlying fill material, resulting in soil erosion and the development of a void under the approaching slab, eventually causing settlement of the approaching slab (Mekkawy et al., 2005; White et al., 2007; Puppala et al., 2012).

Based on the previous available literatures (Stewart, 1985; Wahls, 1990; Briaud et al., 1997; Hoppe, 1999; White et al., 2005; Abu-Hejleh et al., 2006; Lenke, 2006; Williammee, 2008), the factors affecting the efficiency of the drainage system can be

divided into three major categories: the selected backfill soil, design and construction of the drainage system, and pavement joints.

Hoppe (1999) reported, based on the survey results, that the selected backfill soil should provide good drainage. White et al. (2005) recommended the use of porous backfill material, or limiting the percentage of fine particles in the fill material, to reduce material plasticity and enhance drainage properties. The allowable percentage of fine material passing through the ASTM No. 200 sieve in the backfills varied from less than 4 percent to 20 percent by different state agencies (Hoppe, 1999).

White et al. (2005) suggested that using a large-diameter surface drain and gutter system in the shoulder of the approach slab and using a geo-composite vertical drainage system around the embankments have the potential to increase the drainage capacity.

For the MSE wall structure, as presented in Figure 2.23, it is recommended that the drainage systems should be constructed in many locations, such as in the retained soil or behind and beneath the walls. The internal drainage of the reinforced fill can be provided using a free-draining granular material with free of fine particles. The drainage should be provided to the base of the fill for preventing water from exiting the wall face and causing erosion, and face strains and should have suitable outlets for discharge of seepage away from the reinforced soil structure (Elias et al., 2001 and Abu-Hejlah et al., 2006).

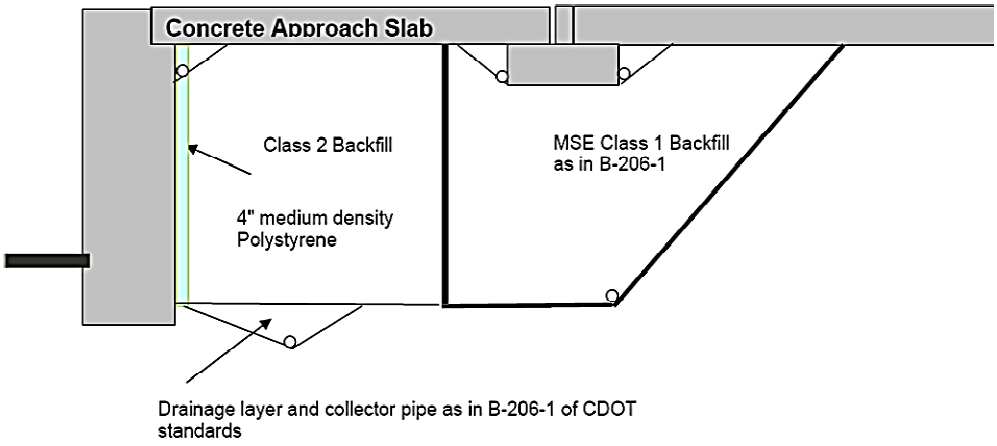

Figure 2.23 MSE walls system under bridge approach slab (Abu-Hejlah et al., 2006)

Abu-Hejlah et al. (2006) proposed another method, as shown in Figure 2.24, to provide an adequate internal drainage system behind the abutment and wing wall. The layer of filter material, granular soil, is filled before placement of the backfill. A 6 in. (150 mm) diameter perforated pipe is installed at the bottom of the filter material to collect excess water and carry it out directly through the wing wall. Providing a system of drainage inlet in the approach slab, or end of deck, to collect the pavement surface water before reaching the expansion joints are also recommended.

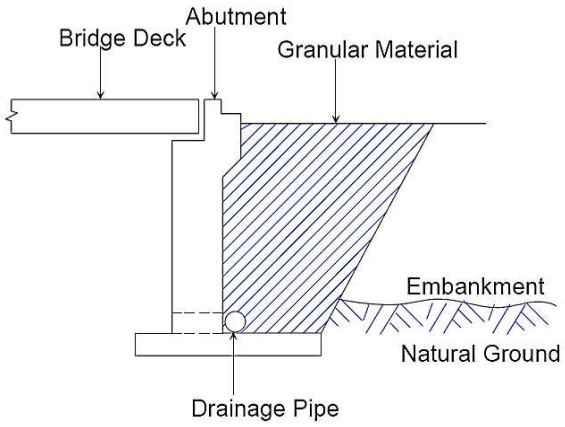

Figure 2.24 Internal drainage system behind the abutment (Abu-Hejlah et al., 2006)

A pavement joints system is the other factor influencing the performance of the drainage system. Improper design practice for the joints between the pavement and curb or abutment wing wall causes water to leak into the backfill and embankment materials, leading to soil erosion and weakening of the granular filter (Briaud et al., 1997). Figure 2.25 presents the two pavement joints systems. The one presented in Figure 2.25a is a poorly designed joints system, which is not recommended for use in bridge construction; whereas, Figure 2.25b shows the system that can prevent water from infiltrating the soil below the approaching slab.

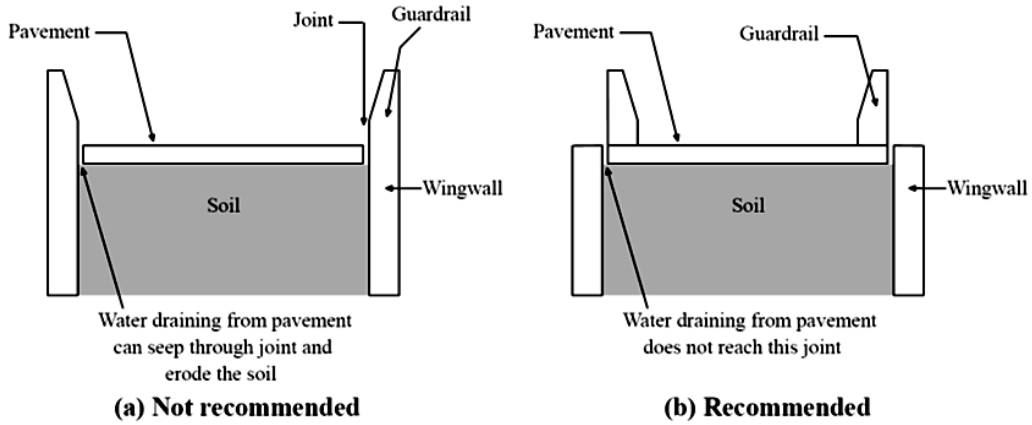

Figure 2.25 Details of the pavement joint systems (Briaud et al., 1997)

Lenke (2006) provided examples good drainage systems and erosion control on the field embankment, as presented in Figure 2.26 and 2.27. The use of rip-rap is effective to prevent erosion under the approach slab and bridge abutments. Similarly, the use of concrete slope protection on the embankment faces, sides, and drainage channels were claimed to be successful in mitigating the erosion problems and in facilitating adequate draining conditions.

Figure 2.26 Rip-rap system used for erosion control (Lenke, 2006)

Figure 2.27 Concrete slope protection and drainage channel (Lenke, 2006)

Dupont and Allen (2002) recommended that the construction cost of providing a good drainage system is not considered too high when compared to the expensive maintenance costs which might be incurred during the service life of the bridge. Thus, the bridge embankments should be constructed with effective seals and good drainage systems in and around the bridge structures.

2.4.4 Use of Lightweight Materials to Mitigate the Bridge Approach Settlements

Cost considerations of the mitigation techniques presented above affect the decisions of engineers to select them as a solution for the bridge approach settlement problem. This leads to the need for researching new methods which have lower construction cost (Saride et al., 2010).

The use of lightweight materials is considered the most cost effective method for mitigating the approach settlement problem (Stark et al., 2004). The concept of this technique is to reduce the vertical loading or stress from the embankment on the underlying foundation soils, resulting in less consolidation settlement of the soils. The reduction of embankment weight also increases the stability of the embankment (Archeewa, 2010 and Puppala et al., 2012).

According to Elias et al. (1998), there are many types of lightweight fill materials that have been used in roadway embankment construction. A summary of the common types of lightweight fills is presented in Table 2.4. It can be seen from the table that the range in density of the lightweight fill materials can vary from 12 kg/m^3 (0.75 pcf) to 1720 kg/m^3 (109 pcf), which is about 1 percent to 70 percent of natural soil density (Stark et al., 2004). The costs shown in the table correspond to the project completed in 1993 to 1994; the current cost may differ due to inflation (Stark et al., 2004).

Table 2.4 Various Types of Lightweight Fill Materials (Stark et al., 2004)

Lightweight fill type	Unit weight, pcf (kN/m^3)	Specific gravity	Approximate cost, \$/yd^3 (\$/m^3)
EPS (expanded polystyrene) geofoam	0.75 to 2.0 (0.12 to 0.31)	0.01 to 0.03	26.76 to 49.70 (35.00 to 65.00)**
Foamed Portland-cement concrete	21 to 48 (3.3 to 7.6)	0.3 to 0.8	49.70 to 72.63 (65.00 to 95.00)***
Wood Fiber	34 to 60 (5.4 to 9.4)	0.6 to 1.0	9.17 to 15.29 (12.00 to 20.00)*
Shredded tires	38 to 56 (5.9 to 8.8)	0.6 to 0.9	15.29 to 22.94 (20.00 to 30.00)*
Expanded shale and clays	38 to 65 (5.9 to 10.2)	0.6 to 1.0	30.58 to 42.05 (40.00 to 55.00)**
Boiler slag	62 to 109 (9.8 to 17.2)	1.0 to 1.8	2.29 to 3.06 (3.00 to 4.00)**
Air cooled blast furnace slag	69 to 94 (10.8 to 14.7)	1.1 to 1.5	5.73 to 6.88 (7.50 to 9.00)**
Fly ash	70 to 90 (11 to 14.1)	1.1 to 1.4	11.47 to 16.06 (15.00 to 21.00)**
Expanded blast furnace slag	N/A	N/A	11.47 to 15.29 (15.00 to 20.00)**

Notes: * Price includes transportation cost

** FOB (freight on board) at the manufacturing site. Transportation costs should be added to this price.

*** Mixed at job site using pumps to inject foaming agents into concrete grout mix.

In the following sections, the details of some lightweight fill materials with their applications related to bridge approach embankment construction are briefly explained.

2.4.4.1 Expanded Polystyrene (EPS) Geofoam

The definition, based on ASTM D 6817-07, of EPS geofoam is a block or planar rigid cellular foam polymeric material used in geotechnical engineering applications. The first use of this material was in 1972 for the construction of an embankment adjacent to a bridge founded on piles in Norway (Frydenlund and Aaboe, 2001). However, the use of

EPS geofoam for lightweight fill in the US dates back to at least the 1980s (Stark et al., 2004). Currently, the use of EPS geofoam as a super light filling material has increased both in volume and types of application on a world wide scale.

As provided in Table 2.4, the unit weight of the EPS geofoam is approximately 100 times lighter than most soils and at least 20 to 30 times lighter than other lightweight fill alternatives (Dusenberry and Bygness, 2006). The advantages of EPS geofoam for highway construction are summarized as listed below:

- Because of its lightweight property, EPS geofoam can be used as an embankment fill to reduce the loads on underlying soils and, consequently, minimize the total settlement of the soils and differential settlement at the bridge ends.
- The use of EPS geofoam provides benefits to construction schedules and decreases the overall cost of construction. This is because it is easy to handle, is less labor intensive, and requires fewer large earth-moving pieces of equipment.

In the following, four examples of projects involving the use of lightweight EPS geofoam in bridge embankment construction are briefly described. More information, such as manufacture of EPS geofoam and its applications, is explained explicitly later in section 2.5.

Thompsett et al. (1995) presented a case study of using the EPS geofoam to raise the road level of a highly settled road near Oslo in 1972. A new 20 in. (50 cm) thick pavement was laid on the top of the EPS geofoam blocks. During the next 12 years, only 3 in. (8 cm) of settlement was noticed, and after that time period, almost zero settlement was recorded.

Frydenlund and Aaboe (2001) described the embankment construction for a temporary bridge, the Lokkeberg Bridge, in Norway. It was built in 1989 as a single-span bridge, using steel truss girders to support a single-lane pavement. The results from a site investigation indicated that the foundation soil of the bridge had low bearing capacity and, therefore, large settlement was expected. For these reasons, the EPS geofoam blocks were considered for use as the fill material for the bridge approaching embankment. The bridge foundation was placed directly on top of the EPS blocks, as presented in Figure 2.28 and 2.29, as an alternative to placing the bridge abutment on piled foundation. After being open to traffic for 12 years, deformation of 6 cm (2.4 in) was all that was observed in the EPS embankment, and most of the deformation occurred during the construction period.

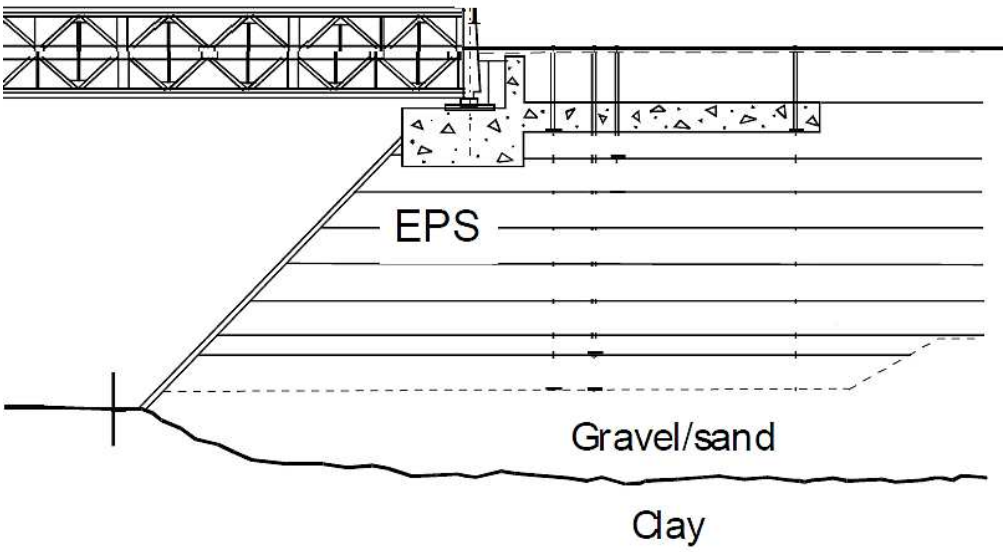

Figure 2.28 Cross section of the Lokkeberg bridge embankment
(Frydenlund and Aaboe, 2001)

Figure 2.29 Abutment construction on EPS embankment at Lokkeberg Bridge (Frydenlund and Aaboe, 2001)

An interesting project underway in Seattle, the reconstruction of the York Bridge on Northeast 116th Street north of Redmond, over the Sammamish River, was reported by Dusenberry and Bygness (2006). Before the reconstruction, the road elevation of the old bridge was very low, causing the Sammamish River to run over the road. For this reason, the King County DOT decided to replace the bridge. The project included a new 220-ft. bridge over the Sammamish River and two river trails, access to the river trails from Northeast 116th Street, 1,400 ft. of new approach roadways, structural earth retaining walls, wetlands mitigation, river enhancement, a three-legged precast concrete box culvert supported on geopiers, and a major geofoam embankment. The west approach of the bridge was over deep unconsolidated peats, clays, and silty sands which would exhibit long-term excessive settlements. To avoid the possible settlement problem, an EPS geofoam material was selected to be used as an alternative fill for the

approaching embankment. The height of the geofoam varied from 1-ft. to about 9 ft. in height at the face of the bridge abutment. The entire geofoam mass was placed on a layer of geogrid-reinforced soil and a 6-in thick sand-draining and leveling blanket. An additional sand-drainage blanket and 6-in thick, reinforced concrete load distribution slab were placed on top of the geofoam layer. The load distribution slab was provided to evenly distribute live loads to the geofoam and to protect the geofoam from solvents that could cause damage. From all appearances, it can be seen that the use of geofoam eliminated the potential for long-term settlement and maintenance of the roadway approach. Figure 2.30 presents the geofoam replacement for the York Bridge approaching embankment.

Figure 2.30 Geofoam replacement for York Bridge embankment
(Dusenberry and Bygness, 2006)

From 1998 to 2001, the Utah Department of Transportation (UDOT) reconstructed a 27.4 km (17.03 miles) portion of Interstate Highway 15 (I-15) in Salt Lake City, Utah (Bartlett et al., 2012). The reconstruction involved the widening of the interstate embankment from 8 lanes to 12 lanes. The I-15 alignment cuts across an extensive deposit of compressible lake bottom sediment. From previous observations along the sections of I-15 performed by UDOT, settlements of up to 1400 mm (55 in) were found for over 30 years for the embankment heights of 6 to 10 meters (20 to 33 ft.). Settlements with same order of magnitude were expected for the I-15 expansion project if conventional earth fill was used (Negussey and Stuedlein, 2003).

The other factor affecting the reconstruction project was that the project had to be finished ahead of the 2002 Winter Olympic Games; thus, the available time to complete the construction was limited. To solve the problems of high soil settlements and to stay within the time schedule constraints, EPS geofoam was selected to be used as the fill material for the embankments. Approximately 100,000 m^3 (130,800 yd^3) of EPS blocks were placed at various locations along I-15. Bartlett et al. (2012) concluded, based on the obtained field measurement data, that using EPS geofoam could successfully reduce the soil settlement problem. A minor 15-mm (0.6-in) settlement was observed in the foundation soil during the EPS block and pavement construction. An additional 25-mm (0.98-in) settlement was measured over a 5-year period after the highway was open to traffic. The total post-construction settlement was expected to be 50 mm (2 in) for a 10-year period. The typical geofoam embankment construction on the I-15 reconstruction project is illustrated in Figure 2.31.

Figure 2.31 Typical geofoam embankment construction on the I-15 reconstruction project in Salt Lake City, Utah (Bartlett et al., 2012)

2.4.4.2 Foamed Cement Concrete

Foamed concrete, sometimes referred to as cellular concrete, is an engineered geotechnical material created by introducing a foaming agent into the Portland cement matrix (Dolton and Hannah, 2006; SCDOT, 2010; NYDOT, 2013). Fly ash may be added to the mixture to partially replace a portion of the cement, but without sand or gravel in the mix (Elias et al., 1998). The foaming agent produces interconnected air voids in the mixture, resulting in a low density, about 25 to 35 percent of natural soil density. The flowability and cementitious properties of this material provide a product that is self-leveling and does not require compaction (NYDOT, 2013). This material is normally mixed at the job site. Pumps are required for delivering the foamed concrete mixture (SCDOT, 2010).

NYDOT (2013) summarized the advantages of using foamed cement, including (1) using foamed cement material in the embankment over a deep, soft organic or clay soil may create significant time and cost savings as compared to other foundation stabilization and settlement mitigation techniques; (2) the foamed concrete exerts little-to-no lateral load acting on the retaining structure when it is properly designed as backfill; (3) because of its flowability property, foamed concrete can be used to fill voids in areas which would be inaccessible to other lightweight materials. Figure 3.32 shows the foamed concrete material filled in a construction site.

Figure 2.32 Foamed concrete filled in a construction site (NYDOT, 2013)

Elias et al. (1998) presented a case history of using foamed concrete to compensate for soil weight. In the procedure of soil weight compensation, the exiting soils are excavated to a depth required to balance the weight of the lightweight foamed concrete fill. The fill is placed at a grade higher than the existing grade so that no additional loads are applied to the foundation soils (Elias et al., 1998). The NYDOT used the foamed concrete in a weight balancing method for a two-span structure that was replaced with a single-span structure. The abutments were structurally sound enough to support the new superstructure; however, the grade of the approaching embankments needed to be increased up to 1-m. (3.3 ft.) higher than the existing level. The foundation

soil supporting the embankments was very soft-to-soft clay underlain by loose silt. An analysis of bearing capacity indicated that raising the grade could cause failure in the structure. In order to solve that problem, the foamed concrete with weight balance technique was used to reduce the loading on the soft foundation soil.

2.4.4.3 Shredded Tires

Shredded tires are the product made by mechanically cutting tires into small pieces. After cutting, the tire is reduced into strips ranging in size from 2 in × 8 in down to 2 in × 2 in, which reduces the volume of the tire up to 75 percent (Lund, 1993; Cecich et al., 1996). The engineering properties of shredded tires, which are required for the design of a retaining wall, were tested by Cecich et al. (1996). Based on the testing results, it can be summarized that: (1) The gradation of shredded tires is comparable to the gradation of sandy or gravelly soils commonly used as backfill materials; thus, the use of shredded tires is acceptable for use as backfill material for retaining walls; (2) The unit weight of shredded tires ranged from 35.1 to 37.3 pcf; thus, the shredded tires are considered as lightweight backfill material for retaining walls. (3) Shredded tires have a high value of hydraulic conductivity, indicating that they will allow free drainage of water. This property makes shredded tires a desirable backfill material for retaining structures. (4) The cohesion of shredded tires is 147 psf and the friction angle is 27 degree. Based on their properties, shredded tires are suitable for use as backfill material for the construction of retaining walls. The other advantage of shredded tires is that they are inexpensive; thus, using shredded tires can reduce the cost of the construction (Engstrom and Lamb, 1994).

2.4.4.4 Expanded Shale and Clay

Expanded shale and clay (ESC) is a granular lightweight fill material. It is also called light weight aggregate (LWA). The process for producing ECS requires heating shale or clays in a rotary kiln to the temperature of 1,000 to 1,200 degree Celsius for at least 15 minutes. With this process, the clay minerals, which are montmorillonite, illite, and kaolinite, become completely dehydrated and will not rehydrate under atmospheric conditions (Elias et al., 1998). The particles of this material may be in rounded, cubical, or sub-angular shapes (SCDOT, 2010). The advantageous properties of ESC are that they are durable, chemically inert, and relatively insensitive to moisture. However, the ESC particles will absorb and retain some water.

Elias et al. (1998) stated that the manufacturing cost for ESC material is relatively high; therefore, these products have generally been used as lightweight aggregates for structural concrete. However, the ESC material is sometimes used for normal roadway or approach embankment construction when the construction is in areas where high-quality, naturally-occurring aggregates are no longer present.

Saride et al. (2008) performed the laboratory tests and field monitoring to evaluate the performance of the ESC material used as an embankment backfill. The test embankment section was constructed using ESC as the fill material along State Highway (SH) 360, Arlington, Texas, in summer 2006. The test section was instrumented with vertical inclinometers extended to a depth of 40 ft. deep at two different locations. The studying results indicated that the ESC material can be utilized successfully as an embankment backfill material.

2.5 Expanded Polystyrene (EPS) Geofoam

This section provides more details of expanded polystyrene (EPS) geofoam material including the definition, manufacturing, properties, and applications.

2.5.1 Definition of Geofoam

Geofoam is one of eight different types of polymeric geosynthetic material; including geotextiles, geogrids, geonets, geomembranes, geosynthetic clay liners, geofoam, geocells, and geocomposites. It has been widely used around the world as a fill for more than 30 years (Koerner, 2005; Dusenberry and Bygness, 2006). The definition of geofoam has been provided by many sources, some of which are presented below.

According to ASTM D 6817-07, “geofoam is a block or planar rigid cellular foam polymeric material used in geotechnical engineering applications”. Koerner (2005) defined the geofoam as “a foamed polymeric geosynthetic material (generally expanded polystyrene) manufactured in slab or block form and used primarily for its lightweight and sometimes for its insulating properties”.

The definition of geofoam provided by Stark et al. (2004) is “any manufactured material created by an internal expansion process that results in a material with a texture of numerous, closed, gas-filled cells using either a fixed plant or an in situ expansion process (Horvath, 1995)”. Based on the previous definitions, it can be summarized that geofoam is a lightweight foamed polymeric material manufactured by an internal expansion process, in slab or block shapes, used primarily in geotechnical engineering applications.

2.5.2 Types of Geofoam and Manufacturing Process

Based on the differences in the manufacturing process, the geofoam material can be classified as (1) expanded polystyrene (EPS) geofoam and (2) extruded polystyrene (XPS) geofoam (Stark et al., 2004; Koerner, 2005).

The EPS geofoam production consists of three processing stages (Koerner, 2005) as presented in Figure 2.33.

In the first stage, the resin styrene, which is the main row material used in the production, and various additives are mixed with the blowing agent (i.e., pentane) and water to form a polymerization unit. The resin is softened by the heat transferred from steam. The increased vapor pressure of the blowing agent expands the resin beads to about 50 times their original size and forms the close-cell foam structure of the beads.

The second stage is called intermediate bead processing. In this stage, steam is again used along with a rotary blower to make the bead particles mechanically stable and to dissipate moisture to the atmosphere, resulting in aiding the flow properties of the beads. The product received from this stage is called stabilized beads and is stored in a silo for 5 to 28 hours. For the final stage, the stabilized beads are formed to slab or block shape. Steam is again used to soften the beads placed in the appropriate forms. The beads are compressed to form a polyhedral structure and to create the bond between the touching surfaces. After that, the system is cooled down and the finished EPS geofoam slabs or blocks are obtained and then, sent to a sizing operation.

XPS geofoam is manufactured by expanding the polystyrene solid resin beads and shaping the cellular product in a continue process by using an extruder (Stark et al., 2004; Koerner, 2005). The final product of XPS geofoam has the appearance of a uniform texture of closed cells; whereas, the EPS geofoam product has the appearance of individual, fused particles (Stark et al., 2004). The XPS geofoam is relatively thin when compared with the EPS geofoam. The application of the XPS geofoam is usually limited to insulation rather than lightweight fill. Moreover, the unit price of XPS geofoam is generally higher than that of EPS geofoam (Koerner, 2005).

In this study, the engineering properties and applications of the EPS geofoam are emphasized rather than those of the XPS geofoam. This is because the EPS geofoam is mostly used as the lightweight fill material in geotechnical related projects.

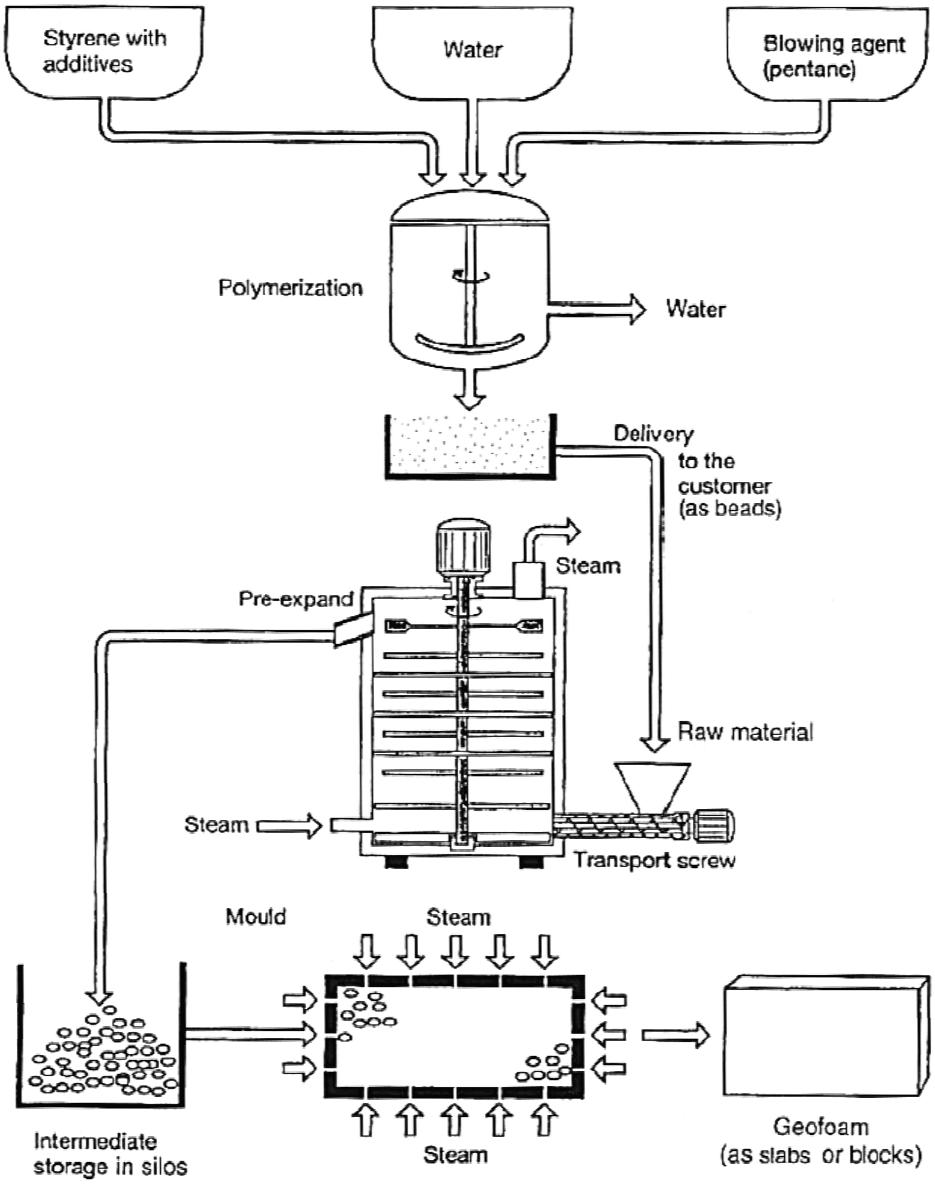

Figure 2.33 Manufacturing process of EPS geofoam (Koerner, 2005)

2.5.3 Properties of EPS Geofoam

Properties of EPS geofoam can be grouped into four major categories including physical properties, mechanical properties, thermal properties, and endurance properties (Koerner, 2005). The property requirements of both EPS and XPS geofoam as per the ASTM D 6817-07 standard are presented in Table 2.5. The following subsections explain the detail of each property and some experiments conducted to test those properties.

2.5.3.1 Physical Properties

The interesting physical properties of EPS geofoam consist of four different types including block dimensions, density, moisture absorption, and oxygen index. As presented in Table 2.5, the minimum values of the density and oxygen index properties are required in the geofoam products.

Table 2.5 Properties Requirements of EPS Geofoam (ASTM D 6817-07)

Type	**EPS12**	**EPS15**	**EPS19**	**EPS22**	**EPS29**	**EPS39**	**EPS46**
Density, min., kg/m^3 (pcf)	11.2 (0.70)	14.4 (0.90)	18.4 (1.15)	21.6 (1.35)	28.8 (1.80)	38.4 (2.40)	45.7 (2.85)
Compressive resistance, min., kPa (psi) at 1%	15 (2.2)	25 (3.6)	40 (5.8)	50 (7.3)	75 (10.9)	103 (15.0)	128 (18.6)
Compressive resistance, min., kPa (psi) at 5%	35 (5.1)	55 (8.0)	90 (13.1)	115 (16.7)	170 (24.7)	241 (35.0)	300 (43.5)
Compressive resistance, min., kPa (psi) at 10%	40 (5.8)	70 (10.2)	110 (16.0)	135 (19.6)	200 (29.0)	276 (40.0)	345 (50.0)
Flexural strength, min., kPa (psi)	69 (10.1)	172 (25.0)	207 (30.0)	276 (40.0)	345 (50.0)	414 (60.0)	517 (75.0)
Oxygen index, min., volume %	24.0	24.0	24.0	24.0	24.0	24.0	24.0

Block dimensions:

Typical dimensions of the EPS-block geofoam commonly available in the U.S.A. are varied from 305 to 1219 mm (12 to 48 in) in width, 1219 to 4877 mm (48 to 192 in) in length, and 25 to 1219 mm (1 to 48 in) in thickness (ASTM D 6817). The block dimensions do not affect any other properties of the EPS geofoam.

Density:

According to the Table 2.5, the density of EPS geofoam ranges from 11 to 46 kg/m^3 (0.70 to 2.9 pcf), which is about 0.6 to 2.4 percent of the weight of a typical sand at a density of 1940 kg/m^3 (121.25 pcf). ASTM standards characterizes the EPS geofoams based on their density in unit of kg/m^3. Because the density of EPS geofoam is very low when compared with the natural soils or granular fill, this material is suitable to be used in lightweight fill applications.

The density of EPS geofoam has been shown to correlate well with geotechnical-relevant mechanical properties such as the compression behavior. Therefore, the density can be used as an index property to estimate some mechanical properties of the EPS geofoam (Stark et al., 2004).

The density variation, (also called density gradient), is a result of the inherent variability in the EPS manufacturing process and can be found in every block. The density at the center of a block is generally assumed to be higher than at the edges, and a small specimen cut from a block can be significantly different from the gross density of the entire block (Stark et al., 2004). The density of the EPS geofoam specimen can be determined in accordance with ASTM D 1622, the standard test method for apparent density of rigid cellular plastics.

Moisture absorption:

Frydenlund and Aaboe (2001) stated in their study that the moisture content in EPS geofoam is hardly changed with time. The water content of EPS geofoam specimens periodically submerged in water for more than 20 years showed a change from 1% to 4% by volume; whereas, the volume of water content in the specimen permanently submerged in water changed from 1% to nearly 10%. These occurrences indicated that a small amount of water can be absorbed by EPS geofoam. According to ASTM C578, the maximum absorption of about 0.3% by volume is specified for geofoam used in thermal insulation applications (Koerner, 2005).

Oxygen index:

This property is listed in the specification provided in ASTM D 6817, as presented in Table 2.5. The oxygen index (OI) is defined as the minimum percentage of oxygen required to support combustion in the site-specific gaseous environment. For example, a material with an OI $\leq$ 21% would burn freely in air, which contains approximately 21% oxygen. According to Table 2.5, the minimum OI of 24% is required for EPS geofoam. Moreover, Horvath (1995) noted that EPS geofoam should not be exposed to the conditions where the temperatures are higher than 95 degree Celsius.

2.5.3.2 Mechanical Properties

The mechanical properties of EPS geofoam are very important for use in lightweight fill applications. These properties affect both the external and internal stability of structures (Stark et al., 2004). In particular, two distinct categories of mechanical properties that need to be addressed include: (1) the compression behavior of EPS geofoam and (2) the interface shear properties for use between EPS blocks, as well as

between EPS block and soils. The details of these two properties are discussed in the following subsections.

The tension and flexure properties of EPS geofoam are also briefly discussed because these two properties are useful in manufacturing quality control and manufacturing quality assurance tests.

Compression behavior:

The compressive strength of an EPS geofoam specimen can be determined in accordance with ASTM C165 or D1621. A cube with dimensions of 50 mm or a cylinder with 2.8-in. diameter and the height that can be varied from 1 in. to not more than the diameter of the specimen is used in the test. The strain rate applied to the EPS specimen is about 10% strain per minute. As presented in Table 2.5, the minimum values of compressive resistance at 1%, 5%, and 10% strain are required for the EPS-block geofoam to be reached. The compression behavior of an EPS geofoam is varied with its density (Koerner, 2005). The compressive strength of EPS geofoam increases with the increase in the density. Typical compression behavior of EPS geofoam at various densities is illustrated in Figure 2.34.

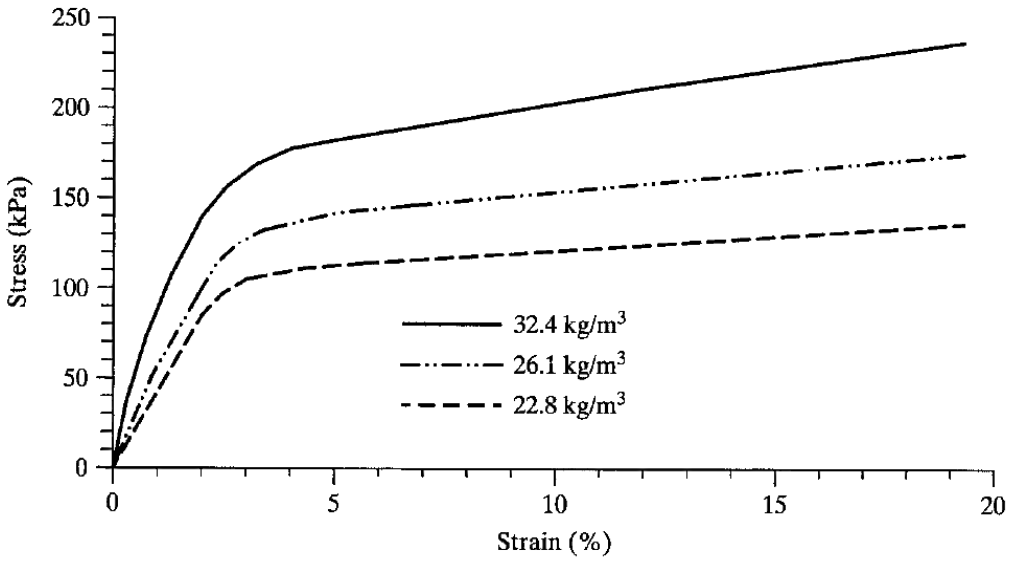

Figure 2.34 Compression behavior of EPS geofoam at various densities (Koerner, 2005)

Stark et al. (2004) introduced the effect of specimen shape on compression behavior of EPS geofoam. By using a specimen in a circular cylindrical shape with dimensions similar to soil specimens used in triaxial test (i.e., approximately 5.9 in (150 mm) in height and 2.75 in (70 mm) in diameter), both the initial tangent Young's modulus and elastic limit stress for such specimen are decreased compared to the values obtained using the standard specimens. However, for the cylindrical specimens with 1.0-in. (25 mm) high and 2.4 in. (60 mm) in diameter, which is similar to soil specimen used for one-dimensional consolidation test, there is no practical difference from the standard 50-mm (2 in) cube specimen.

The effect of specimen size on the compression behavior of EPS geofoam was also discussed in previous literatures (Elragi et al., 2000; Stark et al., 2004; Koerner, 2005; Bartlett et al., 2012). The results from the compression test on EPS specimens in different sizes conducted by Elragi et al. (2000) indicated that the Young's modulus of conventional 5-cm (2-in) cube samples is significantly underestimated when compared

with those of the larger block samples. The initial Young's modulus of a 60-cm (24-in) cube block of EPS is about twice the value obtained from 5-cm (2-in) cube samples. Similar results were mentioned by Eriksson and Trank (1991). The compression test results on 400-mm (16-in) cubes showed that the larger specimens are approximately 50 percent stiffer than the smaller specimens at small strains. Based on these results, it can be expected that the Young's modulus of a full-sized EPS block placed in large embankments may be significantly underestimated using standard 5-cm (2-in) cube samples (Stark et al., 2004).

Compression creep behavior:

The sustained compressive stress applied to EPS geofoam blocks results in creep behavior in the EPS geofoam. Figure 2.35, provided by Negussey (1997), presents the creep behavior of EPS geofoam with density of 23.5 kg/m^3 (1.47 pcf) under various loads applied. It is clearly seen from the figure that higher creep deformation, as presented with the solid line, can occur when a too high load is applied. To reduce the magnitude of creep deformation under sustained loads, the higher density products should be used to support the sustained loads (Koerner, 2005).

Frydenlund and Aaboe (2001) performed a laboratory test at the Norwegian Road Research Laboratory (NRRL) to study the creep behavior of the EPS geofoam blocks. As presented in Figure 2.36, the normal size EPS geofoam blocks, which have compressive strength of 100 kPa (14.5 psi), were stacked to the height of 2 m (6.56 ft.), and then compressed with the pressure of 52.5 kPa (7.6 psi) to simulate deformations observed over a period of 3 years. The test results showed that low deformations, about 1.2% strain, were observed in the EPS geofoam blocks layer.

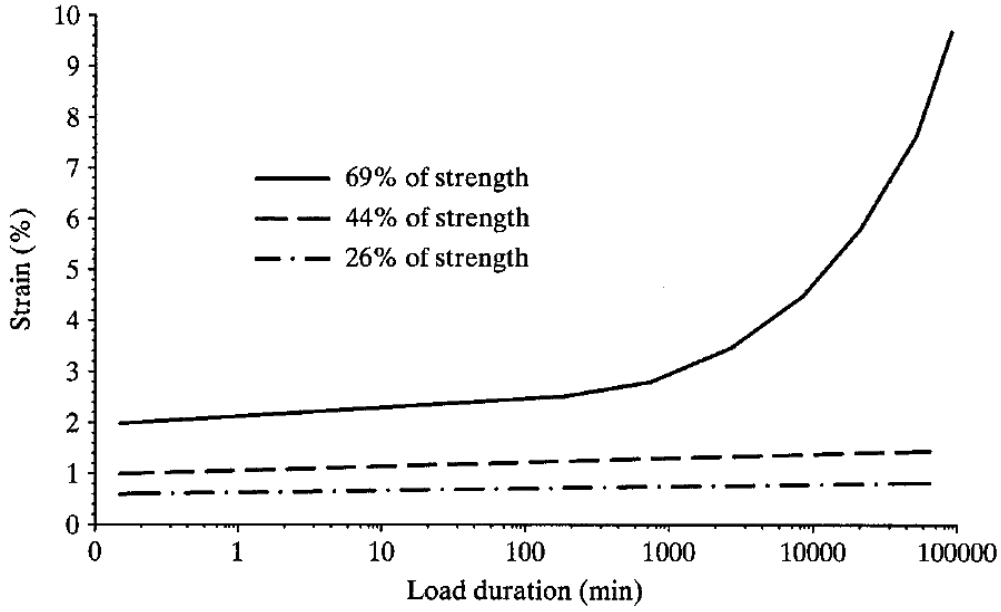

Figure 2.35 EPS geofoam creep behavior (Negussey, 1997)

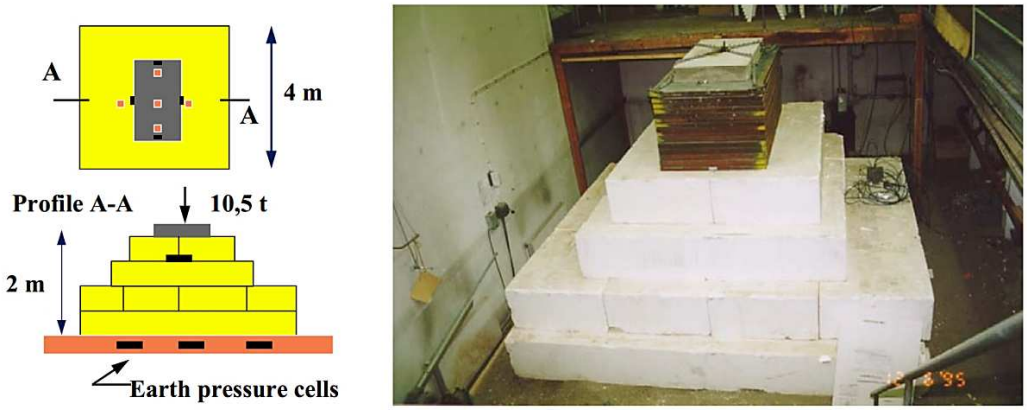

Figure 2.36 EPS test fill at the Norwegian Road Research Laboratory (Frydenlund and Aaboe, 2001)

Tension and flexure resistances:

Tensile strength is an important manufacturing quality control parameter used for evaluating the EPS geofoam fusion (Stark et al., 2004). The tensile test can be performed

in accordance with the ASTM C 1623 standard test method, using a dumbbell-shaped specimen of 645 mm^2 cross section at its narrowest location. During the test, a strain rate of 5% per minute is used, applying it to the specimen until failure (Koerner, 2005). However, because of the difficulty in fabricating the dumbbell-shaped specimen, the tensile testing is not typically conducted (Stark et al., 2004). The alternative testing method, flexure test, is most often used because it is easier to perform and results in the same behavior as the tensile test.

The flexure test can be performed as per the ASTM C 203 standard, using an EPS geofoam beam applied with 3-point transverse loads. The dimension of the beam-shaped specimen is 100 mm (4 in.) wide, 300 mm (12 in.) long, and 25 mm (1 in.) thick. The size of the specimen can be changed based on the geometric setup of the test apparatus (Stark et al., 2004). The flexural strength is defined as the calculated maximum stress at the time when the specimen is ruptured.

Figure 2.37 presents the linear relationship between tensile strength and flexural strength with EPS density. As can be seen from the figure, flexural strength correlates well with the tensile strength. This result validates the assumption that the flexure test can be used routinely, as a measure of bead fusion during the manufacture of EPS (Stark et al., 2004).

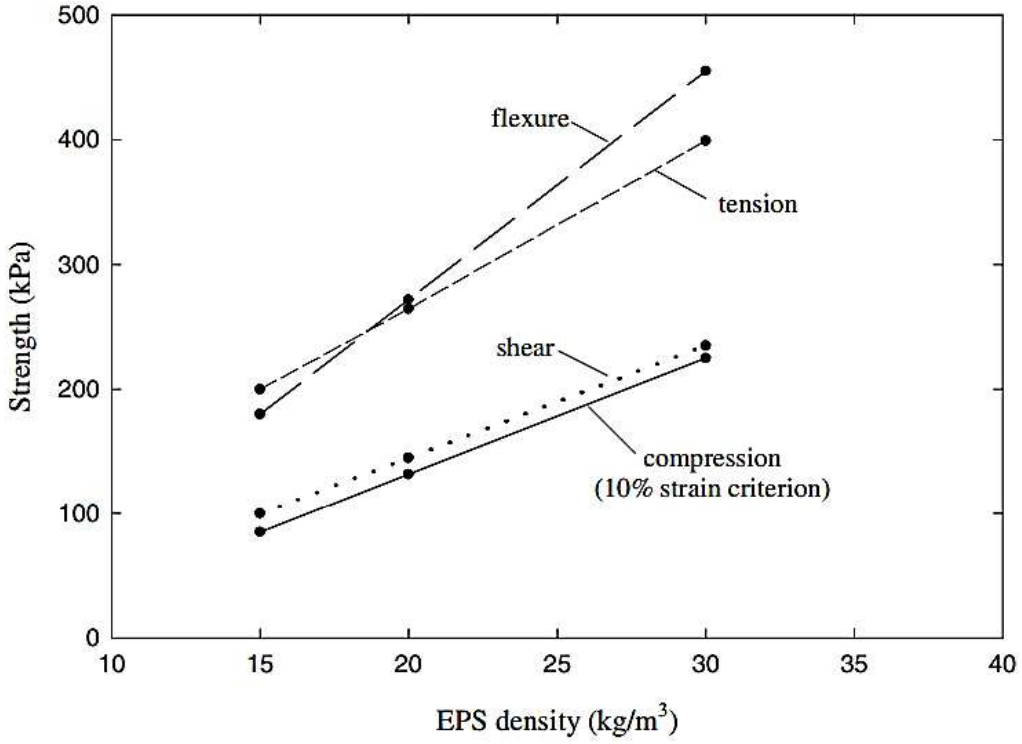

Figure 2.37 Strength values of EPS geofoam as a function of density (Stark et al., 2004)

Shear strength:

In consideration of shear strength of EPS geofoam, both internal shear strength within a specimen of EPS and external shear strength between EPS blocks or between an EPS block and a dissimilar material are interesting (Stark et al., 2004). The internal shear strength of EPS geofoam can be measured in accordance with the ASTM C 273 standard (Stark et al., 2004). Shear loading is applied to a test specimen fairly rapidly until the maximum shear stress is reached. The correlation between shear strength and density of the EPS geofoam block, also presented in Figure 2.37, shows the parallel behavior to the 10% compression response.

The external shear strength, also called interface friction, is an important consideration in external and internal stability assessments under horizontal loads (Stark

et al., 2004). The interface friction can be divided into two types, including EPS/EPS interface and EPS/dissimilar material interface. The test for external shear strength can be conducted similar to the direct shear testing (ASTM D 5321) performed in soils. Based on the testing results reported in previous studies, the values of EPS/EPS interface frictional angle (δ) are varied from 27 to 35 degrees (Stark et al., 2004); whereas, the δ equal to 32 degrees was found in the published study performed in Japan. For routine design, the δ equal to 30 degrees is recommended (Stark et al., 2004). For the EPS/dissimilar material interface, based on the results from previous studies (Stark et al., 2004; Elragi, 2006), the friction angles between the EPS block and various dissimilar materials are summarized in Table 2.6.

Table 2.6 Interface Friction Angles between EPS geofoam and dissimilar materials

Materials		Interface friction angle (degrees)
EPS	Sand	30
EPS	Non-woven geotextile	25
EPS	Geomembrane	52

2.5.3.3 Thermal Properties

The thermal properties are mainly related to the thermal insulation function of EPS-block geofoam, which is not a primary concern for the lightweight fill applications. However, some knowledge of these properties may be necessary to understand the potential problems of differential icing and solar heating on the EPS geofoam (Stark et al., 2004).

Thermal resistance:

Thermal resistance is represented in terms of an R-value, which is the resistance to heat flow in a unit width of geofoam. This R-value can be measured in accordance with

ASTM C578 standard (Koerner, 2005). The R-value of geofoam (both EPS and XPS) is higher than the R-values of soils and concrete. R-value losses of 33 to 44% for EPS and 10 to 22% for XPS have been found for geofoam with full moisture absorption (Koerner, 2005).

2.5.3.4 Endurance Properties

In this section, the endurance properties of EPS geofoam, including chemical resistance, ultraviolet degradation, flammability, and lifetime period are briefly explained. These properties involve the long-term nature of the EPS geofoam (Koerner, 2005).

Chemical resistance:

Polystyrene is typically a stable chemical compound. However, it may dissolve when exposed to petroleum agents or organic fluids. It is recommended that it be covered with a load distributing concrete slab or encapsulated with a geomembrane to protect the EPS blocks placed in an embankment or a road fill (Frydenlund and Aaboe, 2001). However, no incident of the EPS geofoam failure caused by petrol agents has been reported in the nearly 30 years since the first EPS fill was placed.

Ultraviolet degradation:

Ultraviolet (UV) radiation from sunlight does not affect the EPS geofoam much. The surface of an EPS block will turn yellow in color and become brittle and chalky when it is exposed to the UV radiation for a long period (i.e., from months to years). This process is on the surface and does not progress into the block (Stark et al., 2004). Therefore, it is not necessary to protect EPS geofoam from long-term UV radiation, and the short-time it is exposed to sunlight during construction is not a problem (Stark et al., 2004).

Flammability:

EPS geofoam is a combustible material and can burn easily when set on fire. Precautions such as fencing in any stockpiles at the construction site, providing guards round the clock, or placing the blocks directly in the fill after they arrive at the site are recommended during the EPS fill construction. However, after the EPS blocks are covered by the pavement materials (i.e., at least two feet thick) and by the soil on slopes, the oxygen will not be sufficient to sustain a fire (Frydenlund and Aaboe, 2001).

There are two cases of EPS geofoam burning have been reported in Norway. Both cases were caused by welding activities on bridge abutments adjacent to EPS fills, during the construction phase (Frydenlund and Aaboe, 2001).

Lifetime period:

Koerner (2005) stated that the required lifetime period for EPS goefoam is 75 to 100 years. The lifetime period of EPS geofoam can be affected by time-temperature superposition.

Termite protection:

The untreated insulations are susceptible to termite infestation because they can provide the environment that is suitable for termites to live, work, and eat. To prevent this problem, the special type of EPS geofoam, especially used in insulation application, is made by a process that incorporates a termite-resistant additive during the manufacturing process. According to the testing results performed by Foam-Control EPS Company, the EPS geofoam incorporated with the termite resistant additive shows good performance in resisting termites.

2.5.4 EPS Geofoam Applications

Horvath (1992 and 1999) classified the applications of EPS geofoam blocks into six major categories, based on their functions, including lightweight fill, compression inclusion, thermal insulation, small amplitude wave damping, drainage, and structural.

Another way to classify the EPS geofoam applications is by engineering properties. These properties include density, compressibility, thermal resistance, vibration damping, and the self-supporting nature of the EPS geofoam (Elragi, 2006). Elragi (2006) and The EPS Industry Alliance (undated) listed several applications of EPS geofoam block. Some of those applications related to infrastructural construction have been selected and briefly explained in the following subsections.

2.5.4.1 Slope Stabilization

Arellano et al. (2011) provided a good report to be used as a guideline for geofoam applications in slope stability projects. The most important research product provided in the report is a comprehensive design guideline to facilitate the use of EPS geofoam blocks for slope stabilization and repair. The other primary research products of the report include summary of relevant engineering properties, material and construction standards, economic data, and detailed numerical design examples.

The strategy to remedy the slope instability problem found in embankment or other slope areas can usually be classified into three categories including (1) avoid the problem altogether, (2) reduce the driving forces, and (3) increase the resisting forces. Among those, the option of avoiding the problem is generally the simplest solution, but it is typically not feasible. Therefore, the method for constructing a stable slope must be selected from the remaining two strategies.

The simplest solution to reduce the driving forces within a slope is to simply reduce the slope inclination. With this method, the shear stress on the slope material is

reduced, resulting in more stability for the entire slope. However, the total costs of this solution can be considerable.

Replacement of a portion of the slope material with lightweight fill, such as EPS geofoam blocks, can be the other alternative that serves to reduce the driving forces (Elragi, 2006; Arellano et al., 2011). By removing the existing soil in an upper portion of the slope and replacing it with the lightweight EPS blocks, as presented in Figure 2.38, the weight of the upper portion of the slope is significantly reduced, resulting in less driving forces and consequently, less tendency of the slope failure.

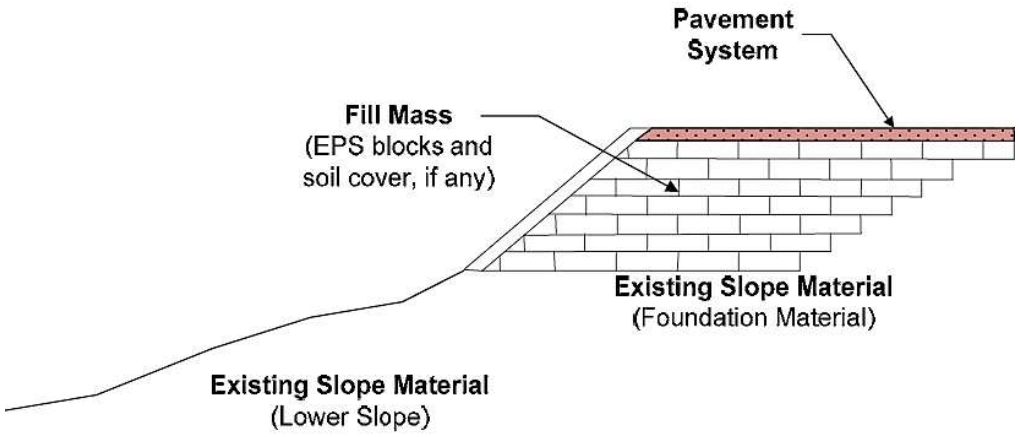

Figure 2.38 Slope stabilization utilizing EPS geofoam (after Arellano et al., 2011)

The EPS geofoam was used to stabilize a road embankment in Japan. The embankment was constructed on a steep hillside. The 1834 cubic meters of EPS geofoam were used in a section of the road of about 341 ft. (104 m) long. The use of EPS geofoam caused a reduction in the overall cost of stabilization efforts and construction time (Suzuki et al., 1996).

Another case involved the use of EPS geofoam to solve the slope instability problem on the slopes along County Highway A in Wisconsin. The slope was 16 ft. (4.9

m) high, with 14 degrees angle with horizontal. It was observed that a deep-seated slip surface was slowly creeping down slope, causing the damage on the pavement. In order to reduce the up-slope driving force of the slide, engineers decided to excavate the embankment fill from the top of the slide and replace it with lightweight fill EPS geofoam blocks. Three layers of 32 in. (0.81 m) thick EPS geofoam, each of 287 in. (7.3 m) width were used in that project (Elragi, 2006).

2.5.4.2 Embankment Fill

Large soil settlement is the problem frequently found occurring when a new embankment is constructed on soft or loose soils, which are incapable of supporting additional loads (Gan and Tan, 2003; Stark et al. 2004; Elragi, 2006; Jones et al., 2008; Sura and Othman, 2011;Puppala and Chittoori, 2012). A comprehensive design guideline for geofoam applications in highway embankments has been provided by Stark et al. (2004). Several design charts and design examples are presented in the guideline.

As discussed previously, there are several techniques to mitigate the settlement in soft foundation soils. Using lightweight materials as an embankment backfill is one effective method for reducing the soil settlement problem.

EPS geofoam can be used to replace the soft ground soils or used in place of heavy fill materials to reduce the stress increase on underlying soils and, consequently, reduce the potential soil settlement magnitude. The EPS geofoam blocks have high compressive resistance which is adequate to support the loads from the pavement system and traffic. Another benefit of using EPS geofoam in the embankment construction is that the EPS blocks can be handled and compacted easily without the need for special equipment, resulting in a savings of time and overall cost of the construction (Stark et al., 2004; Elragi, 2006; The EPS Industry Alliance, undated). Figure

2.39 presents the cross section of embankment and road construction sections using EPS geofoam.

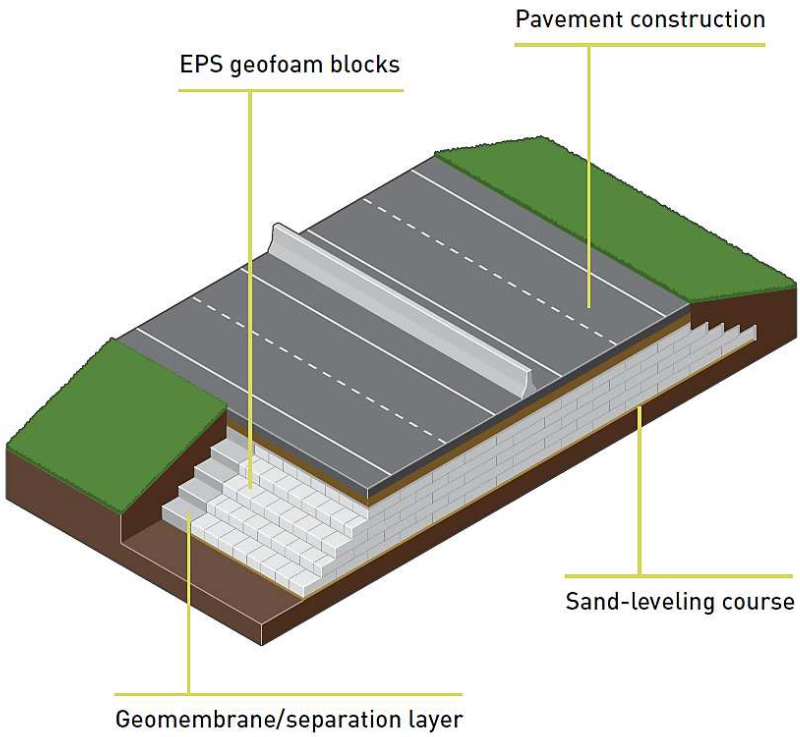

Figure 2.39 Cross section of embankment and road construction using EPS geofoam (after The EPS Industry Alliance)

2.5.4.3 Bridge Support

EPS geofoam blocks can be used as a foundation directly supporting a bridge abutment. Because of its high compressive resistance, EPS geofoam can safely support loads from the bridge structures and traffic without over-stressing the underlying foundation soils (Elragi, 2006; The EPS Industry Alliance, undated).

As presented in Figure 2.40, EPS geofoam blocks were used as supporting the abutments of Hjelmungen Bridge in Norway (Frydenlund and Aaboe, 2001). In 1992, the bridge was completely constructed and its abutments were supported by the soil

consisting partly of waste material-filled embankment over the soft sensitive marine clay. Two years after completion, the soils beneath the abutments (i.e., both embankment and foundation soils) had experienced excessive settlements, causing damage to the bridge deck. Repairs were done from December 1995 to spring 1996. The original filling materials and the old abutments were removed, and the new abutments were constructed and directly supported by the EPS geofoam blocks.

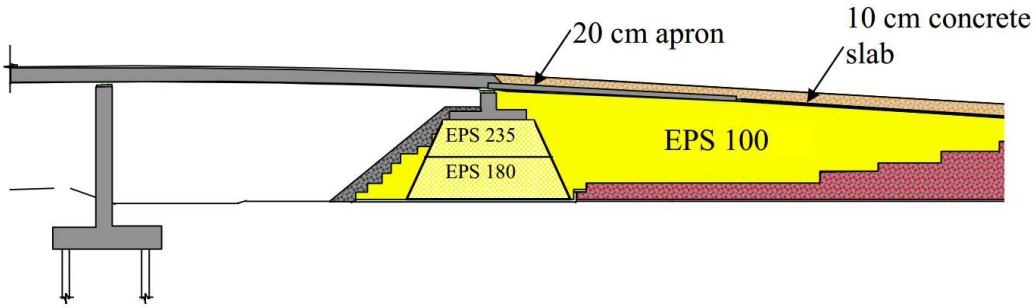

Figure 2.40 EPS geofoam blocks directly supporting bridge abutment (Frydenlund and Aaboe, 2001)

2.5.4.4 Retaining Wall Backfill

Lateral earth pressure is the important parameter affecting the stability of a retaining wall. High lateral pressure, acting on the wall, can cause the failures, such as overturning and sliding to the wall structure (Das, 2010). The factors influencing the magnitude of lateral pressure are unit weight, height, and coefficient of lateral earth pressure of the backfill material. As already known, the EPS geofoam is a lightweight material and the unit weight of it is about 100 times lighter than of natural soils. The other advantages of EPS geofoam over conventional fill are lower Poisson's ratio and coefficient of lateral earth pressure. Hence, using EPS geofoam as the backfill material for retaining wall structures (i.e., as illustrated in Figure 2.41) can result in greatly reduced lateral pressure on the wall (Lutenegger and Ciufetti, 2009).

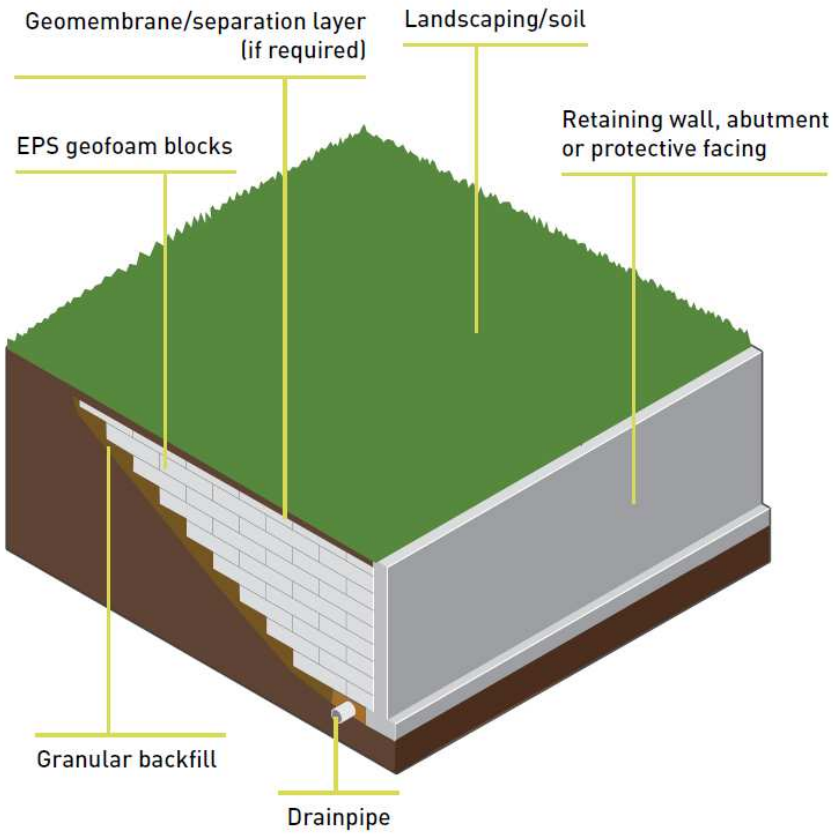

Figure 2.41 Schematic drawing of retaining wall with EPS geofoam backfill
(after The EPS Industry Alliance)

Negussey and Sun (1996) performed a field observation program to study the effectiveness of the EPS geofoam backfill in reducing the lateral pressures against the basement wall in the Syracuse mall, New York. Three earth pressure cells were installed on the outer face of the wall, touching the EPS geofoam blocks. The testing results indicated that the use of EPS geofoam as soil substitute backfill resulted in significantly reducing lateral pressure on the basement wall.

2.5.4.5 Compressible Inclusion against Expansive Soil

Expansive soils are the soils exhibiting shrink-swell behavior due to the changes in moisture level (Puppala et al., 2008). The volume of the expansive soils will increase (i.e., swelling) when water is available and will decrease (i.e., shrink) if water is removed or dried out (Ranjan and Rao, 1993).

EPS geofoam blocks can be used as a compressible inclusion adjacent to a structure element when it is in contact with expansive soil (Horvath, 1996; Elragi, 2006). As presented in Figure 2.42, EPS geofoam is installed below the structure slab and beside the structure wall, as the compression inclusion layer protecting the building structures from soil heaving behavior. The stresses on the structural slab and wall will be limited to a specified value depending on the density of the EPS geofoam (Elragi, 2006).

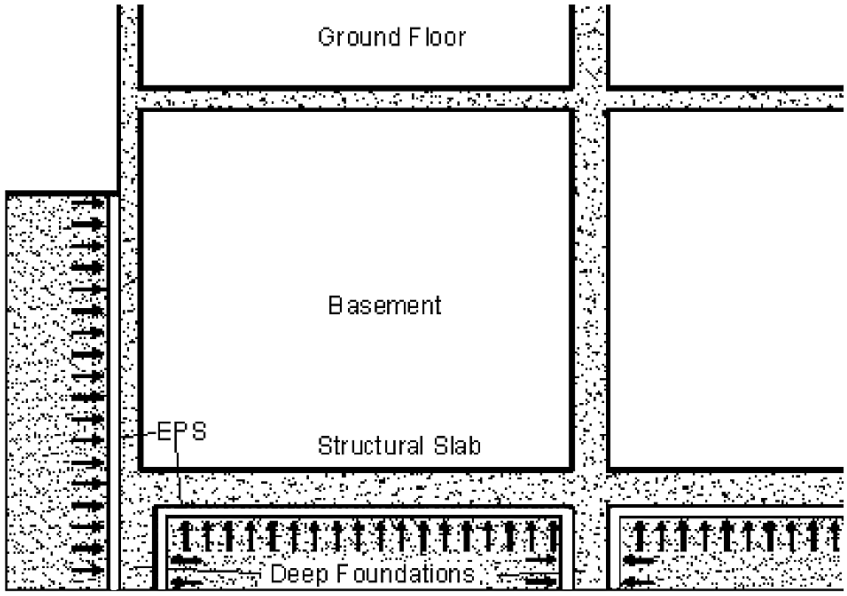

Figure 2.42 Soil expansion stress reduction utilizing EPS geofoam (Elragi, 2006)

2.5.5 Advantages of EPS Geofoam

Archeewa (2010) summarized the benefits of using the EPS geofoam blocks as a lightweight backfill material, as listed in following:

(1) EPS geofoam is approximately 100 times lighter than conventional soils and at least 20 to 30 times lighter than other lightweight fill alternatives.

(2) With its light weight, EPS geofoam can reduce the increasing loads on the underlying subgrade, resulting in the soil settlement reduction.

(3) EPS geofoam can also reduce the lateral stresses on the retaining structures.

(4) Limited labor, without any heavy compaction machine, is required for the EPS geofoam installation process.

(5) Using EPS geofoam can reduce the construction schedule because it is easy to handle and can be installed even in adverse weather conditions.

(6) Although the price per unit of EPS geofoam is relatively high, the overall project costs can be reduced and the maintenance cost for the EPS-used structures can be decreased.

2.6 Summary

This chapter provides a thorough synopsis of the literature review on the problem of the bump at the ends of the bridge and settlement at the bridge approach. The definition of the bump problem and the magnitude of the bump tolerance were first introduced. Then, the factors causing the formation of the bump were summarized and the nine possible factors were briefly explained. Following that, several techniques used to mitigate the bridge approach settlement problems were introduced, with emphasis on the technique of using expanded polystyrene (EPS) geofoam material. The definition,

types and manufacturing process, properties, applications, and advantages of EPS geofoam were presented in the last section.

Chapter 3

Laboratory Experimental Programs

3.1 Introduction

This research study was undertaken at the University of Texas at Arlington with the main objective of evaluating the effectiveness of using the EPS geofoam blocks as an embankment fill material for alleviating the differential settlement problem which occur between the bridge abutment and approach slabs. As a part of the dissertation research, the experimental program aimed at studying a full-scale test section in the real field condition. Hence, a 40-ft high embankment approach to the bridge located on US 67 over SH 174 in Johnson County, Texas was selected as the test site.

In order to study the measured settlement behavior of the tested embankment section, a numerical model was formulated, using a geotechnical finite element software, Plaxis. The properties of the fill and foundation soils as well as an EPS geofoam are necessary for simulating the models. Hence, the samples of embankment fill soil and foundation subgrade soil were collected from the test site and were subjected to a basic laboratory testing program including determination of natural moisture content and in-place unit weight, specific gravity of soil solids, sieve analysis, hydrometer analysis, Atterberg limits tests, falling-head permeability test, and standard Proctor compaction test. Moreover, the tests to find engineering properties of the soils; for example, compressibility characteristics and shear strength of the soils, including consolidation test, direct shear test, and unconsolidated-undrained (UU) triaxial test, were also conducted. In this study, EPS 22 geofoam material samples were used in the laboratory tests. A total eight EPS 22 geofoam samples were tested to investigate its compression behavior.

This chapter presents the details of the experimental testing program performed on the collected soils samples and EPS geofoam, as well as a discussion of the tests results. In the first section, the testing procedures outlined by the American Society of Testing Materials (ASTM) standards were followed; test results obtained from these tests are discussed and summarized in the following sections.

3.2 Experimental Program

In this section, the procedures of the tests performed on the soil samples and EPS geofoam are described. Table 3.1 provides a list of the experiments with corresponding testing standards that were followed in this study.

Table 3.1 Summary of Experiments and Testing Standard Performed in this Study

Materials	Test performed	Standard
Embankment fill soil and foundation subgrade	Determination of natural moisture content	ASTM D-2216-98
	Determination of in-place unit weight	ASTM D-2937-00
	Specific gravity of soil solids test	ASTM D-854
	Sieve analysis test	ASTM D-422
	Hydrometer analysis test	ASTM D-422
	Atterberg limits tests	ASTM D-4318
	Falling-head permeability test	-
	Standard Proctor compaction test	ASTM D-698
	One-dimensional consolidation test	ASTM D-2435-96
	Direct shear test	ASTM D-3080-98
	UU triaxial compression test	ASTM D-2850-95
EPS geofoam	Compression test	ASTM D-1621-00
	Unconfined compression strength test	ASTM D-2166-00

3.2.1 Determination of Natural Moisture Content

According to ASTM D-2216-98, the standard test method for laboratory determination of water (moisture) content of soil and rock by mass, the moisture content of the soil cut samples collected from the test site were measured from the following expression:

$$w\ (\%) = \frac{(\mathrm{m_1} - \mathrm{m_2}) \times 100}{(\mathrm{m_2} - \mathrm{m_c})} \tag{3.1}$$

when, w = moisture content of the soil, %

$\mathrm{m_1}$ = mass of container and moist specimen, g

$\mathrm{m_2}$ = mass of container and oven-dried specimen, g and

$\mathrm{m_C}$ = mass of container, g

3.2.2 Determination of In-Place Unit Weight

To formulate a numerical model of the test embankment site, an in-place unit weight of the fill soil and foundation subgrade needed to be determined. The test procedure performed in this study was partly modified from the procedure provided in ASTM Designation: D 2937-00-Standard test method for density of soil in place by the drive-cylinder method. At first, the total weight and volume of the soil sample were measured. Because the soil samples collected from the site were not in geometrical shape, the volume of the soil samples was determined by using a water-replacement technique instead of calculating it from the soil sample dimensions. After that, moisture content of the soil was determined. The bulk unit weight (γ_t) and dry unit weight (γ_d) of the soil was calculated using the following equations:

$$\gamma_t = \frac{W_t}{V} \quad (3.2)$$

and

$$\gamma_d = \frac{\gamma_t}{(1+w)} \quad (3.3)$$

when, W_t = total weight of the soil sample

V = volume of the soil sample and

w = moisture content of the soil in decimal

3.2.3 Specific Gravity of Soil Solids Test

In soil mechanics, specific gravity of soil solids, represented by G_s, is an important parameter used to calculate the soil weight-volume relationship. Das (2009) provides the definition of the specific gravity of soil solids as the ratio of the density of soil solids to the density of an equal volume of water. In this study, the test to determine the specific gravity of soil solids was conducted as per ASTM D 854 standard test method.

At the beginning of the test, the mass of volumetric flask filled with distilled water up to the 500-ml mark and the temperature of the water were recorded. After that, the approximate mass of 50 g of the air-dried soil that passed through a No. 40 sieve was mixed with distilled water to form a smooth paste and was then transferred into the empty volumetric flask. The distilled water was added to the volumetric flask containing the soil up to about two-third full. In the next step, the air from the soil-water mixture was removed by applying vacuum using a vacuum pump as shown in Figure 3.1. After all of the entrapped air was out, the distilled water was filled to the volumetric flask until reaching the 500-ml mark. Then, the combined mass of the flask, soil, and water was measured. Finally, the mass of the soil dried by the drying-oven was determined and the value of the specific gravity of the soil solids could be calculated with the following relationships:

$$G_s = \frac{M_s}{(M_1 + M_s) - M_2} \quad (3.4)$$

and $$G_{s\,(at\ 20\,℃)} = (G_s)(A) \quad (3.5)$$

when, M_s = mass of dry soil, g

M_1 = mass of volumetric flask with the water filled to 50-ml mark, g

M_2 = mass of volumetric flask, soil and water filled up to 50-ml mark, g

A = the temperature correction factor (given in Table 3.2)

Table 3.2 Temperature Correction Factor

Temperature (℃)	$\boldsymbol{A}$	Temperature (℃)	$\boldsymbol{A}$
17	1.0006	24	0.9991
18	1.0004	25	0.9988
19	1.0002	26	0.9986
20	1.0000	27	0.9983
21	0.9998	28	0.9980
22	0.9996	29	0.9977
23	0.9993	30	0.9974

Figure 3.1 Process of applying vacuum to remove entrapped air

3.2.4 Sieve Analysis Test

The particle-size distribution of a given soil mass is necessary in soil classification for engineering purposes. There are two methods generally used to find the particle-size distribution curve of a soil: (1) sieve analysis, for particle sizes larger than 0.075 mm in diameter; and (2) hydrometer analysis, for particle sizes smaller than 0.075 mm in diameter. In this section, the details of sieve analysis test is presented. The details of the hydrometer analysis test will be explained in Section 3.2.5. Both tests were performed in accordance with ASTM D-422 Standard test method for particle-size analysis of soils.

The wet sieve analysis test was first conducted on the soil sample. About 500 g. of the representative oven-dried soil sample was washed, passing through No. 200 sieve until the wash water was clear. After that, the washed soil retained on the sieve was dried

to constant mass; then, the dry soil sample was tested with the dry sieve analysis test. The soil was passed through a set of sieves, and the stack of sieves was vibrated via a sieve shaker machine, shown in Figure 3.2, for 10-15 minutes. Afterwards, the mass of the soil retained on each sieve and in the bottom pan was measured, and the percentage of the soil retained was calculated.

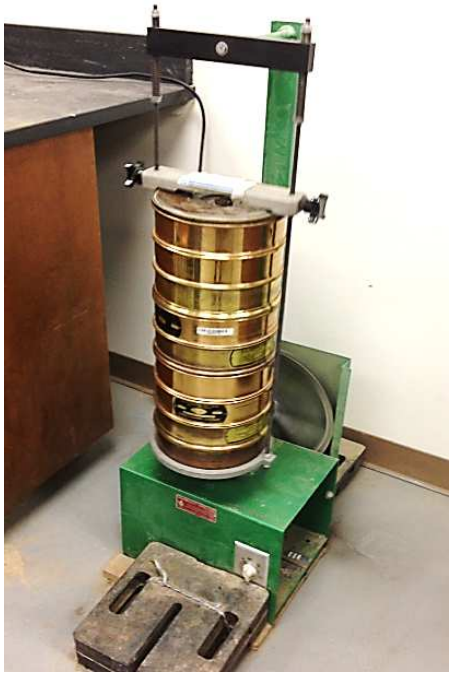

Figure 3.2 Stack of sieves shaken by a sieve shaker machine

3.2.5 Hydrometer Analysis Test

The hydrometer analysis test was developed to determine the particle-size distribution in a soil for the fraction that is smaller than 0.075 mm. in diameter, which is the opening size of No. 200 sieve (Das, 2009). In the test, the ASTM 152 H type hydrometer shown in Figure 3.3(a) was used. In the beginning, 50 g of oven-dried and well-pulverized soil was soaked in a solution of 4% deflocculating agent (sodium hexametaphosphate ($NaPO_3$) or Calgon) for about 8 to 12 hours. Simultaneously, 875

cm^3 of distilled water was mixed with 125 cm^3 of deflocculating agent in a 1000 cm^3 graduated cylinder. Then, meniscus correction and zero correction observed by inserting the hydrometer in to the cylinder were recorded.

The prepared soil was mixed with distilled water by using a mixer machine and then, the entire soil solid inside the mixer cup was transferred to a 1000 cm^3 graduated cylinder. The cylinder was filled with distilled water up to the 1000 cm^3 mark, as shown in Figure 3.3(b). Hydrometer readings were recorded at intervals of 0.25 min., 0.5 min., 1 min., 2 min., 4 min., 8 min., 15 min., 30 min., 1 hr., 2 hr., 4 hr., 8 hr., 12 hr., 24 hr., 48 hr., and 72 hr. After taking the reading initially for the first 2 minutes, the hydrometer was taken out and kept in another cylinder filled with deflocculating solution. Finally, the percent of finer and the diameter of the soil particles were calculated using the cumulative time and the observed hydrometer readings.

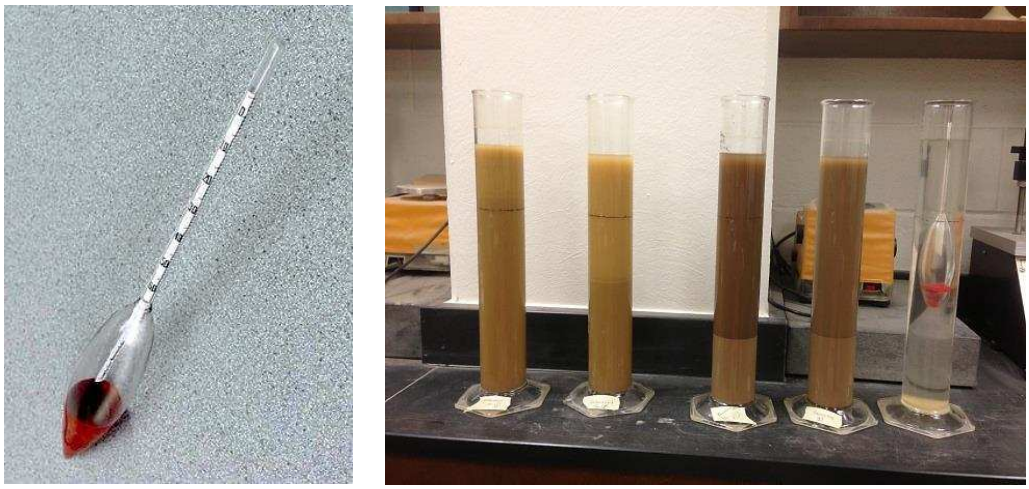

(a) (b)

Figure 3.3 Hydrometer analysis test: (a) ASTM 152 H type hydrometer and (b) Soil-water solutions

3.2.6 Atterberg Limits Tests

With the addition of water to a soil mix, the state of the soil changes from dry, semi-solid, plastic, and finally to liquid state. The water contents at the boundaries of these states are known as shrinkage limit (SL), plastic limit (PL), and liquid limit (LL), respectively.

The liquid limit (LL) refers to the moisture content at which the soil passes from a plastic state to a liquid state or vice versa. The test to find liquid limit of the soil sample was conducted as per ASTM D-4318 standard test method, using the Casagrande liquid limit device. The schematic diagram of a liquid limit device and a grooving tool are illustrated in Figure 3.4. During the test, about 250 g of air-dried soil sieved through No. 40 sieve was mixed with water to form a slurry uniform paste. A portion of the paste was placed in the brass cup of the liquid limit device to the maximum depth of the soil, about 8 mm. Then, using the grooving tool, a groove was created along the centerline of the soil put in the cup. The crank was turned at the rate of 2 revolutions per second and stopped when the soil from two sides had come close through a distance of 1/2 in. The number of blows (N) and moisture content of the soil in the cup were collected. The test was repeated 3-4 times with different amounts of water to determine the exact liquid limit corresponding to the 25 blow count.

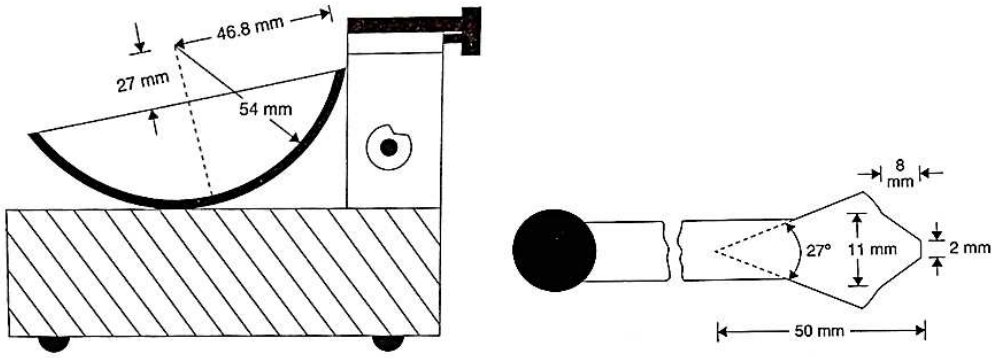

(a) (b)

Figure 3.4 Schematic diagrams: (a) Liquid limit device and (b) Grooving tool (Das, 2009)

The plastic limit (PL) is defined as the moisture content at which the soil passes from a semi-solid state to a plastic state or vice versa. The test to determine plastic limit of the soil sample was also conducted as per the ASTM D-4318 standard test method. Approximately 20 g of a representative air-dried soil sample, passed through No. 40 sieve, was thoroughly mixed with water, then rolled on ground glass. The moisture content at which the mixed soil started crumbling when rolled into a 1/8 in. (3.2 mm) diameter thread was recorded and is referred to as the plastic limit of the soil.

Plasticity index (PI) of a soil can be determined as the numerical difference between liquid limit and plastic limit. The plasticity index is important in classifying fine-grained soil. It is fundamental to the Casagrande plasticity chart (presented in Figure 3.5), which is currently the basis for the Unified Soil Classification System.

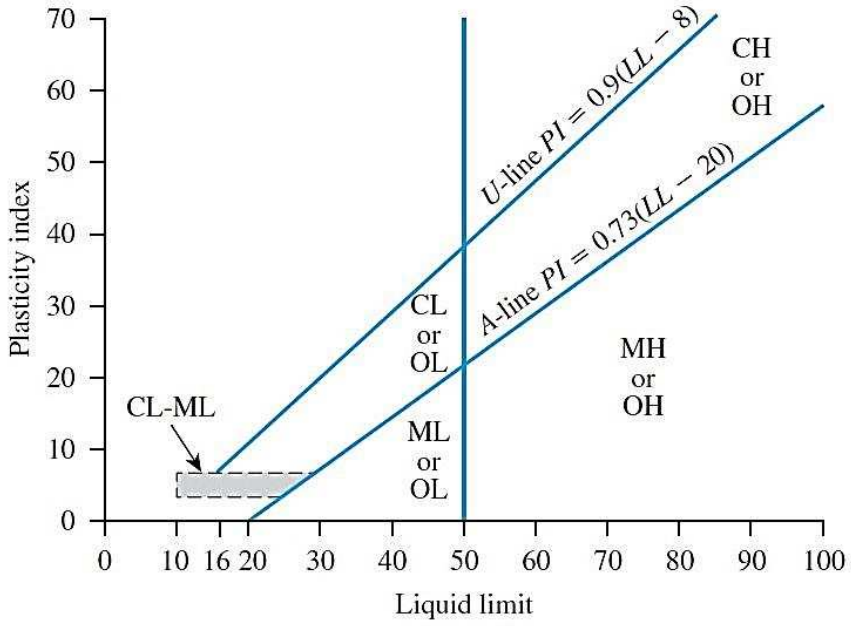

Figure 3.5 Casagrande plasticity chart (Das, 2010)

3.2.7 Falling-Head Permeability Test

Hydraulic conductivity, or sometime called coefficient of permeability, of a soil (k) is a parameter important for predicting the movement of water and contaminants dissolved in the water through the soil (Salarashayeri and Siosemarde, 2012). It is generally expressed in cm/sec or m/sec in SI units and in ft./min or ft./day in English units. The value of hydraulic conductivity varies widely for different soils. Some typical values for saturated soils are presented in Table 3.3 below.

Table 3.3 Typical Values of Hydraulic Conductivity of Saturated soils (Das, 2010)

Soil type	Hydraulic conductivity, k	
	cm/sec	ft./min
Clean gravel	100 – 1.0	200 – 2.0
Coarse sand	1.0 – 0.01	2.0 – 0.02
Fine sand	0.01 – 0.001	0.02 – 0.002
Silty clay	0.001 – 0.00001	0.002 – 0.00002
Clay	< 0.000001	< 0.000002

There are two standard laboratory tests used to determine the hydraulic conductivity of soil: the constant-head test and the falling-head test. The falling-head test was selected for this study because it can be used for both coarse-grained soils and fine-grained soils. The modified falling-head permeability test setup used in this experiment is shown in Figure 3.6.

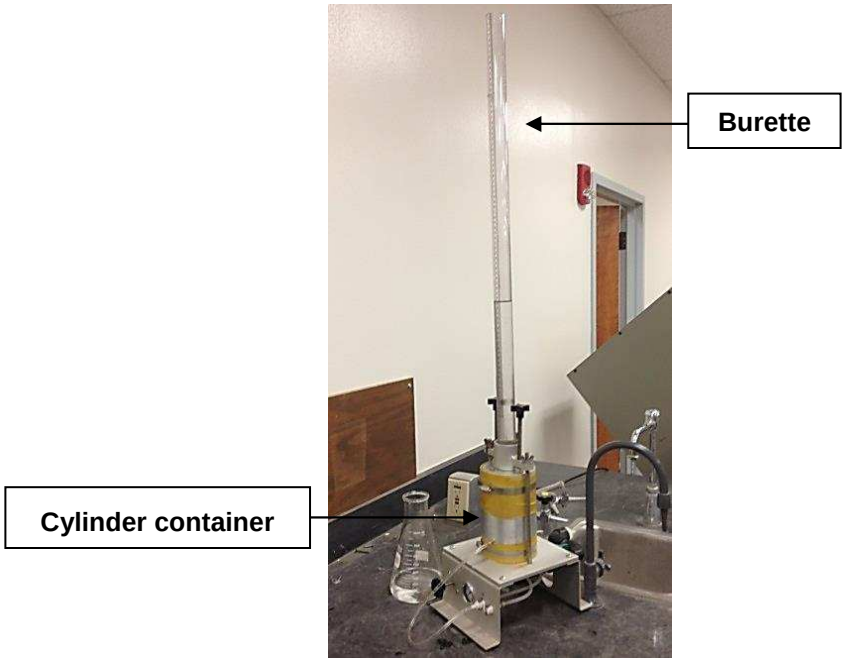

Figure 3.6 Modified falling-head permeability test setup

The oven-dried soil sample was placed in a 4-in. diameter cylinder container, and the test setup was performed. Water was poured into the burette on top of the container and allowed to flow for some time to saturate the soil. After the soil saturation, the water was allowed to flow through the burette to the soil specimen and then out of the channel. During that process, the head difference of water (h) before and after test, flowing time duration, volume of drained water, and temperature of water were recorded. The value of the hydraulic conductivity of the soils could then be calculated.

3.2.8 Standard Proctor Compaction Test

The purpose of standard Proctor compaction test is to establish the compaction moisture content and dry density relationship of a soil. From the relationship, the optimum moisture content (OMC), which is the moisture content at which the soil is compacted to a maximum dry density (MDD) condition, can be determined. The soil compacted at OMC-MDD condition is best for supporting civil infrastructure due to the low volume of voids (Pedarla, 2009). The standard Proctor compaction test was performed as per ASTM D-698 standard procedure on the collected soil samples. During the test, soil samples mixed with different amounts of water were compacted in three layers in the mold size of 4-in. diameter and 6-in. height by using a 5.5 lb. hammer dropped 25 times per layer from a height of 12 in. The weight of the molded soils and corresponding moisture contents were then measured. The compaction curve of the soil was plotted, and the value of OMC and MDD was determined from the curve. Figure 3.7 shows the equipment, including standard Proctor hammer and compaction mold used in this test.

Figure 3.7 Standard Proctor hammer and compaction mold

The results obtained from the test were used to prepare the specimens used in the consolidation test, direct shear test, and UU triaxial compaction test for the collected soil samples. The specimens were prepared at three different moisture content-dry density conditions, including OMC, dry of OMC, and wet of OMC. The points at which the soil specimens were prepared are presented in Figure 3.8.

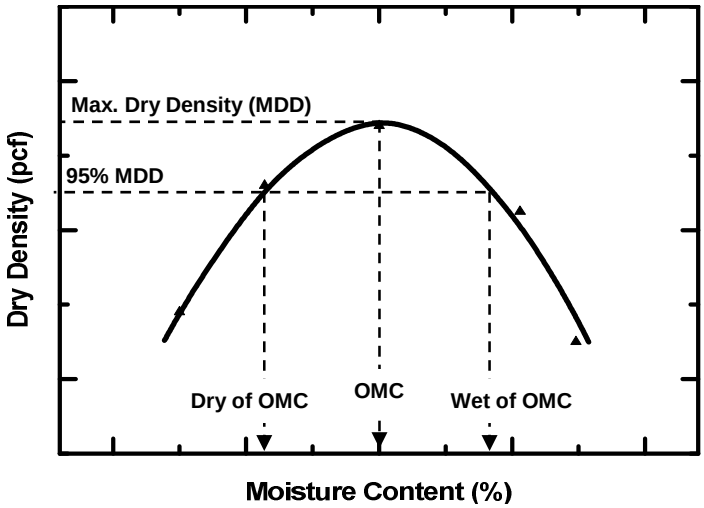

Figure 3.8 Typical standard compaction curve and specimen compaction points

3.2.9 One-Dimension Consolidation Test

The main intent of the one-dimension consolidation test is to determine the compressibility of saturated fine-grained soils, which is considered a time-dependent phenomenon. In this study, the tests were conducted in accordance with the ASTM D-2435-96 standard procedure on the soil specimens prepared at OMC, dry of OMC, wet of OMC and at natural in-situ condition for both embankment fill soil and foundation subgrade soil by using an automated consolidometer test setup shown in Figure 3.9. Porous stones were placed on both top and bottom of the specimens to facilitate water dissipation from the soil. After that, the specimens with porous stones were placed in a consolidation ring and transferred into a consolidometer.

Water was added into the consolidometer to keep the soil saturated. During the saturation process, normally 24 hours, the specimen was loaded under a seating load of 100 psf in order to ensure that the specimens became saturated, with no swelling occurring prior to the loading. The load increments were programmed and specimen deformations were automatically recorded by the GeoJac system unit. At the end of the test, the specimen was carefully removed from the ring and the weight of the specimen immediately after the test was recorded. The weight of the specimen after oven-drying was also measured in order to calculate the moisture content of the saturated specimen. Finally, void ratios were calculated using the height of solids method and plotted with vertical stress to obtain the compression indexes of the specimens.

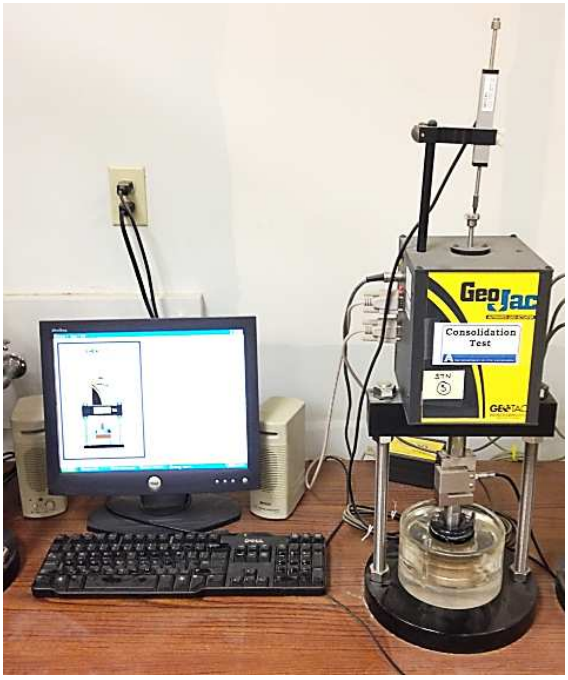

Figure 3.9 Automated consolidometer test setup

3.2.10 Direct Shear Test

The direct shear test is a test method to measure the friction angle, cohesion, and shear strength of soils. The testing method follows closely the ASTM D-3080-98 procedure for performing the standard direct shear test. The direct shear machine used in UTA's geotechnical engineering laboratory provided improvement in electronic deformation devices and automation of data record system over the traditional direct shear device with manual measurement. The soil specimen size of 2.5 in. in diameter and 1.0 in. in height were prepared at OMC, dry of OMC, and wet of OMC conditions for the fill soil and at natural in-situ condition for foundation subgrade soil. The soil specimens were placed in a shear box and installed in the direct shear testing machine. Then, the specimen was pre-consolidated under a water bath with a load increment from the minimum applied normal stress of 250 psf unit the desired normal stress was applied.

During the consolidation stage, the upper and lower shear box halves were held in contact each other with alignment screws. In this test, four normal stresses, including 500 psf, 1000 psf, 2000 psf, and 4000 psf were chosen to characterize the failure envelope.

After completing the consolidation process, the screws holding the two halves of shear box were removed, leaving a gap of approximately 0.025 in. Then, the soil specimen was sheared very slowly in order to allow the dissipation of pore pressure. The equation calculating the estimated minimum time required for the shearing stage is provided in ASTM D-3080, as shown in the following:

$$t_f = 50t_{50} \tag{3.6}$$

when, t_f = total estimated elapsed time to failure, min

t_{50} = time required for the specimen to achieve 50 percent consolidation under the specified normal stress, min

The shearing rate was adjusted for each test run on the GeoTac device; however, because of the difficulty of changing the rate of shear for every normal stress, it was decided to use a lower bound rate of 0.0002 in/min (0.0051 mm/min). From the testing results, the graph of shear strength versus normal stress can be plotted. and the value of friction angle and cohesion of the soil can be determined from the graph. The direct shear test setup used in this study is presented in Figure 3.10.

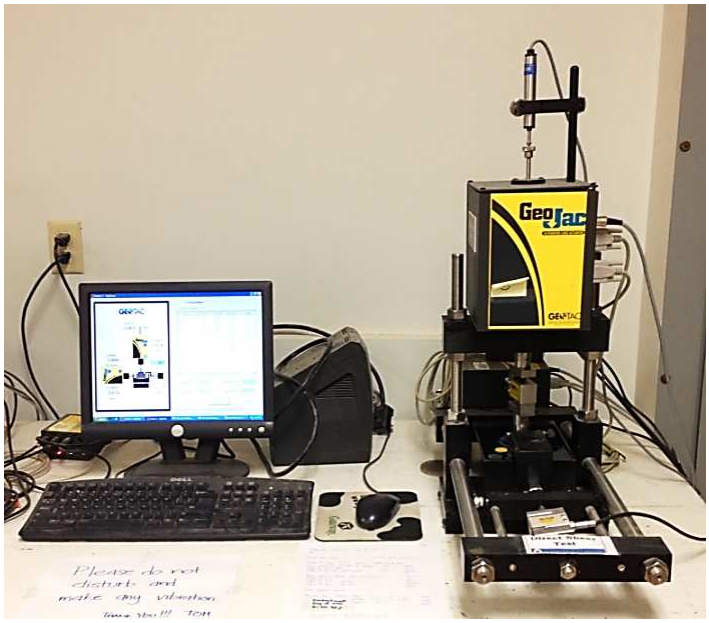

Figure 3.10 Direct shear test setup

3.2.11 Unconsolidated-Undrained (UU) Triaxial Test

The unconsolidated-undrained (UU) triaxial test is a quick test to obtain the shear strength parameters (c and ϕ). This test is applicable to situations where the rate of construction is fast and the loads are assumed to take place rapidly so that there is insufficient time for the induced pore-water pressure to dissipate and for consolidation to occur during the loading period. The test was performed using ASTM D-285-95 standard test method for unconsolidated-undrained triaxial compression test on cohesive soils. The specimens used in the test were remolded to the size of 2.8 in. in diameter and 5.6 in. in height at OMC, dry of OMC, and wet of OMC conditions for the embankment fill soil and at natural in-situ condition for the foundation soil. Before testing, the prepared specimens were placed in a moisture room for at least 7 days to make the moisture inside the specimens homogeneous. In the test, the soil specimens were sealed with a rubber membrane, then placed on a base in a triaxial chamber filled with water. Required

confinement was applied by not allowing water to dissipate from the specimen and waiting for about 10 min to allow the specimen to stabilize. After that, the specimen was tested by applying the constant rate of strain at 1.0 % per min., as per ASTM specifications. The test was stopped when a drop was observed in the load-displacement curve or when at least 15% of the axial strain was reached. Figure 3.11 presents the UU triaxial test setup and the failed specimen obtained from the test.

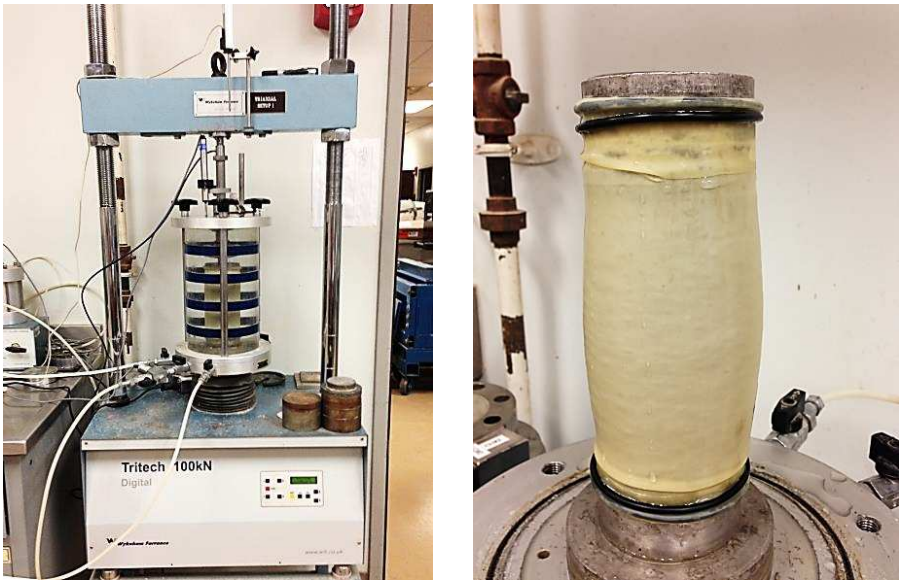

(a) (b)

Figure 3.11 Unconsolidated-undrained triaxial test: (a) the test setup and (b) the failed specimen

3.2.12 Compression Test on EPS 22 Geofoam

The compression behavior, such as compressive strength and modulus of elasticity of the geofoam specimen, is the important mechanical property necessary for designing with geofoam material. In this study, the compression tests were performed on EPS 22 geofoam specimens in accordance with ASTM D-1621-00, standard test method

for compressive properties of rigid cellular plastics. The test specimens were prepared in a cylindrical shape with the diameter of about 2.8 in. The minimum height of the specimens was assigned to be 1 in. and the maximum height was not greater than the diameter of the specimen. The triaxial testing machine was used to perform the test. Before testing, the weigth and dimension of the specimens were measured. Then, the EPS 22 geofoam specimens were installed on the base in a triaxial chamber. After that, the specimens were tested by applying the constant rate of the base plate movement at 2.5 mm / min., as per ASTM specifications. The test was continued until a yield point was reached, or until the specimen was compressed to about 13 % of its original thickness. The compression test setup and the EPS 22 geofoam specimens used in this test are presented in Figure 3.12.

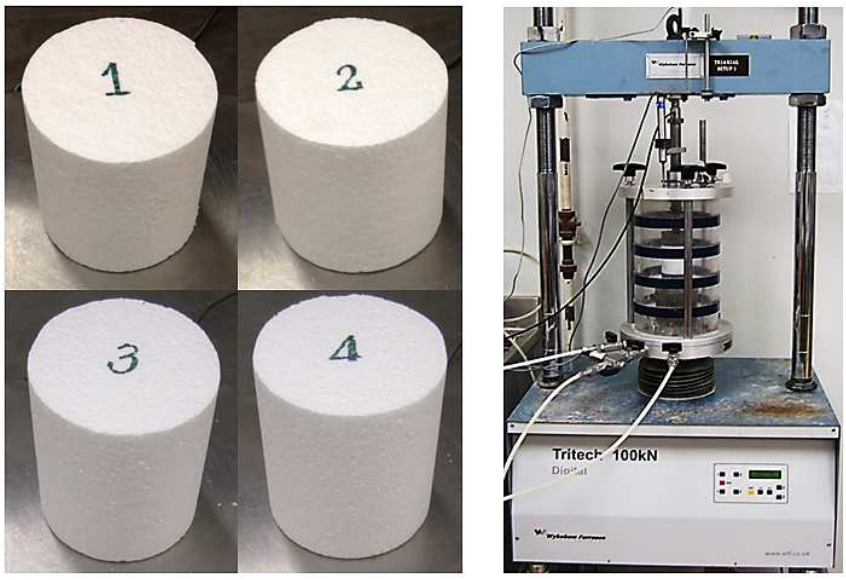

(a) (b)

Figure 3.12 Compression test on EPS 22 geofoam: (a) the test specimens and (b) the test setup

3.2.13 Unconfined Compression Strength Test on EPS 22 Geofoam

Expanded Polystyrene (EPS) Geofoam is successfully used as a construction material in the field of geotechnical engineering. For example, the EPS geofoam is recommended to be used as the fill material in many bridge embankment constructions in order to reduce the settlement problem on the embankment. In this research, the behavior of EPS 22 geofoam under the unconfined compression strength (UCS) test has been studied. Four EPS 22 geofoam specimens were prepared in a cylindrical shape, with the ratio of diameter to height equal to 1:2, and were tested in accordance with ASTM D-2166-00 standard test method for unconfined compressive strength of cohesive soil. During the test, the specimen was applied to a constant strain rate of 1.27 mm / min., and the test was stopped when the specimen was compressed to 15 % of its initial height. Figure 3.13 presents the EPS 22 geofoam specimens and the UCS testing setup performed in this test.

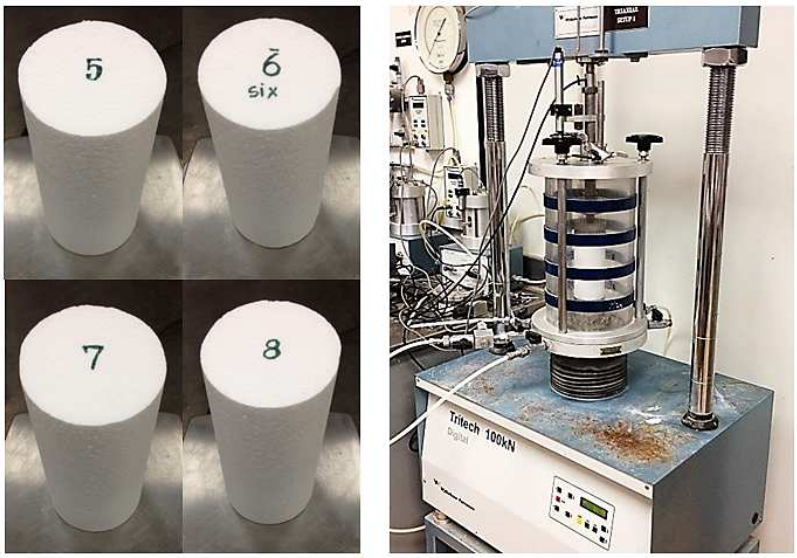

(a) (b)

Figure 3.13 Unconfined compression strength test on EPS 22 geofoam: (a) the test specimens and (b) the test setup

3.3 Analysis and Discussion of Test Results

This section presents the results obtained from laboratory tests mentioned in the previous section. The discussions on the testing results are also provided briefly. The explanation is divided into three parts, based on the types of soil properties and the properties of EPS geofoam: (1) Physical properties of soils, (2) Engineering properties of soils, and (3) Properties of EPS 22 geofoam.

3.3.1 Physical Properties of Soils

The laboratory tests performed to find the physical properties of the collected soil samples consisted of determination of natural moisture content, determination of in-place density, specific gravity of soil solid test, sieve analysis test, hydrometer analysis test, Atterberg limits tests, falling-head permeability test, and standard Proctor compaction test. From the testing results, the collected soil samples could be classified based on Unified Soil Classification System (USCS).

3.3.1.1 Determination of Natural Moisture Content and In-place Unit Weight

The tests to find the natural in-situ moisture content and the bulk unit weight of the collected soil samples were performed immediately after the soils were transferred to the geotechnical engineering laboratory at the University of Texas at Arlington. The results obtained from the tests showed that natural moisture content of the embankment fill soil and foundation soil were 18.0 % and 17.2 % respectively. Whereas, the in-place bulk unit weight of 119.2 pcf and 131.4 pcf were observed respectively for the embankment fill soil and foundation soil.

3.3.1.2 Specific Gravity of Soil Solids Test

The tests to determine the specific gravity of soil solids (G_s) of the collected soil samples were performed in the geotechnical engineering laboratory at UTA. The

temperature of water used in the tests was recorded equal to 22 °C; therefore, the temperature correction factor (A) of 0.9996 was selected to be used in the calculation of G_s at standard temperature (20 °C). From the calculation, the values of $G_{s\ (at\ 20\ °C)}$ of the embankment fill soil and foundation soil equal to 2.67 and 2.70 respectively were obtained.

3.3.1.3 Sieve Analysis and Hydrometer Analysis Tests

Sieve analysis and hydrometer analysis tests were performed in order to find grain size distributions of the soil samples. The result of these tests is one of the important parameters used in soil classification. Table 3.4, provided below, presents the results of the sieve analysis tests conducted on the collected soil samples. The grain size distributions of the soils plotted with the results of the sieve analysis test and hydrometer analysis test are also illustrated in Figure 3.14.

Table 3.4 Sieve Analysis Testing Results

Sieve No.	**Sieve opening (mm)**	**Percent finer (%)**	
		Embankment fill soil	**Foundation soil**
4	4.750	99.43	99.96
10	2.000	97.35	96.88
20	0.850	95.54	95.35
30	0.600	95.13	94.94
40	0.425	94.90	94.46
60	0.250	93.08	90.29
80	0.180	77.51	81.14
100	0.150	67.71	74.90
200	0.075	38.28	51.29
Pan	-	0.00	0.00

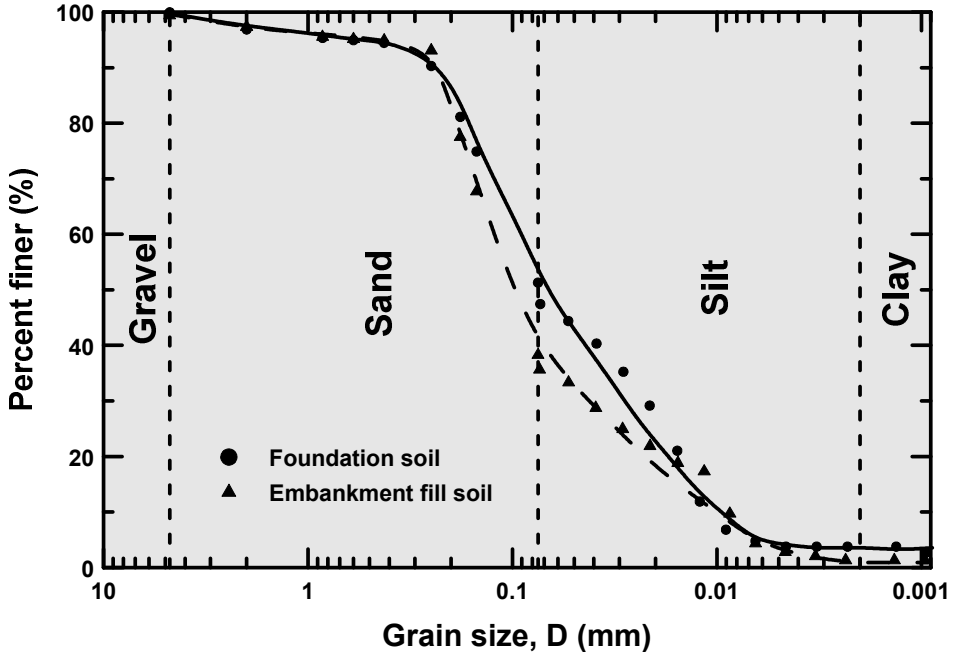

Figure 3.14 Grain size distribution curves of embankment fill soil and foundation soil

3.3.1.4 Atterberg Limits Tests

Atterberg limits tests, including liquid limit (LL) test and plastic limit (PL) test, were conducted on the representative soil samples collected from the test site. From the testing results, the value of plasticity index (PI) of the soils was calculated. Based on the Unified Soil Classification System (USCS), the values of LL and PI are the other two important parameters used in soil classification. The testing results for the collected soil samples are presented in Table 3.5 provided at the end of this section.

3.3.1.5 Falling-Head Permeability Test

The falling-head permeability tests were performed in order to find the value of hydraulic conductivity (k) of the soil samples. The results showed that k for the embankment fill soil was 4.8×10^{-6} cm/sec or 0.0041 m/day (0.013 ft./day), and k for the foundation soil was 5×10^{-7} cm/sec or 0.00043 m/day (0.0014 ft./day).

3.3.1.6 Standard Proctor Compaction Test

The test results obtained from the standard Proctor compaction tests performed on the soil samples are presented in the form of compaction dry density and moisture content relationship curves, as shown in Figures 3.15 and 3.16. From the curves, the values of optimum moisture content (OMC) and maximum dry density (MDD) of the soils can be determined.

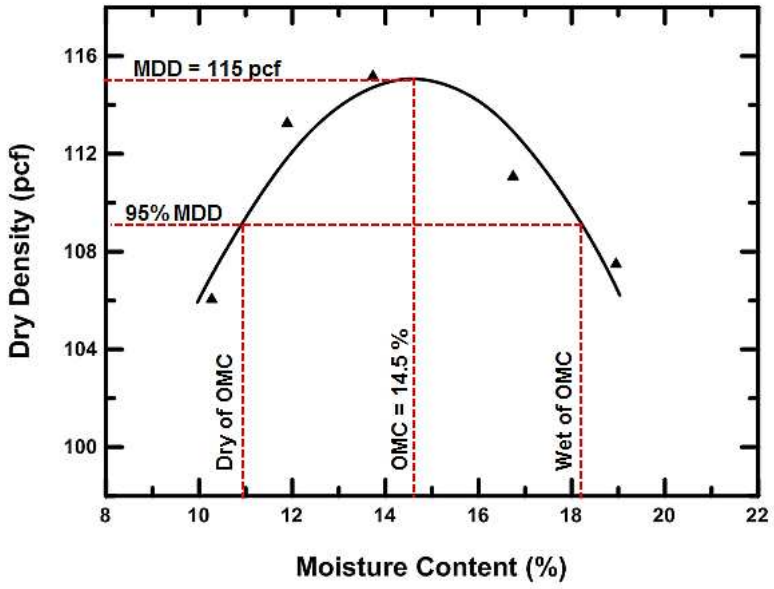

Figure 3.15 Standard Proctor compaction curve of embankment fill soil

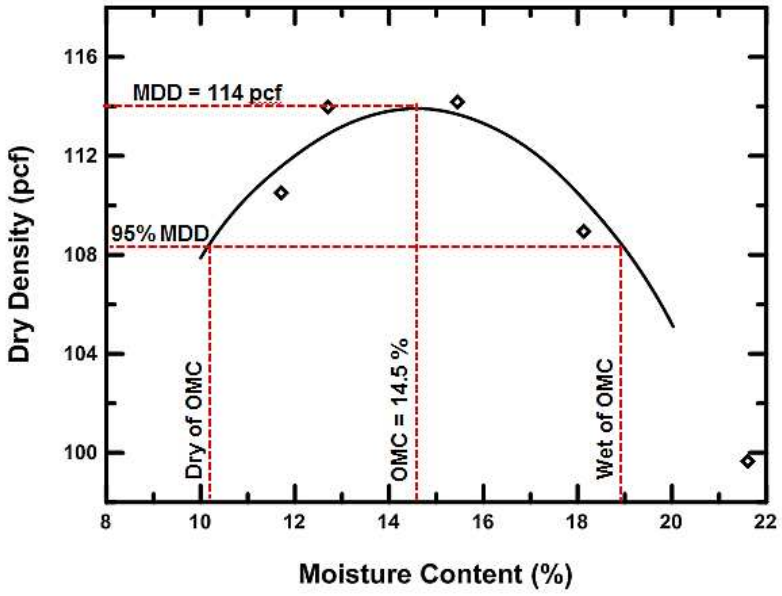

Figure 3.16 Standard Proctor compaction curve of foundation soil

The summary of physical properties of the collected soil samples is provided in Table 3.5. From the results, the soils can be classified based on USCS classification system. The embankment fill soil was classified as sandy soil with low-to-medium plasticity clay (SC); whereas the foundation soil was classified as low-to-medium plasticity sandy clays (CL).

As expressed in Table 3.5, when compared with the data provided in the website (Natural Resources Conservation Service (NRCS) Web Soil Survey), the percent of sand in the foundation soil sample measured from the laboratory test showed the higher value; whereas, the testing results of liquid limit (LL) and plastic index (PI) were lower. The cause of the difference was analyzed, and was concluded that it was because, in the several years past after the embankment construction, some sand from the embankment fill soil had been transported by rainfalls and deposited on or penetrated into the top layer of the surrounding natural foundation soil. Moreover, the foundation soil sample collected

was not very deep and quite close to the embankment toe, resulting in the high percentage of sand found in the collected foundation soil sample. This high fraction of sand resulted in the foundation soil sample having lower values of LL and PI.

Table 3.5 Physical Properties of the Collected Soil Samples

Soil properties	Unit	Embankment fill soil	Foundation soil	
			Laboratory test	From NRCS
Natural moisture content, ω_n	%	18.0	17.2	-
In-place dry unit weight	pcf	101.0	112.1	-
In-place bulk unit weight	pcf	119.2	131.4	-
Specific gravity of soil solids, G_s	-	2.67	2.70	-
Percent gravel	%	0.57	0.04	0.00
Percent sand	%	61.15	48.67	22.10
Percent fine	%	38.28	51.29	77.90
Liquid limit, LL	-	32.0	38.0	50.0
Plastic limit, PL	-	15.0	17.0	15.0
Plasticity index, PI	-	17.0	21.0	35.0
Hydraulic conductivity, k	ft./day	0.013	0.0014	-
Maximum dry density, MDD	pcf	115	114	-
Optimum moisture content, OMC	%	14.5	14.5	-
USCS classification	-	SC	CL	CH

3.3.2 Engineering Properties of Soils

In this study, the laboratory tests conducted to find engineering properties of the soil samples were selected based on the properties which are necessary for the numerical modeling. The tests consisted of one-dimension consolidation test, direct shear test, and unconsolidated-undrained (UU) triaxial test. The results obtained from the tests are described in following:

3.3.2.1 One-Dimension Consolidation Test

During the one-dimension consolidation test, the initial moisture content (w_o), final moisture content and specimen size were measured. The load increments were applied on soil specimens, and specimen deformations were recorded. From the results, void ratios of the soil specimens were calculated and plotted, with corresponding pressures applied in a semi-log scale (consolidation curve) as illustrated in Figure 3.17 and 3.18.

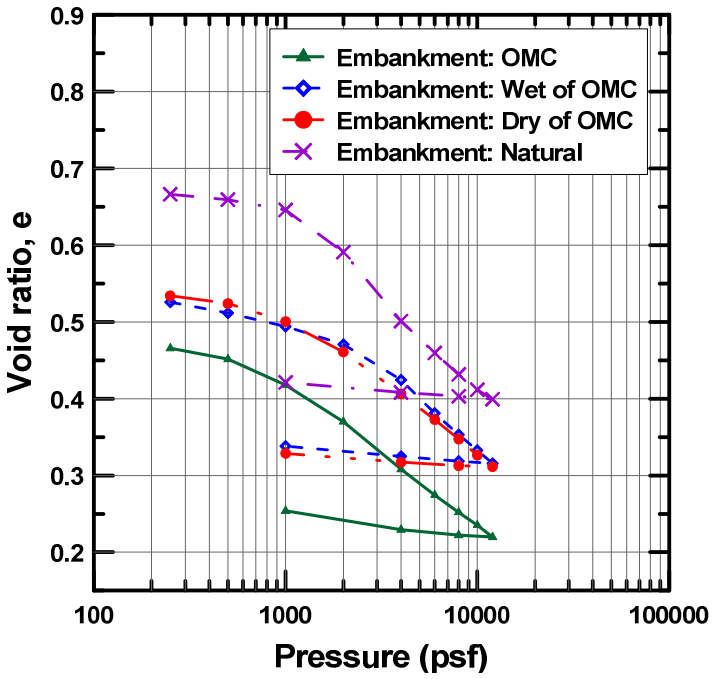

Figure 3.17 Consolidation curves of embankment soil specimens

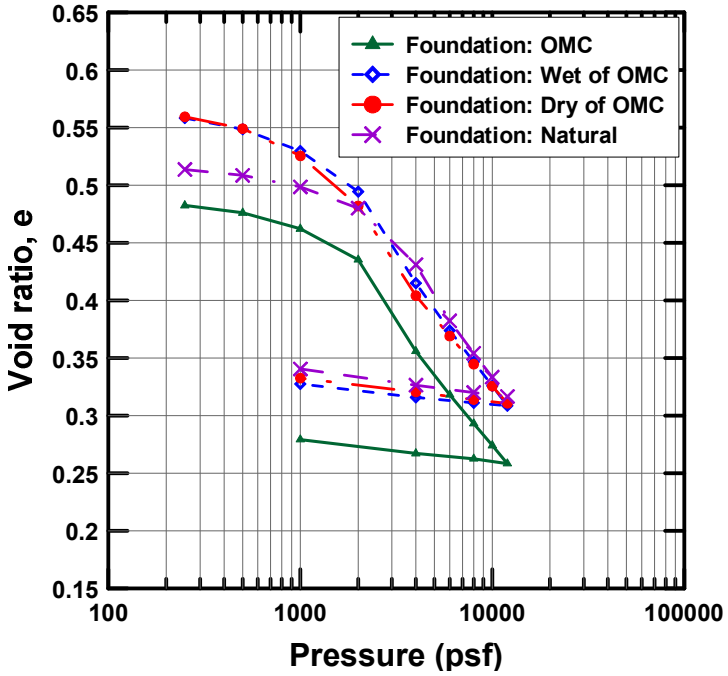

Figure 3.18 Consolidation curves of foundation soil specimens

According to Casagrande (1936), the value of pre-consolidation pressure (σ_c') of the soil samples can be determined from the laboratory e-log P curve. Figure 3.19 presents the graphical procedure used to determine pre-consolidation pressure. At first, point a is established at which the e-log P curve has a minimum radius of curvature. Then, a horizontal line ab and a tangent line ac are drawn. The line ad, which is the bisector of the angle bac, is created and finally, the straight-line portion gh of the e-log P curve is projected back to intersect the line ad at point f. The abscissa of point f is the pre-consolidation pressure.

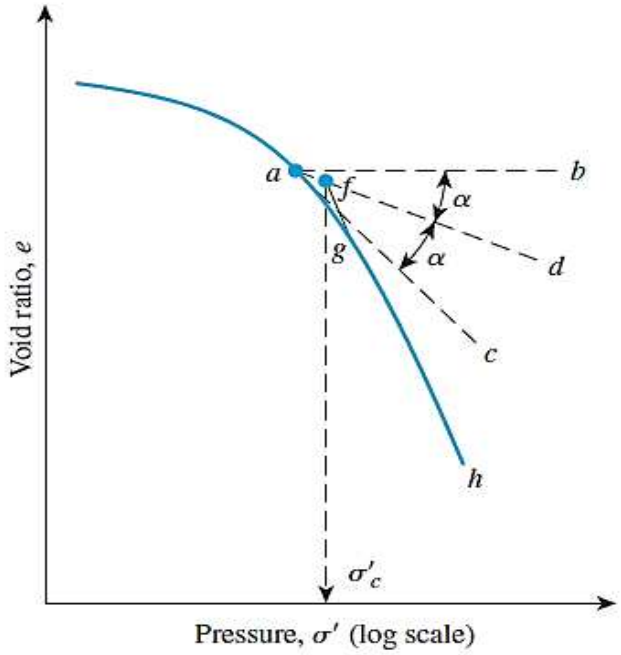

Figure 3.19 Graphic procedure for determining pre-consolidation pressure (after Das, 2010)

Because the soil specimens were remolded, the field consolidation curve needed to be reconstructed from the laboratory test results. The compression index (C_c) and recompression index (C_r) of the soil specimens were calculated as the slope of the compression and recompression parts of the field consolidation curve, respectively. The values of C_c and C_r of the soil samples are provided in Table 3.6.

Table 3.6 Consolidation Parameters (σ_c', e_o, C_c, and C_r) of the Soil Specimens

Soil	Compaction condition	Consolidation parameters			
		σ_c' (psf)	e_o	C_c	C_r
Embankment fill soil	Dry of OMC	1,050	0.53	0.22	0.02
	OMC	1,040	0.47	0.22	0.03
	Wet of OMC	1,100	0.54	0.23	0.02
	Natural in-situ	1,050	0.67	0.26	0.02
Foundation soil	Dry of OMC	1,700	0.56	0.27	0.02
	OMC	1,900	0.49	0.28	0.02
	Wet of OMC	1,900	0.56	0.27	0.02
	Natural in-situ	1,800	0.54	0.25	0.02

3.3.2.2 Direct Shear Tests

The results received from the tests performed in accordance with the procedure explained in Section 3.2.10 can be presented as the relationship curves between shear stress (τ) and horizontal displacement of the soil specimens. From the curves, shear strength (*s*) of each soil specimen was determined. Finally, the graphs of shear strength versus normal stress were plotted to determine the values of cohesion (c') and friction angle (ϕ') of the soils, as presented in Figures 3.20 to 3.23 and Table 3.7, respectively.

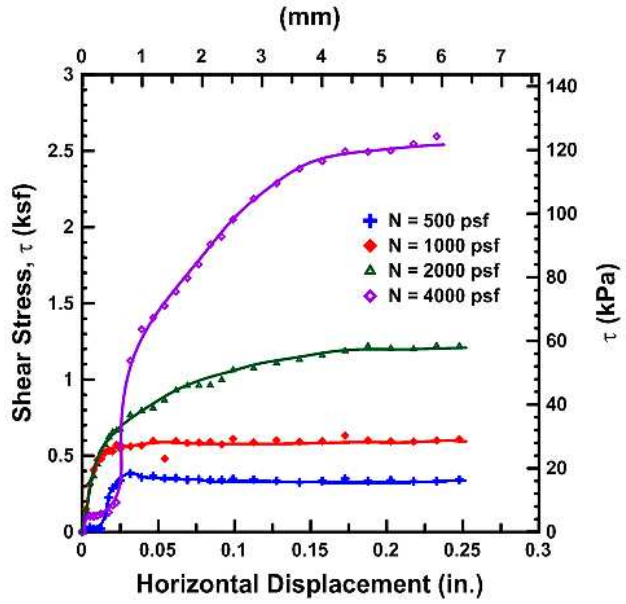

(a)

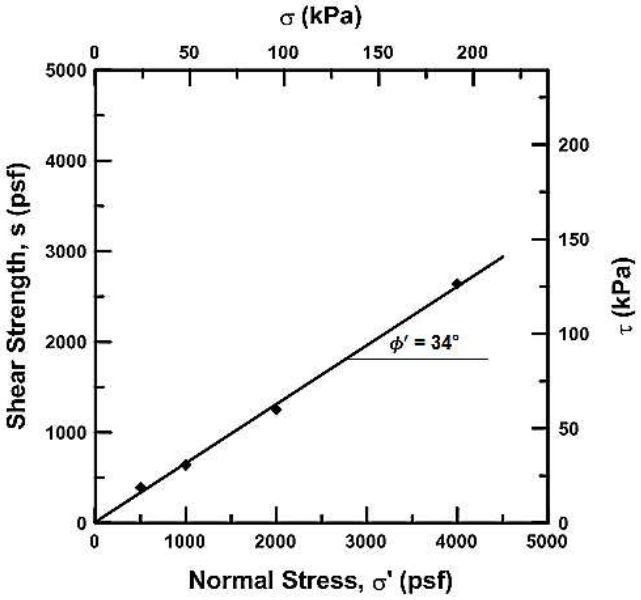

(b)

Figure 3.20 Direct shear test results of embankment soil specimens compacted at Dry of OMC: (a) Graphs of shear stress versus horizontal displacement and (b) Graph of shear strength versus normal stress

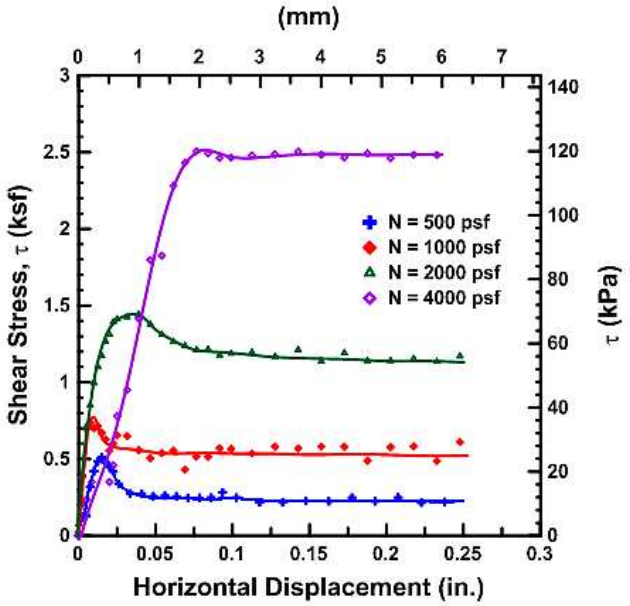

(a)

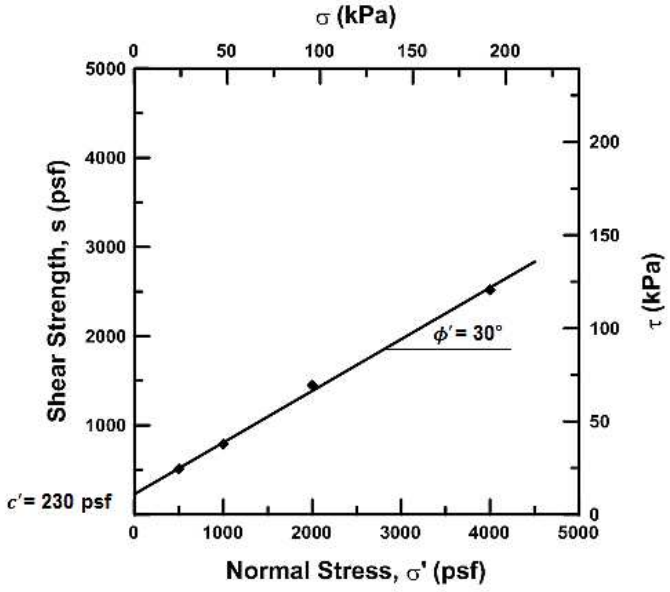

(b)

Figure 3.21 Direct shear test results of embankment soil specimens compacted at OMC: (a) Graphs of shear stress versus horizontal displacement and (b) Graph of shear strength versus normal stress

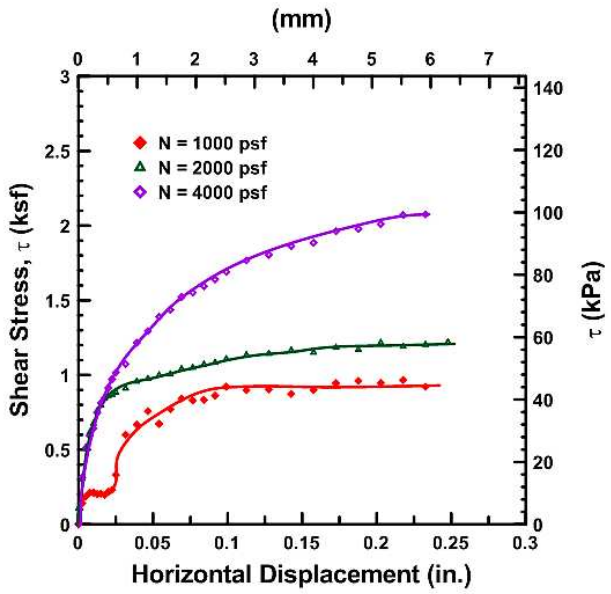

(a)

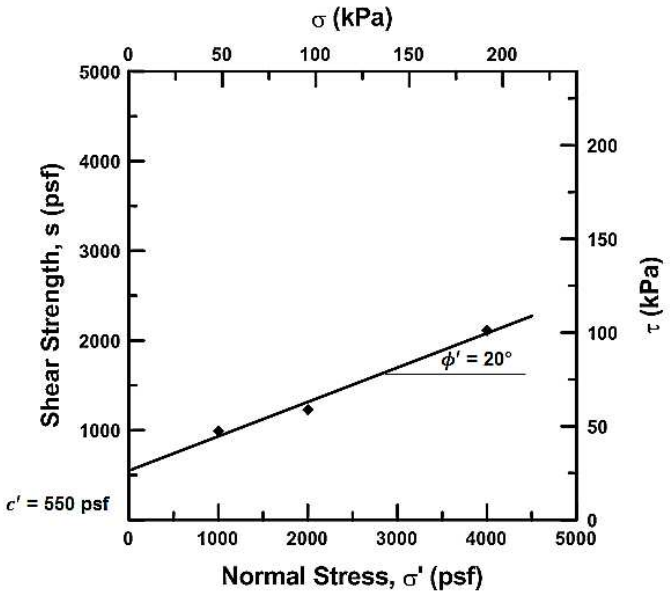

(b)

Figure 3.22 Direct shear test results of embankment soil specimens compacted at Wet of OMC: (a) Graphs of shear stress versus horizontal displacement and (b) Graph of shear strength versus normal stress

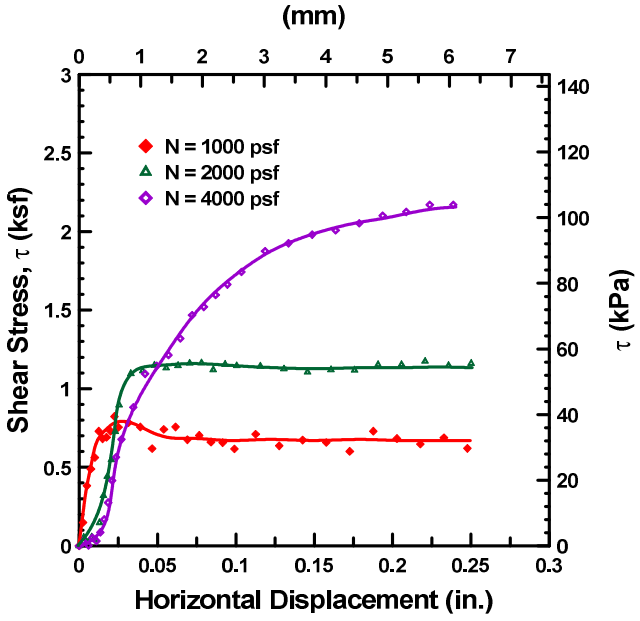

(a)

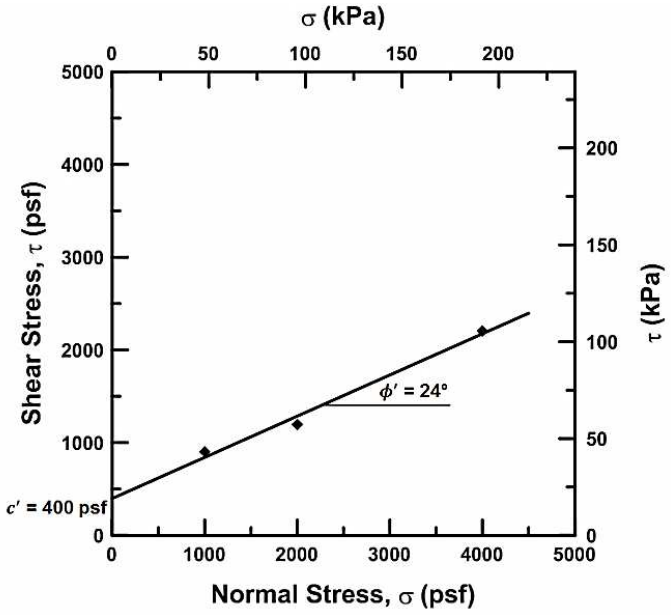

(b)

Figure 3.23 Direct shear test results of Foundation soil specimens compacted at in-situ condition: (a) Graphs of shear stress versus horizontal displacement and (b) Graph of shear strength versus normal stress

Table 3.7 Cohesion (c') and Friction Angle (ϕ') received from Direct Shear Test

Soil	Compaction condition	Cohesion, c' (psf)	Friction angle, ϕ' (degree)
Embankment fill soil	Dry of OMC	0	34
	OMC	230	30
	Wet of OMC	550	20
Foundation soil	Natural in-situ	400	24

3.3.2.3 Unconsolidated-Undrained (UU) Triaxial Tests

Unconsolidated-undrained (UU) triaxial tests were performed on each type of the prepared soil specimens by applying three different confining pressures; 7.25 psi (50 kPa), 14.5 psi (100 kPa), and 29 psi (200 kPa). From the test results, the graph of the axial strain (ε) versus deviatoric stress (σ_d) was plotted.

The minor principal stress (σ_3) and the major principal stress (σ_1) on the soil specimens at failure was determined and used to draw Mohr's circles. A failure envelop line was drawn as the tangent line of the Mohr's circles. The values of cohesion (*c*) and friction angle (ϕ) of the soils were determined as the point at which the failure envelope line cut the y-axis, and the angle between the failure envelope with horizontal line respectively. The graphs of axial strain (ε) versus deviatoric stress (σ_d) and the Mohr's circles of the soil specimens are presented in Figures 3.24 to 3.27.

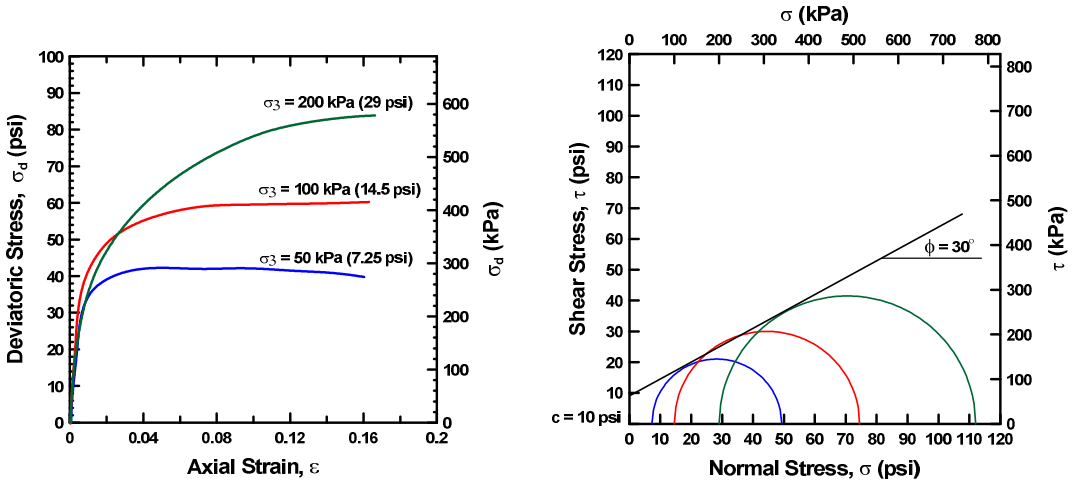

(a) (b)

Figure 3.24 UU triaxial test results of embankment soil specimens compacted at Dry of OMC: (a) Graphs of the axial strain versus deviatoric stress and (b) Mohr's circles at failure

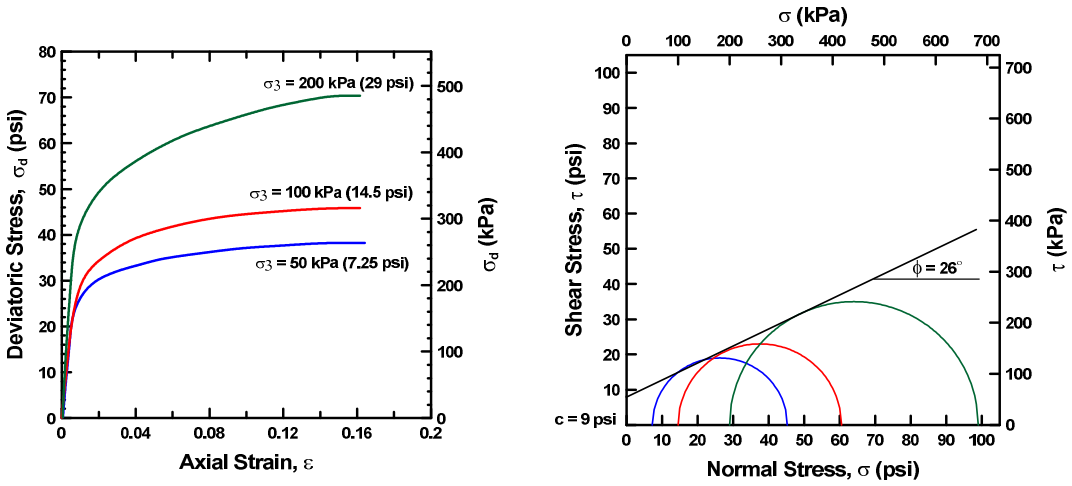

(a) (b)

Figure 3.25 UU triaxial test results of embankment soil specimens compacted at OMC: (a) Graphs of the axial strain versus deviatoric stress and (b) Mohr's circles at failure

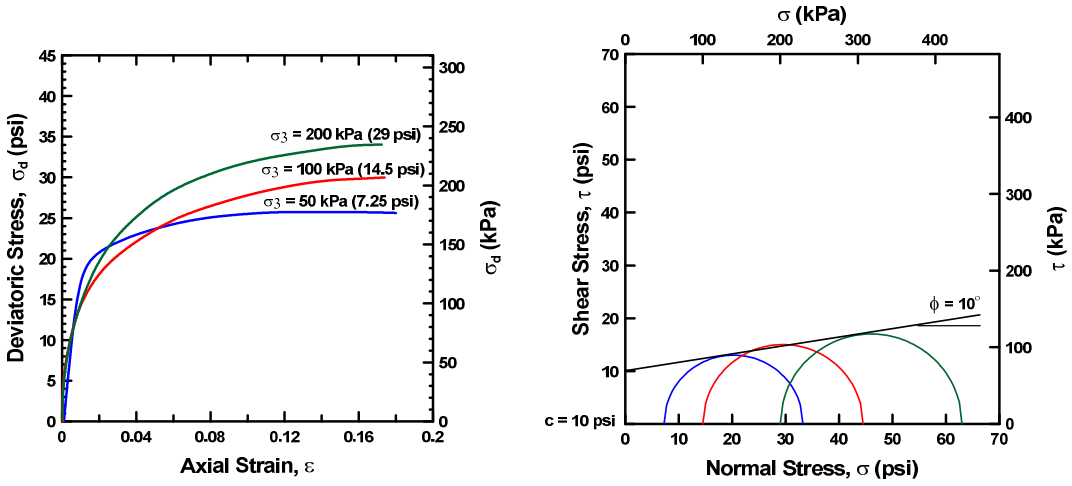

(a) (b)

Figure 3.26 UU triaxial test results of embankment soil specimens compacted at Wet of OMC: (a) Graphs of the axial strain versus deviatoric stress and (b) Mohr's circles at failure

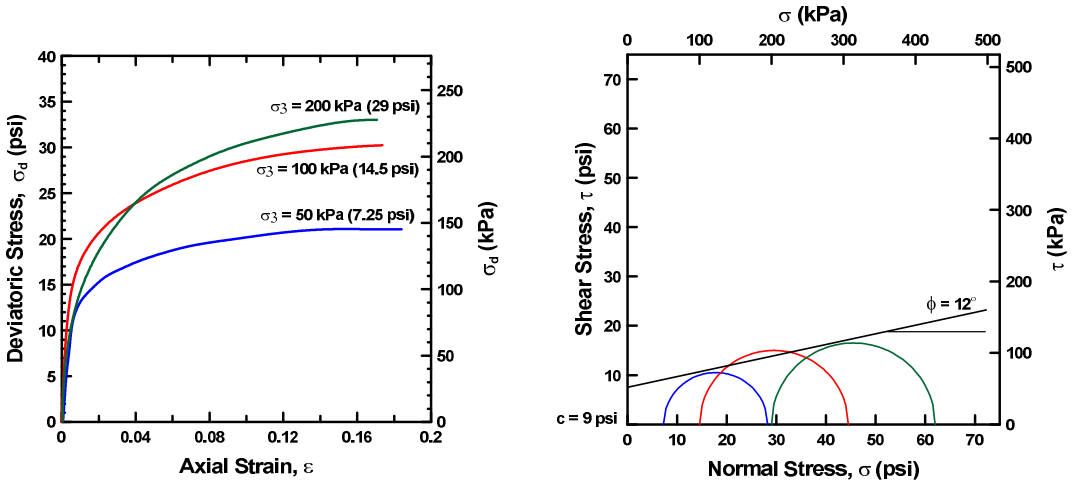

(a) (b)

Figure 3.27 UU triaxial test result of foundation soil specimens compacted at in-situ condition: (a) Graphs of the axial strain versus deviatoric stress and (b) Mohr's circles at failure

Table 3.8 (below) presents the values of cohesion (c) and friction angle (ϕ) of the soil samples measured from the plots of Mohr's circles and failure envelope line.

Table 3.8 Cohesion (c) and Friction Angle (ϕ) of the Soil Samples

Soil	**Compaction condition**	**Cohesion, c (psi)**	**Friction angle, ϕ (degree)**
Embankment fill soil	Dry of OMC	10	30
	OMC	9	26
	Wet of OMC	10	10
Foundation soil	Natural in-situ	9	12

3.3.3 Properties of EPS 22 Geofoam

In this research, some properties, such as density and compression behavior of the EPS 22 geofoam, were investigated in order to verify the values specified in the ASTM standard. Moreover, the geofoam samples were tested with the standard tests used to find engineering properties of soils, i.e. unconfined compressive strength (UCS) test. Those properties are necessary in the designing of geofoam material. The results from the tests are presented in the following sections.

3.3.3.1 Unit Weight of EPS 22 Geofoam

Before starting the compression test and UCS test, the weight and dimensions, including diameter and length of the total eight EPS 22 geofoam specimens, were measured exhaustively with a sensitive vernier caliper. The values of unit weight were estimated from the measurements. Table 3.9 provided below presents the measured values of weight and dimensions and the calculated unit weight of the EPS 22 geofoam specimens. It can be observed from the table that all specimens have the unit weight higher than the minimum value specified in ASTM D-6817-07.

Table 3.9 Weight, Dimensions, and Unit Weight of the EPS 22 Geofoam Specimens

Specimen No.	Weight (lb.)	Diameter (in)	Length (in)	Unit Weight (pcf)		Tests
				Measured	Minimum	
1	0.0148	2.746	2.838	1.52	1.35	Compression
2	0.0148	2.750	2.762	1.56	1.35	Compression
3	0.0165	2.757	2.824	1.70	1.35	Compression
4	0.0163	2.761	2.769	1.70	1.35	Compression
5	0.030	2.753	5.642	1.52	1.35	UCS
6	0.032	2.758	5.644	1.65	1.35	UCS
7	0.034	2.766	5.638	1.73	1.35	UCS
8	0.031	2.768	5.652	1.58	1.35	UCS

3.3.3.2 Compression Test

As mentioned in Section 3.2.12 and Table 3.9, the compression tests were conducted on four specimens of EPS 22 geofoam. The test results were recorded with an accurate data logger. From the results, it can be concluded that the values of stress (σ) and axial strain (ε) that occurred on the specimen can be calculated and plotted as the graphs presented in Figure 3.28.

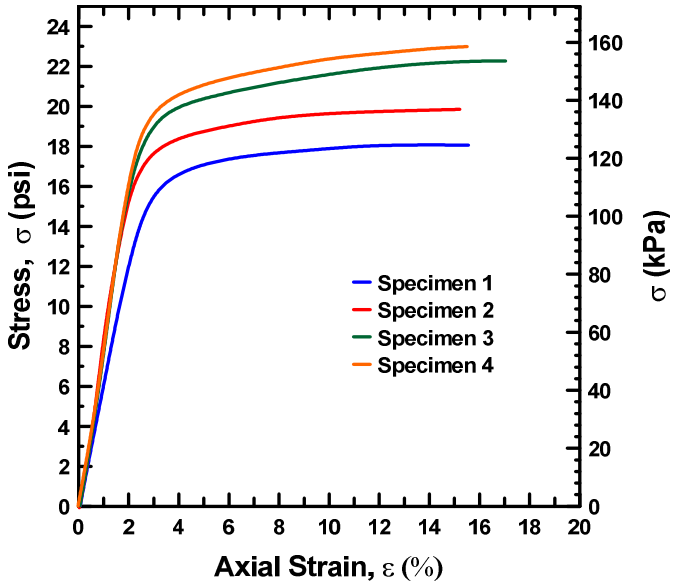

Figure 3.28 Stress - strain curves of EPS 22 geofoam specimens (Compression test)

Furthermore, the important compression behavior, including the compressive resistance at 1 %, 5 %, and 10 % strain, is estimated and provided in Table 3.10. From the table, it can be observed that one of the four EPS 22 geofoam specimens showed some lower compressive resistances; whereas, the rest of them gave higher values when compared with the minimum values of those properties specified in ASTM C-6817-07.

Table 3.10 Compressive Resistances of EPS 22 Geofoam Samples

Compressive resistances	**Specimen No.**				**Minimum value**
	1	**2**	**3**	**4**	**(ASTM)**
At 1 % strain, psi (kPa)	6.5 (45)	8.7 (60)	8.6 (59)	8.1 (56)	7.3 (50)
At 5 % strain, psi (kPa)	17.2 (118)	18.7 (129)	20.4 (141)	21.0 (145)	16.7 (115)
At 10 % strain, psi (kPa)	17.8 (123)	19.7 (136)	21.6 (149)	22.2 (153)	19.6 (135)

3.3.3.3 Unconfined Compression Strength (UCS) Test

As mentioned in Section 3.2.13, this test was performed in order to investigate the equivalent of unconfined compression strength of EPS 22 geofoam material compared with the normal fill soil. From the tests, it can be observed that most of the specimens failed in buckling shape, as shown in Figure 3.29. This is because the specimens that were tested with the UCS test had a length that was greater than the diameter, which is not in accordance with the specified standard for the compression test (ASTM C-6817-07).

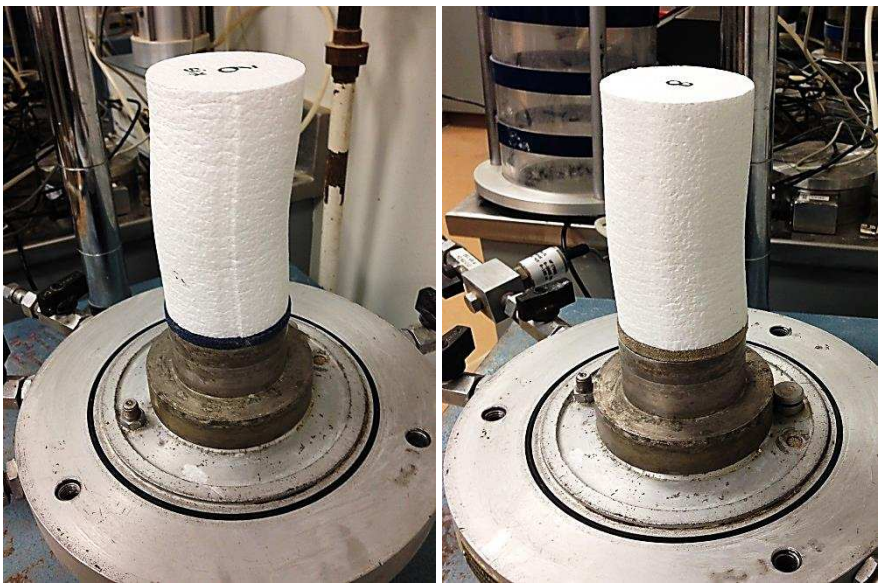

Figure 3.29 Buckling failure occurred on the EPS 22 geofoam specimens

The results obtained from the test were used in the calculation of the stress (σ) and axial strain (ε) developed on the specimen during the test. The plots of stress versus strain of the EPS 22 geofoam specimens are illustrated in Figure 3.30.

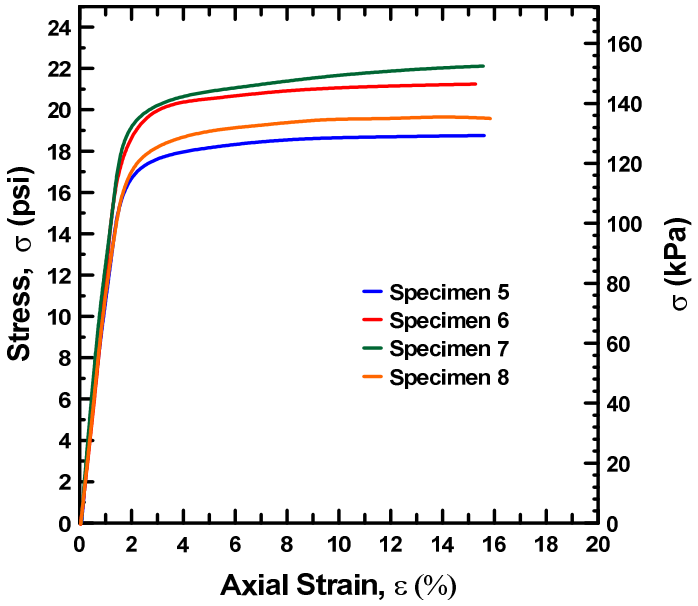

Figure 3.30 Stress - strain curves of EPS 22 geofoam specimens (UCS test)

From the stress-strain curves, the unconfined compression strength, q_u, of the specimens can be estimated as the stress corresponding to 15 % strain. The equivalent undrained shear strength (s_u) of the EPS 22 geofoam can be calculated as half of q_u. Table 3.11 presents the values of q_u and s_u of the tested EPS 22 geofoam specimens.

Table 3.11 Unconfined Compression Strength (q_u) and Undrained Shear Strength (S_u) of EPS 22 Geofoam Specimens

EPS 22 Geofoam Specimens	**q_u psi (kPa)**	**s_u psi (kPa)**
Specimen No. 5	18.7 (129)	9.35 (64.5)
Specimen No. 6	21.2 (146)	10.6 (73)
Specimen No. 7	22.0 (152)	11.0 (76)
Specimen No. 8	19.5 (134)	9.75 (67)

3.4 Summary

This chapter presents the laboratory testing program conducted on embankment fill soil and foundation soil collected from the test site (i.e., the bridge located on US 67 over SH 174 in Cleburne, Texas), as well as the EPS22 geofoam specimens. The embankment fill and foundation soils were classified, based on the unified soil classification system (USCS), as clayey sand (SC) soil and low-to-medium plasticity clay (CL,) respectively. The soils were also tested to evaluate their compressibility and strength characteristics. The results obtained from laboratory tests were used as the input parameter in the numerical model analysis created to study the settlement behavior of the test embankment. The compression behavior of EPS22 geofoam was also investigated. The results were compared with the required minimum value specified in the ASTM standard, and these values were in agreement with those reported in the literature.

Chapter 4

Construction and Instrumentation of EPS Geofoam Embankment Test Section

4.1 Introduction

In this study, the lightweight EPS geofoam was selected to be used as an alternative fill material replaced on top of the US 67 bridge approach embankment test site to mitigate the settlement problem underneath the approach slabs. To evaluate the application of EPS geofoam in real field conditions, a study of the EPS geofoam-embedded embankment test section was performed and monitored by using instruments. The instrumentations used for monitoring the field performance included horizontal inclinometer and earth pressure cells.

This chapter presents the site description, procedures of test site construction, and instrumentation used in the field.

4.2 Site Description

During 1995 and 1996, the US 67 bypass was constructed in Cleburne, Texas to divert US Highway 67 traffic around the downtown district. One of the four bridges constructed in the project is the 40-ft high overpass bridge situated at the intersection between US 67 and State Highway 174. as illustrated in Figure 4.1. The bridge was designed for two-lane traffic conditions. Both ends of the bridge structure were placed on the abutments supported by drilled-shaft foundations. Adjacent to the bridge abutments, approach embankments were built to support the interfacing bridge approach slabs and roadways. Within approximately 16 years after the initial construction, the approach slab of the bridge had experienced approximately 17 inches of settlements, as shown in Figure 4.2. During that period, several treatment methods, including hot mix overlays,

grout injections, soil nailings, and others were attempted; however, those methods were not proven to be effective in mitigating the settlements.

Figure 4.1 Location of the test site: Cleburne, TX (source: Google Earth)

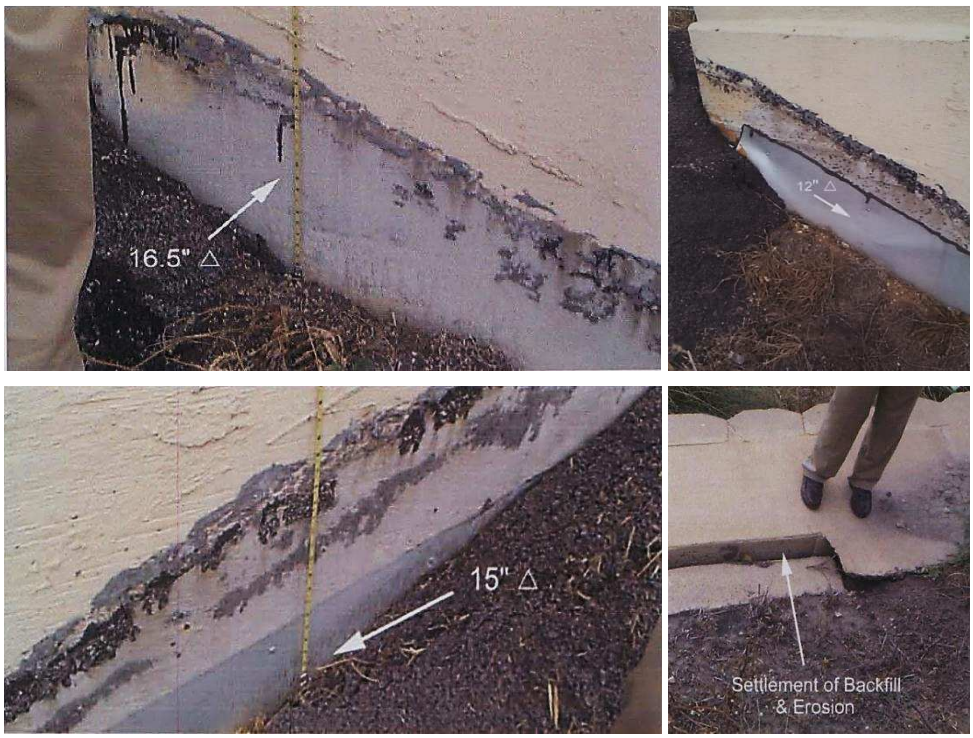

Figure 4.2 US 67 bridge approach settlement occurred in 16 years since the initial construction (Courtesy of TxDOT)

4.3 Construction of Test Section

In order to alleviate the settlement problems that occurred on the approach embankments of the overpass bridge situated on US 67 over SH 174 in Johnson County, Cleburne, Texas, the research team worked with TxDOT's Fort Worth district to study the potential of using the Geofoam embankment system to mitigate settlements. This is because the geofoam can reduce the loads acting on existing soils by replacing parts of the embankment with this lightweight fill material. For this reason, EPS 22 geofoam blocks were recommended to be used as the fill material. This material was used to replace a 6 ft. depth of the top part of the embankment on the east end of the bridge for the present test section (see Figure 4.1).

The rehabilitation work began in January 2012 and was completed at the end of February 2012. At the beginning of this work, 9 to 10 ft. of the original fill material was excavated, and the underdrain systems were installed at the bottom of the excavation. Following that, 2 to 6 inches of a sand-leveling layer was compacted on the underdrain systems, as presented in Figure 4.3. The 6 ft. high stack of three layers of the EPS 22 geofoam was then encapsulated with a layer of impermeable geomembrane and was placed on the compacted sand blanket. Figure 4.4 shows the barbed plates used to connect the EPS geofoam blocks, and Figure 4.5 illustrates the process of geofoam removal and installation.

The EPS geofoam's shape adjustment for filling in narrow spaces between the bridge abutment wall and geofoam blocks is shown in Figure 4.6. The layer of EPS geofoam completely filled in the embankment and encapsulated it with a layer of geomembrane, as presented in Figure 4.7. Finally, about 2 ft. height of the pavement structure, including lightweight aggregates, flex base, hot mix asphalt concrete (HMAC),

and concrete pavement, was constructed on top of the embankment. The layers of fill materials and dimensions of the repaired embankment as illustrated in Figure 4.8.

Figure 4.3 Compaction of sand leveling layer

Figure 4.4 Barbed connection plates for geofoam

Figure 4.5 Geofoam removal and installation

Figure 4.6 Geofoam's shape adjustment for filling in narrow space

Figure 4.7 EPS geofoam layer encapsulated with a layer of geomembrane

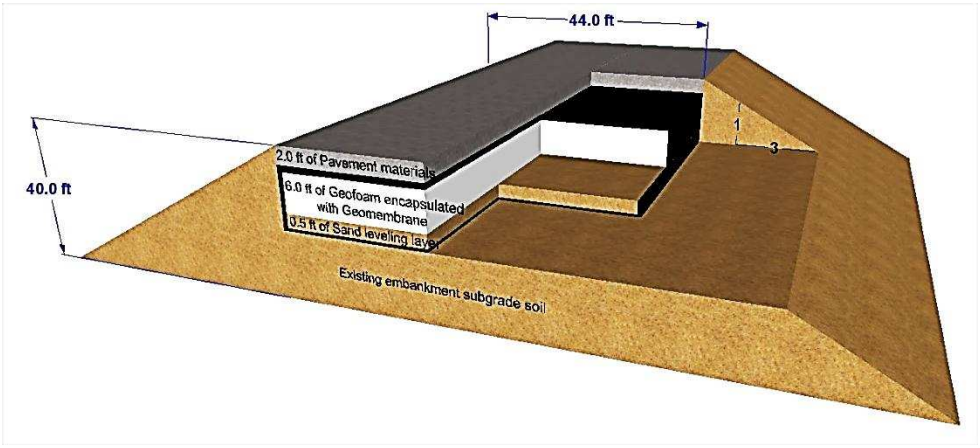

Figure 4.8 Dimension and layers of fill materials in the repaired embankment (not to scale)

4.4 Instrumentation

In order to evaluate the effectiveness of the geofoam material in mitigating the settlement problem of the embankment system, the field test site was instrumented with horizontal inclinometers and pressure cells for monitoring the settlement and loading behaviors of the embankment. The details of the instruments used and the installation procedures followed are presented in the subsequent sections.

4.4.1 Horizontal Inclinometer

The general definition of an inclinometer is the device that is used for monitoring deformations of surfaces or subsurface, in a direction perpendicular to the axis of a flexible plastic casing, by means of passing a probe through the casing (EM 1110-2-1908-US Army Corps). It can be clearly understood by the definition that the typical application of a horizontal inclinometer is to measure the settlement and/or heave under storage tanks, dams, and embankments. (Archeewa, 2010). The horizontal inclinometers generally consists of seven components: inclinometer casing, horizontal probe, pull-cap, pull cable, dead-end pulley, control cable, and readout. However, in this study, the

components used for passing the probe through the casing were modified by using a long connected pipe delivering the probe into the casing instead of using the pull cable with the dead-end pulley to pull the probe. The inclinometer casing is an acrylonitrile butadiene styrene (ABS) plastic pipe, which has four grooves inside, perpendicular to each other. The typical details of the casing used in this study are presented in Figures 4.9 and 4.10. More details about preparing and assembling the casings can be searched in Slope Indicator (2011).

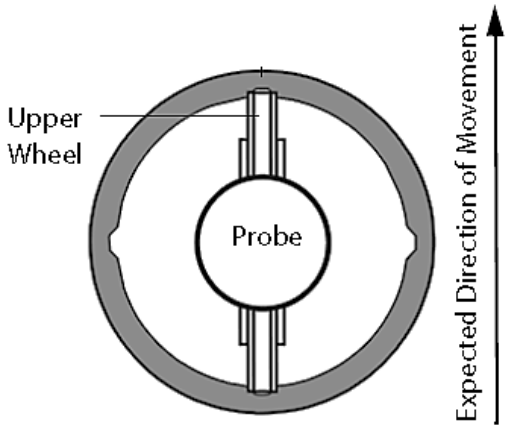

Figure 4.9 The grooves inside inclinometer casing (Slope Indicator, 2011)

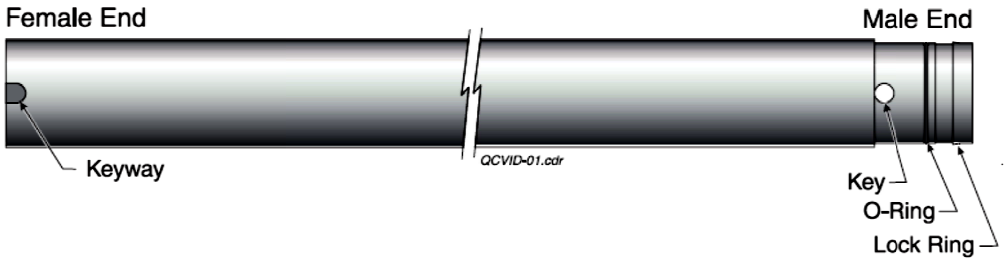

Figure 4.10 Detail of assembling system of the inclinometer casing
(Slope Indicator, 2009)

During the reconstruction of the test embankment, the total four inclinometer casings of diameter 3.34 in. (8.5 cm) were placed on the top of EPS 22 geofoam layer, about 2 ft. (0.6 m) below the pavement surface, in the test embankment. The length of each casing is more than 22 ft. (6.7 m). The positions of the installed inclinometer casings are illustrated in Figure 4.11.

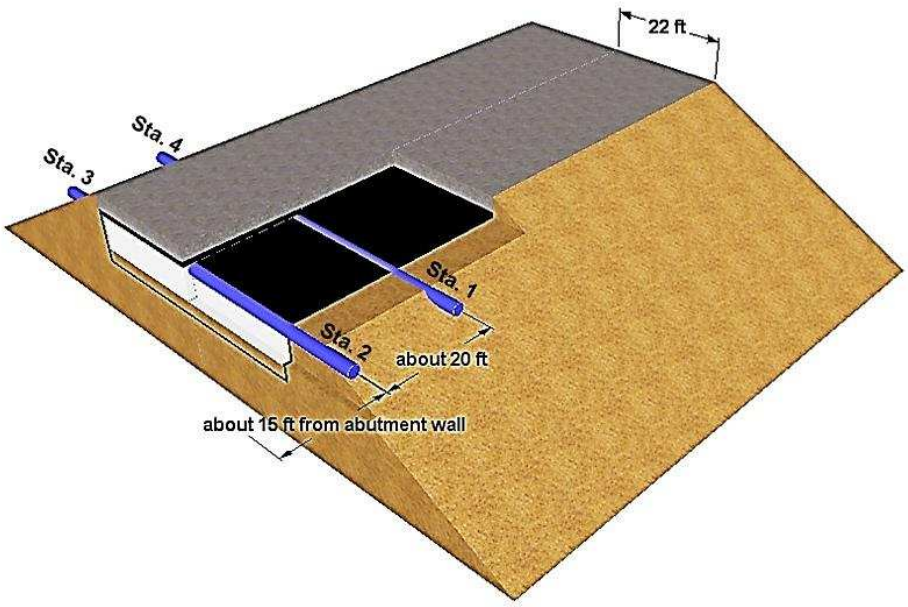

Figure 4.11 Positions of the inclinometer casings installed in the test embankment

The following steps describe the procedure of installation of inclinometer casings in the test embankment:

1. After completing the installation of compacted EPS 22 geofoam blocks in the test embankment, the four trenches fitting to the size of inclinometer casing were excavated at selected locations. According to the Slope Indicator manual (2006), a gradient of 3% is maintained along the length of the casing for drainage. Figure 4.12 presents a trench prepared for installation of the inclinometer casing.

2. The trenches were then cleaned. After that, the casings were carefully placed into the trenches, as illustrated in Figure 4.13. The casings were closed at the end that was embedded in the embankment; whereas, the other end that extended out of the embankment was covered with a cap.
3. The vertical of a pair of top and bottom grooves was checked at initiation and when the casings were assembled.
4. The trenches were backfilled with compacted sand and then covered with a layer of geomembranes, as shown in Figure 4.14.
5. Finally, the extended end of the casings was fastened with cast-in-place concrete bases. See Figure 4.15.

Figure 4.12 Trench prepared for installing the inclinometer casing

Figure 4.13 Inclinometer casing placed in prepared trench

Figure 4.14 Backfilled trenches and covering geomembrane

Figure 4.15 Cast-in-place concrete base

An inclinometer survey consists of readings acquired from two passes of the horizontal probe through the inclinometer casing. Figure 4.16 shows the schematic diagram of the horizontal probe. The probe has identical connectors at each end. In the first pass, the connector 2 is connected to the control cable and readout device. Then, the connectors are swapped and the second pass is conducted. The wheels on one side of the probe are fixed. These fixed wheels are always kept in the bottom groove of the casing during the inclinometer survey.

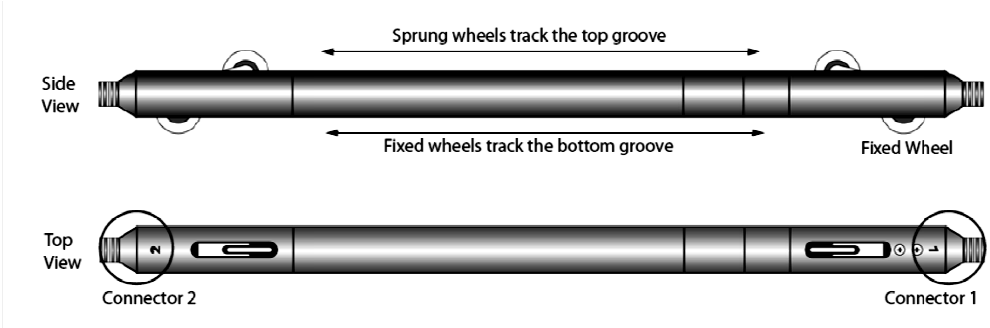

Figure 4.16 Schematic diagram of horizontal probe (Slope Indicator, 2006)

The probe is delivered into the casing with a long connected pipe. The readings are taken every two feet, beginning at the far end of the casing, and are recorded with the readout device called Digitilt DataMate. The profile of the casing can be obtained by plotting the measurements. Any change in the profile of the casing compared to the initial profile from a subsequent survey indicates surface movement. Figure 4.17 presents the process of the inclinometer survey performed at the test site.

(a) (b)

(c) (d)

Figure 4.17 Process of an inclinometer survey: (a), (b), and (c) the process of passing horizontal probe into a casing; and (d) Digitilt DataMate used to record the readings

4.4.2 Pressure Cells

The earth pressure cell, also known as total pressure cell, is the device used in the applications of monitoring total pressure exerted on a structure to verify design assumption and determine the magnitude, distribution, and orientation of stresses (Slope Indicator, 2004). The pressure cell is made from two circular stainless steel plates welded together around their edges to form a sealed cavity. The cavity is filled with a non-compressible fluid and a pressure transducer is connected to the cell. In the present study, four pressure cells have been installed at different locations in the reconstructed embankment. The details of the pressure cell locations are provided in Table 4.1, presented below.

Table 4.1 Pressure Cell Locations (source: TxDOT)

Pressure Cell No.	**1**	**2**	**3**	**4**
Serial Number	09-1836	09-1837	09-1833	09-1834
Longitudinal distance	10 ft. east of east abutment	10 ft. east of east abutment	On east abutment backwall	On inside of north wingwall
Transverse distance	10 ft. south of north wingwall	10 ft. south of north wingwall	13 ft. south of north wingwall	9.3 ft. west of north wingwall
Depth	8 ft. below pavement surface	2 ft. below pavement surface	34 in. below bottom of north wingwall rail	45 in. below bottom of north wingwall rail
Date Placed	Jan. 17, 2012	Jan. 19, 2012	Jan. 18, 2012	Jan. 18, 2012

During the reconstruction of the test embankment, two pressure cells were embedded in the sand-leveling layer and in the top part of the EPS 22 geofoam layer; whereas, the other two pressure cells were attached to the east abutment backwall and to the inside of the north wingwall. In the case of embedded ones in fill, the cells were placed in excavated pockets and covered with hand-compacted fill before the normal fill and compaction operations resumed. Figure 4.18 presents the pressure cells installed in the test embankment.

Figure 4.18 The pressure cells installed in the test embankment

In this study, a compact data logger named Quattro Logger was used to monitor the four installed pressure cells. After installation, the pressure cells were connected to the Quattro Logger which was set to record the data from the pressure cells once per 15 minutes. The recorded data stored in the logger was retrieved via Manager software. The software needs to be installed in a computer prior to connecting the Quattro Logger. Figure 4.19 presents the external and internal appearance of the Quattro Logger.

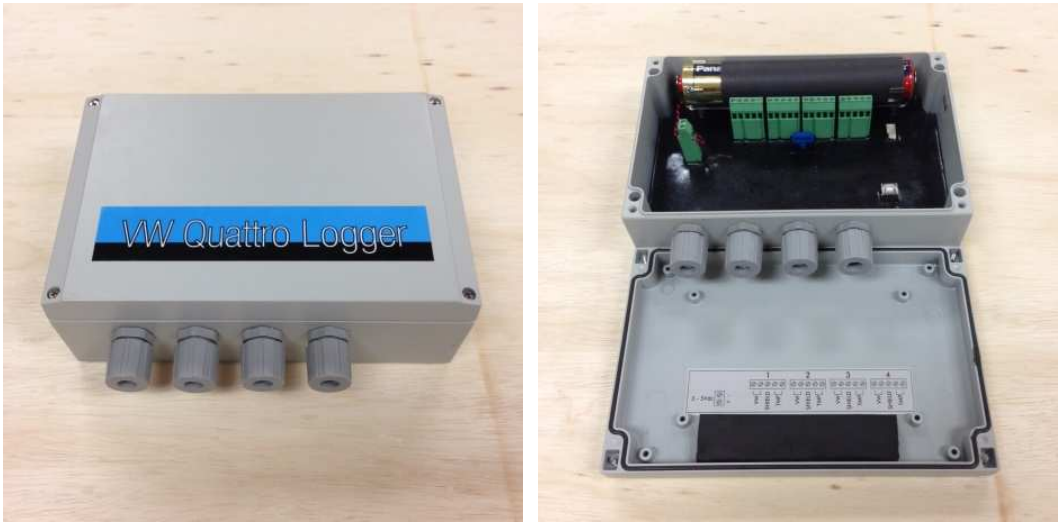

(a) (b)

Figure 4.19 Quattro Logger: (a) external appearance and (b) inside

4.5 Summary

This chapter presents the construction procedure on the test embankment and field instrumentation used to study settlement behavior of the embankment and pressure response of EPS geofoam blocks. The EPS22 geofoam was used to replace the top 6ft. of the approach embankment adjacent to the bridge on US 67 in Cleburne, Texas in order to mitigate the bridge approach settlement problem. Horizontal inclinometers and pressure cells were installed in the test embankment during the construction process. The results obtained from field visual inspection and filed instrumentation data are discussed and analyzed in the next chapter.

Chapter 5

Analysis of Field Monitored Data

5.1 Introduction

In this study, the field performance monitoring data from January 2012 to October 2014 was comprehensively analyzed to address the efficacy of the Geofoam section to mitigate the settlement of the high embankment. The field visits for collecting monitoring data from the horizontal inclinometer and pressure plates were performed every week for the first three months, and then once every two weeks thereafter for another three months. After that, the data collection was made at least once a month. The collected field data and its analysis are provided in this section.

5.2 Visual Inspections

During the site visits, visual inspections were performed to investigate the performance of the reconstructed EPS geofoam embankment. The figures provided in following present the external appearances of the embankment at several different times after being open to traffic. Figure 5.1 was taken in August 2014, 30 months after being open to traffic, and presents the bridge approach slab constructed on the test embankment. An insignificant differential settlement between the approach slab and bridge structure was observed. However, more than 1 in. (25.4 mm) of differential settlement between the sections of pavement with and without the EPS geofoam layer was noticed within a few months after the test sections were subjected to the traffic, as illustrated in Figure 5.2. In November 2013, more than 3 in. (76.2 mm) of the differential settlement happened at the section where the horizontal inclinometer (HI #2) casing had been installed and caused a break in the casing, as presented in Figure 5.3. The broken

HI #2 casing was repaired in June 17th 2014. The appearance of the HI #2 casing after the repair is shown in Figure 5.4.

Figure 5.1 Bridge approach slab constructed on the EPS geofoam layer

Figure 5.2 Differential settlements occurred in a few months after opening to the traffic

Figure 5.3 Differential settlement occurred in November 2013

Figure 5.4 HI #2 inclinometer casing after repairing

5.3 Pressure Responses of the EPS Geofoam Embankment

As mentioned in the previous chapter, four pressure cells were installed at different locations in the reconstructed embankment. Two of the total four pressure cells (PC #1 and PC #2) were installed horizontally at 2 ft. (0.6 m) and 8 ft. (2.4 m) under the pavement surface to monitor the vertical pressures on top and bottom of the geofoam layer. The other two pressure cells (PC #3 and PC #4) were attached vertically on the east abutment back wall and on the inside of the north wingwall for monitoring lateral pressures induced by the geofoam layer.

The pressure cells were connected to a compact data logger which was set to record the pressure data every 15 minutes. The recorded data stored in the logger were downloaded at all of site visits. Figure 5.5 presents the plots of the pressure data obtained from the pressure cells with time. The data presented in the plots was collected from March 2012 to August 2014. It can be noticed from the plots that the average vertical pressure of 4.9 psi (33.8 kPa) and 1.8 psi (12.4 kPa) were obtained from pressure cells, PC #1 and PC #2, respectively. However, the lateral pressures obtained from the pressure cells PC #3 and PC #4, showed negative values, which do not quite represent the true field behavior. This may be because the vertically-installed pressure cells, PC #3 and PC #4, were not in proper contact with the installed EPS geofoam layer and abutment walls.

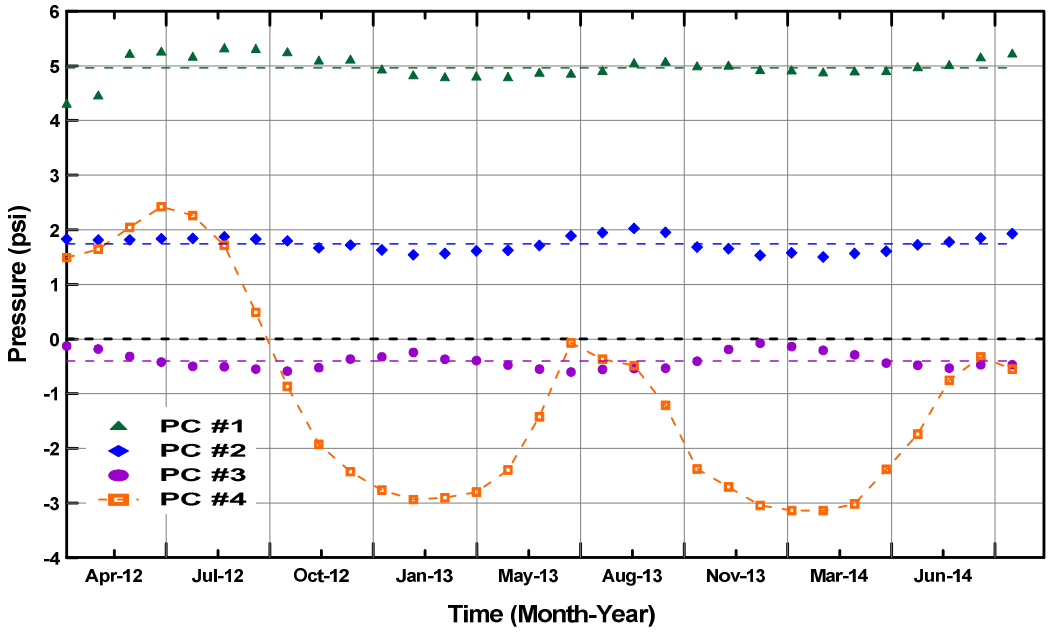

Figure 5.5 Pressure data collected from the installed pressure cells

5.3.1 Analysis of Vertical Stress Distribution in EPS Geofoam Layer

According to Frydenlund and Aaboe (2001), the load distribution mechanisms in EPS geofoam fills are complicated and are not fully understood. Tsukamoto (2011) proposed the chart of vertical stress distribution in a pavement system and EPS geofoam layer, as presented in Figure 5.6. The chart is provided in the EPS embankment design method by the EPS method Development Organization (EDO), Japan. The load distribution angle measured vertically inside the EPS geofoam layer is assigned to be 20 degrees. Besides that, the NCHRP Report 529 (2004) proposes a simple approach for estimating the vertical stress distribution in the EPS geofoam embankment from traffic loads. The method of 2V:1H distribution is recommended to be used in the calculation of vertical stress distribution in the EPS geofoam layer.

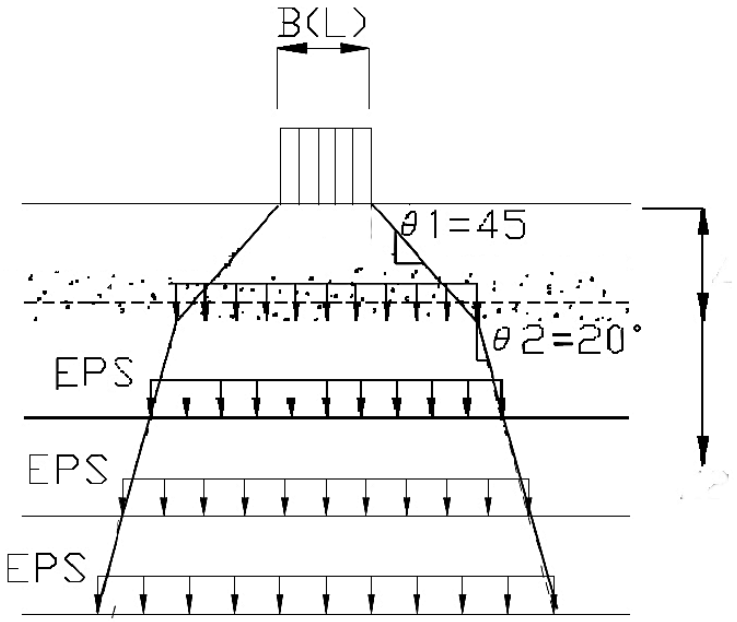

Figure 5.6 Vertical stress redistribution chart for EDO design method (Tsukamoto 2011)

The vertical stress results obtained from the pressure cell PC #1 installed at the bottom of the layer of stacked EPS geofoam blocks ($\sigma_{PC\ \#1}$) can be used to analyze the stress distribution in the EPS geofoam material. Other parameters needed in the analysis consist of the design dead weight of a concrete pavement system, the density of EPS 22 geofoam, and design live loads from traffic. Based on the preliminary design of the test embankment, the design stress for the dead weight of the concrete pavement system ($\sigma_{pavement}$) is 2.4 psi (16.55 kN/m^2). The unit weight of EPS 22 geofoam defined in ASTM D 6817-07 is 1.35 pcf (0.22 kN/m^3), and according to AASHTO LRFD Bridge Design Specification (2012), the standard truck HS-20 (a 20-ton semi-trailer truck) is used as the design truck for a bridge design. The design live loads ($\sigma_{design\ LL}$) of 6.68 psi (46.0 kN/m^2)

is estimated to be used in this analysis. The details of the design live loads calculation is provided in Chapter 6.

Based on the stress observations and the values of related parameters provided previously, the stress distribution from the design live load in the EPS geofoam layer was estimated. The following equations present a rough calculation of the stress increase induced by the design live loads ($\Delta\sigma_{LL}$) at the bottom of the 6-ft depth EPS geofoam layer:

$$\Delta\sigma_{LL} = (\sigma_{PC\ \#1}) - (\sigma_{pavement}) - (\gamma H)_{EPS\ geofoam} \quad (5.1a)$$

$$\Delta\sigma_{LL} = (4.9\ psi) - (2.4\ psi) - [(1.35\ pcf) \times (6\ ft) \times (0.00694) psi] \quad (5.1b)$$

$$\Delta\sigma_{LL} = 2.44\ psi \quad (16.55\ kN/m^2) \quad (5.1c)$$

From the calculation, it can be observed that about 36.5% of the design live load was distributed to the bottom of the 6 ft. deep EPS geofoam layer. The result was slightly different from the vertical stress distributions calculated by EDO design method and 2V:1H distribution method. The load distribution angle, inside the EPS geofoam layer, of about 16 degrees measured vertically can be estimated from the stress observations results. This load distribution angle is close to the one specified in the EDO design method (i.e., 20 degrees).

5.4 Vertical Movement of the Test Embankment

In addition to the pressure response of the EPS geofoam backfill, the field observation program was also planned to assess the settlement behavior of the EPS geofoam embankment. As previous discussed, four inclinometer casings were installed on the top of EPS 22 geofoam layer in order to measure the vertical movement of the test embankment. The details of the horizontal inclinometer probe and the locations and

installation procedure of the inclinometer casings were explained and presented in the previous chapter.

Vertical displacements at the top of the EPS geofoam layer were measured at 2 ft. intervals, beginning at the far end of the inclinometer casings. The collected data is presented in the form of graphs plotted between the vertical displacements in inch versus the length of the casing, in feet. The vertical displacements were recorded cumulatively from the initial one at the time of installation (01/30/2012), which is used as a reference, until October 2014. However, in this section, the data had been collected from January 2012 to August 2014 is used in analysis.

Figures 5.7 to 5.10 present the settlement data collected from the horizontal inclinometer casings HI #1 to HI #4, respectively. It can be noticed that the data of the casing HI #2 from November 2013 to May 2014 were missing because in the range of that time, the casing HI #2 had been broken. It was fixed on June 17^{th,} 2014; however, the results received from the casing HI #2 after the repair show that the settlement of the embankment was less than what is expected. For the others casings, the maximum settlements of about 1.25 in. (32 mm) to 1.50 in. (38 mm) have been observed at the middle of the pavement (the distance of 20 ft.in the plots). Moreover, the settlement data measured from inclinometer casings HI #1, HI #3, and HI #4 in the last six months is slightly changed.

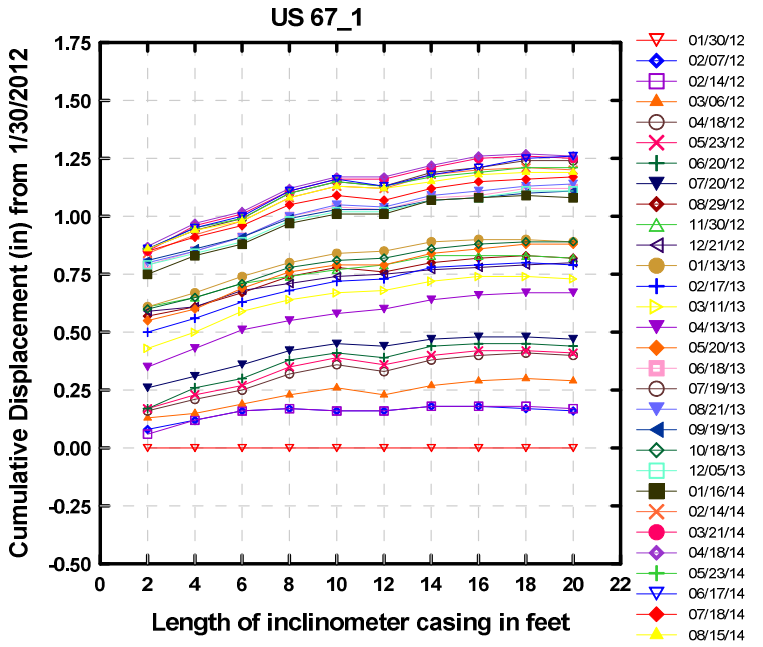

Figure 5.7 Cumulative vertical displacements recorded from inclinometer casing HI #1

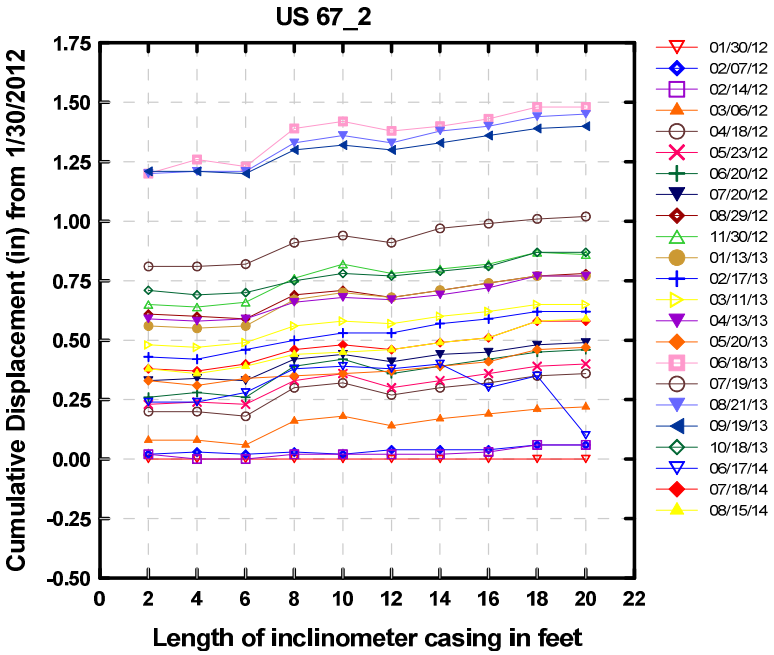

Figure 5.8 Cumulative vertical displacements recorded from inclinometer casing HI #2

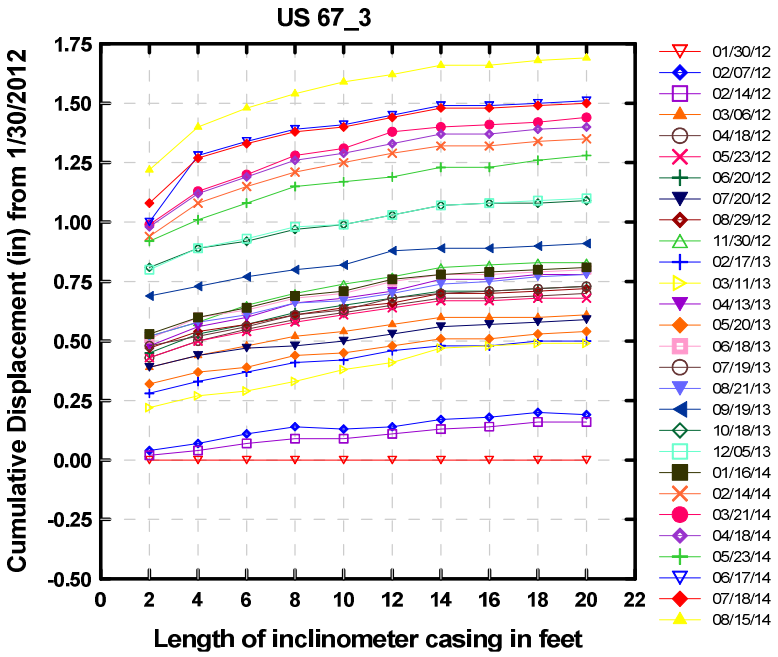

Figure 5.9 Cumulative vertical displacements recorded from inclinometer casing HI #3

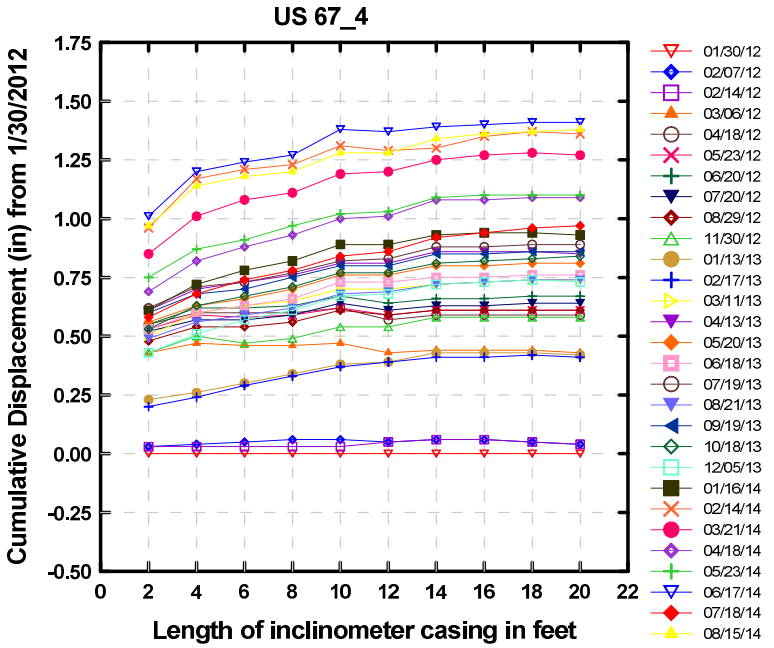

Figure 5.10 Cumulative vertical displacements recorded from inclinometer casing HI #4

Considering the maximum vertical movements of the test embankment measured at the middle of the pavement, the plots of vertical displacement of the embankment versus time can be provided, as illustrated in Figure 5.11. The vertical displacements plotted in the graph were calculated as an average of the data collected from the four inclinometer casings. In the plot, there are two sets of the displacement data, which are blue and orange sets.

The blue dots and a dash line present the total vertical displacement, including those obtained during the embankment reconstruction process. The orange dots and a dash line present the vertical displacement of the embankment after the reconstruction was completed. The total vertical displacement increased considerably at the beginning and gradually increased with time. The trend of the total vertical displacement became constant at the settlement of about 1.30 to 1.40 in. (33 to 35.6 mm).

The vertical displacement of about 0.25 in. (6.35 mm) occurring during the reconstruction process (i.e., 28 days from the casing installation) was estimated from the graph. The average vertical settlement of the embankment that occurred at any time after reconstruction can be determined by subtracting the settlement that occurred at 28 days from the data of total vertical settlement that had occurred at that time. The maximum vertical displacement of the embankment excluded the displacement that occurred during the reconstruction process and was estimated from the plot and the magnitude of the displacement to be about 1.0 to 1.1 in. (25.4 to 28 mm).

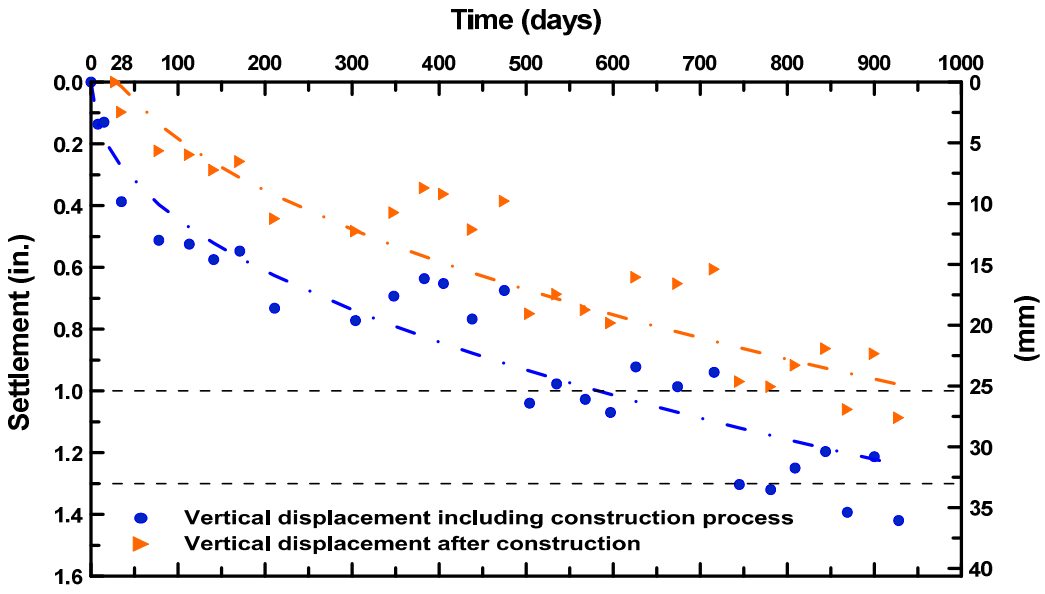

Figure 5.11 Plot of average vertical displacement of the test embankment versus time

5.4.1 Statistical Analysis of the Post-Construction Vertical Displacement Data

As mentioned previously in Chapter 2, the thresholds for initiation of repair of the bridge approach settlement problem have been proposed in several literatures. According to Long et al. (1998), the differential settlement of 1 in. (25 mm) is considered as a slight bump; whereas, the differential settlement of 2 in. (51 mm) and 3 in. (76 mm) or larger is regarded as a moderate bump and a significant bump, which require a repair, respectively.

In this section, the data of post-construction vertical displacement which occurred at the middle of the pavement on the test embankment was statistically analyzed. The statistical analysis was performed in order to check whether the post-construction settlement which occurred from March 2012 to August 2014 was less than 1.0 in. (25 mm), which is regarded as the slight bump. However, because the data collected from the inclinometer casing HI #2 was missing during November 2013 to May 2014, due to

the break in the casing; thus, the data received from the casing HI #2 is not included in this analysis. The post-construction vertical displacement data obtained from the inclinometer casings HI #1, HI #2, and HI #4, as presented in Table 5.1, was used in this analysis. It should be noted that the data was measured at the middle of pavement and was collected almost every month.

Table 5.1 Post-construction Vertical Displacement Measured at the Middle of Pavement from March 2012 to August 2014

Date	**Vertical displacement after construction (in)**				
	HI #1	**HI #3**	**HI #4**	$y_{i.}$	$\bar{y}_{i.}$
03/06/2012	0.04	0.16	0.13	0.33	0.11
04/18/2012	0.15	0.25	0.29	0.69	0.23
05/23/2012	0.16	0.23	0.31	0.70	0.23
06/20/2012	0.19	0.28	0.37	0.84	0.28
07/20/2012	0.22	0.14	0.34	0.70	0.23
08/29/2012	0.57	0.27	0.31	1.15	0.38
11/30/2012	0.57	0.38	0.28	1.23	0.41
01/13/2013	0.64	0.32	0.12	1.08	0.36
02/17/2013	0.54	0.05	0.11	0.70	0.23
03/11/2013	0.48	0.04	0.44	0.96	0.32
04/13/2013	0.42	0.33	0.55	1.30	0.43
05/20/2013	0.63	0.09	0.51	1.23	0.41
06/18/2013	0.87	0.35	0.46	1.68	0.56
07/19/2013	0.99	0.28	0.59	1.86	0.62
08/21/2013	0.89	0.33	0.44	1.66	0.55
09/19/2013	0.86	0.46	0.56	1.88	0.63
10/18/2013	0.64	0.64	0.54	1.82	0.61
12/05/2013	0.86	0.65	0.43	1.94	0.65
01/16/2014	0.83	0.36	0.63	1.82	0.61
02/14/2014	0.95	0.90	1.06	2.91	0.97
03/21/2014	1.00	0.99	0.97	2.96	0.99

Table 5.1 – *Continued*

Date	Vertical displacement after construction (in)				
	HI #1	HI #3	HI #4	$y_{i.}$	$\bar{y}_{i.}$
04/18/2014	1.01	0.95	0.79	2.75	0.92
05/23/2014	0.96	0.83	0.80	2.59	0.86
06/17/2014	1.01	1.06	1.11	3.18	1.06
07/18/2014	0.92	1.05	0.67	2.64	0.88
08/15/2014	0.94	1.24	1.08	3.26	1.09
$y_{.j}$	17.34	12.63	13.89	$y_{..}$ = 43.86	
$\bar{y}_{.j}$	0.67	0.49	0.53	$\bar{y}_{..}$ = 0.56	

The different locations of the inclinometer casings probably have an effect on the data observations; however, the effect is not significantly interesting. Therefore, the locations of casings HI #1, HI #3, and HI #4 can be considered as a nuisance factor. Because the existence of the nuisance factor is known and it will not change levels while the experiment is being conducted, the location of the casings is classified as a known and controllable nuisance factor. According to Montgomery (2013), the effect of the known and controllable nuisance factor can be systematically eliminated by using the statistical technique called blocking. Based on Table 5.1, it can be noticed that each block of the table contains all the data. Therefore, the technique called randomized complete block design (RCBD) was selected to be used in analyzing this data.

In this analysis, the equality of the vertical displacement means was first tested by using RCBD technique. Then, the Fisher Least Significant Difference (LSD) method was used to make comparisons among the vertical displacements. Finally, the data in the months which have statistically equal and highest means was used for claiming that the post-construction vertical displacement was less than the thresholds for initiation of repairing.

5.4.1.1 Statistical Analysis for the RCBD

The randomized complete block design of ***a*** treatments and ***b*** blocks is shown in Figure 5.12. Only one observation per treatment is presented in each block, and the order in which the treatments are run within each block was determined randomly (Montgomery, D. C. 2013).

Treatment	Block 1	Block 2		Block 3
1	y_{11}	y_{12}		y_{1b}
2	y_{21}	y_{22}		y_{2b}
3	y_{31}	y_{32}	…	y_{3b}
.	.	.		
.	.	.		
.	.	.		
A	y_{a1}	y_{a2}		y_{ab}

Figure 5.12 The randomized complete block design (Montgomery, D. C. 2013)

The statistical model for the RCBD is given as:

$$y_{ij} = \mu + \tau_i + \beta_j + \epsilon_{ij} \quad ; i = 1, 2, \ldots, a;\ j = 1, 2, \ldots, b \qquad (5.2)$$

when μ is an overall mean; τ_i is the effect of the i th treatment; β_j is the effect of the j th block; and ϵ_{ij} is a random error term. The main assumptions of this model are that the errors are normally and independently distributed with mean zero and constant, but unknown variance σ^2, and the treatment and block effects are considered as deviations from the overall mean. So that:

$$\epsilon_{ij} \sim NID\ (0, \sigma^2); \sum_{i=1}^{a} \tau_i = 0; \text{ and } \sum_{j=1}^{b} \beta_j = 0 \qquad (5.3)$$

In an experiment involving the RCBD, testing of the equality of the treatment means is taken an interest. The testing hypotheses can be set up as:

$$H_o: \mu_1 = \mu_2 = \mu_3 = \cdots = \mu_a \text{ and } H_1: \text{at least one } \mu_i \neq \mu_j \quad (5.4)$$

The testing hypotheses presented in Eq. (5.4) can be written in an equivalent way in terms of the treatment effects:

$$H_o: \tau_1 = \tau_2 = \cdots = \tau_a = 0 \text{ and } H_1: \tau_i \neq 0 \text{ at least one } i \quad (5.5)$$

To test the hypotheses, the analysis of variance (ANOVA) extended to the RCBD is performed. The procedure is usually summarized in an ANOVA table, such as the one presented in Table 5.2.

Table 5.2 Analysis of Variance for a Randomized Complete Block Design

Source of Variation	Sum of Squares	Degree of Freedom	Mean Square	F_o
Treatments	$SS_{Treatments}$	$a-1$	$\frac{SS_{Treatments}}{a-1}$	$\frac{MS_{Treatments}}{MS_E}$
Blocks	SS_{Blocks}	$b-1$	$\frac{SS_{Blocks}}{b-1}$	
Error	SS_E	$(a-1)(b-1)$	$\frac{SS_E}{(a-1)(b-1)}$	
Total	SS_T	$N-1$		

When a is the number of treatments; b is the number of blocks; and N is the number of observations. The formulas to compute $SS_{Treatments}, SS_{Blocks}, SS_E,$ and SS_T are presented below:

$$SS_T = \sum_{i=1}^{a}\sum_{j=1}^{b} y_{ij}^2 - \frac{y_{..}^2}{N} \quad (5.6)$$

$$SS_{Treatments} = \frac{1}{b}\sum_{i=1}^{a} y_{i.}^2 - \frac{y_{..}^2}{N} \quad (5.7)$$

$$SS_{Blocks} = \frac{1}{a}\sum_{j=1}^{b} y_{.j}^2 - \frac{y_{..}^2}{N} \quad (5.8)$$

and

$$SS_E = SS_T - SS_{Treatments} - SS_{Blocks} \quad (5.9)$$

when y_{ij} is the ij th observation; $y_{..}$ is the summation of all observations; $y_{i.}$ is the summation of observations in the *i* th treatment; and $y_{.j}$ is the summation of observations in the j th block.

The null hypothesis (H_o) is rejected if $F_o > F_{\alpha,\ a-1,\ (a-1)(b-1)}$.

5.4.1.2 Testing of the Equality of the Post-Construction Vertical Displacement Means

According to the data presented previously in Table 5.1, the time schedule for collecting the field data and the location of the inclinometer casings is defined as the treatment and block, respectively. The objective of this experimental design is to test the equality of the treatment means. The first step of this test is to set up the testing hypotheses, as presented in following:

Null hypothesis: $H_o: \mu_1 = \mu_2 = \mu_3 = \cdots = \mu_{26}$

and Alternative hypothesis: H_1: at least one $\mu_i \neq \mu_j$

Based on the data given in Table 5.1, the parameters for ANOVA table were calculated as presented in Table 5.3.

Table 5.3 Analysis of Variance (ANOVA)

Source of Variation	Sum of Squares	Degree of Freedom	Mean Square	F_o
Treatments	5.85	25	0.234	6.32
Blocks	0.46	2	0.230	
Error	1.85	50	0.037	
Total	8.16	77		

The test statistic F_o equal to 6.32 was estimated based on Table 5.3. This test statistic was tested against the significance level, α, of 0.05 with the degree of freedom of

the treatment and error equal to 25 and 50, respectively. The value of $F_{\alpha,\ (a-1),\ (a-1)(b-1)}$ = $F_{0.05,\ 25,\ 50}$ obtained from the F-distribution charts was equal to 1.727, which was less than the value of the test statistic. Therefore, the null hypothesis (H_o) was rejected, and it can be concluded that there is a strong evidence to claim that the means of the post-construction vertical displacement measured from March 2012 to August 2014 are not equal. This can be verified by the fact that the vertical displacements changed with the time increment.

Generally, it is unwise to rely on the analysis of variance until the validity of the assumptions of the statistical model have been checked. In order to validate the assumptions and model adequacy, the residuals are investigated for normality and variance. For the RCBD, the residuals (e_{ij}) are calculated from the following equation:

$$e_{ij} = y_{ij} - \bar{y}_{i.} - \bar{y}_{.j} + \bar{y}_{..} \tag{5.10}$$

when y_{ij} is the observation; $\bar{y}_{i.}$ is the average of observations in the *i* th treatment; $\bar{y}_{.j}$ is the average of observations in the *j* th block; and $\bar{y}_{..}$ is the average of all observations.

The residual of the post-construction vertical displacement observations was calculated by employing Eq. 5.10. The predicted values of the displacements were estimated by subtracting the residual from the actual value of the displacement. These values were used to draw the normal quantile plot, the plot of residuals versus predicted values, the plot of residuals versus date (treatments), and the plot of residuals versus location of the inclinometer casings (blocks), as illustrated in Figures 5.13 to 5.16, respectively.

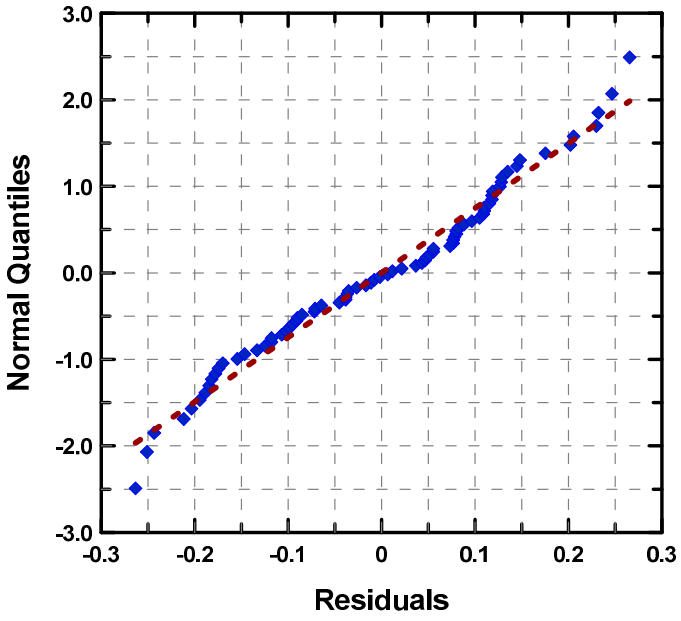

Figure 5.13 Normal quantile plot of residuals

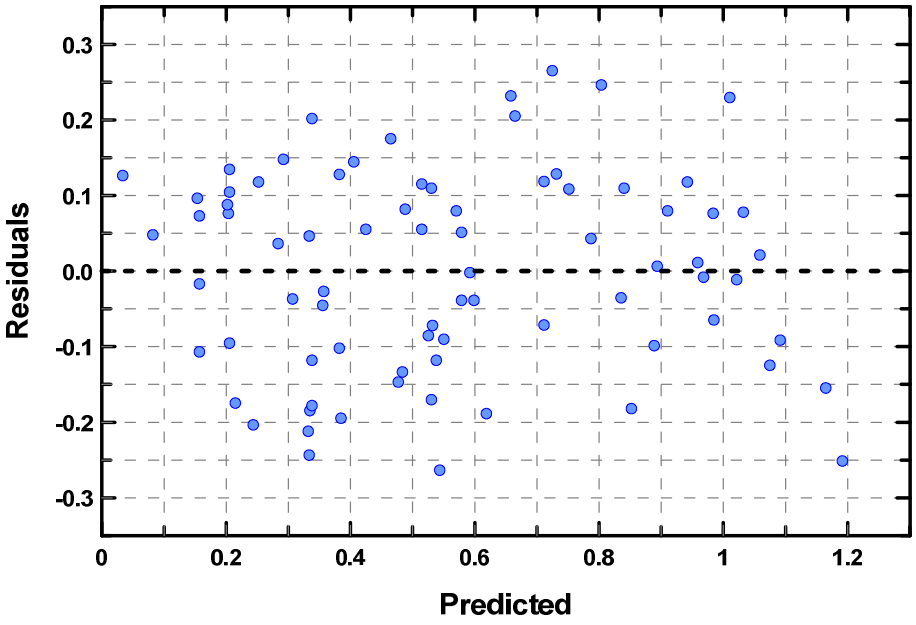

Figure 5.14 Plot of residuals versus predicted values

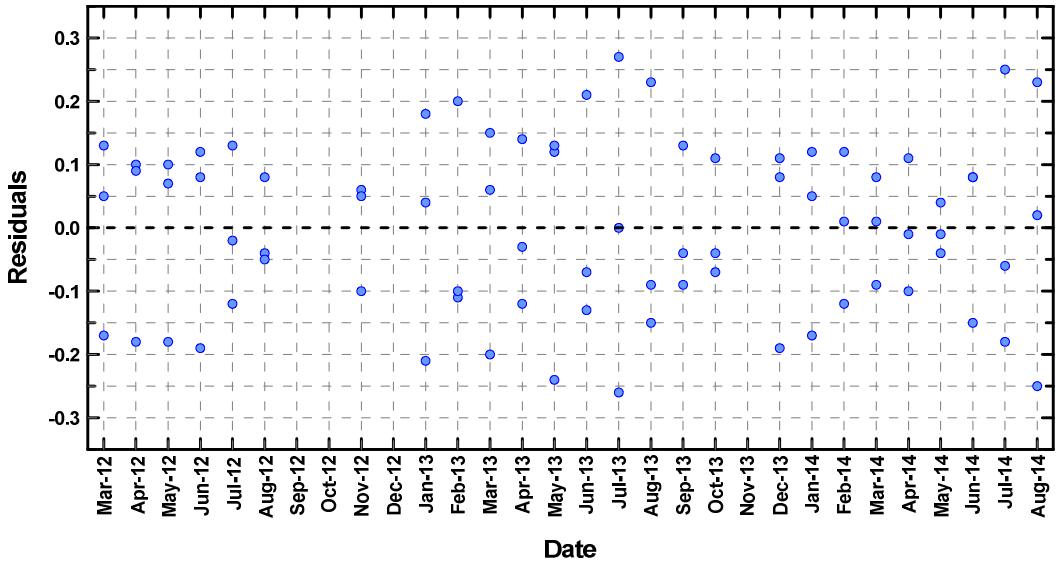

Figure 5.15 Plot of residuals versus date (treatments)

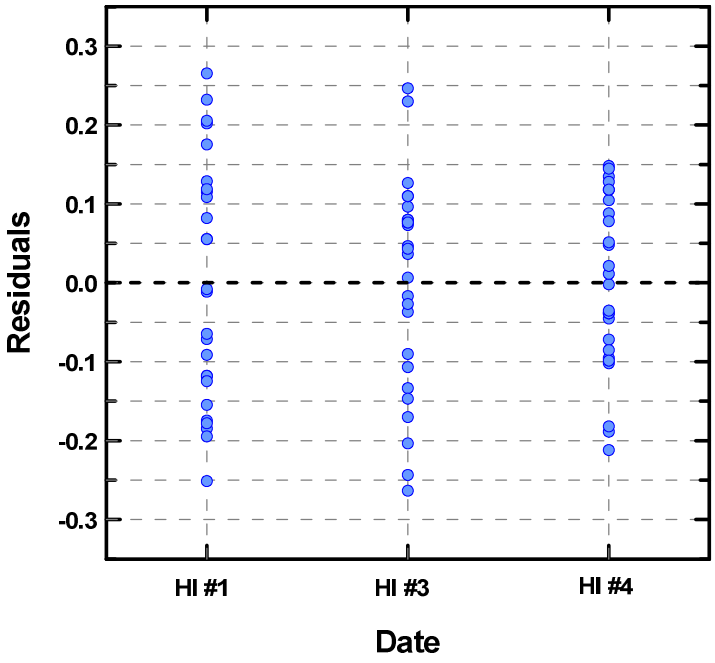

Figure 5.16 Plot of residuals versus the locations of horizontal inclinometer casing (block)

From the figures, it can be observed that the normal quantile plot of the residuals shown in Figure 5.13 was approximately linear. There was no severe indication of non-normality, nor was there any evidence pointing to possible outliers. This indicatedthat the normality assumption was satisfied. The plot provided in Figure 5.14 shows that there was no relationship between the residuals and the predicted values, which means that there was no interaction between blocks and treatments. Whereas, the plot of residuals versus the date (treatment) and locations of horizontal inclinometer casing (block), presented in Figures 5.15 and 5.16, respectively, provided no indication of inequality of variance, the assumption of homogeneity of variances was satisfied. Consequently, it can be concluded that the model is adequate and the analysis of variance can be relied upon.

5.4.1.3 Comparing Pairs of the Post-Construction Vertical Displacement Means

In this section, the Fisher Least Significant Difference (LSD) method is used to make comparisons among the post-construction vertical displacements. Similar to the test of the equality of the treatment means, the significance level, α, of 0.05 is used in the Fisher LSD method. The LSD is calculated as:

$$LSD = t_{\frac{\alpha}{2},\ (a-1)(b-1)} \sqrt{\frac{2\,MS_E}{b}} = t_{0.025,\ 50} \sqrt{\frac{2 \times 0.037}{3}} = 2.009 \times \sqrt{\frac{2 \times 0.037}{3}} = 0.3155 \quad (5.11)$$

The calculated LSD value was compared with the differences in average of the vertical displacement ($\bar{y}_{j.}$) between each pair of the date, which are provided in Table 5.4. It should be noted that the numbers 1 to 26 shown in the table represent the dates of field data measurements. If the difference in average of the vertical displacement is larger than the value of LSD (i.e., 0.3155), it can be concluded that the vertical displacement means for the pair of the date are different.

From the results presented in Tables 5.1 and 5.4 and based on the assumption defined in the Fisher LSD method, it can be concluded that the means of the post-construction vertical displacement measured from February 2014 ($\bar{y}_{20.}$) to August 2014 ($\bar{y}_{26.}$) are equal, and those means are higher than the others. This result confirms that the settlement that occurred on the test embankment has been close to the equilibrium condition.

Table 5.4 The difference in average of the post-construction vertical displacement between each pair of the date of measurement

j	1	2	3	4	5	6	7	8	9	10	11	12	13	14	15	16	17	18	19	20	21	22	23	24	25	26
1																										
2	0.12																									
3	0.12	0.00																								
4	0.17	0.05	0.05																							
5	0.12	0.00	0.00	0.05																						
6	0.27	0.15	0.15	0.10	0.15																					
7	0.30	0.18	0.18	0.13	0.18	0.03																				
8	0.25	0.13	0.13	0.08	0.13	0.02	0.05																			
9	0.12	0.00	0.00	0.05	0.00	0.15	0.18	0.13																		
10	0.21	0.09	0.09	0.04	0.09	0.06	0.09	0.04	0.09																	
11	0.32	0.20	0.20	0.15	0.20	0.05	0.02	0.07	0.20	0.11																
12	0.30	0.18	0.18	0.13	0.18	0.03	0.00	0.05	0.18	0.09	0.02															
13	0.45	0.33	0.33	0.28	0.33	0.18	0.15	0.20	0.33	0.24	0.13	0.15														
14	0.51	0.39	0.39	0.34	0.39	0.24	0.21	0.26	0.39	0.30	0.19	0.21	0.06													
15	0.44	0.32	0.32	0.27	0.32	0.17	0.14	0.19	0.32	0.23	0.12	0.14	0.01	0.07												
16	0.52	0.40	0.39	0.35	0.39	0.24	0.22	0.27	0.39	0.31	0.19	0.22	0.07	0.01	0.07											
17	0.50	0.38	0.37	0.33	0.37	0.22	0.20	0.25	0.37	0.29	0.17	0.20	0.05	0.01	0.05	0.02										
18	0.54	0.42	0.41	0.37	0.41	0.26	0.24	0.29	0.41	0.33	0.21	0.24	0.09	0.03	0.09	0.02	0.04									
19	0.50	0.38	0.37	0.33	0.37	0.22	0.20	0.25	0.37	0.29	0.17	0.20	0.05	0.01	0.05	0.02	0.00	0.04								
20	0.86	0.74	0.74	0.69	0.74	0.59	0.56	0.61	0.74	0.65	0.54	0.56	0.41	0.35	0.42	0.34	0.36	0.32	0.36							
21	0.88	0.76	0.75	0.71	0.75	0.60	0.58	0.63	0.75	0.67	0.55	0.58	0.43	0.37	0.43	0.36	0.38	0.34	0.38	0.02						
22	0.81	0.69	0.68	0.64	0.68	0.53	0.51	0.56	0.68	0.60	0.48	0.51	0.36	0.30	0.36	0.29	0.31	0.27	0.31	0.05	0.07					
23	0.75	0.63	0.63	0.58	0.63	0.48	0.45	0.50	0.63	0.54	0.43	0.45	0.30	0.24	0.31	0.24	0.26	0.22	0.26	0.11	0.12	0.05				
24	0.95	0.83	0.83	0.78	0.83	0.68	0.65	0.70	0.83	0.74	0.63	0.65	0.50	0.44	0.51	0.43	0.45	0.41	0.45	0.09	0.07	0.14	0.20			
25	0.77	0.65	0.65	0.60	0.65	0.50	0.47	0.52	0.65	0.56	0.45	0.47	0.32	0.26	0.33	0.25	0.27	0.23	0.27	0.09	0.11	0.04	0.02	0.18		
26	0.98	0.86	0.85	0.81	0.85	0.70	0.68	0.73	0.85	0.77	0.65	0.68	0.53	0.47	0.53	0.46	0.48	0.44	0.48	0.12	0.10	0.17	0.22	0.03	0.21	

5.4.1.4 Testing to Claim the Mean of the Post-Construction Vertical Displacement Measured from February 2014 to August 2014 is less than 1.0 inch

As discussed in the previous section, the means of post-construction vertical displacement measured from February 2014 to August 2014 were equal, and those means were higher than the others. Therefore, the field data collected in those seven months was used to check whether or not the mean of the post-construction vertical displacements that occurred on the test embankment was less than 1.0 in. (25 mm). The 1.0-in (25-mm) vertical displacement is considered to cause only a slight bump on a bridge approach.

At the beginning, the normal quantile plot of the data measured from February 2014 to August 2014 was drawn, as presented in Figure 5.17, in order to check the assumption that the data is normally distributed. From the figure, it can be observed that the plot is approximately linear. Thus, the normality assumption of the data was satisfied. The values of mean ($\bar{y}$) and standard deviation (S) of the data were also calculated equal to 0.97 in. and 0.125, respectively.

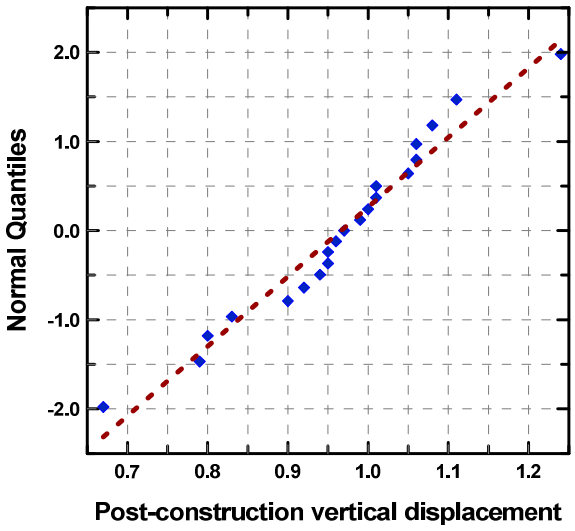

Figure 5.17 Normal quantile plot of the post-construction vertical displacement measured from February 2014 to August 2014

The hypotheses for this test were set up as:

Null hypothesis: $H_o: \mu = 1.0$

and Alternative hypothesis: $H_1: \mu < 1.0$

The test statistic is

$$t_o = \frac{\bar{y} - \mu_o}{S / \sqrt{n}} = \frac{0.97 - 1.0}{0.125 / \sqrt{21}} = -1.0998$$

Use α = 0.05 and from the table of the t-distribution, the value of $-t_{\alpha,\ n-1}$ can be determined:

$$-t_{\alpha,\ n-1} = -t_{0.05,\ 20} = -1.725$$

Because $t_o > -t_{\alpha,\ n-1}$, the null hypothesis (H_o) was not rejected. Consequently, it can be concluded that there is strong evidence to support the conclusion that the mean of the post-construction vertical displacement of the test embankment was currently more than 1.0 inch. However, if the data was changed to be compared with 1.5 in. (38 mm) settlement, the value of t_o would be changed to -19.43.Then, $t_o < -t_{\alpha,\ n-1}$ and the null hypothesis would be rejected. That means that the post-construction vertical displacement was less than 1.5 in. (38 mm).

5.4.2 Prediction of a Long Term Settlement of the Test Embankment

A long term settlement of the test embankment can be predicted from the collected survey data by using the hyperbolic method (Lin and Wong 1999). The rate of settlement is assumed to be decreased hyperbolically with time. The relationship between the settlement and time can be presented by the hyperbolic equation, as provided in following:

$$\frac{t}{S} = \alpha + \beta(t) \qquad (5.12)$$

where t is time from the start of embankment fill (days); S is measured settlement as any specific time (mm); β is gradient of the straight line between t and $\frac{t}{S}$; and α is intersection of the straight line on the $\frac{t}{S}$ axis.

According to Eq. 5.12, the data of total vertical movements of the test embankment measured at the middle of pavement were plotted with a function of time-settlement ratio, as illustrated in Figure 5.18.

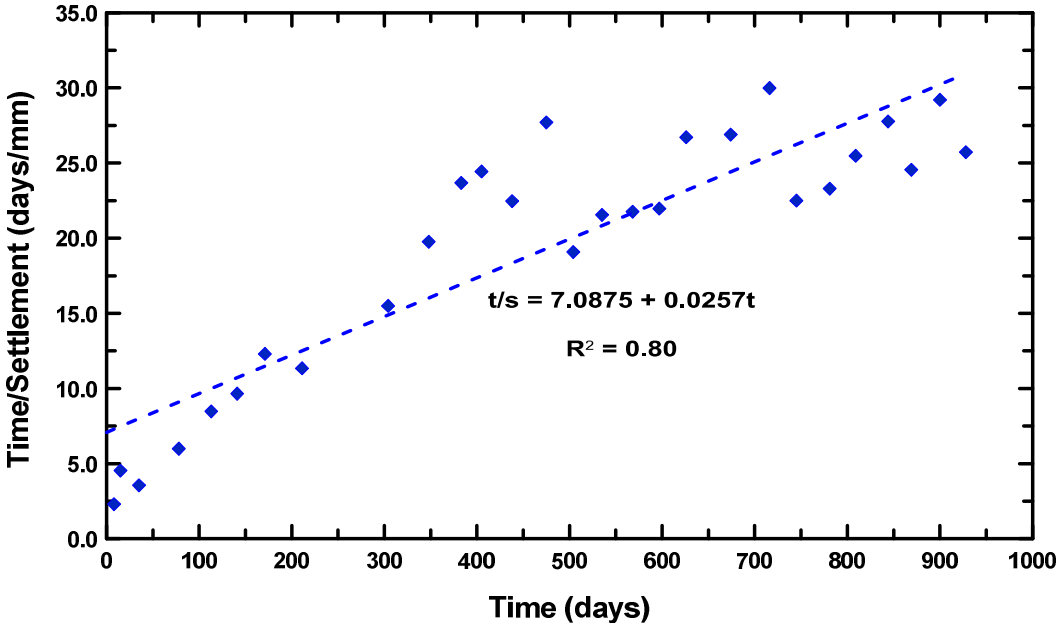

Figure 5.18 Relationship between time-settlement ratio of the test embankment with specific time and a regression equation

By using linear regression analysis, the values of parameters β and α can be estimated. The magnitude of the settlements at a specific time (t) of the test embankment can be calculated by substituting the parameters back into the Eq. 5.12 and rewriting the equation as follows.

$$S = \frac{t}{(\alpha + \beta t)} \tag{5.13a}$$

$$S = \frac{t}{(7.0875 + 0.0257\ t)} \tag{5.13b}$$

Based on Eq. (5.13b), the plot of the predicted vertical displacement which occurred in the test embankment at the specific time interval can be provided, as presented in Figure 5.19. The field data and its best-fit curve are also plotted in the figure. From the plots, it can be observed that the vertical displacements of the test embankment, predicted by hyperbolic method, are in good agreement with the best-fit curve of the measured field data from the horizontal inclinometer surveys. Based on the hyperbolic equation presented in Eq. (5.13b), the settlements of 1.42 in. (36 mm) and 1.50 in. (38 mm) are predicted to occur on the test embankment at 10 year (i.e., 3,650 days) and 20-years (i.e., 7,300 days) intervals.

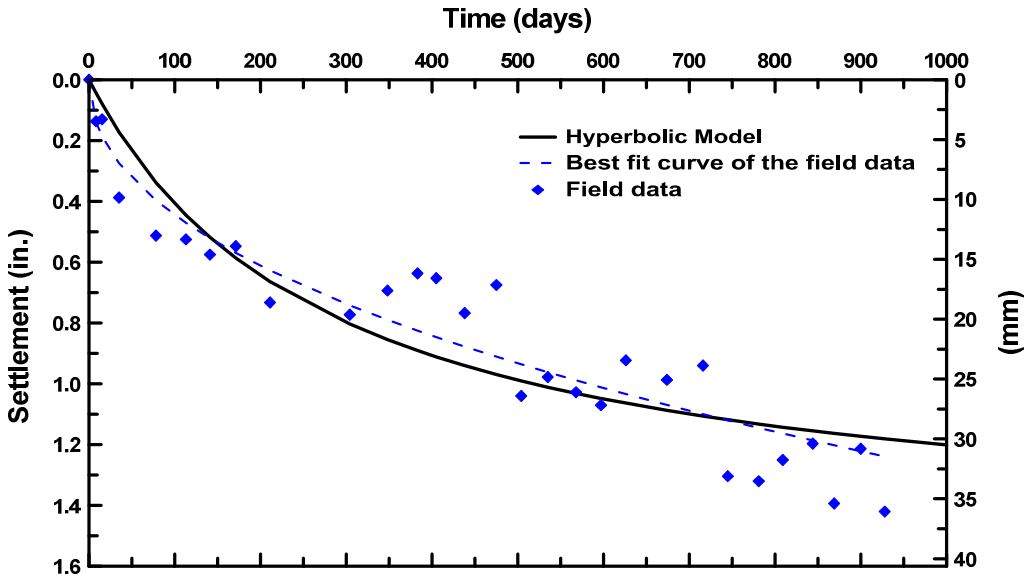

Figure 5.19 Time-settlement relation of the test embankment

Similarly, it's possible to predict the post-construction vertical displacement that will occur in long term. Figure 5.20 presents the plot of prediction of the vertical

displacement after construction on the test embankment. Similar to the total settlement, the post-construction vertical displacement prediction shows good agreement with the best-fit curve of the field data. The settlements of 1.23 in. (31 mm) and 1.30 in. (33 mm) are predicted to be occur on the test embankment at 10 year (i.e., 3,650 days) and 20-years (i.e., 7,300 days) intervals.

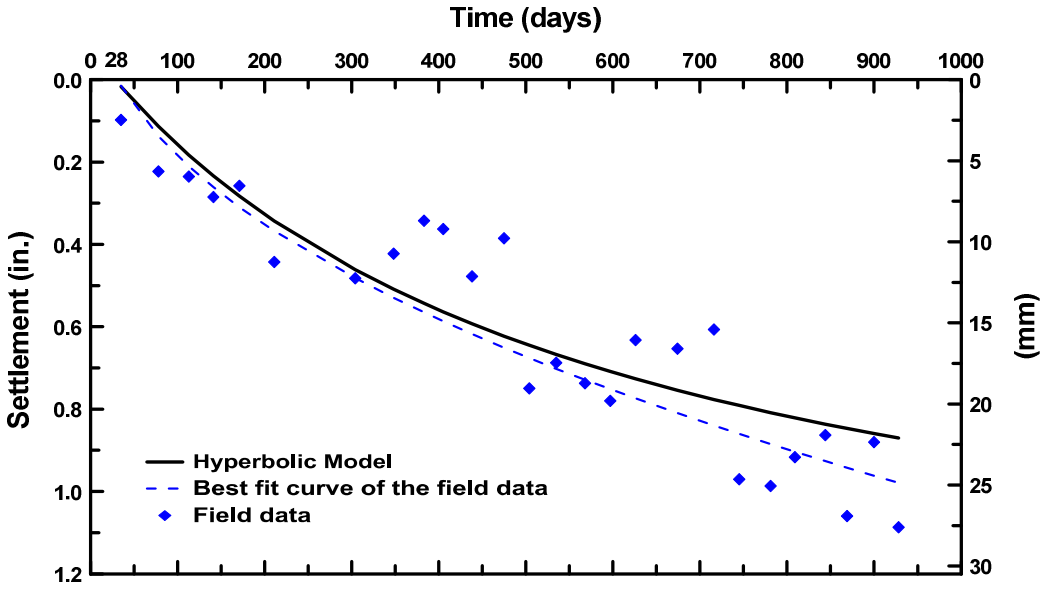

Figure 5.20 Relation of time and post-construction vertical displacement of the test embankment

5.5 Summary

This chapter presents the field monitored data collected during the site visits to the test section of EPS geofoam embankment (US 67, Cleburne, TX). The instruments, including pressure cells and a horizontal inclinometer, were installed in the test embankment to evaluate the benefits of using EPS geofoam in mitigating the bridge approach settlement problems. The field data used in this study was collected periodically from January 2012 to August 2014. The pressure data obtained from pressure cells showed that the average vertical pressure of 1.8 psi (12.4 kPa) and 4.9 psi

(33.8 kPa) were measured at top and bottom of the EPS geofoam layer. From the analysis of stress distribution in EPS geofoam layer, it was observed that only 36.5% of the designed traffic loads was distributed to the bottom of the 6-ft depth EPS geofoam layer. However, the lateral pressure data collected from the vertically-installed pressure cells showed negative values, which do not represent the true field behavior. This may be because the vertically installed pressure cells were not in proper contact with the installed EPS geofoam layer and abutment walls.

The results from vertical movement monitoring collected by the horizontal inclinometer device were statistically analyzed to check whether the current post-construction vertical displacement of the test embankment was less than 1 in. (25 mm), which is regarded as a slight bump. Based on the analysis results, it can be concluded that the post-construction vertical displacement of the test embankment was more than 1.0 in (25 mm) but, less than 1.5 in (38 mm). The Hyperbolic method was used to predict long term settlement of the test embankment (i.e., EPS geofoam embankment). Based on the results, it was predicted that over the service period of ten years, there would be the total settlement of 1.42 in (36 mm), and the post-construction settlement of 1.23 in (31 mm) occurring on the test embankment.

Based on the collected field data and its analysis, it can be concluded that EPS geofoam performs well in mitigating settlements that occur on bridge approach embankments.

Chapter 6

Numerical Modeling of Geofoam Embankment System

6.1 Introduction

The modeling solutions of geotechnical engineering problems can be solved by several different methods. The numerical method is one of the methods that is widely used in the analysis and design of complex geotechnical structures (Booker et al., 1989; Budhu, 2000; Zdravkovic and Potts, 2010). It usually involves solving a set of simultaneous partial differential equations (PDEs) formulated for the problems. There are five different types of numerical methods available for solving the PDEs encountered in geotechnical engineering: (1) the finite element method, (2) the finite difference method, (3) the boundary element method, (4) the discrete element method, and (5) the combined boundary/finite element method. For each of these methods, the way to formulate and solve the PDEs is different.

In this chapter, the numerical analyses using the finite element methods (FEM) were performed to understand the settlement behavior of the test embankment. The commercial geotechnical finite element software (Plaxis) was used in the analysis. The properties of foundation and backfill soils obtained from laboratory testing and presented in Chapter 3 were used as the input model parameters in the numerical analysis. The modeling analysis was validated by comparing the results with the data measured from the field. After the modeling analysis results were satisfied, the numerical model was extended to other embankment configurations for estimating the change in settlement with the varying in heights and types of EPS geofoam in the embankment.

6.2 Finite Element Method (FEM) Studies

The finite element method (FEM) analysis is the numerical technique to solve the problems in the mechanics of continuous media, such as soils (Bartlett, 2012). According to Booker et al. (1989), the FEM has been widely accepted by geotechnical engineers to be a valuable method for analyzing and solving complicated geotechnical problems. However, the FEM plays an important role for the analysis and design of the structures not only in geotechnical field, but also in all branches of engineering (Bathe, 2003). In practice, there are three principal steps in finite element analysis. In the first step, a model of the part to be analyzed is constructed, and the geometry of the model is then divided into a number of discrete elements connected each other at discrete points called nodes. Figure 6.1 illustrates a typical two-dimensional element crated with 6 nodes.

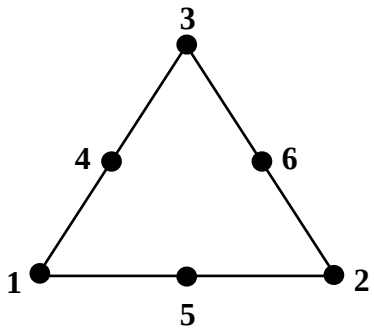

Figure 6.1 Six-node triangular element (Plaxis Manual)

For the second step, the quantities of interested parameters, such as stress, strain, and deformation at the points of interest can be approximately estimated by solving the numerical models, using a system of linear or nonlinear algebraic equations. Finally, the solution for each element is then interpolated to obtain the solution of the entire structure (Roylance, 2001; Archeewa, 2010).

In this study, the commercial geotechnical finite element software, PLAXIS, was used in the numerical study to understand the settlement behavior of the test

embankment. The phenomenon of consolidation of soil can be described by Terzaghi's one-dimensional consolidation equation:

$$\frac{\partial p}{\partial t} = C_{\mathrm{v}} \frac{\partial^2 p}{\partial z^2} \tag{6.1}$$

where $C_{\mathrm{v}} = \frac{k\, E_{OED}}{\gamma_w}$; $E_{OED} = \frac{(1-\upsilon)E}{(1+\upsilon)(1-2\upsilon)}$; $Z = H - y$; k is permeability of soil; E is the Young's modulus; υ is the Poisson's ratio; γ_w is unit weight of water; and E_{OED} is oedometer modulus.

In 1941, Biot developed a more general theory for three-dimensional consolidation coupling the soil deformation and the pore pressure (Krishnamoorthy, 2008). The governing equations of consolidation used in PLAXIS follow the Biot's theory:

$$G\nabla^2 \mathrm{u} + \frac{G}{1-2\upsilon}\frac{\partial \varepsilon}{\partial x} - \alpha \frac{\partial \sigma}{\partial x} = 0 \tag{6.2a}$$

$$G\nabla^2 \mathrm{v} + \frac{G}{1-2\upsilon}\frac{\partial \varepsilon}{\partial y} - \alpha \frac{\partial \sigma}{\partial y} = 0 \tag{6.2b}$$

$$G\nabla^2 \mathrm{w} + \frac{G}{1-2\upsilon}\frac{\partial \varepsilon}{\partial z} - \alpha \frac{\partial \sigma}{\partial z} = 0 \tag{6.2c}$$

and

$$k\nabla^2 \sigma = \alpha \frac{\partial \varepsilon}{\partial t} + \frac{1}{Q}\frac{\partial \sigma}{\partial t} \tag{6.3}$$

when u, v, and w are the components of the displacement of the soil; G is the shear modulus of the soil; υ is Poisson's ratio of the soil; ε is the volume increase of the soil per unit initial volume; σ is pore water pressure; k is coefficient of permeability of the soil; t is time; $\alpha = \frac{2\,(1+\upsilon)\,G}{3\,(1-2\upsilon)\,H}$; Q and H are the physical constants.

During the FEM analysis, a relationship between stress-strain of a material behavior, usually termed as a constitutive law, is used to calculate the stress that has occurred in the mesh (Archeewa, 2010). The PLAXIS program provides several types of material models, such as Linear Elastic model (LE), Mohr-Coulomb model (MC), Hardening Soil model (HS), Hardening Soil model with small-strain stiffness (HSsmall),

Soft Soil model (SS), Soft Soil Creep model (SSC), Jointed Rock model (JR), and Modified Cam-Clay model (MCC). A brief description of the use of those models is provided in the following. More details of the models can be searched in PLAXIS material models manual (2012).

Linear Elastic soil model (LE)

The linear elastic soil model is based on Hooke's law of isotropic elasticity. It involves two basic elastic parameters, which are Young's modulus, *E* and Poisson's ratio, υ. The linear elastic model is not suitable for modeling soil because it is insufficient for capturing the essential features of soil, which is considered to be a highly non-linear and irreversible material. However, the linear elastic model may be used to model stiff volumes in the soil, such as concrete walls or intact rock formations.

Mohr-Coulomb model (MC)

The Mohr-Coulomb model, also called linear elastic perfectly-plastic model, involves five input parameters, which are *E* and υ for soil elasticity; frictional angle, ϕ and cohesion, c for soil plasticity; and ψ as an angle of dilatancy. This model represents a first-order approximation of soil or rock behavior. It includes only a limited number of features that soil behavior shows in reality. However, this Mohr-Coulomb model is recommended to be used for the first analysis of the problem considered.

Hardening Soil model (HS)

The Hardening Soil model is an advanced model for simulation of soil behavior. In this model, soil stiffness is described more accurately than that in the Mohr-Coulomb mode,l by using three different inputs of stiffness: (1) the triaxial-loading stiffness, E_{50}, (2) the triaxial-unloading stiffness, E_{ur}, and (3) the oedometer-loading stiffness, E_{oed}. However, a number of features of soil behavior are not included in this model. For example, the model does not account for softening due to soil dilatancy and de-bonding

effects. Moreover, the model does not distinguish between large stiffness at small strains and reduced stiffness at engineering strain levels.

Hardening Soil model with small-strain stiffness (HSsmall)

The Hardening Soil model with small-strain stiffness is a modification of the Hardening Soil model. This model accounts for the increased stiffness of soils at low strain level. The behavior of soil stiffness at small strain is described in the model using an additional strain-history parameter and two additional material parameters, which are the small-strain shear modulus, G_o^{ref} and the strain level at which the shear modulus has reduced to about 70% of the small-strain shear modulus, $\gamma_{0.7}$. The HSsmall model provides more reliable displacements than the HS model. However, just as in the HS model, the softening due to soil dilatancy and de-bonding effects are not taken into account in the HSsmall model.

Soft Soil model (SS)

The Soft Soil model is a Cam-Clay type model especially meant for primary compression of near normally consolidated clay soil. Compared with the Hardening Soil model, the Soft Soil model is better capable of modeling the compression behavior of very soft soil. However, this model is not recommended for use in excavation problems because it hardly supersedes the Mohr-Coulomb model in unloading problems.

Soft Soil Creep model (SSC)

In reality, all soils exhibit some creep behavior; therefore, primary compression is followed by a certain amount of secondary compression. With this fact in mind, the Soft Soil Creep model has been developed primarily for application to settlement problems of foundation, embankment, etc., by including an additional material parameter, i.e. modified creep index, μ^*, which can be calculated when the creep index for secondary compression, c_α of soil is known. However, the same as the SS model, the SSC model

hardly supersedes the Mohr-Coulomb model for the unloading problems such as tunneling and other excavation problems.

Jointed Rock model (JR)

The Jointed Rock model is an anisotropic elastic-plastic model especially meant to simulate the behavior of rock layers involving stratification and particular fault directions. This model includes a limited number of features of rock behavior. The parameters involving to this model consist of the stiffness properties of the rock, *E* and υ, and the strength parameters in joint directions; c, ϕ, and ψ.

Modified Cam-Clay model (MCC)

The Modified Cam-Clay model is a well-known model from international soil modeling literature. It is meant primarily for modeling of near normally-consolidation clay-type soils. PLAXIS has added this model in order to allow for a comparison with other codes.

6.3 Modeling of EPS Geofoam Embedded Embankment

6.3.1 Geometry of Test Embankment Section

With information received from TxDOT, a cross-section and subsurface profile of the test embankment can be provided, as illustrated in Figure 6.2. The total 40-ft. (12.2 m) high embankment was constructed with a side slope of 3H:1V. The embankment was placed on the layer of foundation clay soil with an average thickness about 12 ft. (3.7 m), underlain by a layer of hard-to-very-hard limestone. The top of the embankment was replaced with 6 ft. (2 m) of EPS 22 geofoam, stacked in three layers.

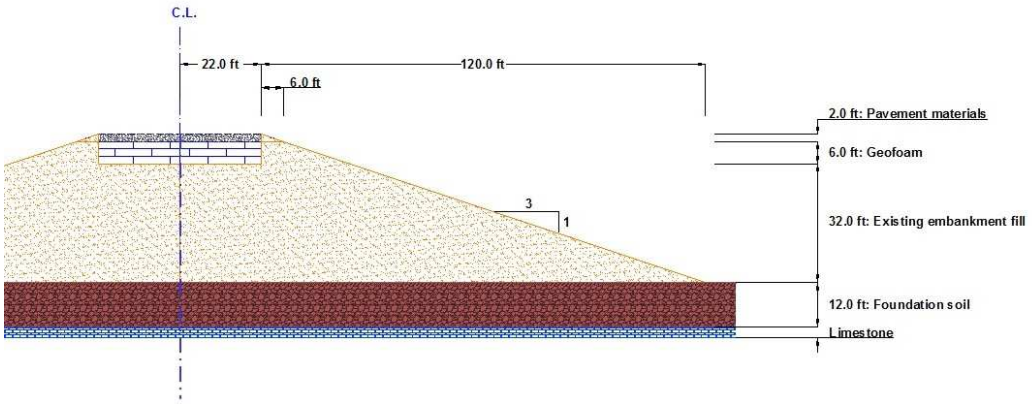

Figure 6.2 Geometry of the test embankment section

6.3.2 Material Properties

In this study, a soft soil model was used to simulate the foundation clay soil and the existing embankment backfill. A linear elastic model was used to simulate the hard limestone and EPS 22 geofoam material. The properties of the embankment fill and foundation soil used in the model were derived from the laboratory test results presented previously in Chapter 3. The properties of the hard limestone, the typical values of Young's modulus, *E*, equal to 1.15×10^9 psf (55 GPa) and Poisson's ratio, υ, of 0.25, were obtained from literature.

For the EPS 22 geofoam, the properties provided in ASTM D 6817-07 standard specification for rigid cellular polystyrene geofoam, were used in the model. However, Barlett et al. (2012) suggested that the size of specimen tested in the laboratory influences Young's modulus of the EPS geofoam. The authors presented the testing results provided by Elragi et al. (2000). The results showed that the initial Young's modulus of 24-in. (60-cm) cube block of EPS19 is approximated twice of the value received from 2-in. (5-cm) cube specimens. The authors also suggested that the current design methods for EPS geofoam embankment, which are based on the test results from 2-in. (5-cm) cube samples, may be significantly conservative. Hence, the Young's

modulus for full size of EPS 22 geofoam block used in the model was modified to be greater than the values provided in ASTM D 6817-07. Based on the test results provided by Elragi et al. (2000), the relationship between multiplying factor for Young's modulus of EPS geofoam versus the scaling of volume of standard specimen, which is 125 cm^3 (5 cm × 5 cm × 5 cm), was plotted as presented in Figure 6.3. From the plot, a multiplying factor of 3 was estimated to be used for modifying the value of Young's modulus of the EPS geofoam blocks with the dimension of 2 ft. × 3 ft. × 8 ft.

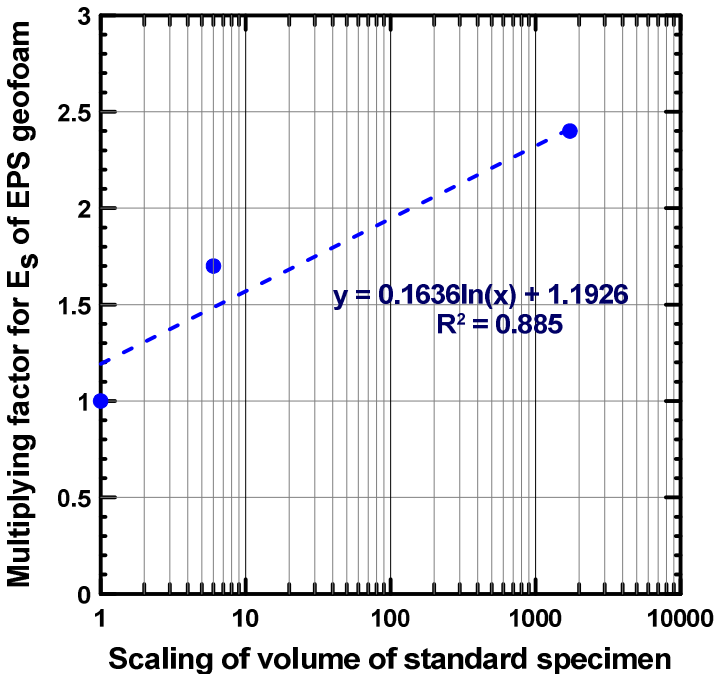

Figure 6.3 the plot of multiplying factor for Young's modulus of EPS geofoam versus the scaling of volume of standard specimen

The pavement layer placed on the top of the embankment was simulated as a plate element. The typical value of Young's modulus of a concrete pavement is equal to 6.27×10^8 psf (30 GPa), and this value was obtained from literature (Kalla, 2010). As per the information provided by TxDOT, the thickness and width of the concrete pavement

section were 0.83 ft. (0.25 m) and 22 ft. (6.7 m), respectively. The material properties used in the current modeling analysis are given in Table 6.1 and 6.2.

Table 6.1 Materials properties and model types used in the numerical model analysis

Properties	Unit	EPS 22 Geofoam	Embankment fill	Foundation soil	Limestone
Material Model	-	*LE model*	*SS model*	*SS model*	*LE model*
Type of behavior	-	Non-porous	Drained	Drained	Drained
Moist unit weight, γ_{unsat}	Pcf	1.35	119.2	131.4	132.8
Saturated unit weight, γ_{sat}	Pcf	-	133.3	132.2	132.8
Horizontal permeability, k_x	ft./day	-	0.013	0.0014	0.00002
Vertical permeability, k_y	ft./day	-	0.013	0.0014	0.00002
Young's modulus, *E*	Psf	3 × 104,400	-	-	1.15×10^9
Poisson's ratio, υ	-	0.12	-	-	0.25
Cohesion, *c*	Psf	-	1,300	1,300	-
Friction angle, ϕ	degree	-	26°	12°	-
Initial void ratio, e_o	-	-	0.47	0.54	-
Compression index, C_c	-	-	0.23	0.27	-
Recompression index, C_s	-	-	0.02	0.02	-
Overconsolidation ratio	-	-	3.0	4.0	-

Table 6.2 Pavement properties used in the model analysis

Pavement properties	Concrete
EA (lb.)	1.144×10^{10}
EI (lb-ft^2)	6.569×10^8
μ	0.15

6.3.3 Gravity Load of Pavement Materials and Traffic Load

The distributed loads used in the model analysis are classified into two categories, consisting of a gravity load of the pavement materials and a traffic uniform load. According to the preliminary design of the embankment provided by TxDOT, the materials used in a construction of the pavement consisted of the layers of flexible base,

hot mix asphalt concrete (HMAC), and continuously-reinforced concrete pavement (CRCP). The design stress of the dead loads of the pavement system, equal to 2.4 psi (346 psf or 16.55 kPa), was estimated and used in the design.

According to AASHTO LRFD Bridge Design Specification (2012), the standard truck used in a bridge design is HS-20 (a 20-ton semi-trailer truck). Characteristics of the design truck are presented in Figure 6.4. It should be noted that the design truck has three axles. The axle at the front is a single axle with single wheel; whereas, at the middle and the rear, the axles are single axle with dual wheels. For the dual wheels system, the vehicle load of 32.0 kip is designated; thus, the wheel load on one side of the axle is 16.0 kips. The tire contact area of the dual wheel is assigned to be 200 square inches (20 in 10 in).

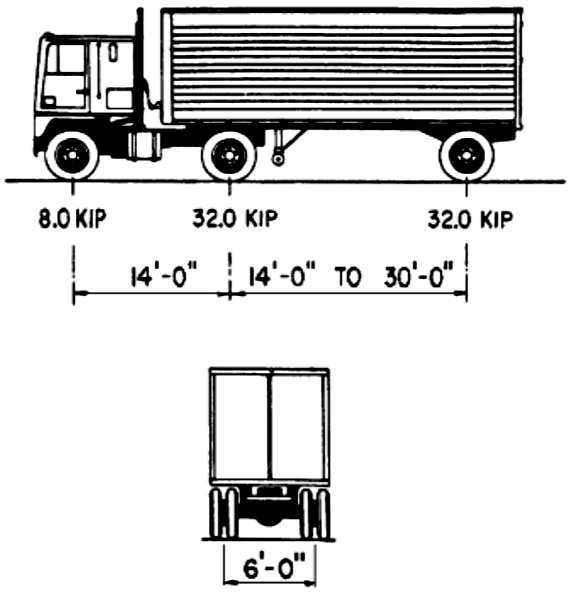

Figure 6.4 Characteristics of the design truck (AASHTO, 2012)

In the model, the vertical stress, induced on top of the EPS22 geofoam layer embedded at the depth of 24 in. (610 mm) underneath the pavement surface, can be

obtained by estimating the dissipation of the traffic stress through the pavement system. The geofoam application guideline provided in NCHRP 529 recommended the use of the Burmister (1943) method to calculate the vertical stress distribution on the top of EPS geofoam layer. The Burmister (1943) solution considers the influence of different elastic properties of the multi-layered systems. The vertical stress depends on the modular ratio between Young's modulus of material in layer 1 to the Young's modulus of material in layer 2 ( ). The stress distribution decreases considerably with the increasing of the modular ratio. Figure 6.5 presents the relationship between the vertical stress influence coefficient, modular ratio, and parameter , when is the depth of the layer and is the radius of equivalent circular load area.

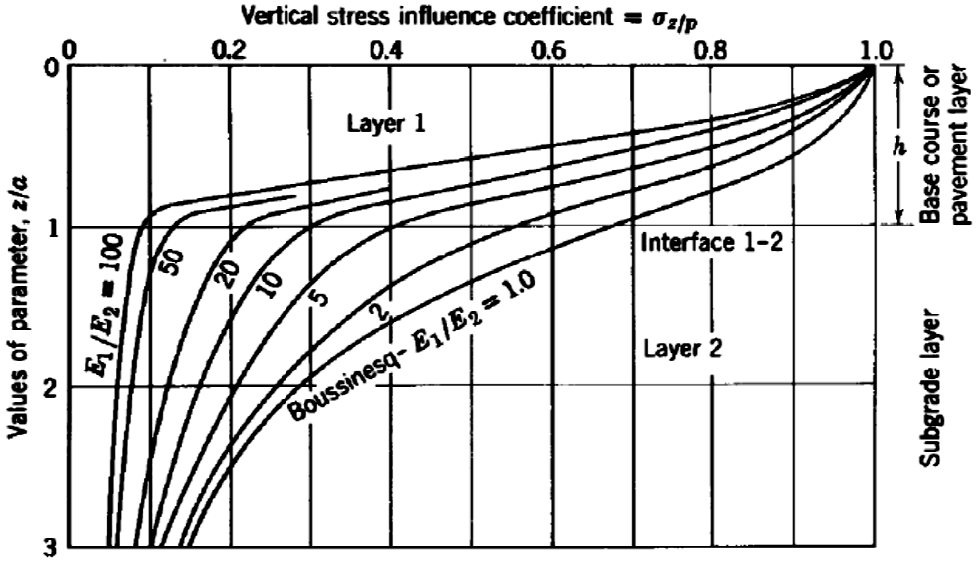

Figure 6.5 Vertical stress in a two-layered system (after Burmister 1958)

For the test embankment section, the thickness of the pavement system ( ) was 24 in. (610 mm) and the modular ratio between concrete pavement and base material ( ) was about 100. The radius, , can be estimated by comparing the equivalent

circular load area with the tire contact area of the standard truck, as presented in the following equation:

$$\pi a^2 = Tire\ conteact\ area \quad (6.4a)$$

$$\pi a^2 = 20 \times 10\ in^2 \quad (6.4b)$$

$$a = 8\ in. \quad (6.4c)$$

Therefore, the parameter z/a is equal to 3. Based on the plot provided in Figure 6.5, the vertical stress influence coefficient of 0.05 was obtained. The vertical stress induced on the top of the EPS22 geofoam layer (σ_Z) equal to 4.0 psi (576 psf or 27.6 kPa) was calculated as follows:

$$\sigma_Z = 0.05 \times (32.0\ kip\ /\ 2)\ /\ (20 \times 10\ in^2)$$

$$\sigma_Z = 0.004\ ksi = 4.0\ psi = 576\ psf$$

The EPS method Development Organization (EDO,) established to promote the EPS geofoam applications in Japan introduces a simplistic approach to calculate the traffic stress distribution throughout the concrete pavement system. The angle of stress redistribution is assigned to be 45 degrees for the pavement section,n as illustrated in Figure 6.6.

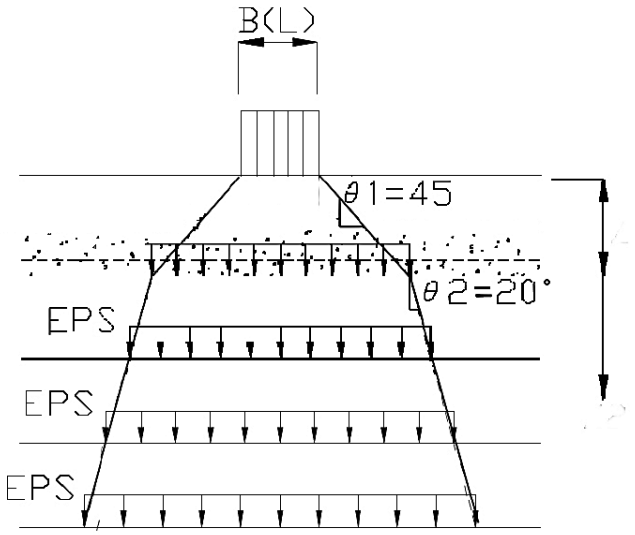

Figure 6.6 Vertical stress redistribution chart for EDO design method (Tsukamoto 2011)

From this method, the area of vertical stress distribution on top of the EPS geofoam layer can be calculated. As presented in Figure 6.7, the spread area of 3,944 in^2 (68 in × 58 in) was estimated and the vertical stress increase on the top of EPS geofoam layer was (16,000 lb.) / (3,944 in^2) = 4.06 psi (585 psf or 28 kPa).

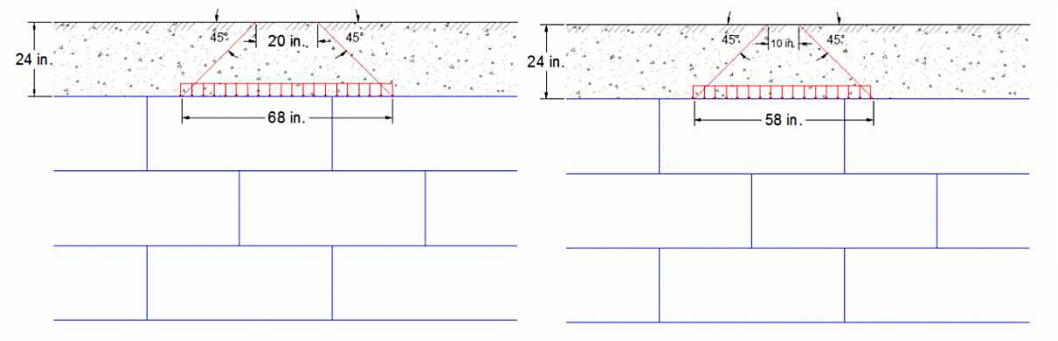

Figure 6.7 Stress increase on EPS22 geofoam layer caused by wheel load

The effects of dynamic loads and vibratory conditions from traffic are generally considered adjacent to a bridge abutment in terms of the impact allowance. An impact coefficient of 0.3 is recommended by NCHRP 529 to be used for design of EPS geofoam

embankments. Therefore, the stress from the design truck load with the impact allowance can be estimated, as shown in Equation 6.5.

$$\sigma_{truck} = \sigma_Z \times (1 + I) = (4.0\ psi) \times (1 + 0.3) = 5.2\ psi = 748.8\ psf \quad (6.5)$$

where σ_{truck} is design truck load with an impact allowance, σ_Z is vertical stress induced on the top of the EPS geofoam layer, and I is an impact coefficient.

In addition to the stress from the design truck (HS-20), a design lane load of 0.64 k/ft. as an uniformly distributed load in longitudinal direction is used as one type of the live loads for the highway bridge design. The design lane load is assumed to be uniformly distributed over the 12-ft lane width, and the stress effects from the design lane load are not subjected to dynamic load allowance (AASHTO 2012). The magnitude of the stress due to the lane load can calculated with the following Equation:

$$\sigma_{Lane\ Load} = (0.64\ k/ft) / 12\ ft = 0.053\ ksf = 53\ psf \quad (6.6)$$

The design live load from the traffic load was calculated and was equivalent to multiplication of safety factor and the live loads:

$$\text{Design live load} = 1.2 \times (748.8 + 53) = 962\ psf \quad (6.7)$$

In the modeling of embankment systems, the dead weight of pavement system is placed on the whole area of the pavement (22-ft width); whereas, the stress increase from wheel loading is placed only on the part of roadway lane (12-ft width) as presented in Figure 6.8.

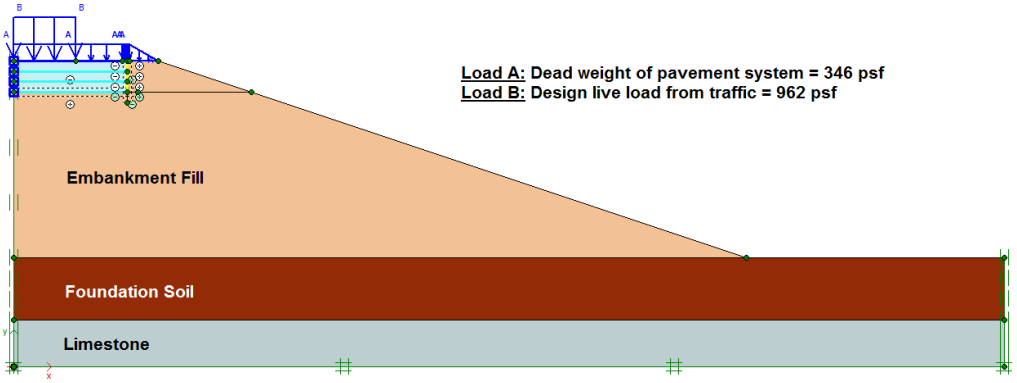

Figure 6.8 Test embankment profile and loads distribution on EPS geofoam layer

6.3.4 Discretization of the Test Section

There are two types of triangular elements provided in the PLAXIS program, and these are 6-noded triangular elements and 15-noded triangular elements. The higher order triangular elements provide better descriptions of continuous strain profiling, stress variation, and displacements that occurred within the discretized area. However, the calculations with higher order triangular elements are more time consuming than the lower order triangular elements.

In PLAXIS, an unstructured mesh is automatically created on the model. The size of the mesh cannot be set explicitly. In the current analysis, the two-dimensional plain-strain modeling with 15-noded triangular elements was used to model the test embankment configuration. Figure 6.9 illustrates the mesh generated on the test embankment model.

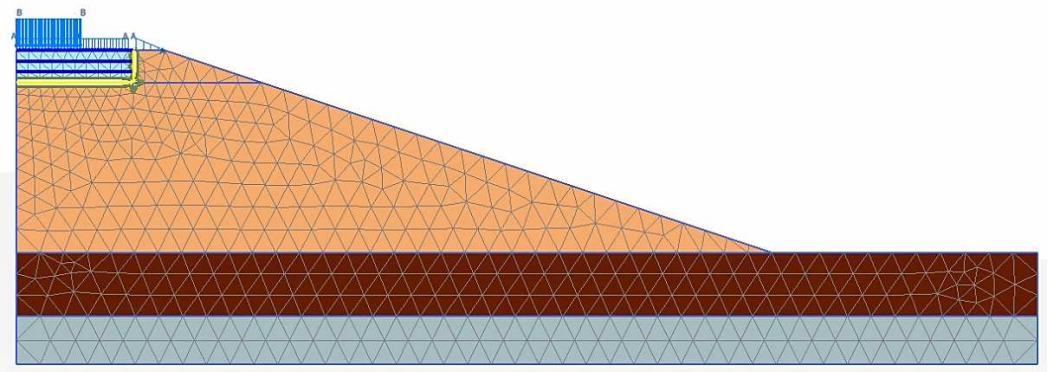

Figure 6.9 Mesh generated on the test embankment model

6.3.5 Initial Boundary Conditions

In PLAXIS modeling analysis, the initial conditions, such as a general phreatic level, needs to be assigned before the analysis. Water pressure is generated based on the phreatic level condition. During the analysis, constant ground water level has been considered. For the test embankment site, the level of ground water table was not reported. Therefore the phreatic level at the middle of the foundation soil layer was assumed in the present numerical modeling. In addition to the phreatic level, the boundary condition for consolidation analysis is also needed to be provided as input conditions. The lines of consolidation are selected in a vertical direction, which means that the vertical boundaries of the model must be close to restrain the horizontal flow, and no free outflow is allowed at the boundary (Kalla, 2010).

6.3.6 Settlement Analysis

In the modeling analysis, different phases of the test embankment reconstruction and loading applications were simulated following the time schedule provided by the original construction plans of the local DOT office. The process of pavement construction was completed within 15 days. During this process, undrained behavior of soils was considered; thus, a plastic calculation approach was used in analysis. After the

construction, concrete curing and a consolidation period of 30 days was introduced to allow some excess pore pressure to dissipate.

During the process of concrete curing and consolidation, the dead weight of the pavement system had been applied to the embankment area. Then, the embankment was opened to traffic service conditions, and the stress increase induced by wheel load was placed on the roadway section. The calculation of the settlement analysis was performed until the minimum excess pore pressure reached a very low value of 0.1 psf (0.005 kPa), indicating complete dissipation condition. Table 6.3 presents different phases of the embankment reconstruction and load-applying conditions, as implemented in the PLAXIS program.

Table 6.3 Calculation phases assigned in the modeling analysis

Phase	Calculation	Loading input	Time
Initial phase	K0 procedure	Unassigned	0 day
Pavement construction	Plastic analysis	Staged construction	15 day
Pavement + curing	Consolidation	Staged construction	30 day
Traffic 1 month	Consolidation	Staged construction	30 day
Traffic 2 months	Consolidation	Staged construction	30 day
Traffic 3 months	Consolidation	Staged construction	30 day
Traffic 4 months	Consolidation	Staged construction	30 day
Traffic 5 months	Consolidation	Staged construction	30 day
Traffic 6 months	Consolidation	Staged construction	30 day
Next 1000 days	Consolidation	Staged construction	1000 day
Minimum pore water	Consolidation	Minimum pore pressure	0 day

During the numerical analysis, five specific points were selected for studying the total vertical movements which occurred in the embankment system. Figure 6.10 presents the five selected points. Points A, B, and C were selected atop the EPS geofoam layer at the middle, 10 ft. from the middle, and 18 ft. from the middle of concrete

pavement, respectively. The results of vertical displacements at those points were used for comparison with the collected field data in order to verify the accuracy of the numerical model. Additionally, Points D and E were selected as the coordinates under the center of pavement and on top of backfill soil and foundation soil, respectively. In addition to the results of vertical displacement at points A, B, and C, the result of total stress atop the backfill soil layer were also used in the model verification by comparing them with the field data obtained from the PC #1 pressure cell.

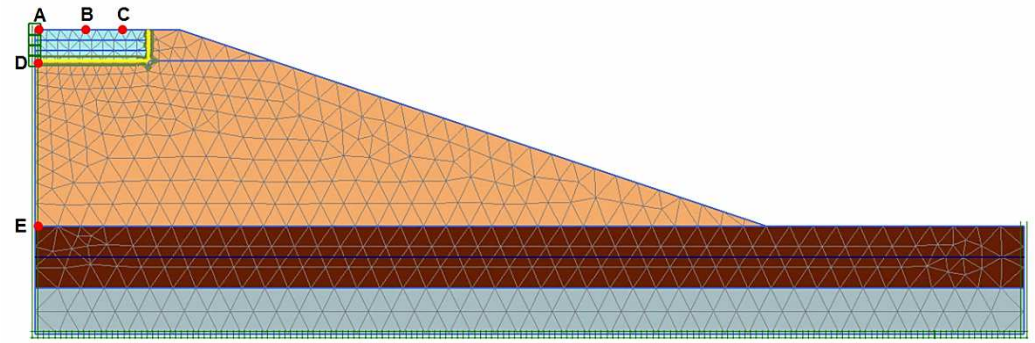

Figure 6.10 Observation points in the settlement analysis

6.3.7 Results of the Numerical Modeling Analysis and Model Validation

The PLAXIS output program has two main output results of finite element analyses and calculations, which are the displacements and stresses. Figure 6.11 shows the deformed mesh after most of the excess pore water has been dissipated. It should be noted that the deformed mesh was scaled up to 25 times. From the figure, it can be observed that the maximum vertical displacement occurred at the middle of the slab (point A in Figure 6.10).

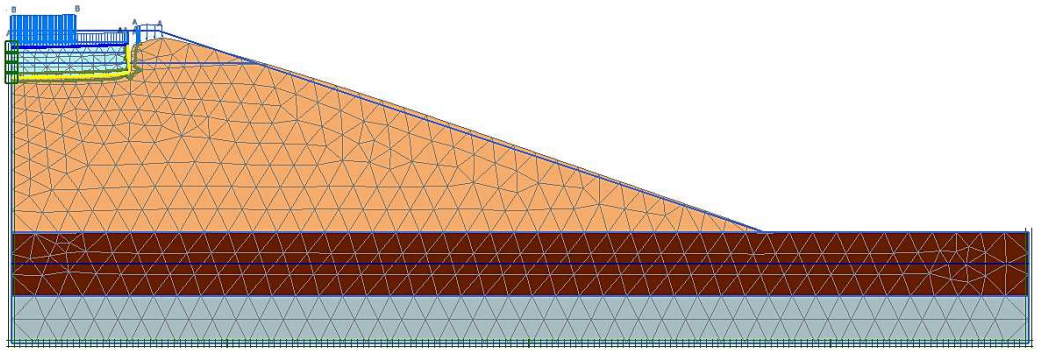

Figure 6.11 Deformed mesh of the model (scaled up 25 times)

To obtain the values of vertical displacement results, the function of total displacement in deformation calculation is selected. Figure 6.12 presents the contours of the total vertical displacement, u_y, which occurred on the EPS geofoam embankment model after full dissipation of pore pressure. The vertical displacements at points A, B, C, D, and E, assigned in Figure 6.10, can be determined and presented in the plots of vertical displacement versus time. Figure 6.13 shows the vertical displacement – time plots at points A, B, and C; the points were selected on the same level, but at different locations.

Figure 6.14 presents the vertical displacement – time plots at points A, D, and E; the points were selected along the center of the concrete pavement, but at different depths. The results shown in the plots depict that the maximum vertical displacement of 1.52 in. (38.6 mm) occurred at the selected point A, and most of the displacement occurred within the layer of backfill soil (i.e., 1.24 in.).

The results of the modeling analysis also show that the settlement occurred in the foundation soil layer was quite low (i.e., about 0.1 in.). This is because in this case, the embankment was reconstructed by replacing EPS geofoam blocks on the top 6 ft. (2 m). In the numerical model, the foundation and backfill soils were assigned to be as they were at the beginning of the analysis, and the software (Plaxis) analyzed the foundation

soil as a deeper layer of backfill soil. The long-term deformation of 0.2 in. (5.08 mm) was predicted occur for the EPS geofoam.

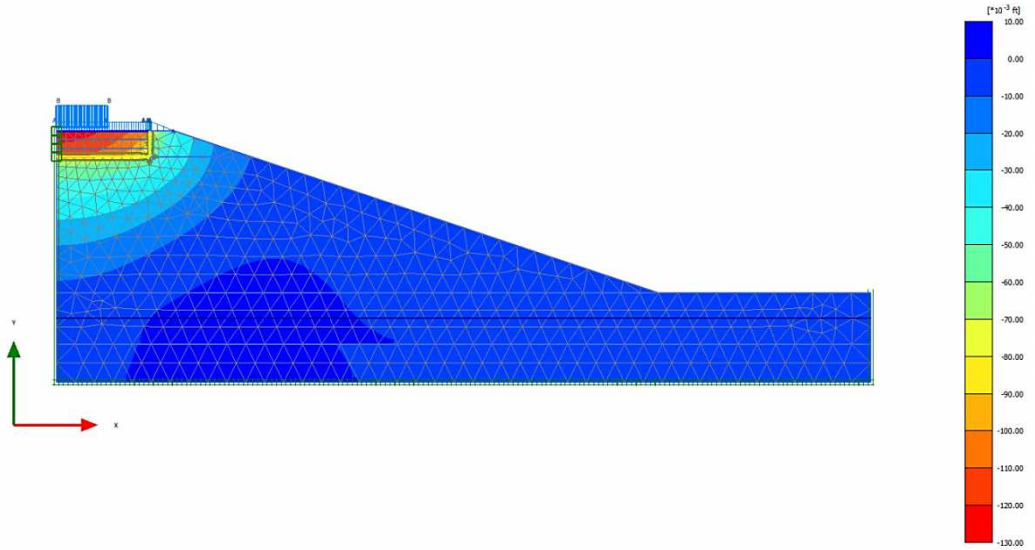

Figure 6.12 The contours of total vertical displacement, u_y, in the embankment

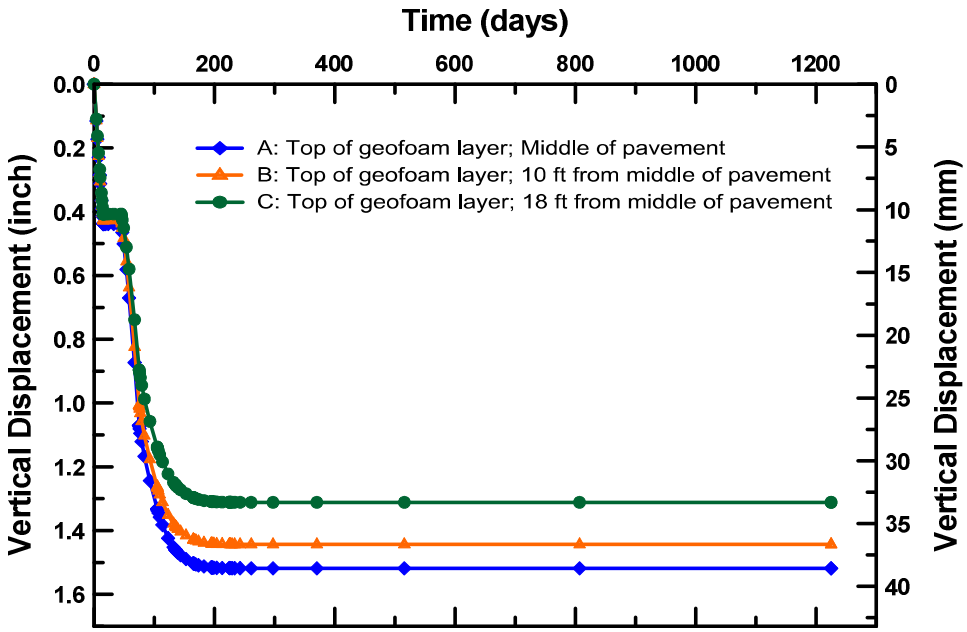

Figure 6.13 Vertical displacement at points A, B, and C from numerical analysis

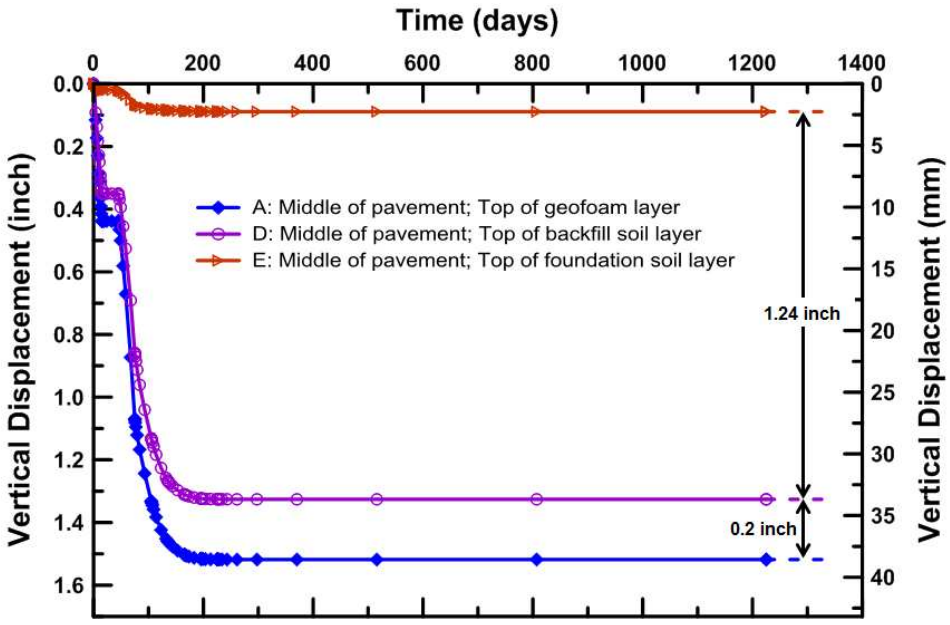

Figure 6.14 Vertical displacement at points A, D, and E from numerical analysis

In addition to the vertical displacements, the result of total stress in a vertical direction is also required in this study. Figure 6.15 presents the contours of the total vertical stress, σ_{yy}, received from the numerical analyses. The vertical stress distributions that occurred on top of the backfill soil, underneath the layer of EPS geofoam were considered and were used to compare with the pressure response collected from the PC #1 pressure cell. The results obtained from the modeling analysis show that after the traffic load was applied to the embankment, an average vertical stress of 700 psf (33.5 kPa) was transmitted at the top of the backfill soil layer.

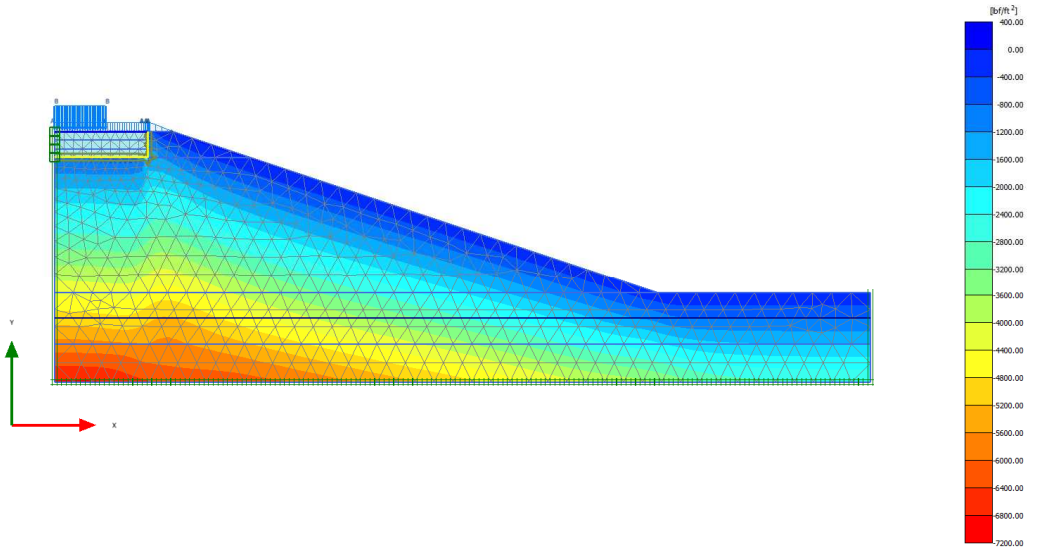

Figure 6.15 Vertical stress contours in the embankment
after full dissipation of pore pressure

In order to validate the model and the parameters used in the numerical analysis, the results obtained from the model analysis were compared with the data collected from the test field. Figures 6.16 to 6.18 present the comparisons of the settlements of the embankment obtained from both field testing and numerical analysis attempted at points A, B, and C, respectively. It can be noticed from the plots that the results from numerical analysis showed the rapid increase in settlement within the first 150 days and then, after 200 days, the settlement remained constant at the maximum values of 1.52 in (38.6 mm), 1.44 in (36.6 mm), and 1.31 in (33.3 mm) for the points A, B, and C, respectively.

The field testing monitoring data showed that the settlements measured at points A, B, and C showed trends that were close to the maximum prediction results from the numerical modeling. However, the time intervals to reach the maximum settlements observed in the field data were significantly different from those obtained in the numerical analysis. This is because of the limitation of loads assignment in the numerical model.

For the numerical analysis, the traffic load was assigned as a static load. However, in the real condition, this load is a dynamic repeated load on the pavement structure.

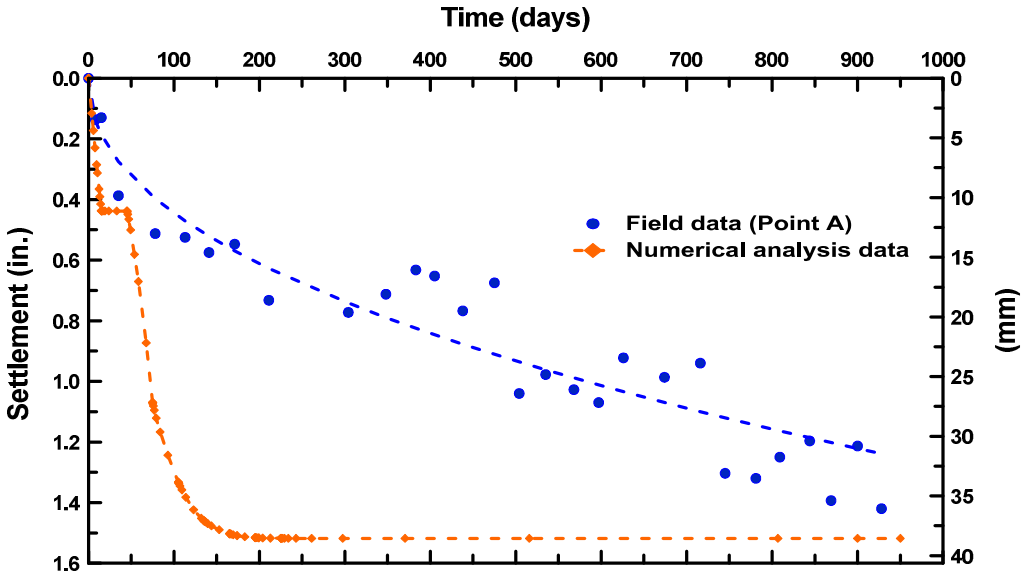

Figure 6.16 Comparison of the settlement at point A (middle of the pavement) obtained from field data and FEM modeling analysis

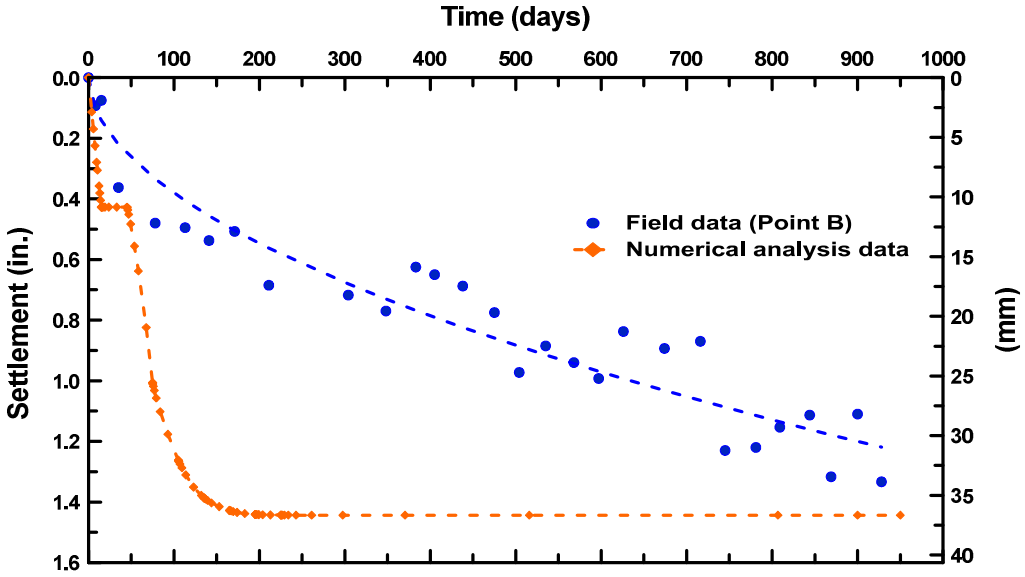

Figure 6.17 Comparison of the settlement at point B (10 ft. from the middle of the pavement) obtained from field data and FEM modeling analysis

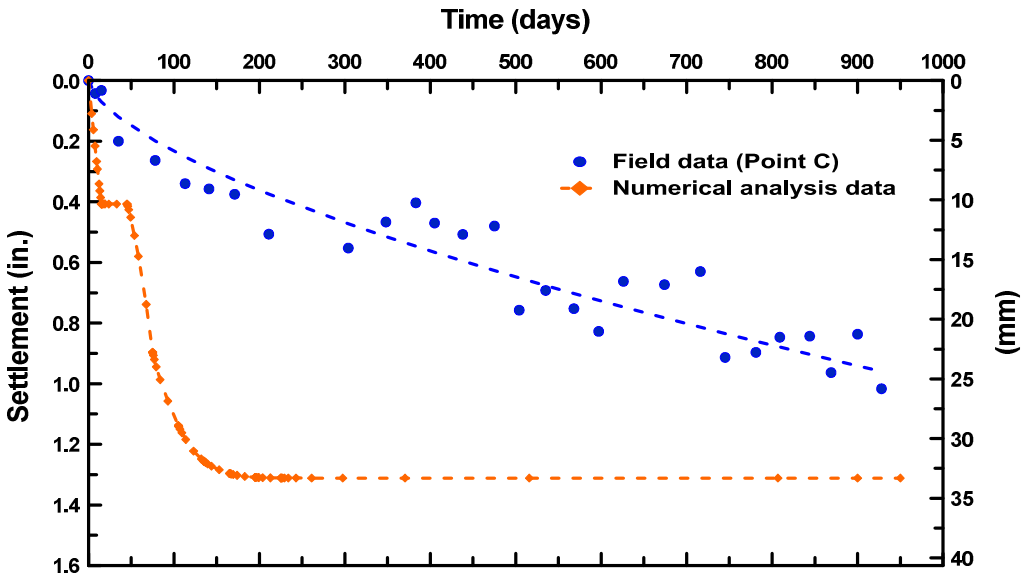

Figure 6.18 Comparison of the settlement at point C (18 ft. from the middle of the pavement) obtained from field data and FEM modeling analysis

Referring to Figure 5.5 in the previous chapter, the average vertical pressure of 4.9 psi (705.6 psf) was obtained from the pressure cell PC #1, which was installed on the top of the backfill soil layer. This value is very close to the result obtained from the modeling analysis, which was equal to 4.86 psi (700 psf).

Based on the comparisons of the settlement that occurred at three different locations on the embankment and the results of vertical pressure on the top of the backfill soil layer, it can be mentioned that the numerical analysis and model input parameters used in this study provided the results that are in a good agreement with the performance of the test section and soils in the field. The final settlement results were in good agreement. The time rate of settlements did not match with the field measurements. Despite this limitation, the model can be confidently used for predicting the settlement of the embankment with the varying heights of the EPS geofoam layer. The effect of the EPS geofoam type on the vertical displacement that occurred on the embankment was also studied by changing the input parameters of the EPS geofoams in the model.

6.4 Prediction of Vertical Movements with Variations of Height of EPS Geofoam Layer

The thickness or height of the EPS geofoam layer is an important factor in geofoam embankment design. The cost per unit of EPS geofoam is relatively high when compared to the cost of soil fill. The excessive height of the EPS geofoam layer can increase the overall cost of an embankment construction. Therefore, the design of the EPS geofoam layer needs to strive for the minimum height that will provide the tolerable magnitude of settlement in the embankment.

To investigate the effects of the EPS geofoam layer height on the vertical displacements that occurred on the embankment section, the numerical model, model input parameters, and the same procedure performed in the previous section were used, varying in the EPS geofoam layer height from 0 to 36 ft. (0 to 11 m) with the increment of 4 ft. (1.2 m). In this study, the results of maximum vertical displacement which occurred at the middle of pavement atop the embankment (i.e., point A in Figure 6.10) were considered.

Figure 6.19 presents the relationship between the vertical displacements which occurred on the embankments versus time. The results of the maximum vertical displacements from the numerical analyses, with various heights of EPS geofoam layer, are provided in Figure 6.20. It can be seen from the figures that the vertical displacement of about 2.1 in. (53.3 mm) was predicted to occur on the embankment without the layer of EPS geofoam. However, in the real condition, the settlement may occur greater than the predicted value. This is because of the potential erosion in the embankment fill that will increase the vertical displacements on the embankment.

Moreover, it can be clearly seen that the vertical displacements occurring over the EPS geofoam embankment reduces in a hyperbolic shape when the height of EPS geofoam layer is increased from 0 to 36 ft. (0 to 11 m). The vertical displacement sharply

decreased when the height of the EPS geofoam increased from 0 to 16 ft. (0 to 5 m) and then, the decrease was small.

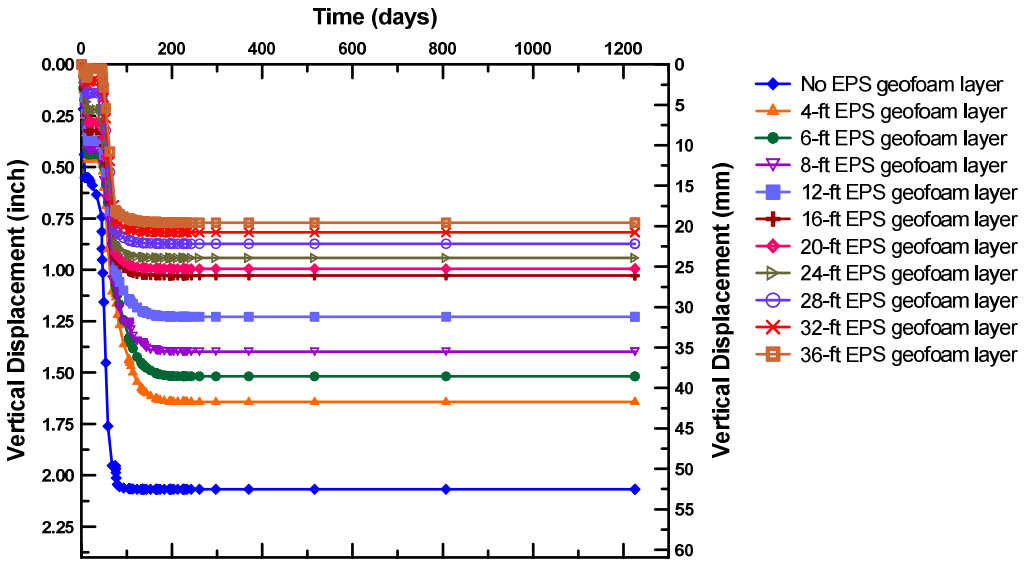

Figure 6.19 Settlement-time in the embankment with various heights of EPS geofoam layer

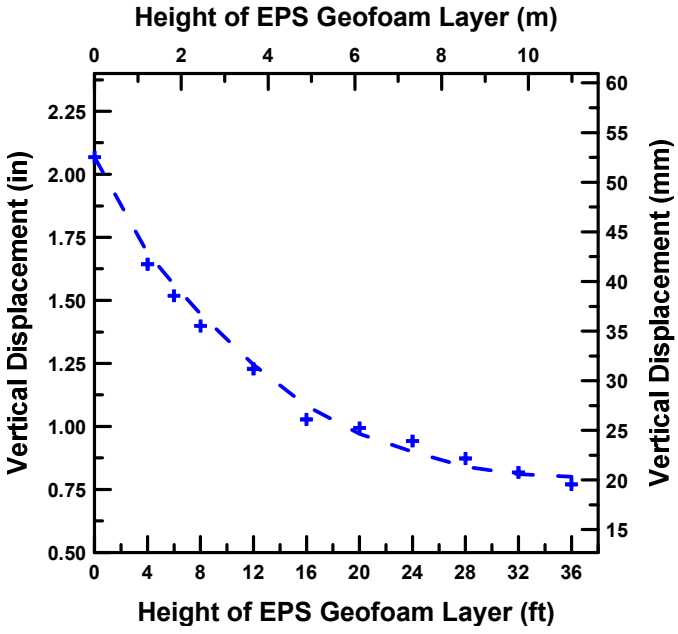

Figure 6.20 Maximum vertical displacement with various height of EPS geofoam layer

6.5 Prediction of Vertical Movements with Variations of EPS Geofoam Types

Based on the ASTM D 6817-07 standard, the number designation for EPS geofoam type indicates a minimum density in kg/m^3 of the geofoam. The density of EPS geofoam is the other factor that affects the cost of a geofoam embankment construction. The cost of EPS geofoam increases with an increase in its density. EPSs are not only different due to their density values, but they are also different due to properties such as compressive resistances and initial modulus values. All these properties can affect the magnitude of the vertical displacements occurring over an EPS geofoam embankment.

In this study, the effects of the EPS geofoam types on the magnitude of vertical displacement which occurred on the embankment are investigated in the numerical modeling. The model of the embankment with a 6-ft. (2-m) depth of EPS geofoam layer created previously in Section 6.3 was used with varying properties of different types of EPS geofoams. Table 6.4 presents the different types of EPS geofoam with their properties used as the model input parameters. It should be noted that the Young's modulus of the EPS geofoam used in the model had to be modified by multiplying the shape factor, which was estimated equal to 3, with the modulus provided in the ASTM standard.

Table 6.4 Types of EPS Geofoam and Properties used in the Numerical Model Analysis

Type	Properties		
	Unit weight (pcf)	Young's modulus (psf)	Poisson's ratio
EPS12	0.70	3 × 31,680	0.12
EPS15	0.90	3 × 51,840	0.12
EPS19	1.15	3 × 83,520	0.12
EPS22	1.35	3 × 104,400	0.12
EPS29	1.80	3 × 156,960	0.12
EPS39	2.40	3 × 216,000	0.12
EPS46	2.85	3 × 267,840	0.12

Similar to the previous section, the modeling results of maximum vertical displacement occurred at the center of the pavement, atop the embankment. Figure 6.21 illustrates the time-vertical displacement relationship of the embankment with the variance in types of EPS geofoam used. In addition, Figure 6.22 presents the relationship between the maximum vertical displacements analyzed from the numerical model and the various types of EPS geofoam. As presented from the figures, the vertical displacement decreased when the density and elastic modulus of EPS geofoam increased. The EPS12 geofoam showed highest magnitude of the vertical displacement, which was equal to 2.01 in (51.0 mm); whereas, the lowest vertical displacement of 1.32 in (33.5 mm) was shown in the EPS46 geofoam. Similar to the relationship between the vertical displacement and the height of EPS geofoam layer, the vertical displacements which occurred on the embankment decreased in a hyperbolic shape when the types of EPS geofoam were changed from EPS12 to EPS46.

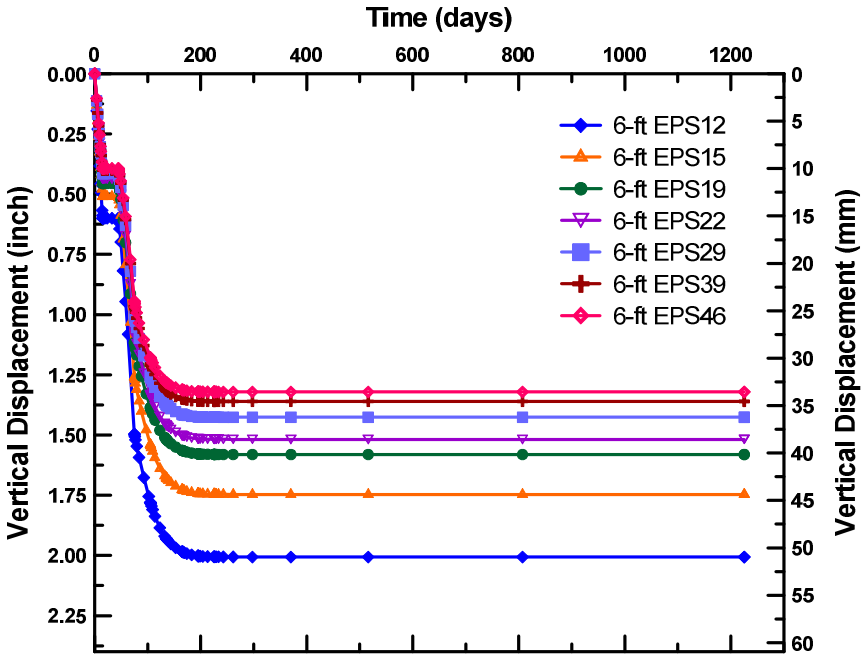

Figure 6.21 Settlement-time in the embankment with various types of EPS geofoam

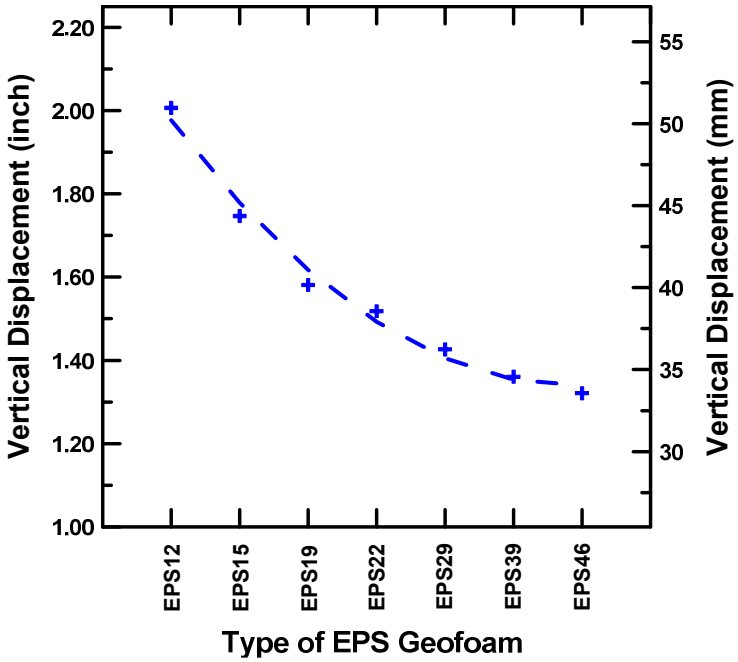

Figure 6.22 Maximum vertical displacement with various types of EPS geofoam layer

6.6 Summary

This chapter presents the details of the numerical finite element modeling analysis of the test embankment system. The numerical models were created using the laboratory test results, presented in Chapter 3, as the model input parameters. The value of designed dead load from the pavement system assigned in the model was 2.4 psi (346 psf). Whereas, the designed live load of 6.68 psi (962 psf) was calculated from the vehicle load of the bridge design standard truck, HS-20, defined in AASHTO standard. The results of settlements at the specified points and vertical pressure at the bottom of the EPS geofoam layer obtained from the model analysis were compared with the field monitored data provided in Chapter 5 in order to validate the model. The validated numerical model was used to predict the vertical movements of the embankment with variations of EPS geofoam layer height and types of the EPS geofoam.

The monitored field data and numerical model analysis results indicate that using the lightweight EPS geofoam as an embankment backfill material is an effective method to reduce the amount of settlements which occur in an embankment. Moreover, it was also found that the magnitude of the settlements decreases with the increase in the height and the density of EPS geofoam.

Chapter 7

Design Guidelines for the EPS Geofoam Embankment

7.1 Introduction

This chapter provides the design guidelines and recommendations for possible future use in the EPS geofoam embankment projects. The guidelines are summarized from three different standards, which are NCHRP 529, European standard, and Japanese standard, along with the results investigated from the field test and obtained from the FEM models. Design charts to estimate the thickness of concrete pavement and EPS geofoam layer are provided in the guidelines.

At the beginning, the scopes and assumptions for the guidelines, as well as the design methodology, are described. Then, the step-by-step procedures and design charts utilized in selecting the appropriate type of EPS geofoam and evaluating the thickness of the EPS blocks layer are provided. Additionally, an example of the EPS geofoam embankment design is presented in order to provide a clear understanding of how to apply the proposed guidelines. Finally, the recommendations for the construction of EPS geofoam embankments are summarized and briefly explained.

7.2 Scope and Assumptions for the Design Guidelines

The scopes and assumptions for the proposed EPS geofoam embankment design guidelines are listed in following:

1. This design guideline is limited to the sloped-side fill (i.e., trapezoidal shaped) EPS geofoam embankments. The major components of an EPS-block geofoam embankment, as presented in Figure 7.1, consist of the pavement system, the proposed embankment backfill, and the existing foundation soil.

Figure 7.1 Sloped-side fill EPS geofoam embankment and its components

2. The materials used for the embankment backfill are EPS geofoam blocks and some volume of soil fill, as illustrated in Figure 7.1.
3. Based on the modeling analysis results presented in Chapter 6, the EPS22, EPS29, EPS39, and EPS46 geofoams show a good performance in reducing the settlement of the approach embankment. However, in this guideline, the EPS22, EPS29, and EPS39 geofoams are considered as the best choices of selected fill materials in the designed embankment.
4. The embankment fill soil is assumed to be borrowed from the existing foundation soil. Therefore, the properties, such as undrained shear strength (S_u) and compressibility (e_o, C_c, C_s, *and OCR*), of the fill soil and foundation soil are considered to be the same.
5. The unit weight of the compacted backfill soil is assumed to be 120 pcf (18.85 kN/m^3).
6. According to Archeewa (2010), there are two types of the approach slabs used by highway agencies: bituminous approach pavement and reinforced concrete pavement. However, the use of bituminous approaches is still not highly preferred by the DOTs (Wahls, 1990). Thus, in this design guideline, the EPS geofoam embankment is designed primarily for supporting the reinforced concrete pavement system.

7. Flexible (unbonded) base with 15 to 20-in. (381 to 508 mm) thickness is assumed to be used as the subbase layer of the concrete pavement system (TxDOT, 2008). The thickness of the concrete pavement varies with the summation of equivalent 18-kip (80-kN) single-axial loads (ESAL).
8. According to the preliminary design of the reconstructed US 67 bridge embankment, using EPS geofoam as a partially filled material, provided by TxDOT, the various component layers of the pavement system are assumed to have an average unit weight of 140 pcf (22 kN/m^3).
9. This design guideline is provided for the EPS geofoam embankment that has the geometries as listed below:
    a) The width of a traffic lane is assumed to be 12 ft. (3.66 m).
    b) Widths at the top of the embankment are 36 ft. (11 m) for a two-lane roadway with two 6-ft. (1.8-m) shoulders, and 76 ft. (23 m) for a four-lane roadway with two 10-ft. (3-m) exterior shoulders and two 4-ft. (1.2 m) interior shoulders.
    c) Embankment side slopes are 2H:1V; 3H:1V; and 4H:1V. It should be noted that H and V stand for horizontal and vertical, respectively.
    d) Height of embankment, excluding pavement layer, varies from 10 ft. (3 m) to 50 ft. (15.24 m), with the increment of 10 ft. (3 m).
10. Both English unit system and International System of Units (SI unit) are used in this guideline.
11. The purpose of this design guideline is to provide guidance for a preliminary design of the EPS geofoam embankment. More detailed design is required for the final design.

7.3 Design Methodology

In the design of earth structures, such as retaining walls, foundations, and slope stability, the service loads and Allowable Stress Design (ASD) methodology with factor of safety are generally used. According to Stark et al. (2004), in the present time, only the ASD methodology is used in the design of the earthworks involving EPS geofoam material. The EPS-block geofoam embankments must be designed for both internal and external stability conditions.

The main concern of designing for internal stability of the EPS geofoam embankment is to properly select the appropriate type of EPS geofoam that can support the loads from the pavement system and traffic without excessive deformations. The design for external stability considers the failures of the embankment for both serviceability and ultimate failures (Stark, et al., 2004). In this study, the external stability of EPS geofoam embankment, including the issues of soil settlement and bearing capacity, is primarily considered.

The main objective of this design guideline exercise is to optimize the design by minimizing the thickness of EPS geofoam layer to be used in the embankment and using the EPS block with the lowest possible density. Therefore, the present design guideline has potential to produce a cost-effective design for the EPS geofoam embankment, but still meet the design criteria pertaining to the settlement and stability of the embankment section.

7.4 Step-by-Step Design Procedure

As presented in Figure 7.2, the design procedure starts with the selection of the concrete pavement thickness. According to the AASHTO 1993 design procedure, the thickness of rigid pavement (i.e., concrete pavement) is dependent on the value of resilient modulus of subgrade, which is EPS geofoam in this case; level of percent of

reliability and ESALs, which is the statistic represents a mixed traffic of different axle configurations converted into an equivalent number of 18-kip (80-kN) single-axle loads summed over the performance period (Stark et al., 2004).

The second step is calculating the vertical stresses at the top of EPS geofoam layer. In this step, the vertical stresses from the weight of the overlying pavement system and traffic loads are calculated.

In the third step, the appropriate type of EPS geofoam is selected by comparing the allowable compressive stress of the EPS block with the factored vertical stress on top of the EPS geofoam layer.

Next, the minimum thickness of EPS geofoam layer is calculated based on the bearing capacity of the foundation soil.

Finally, the settlement of the EPS geofoam embankment is calculated and compared with the allowable settlement. The thickness of EPS geofoam layer should be increased if the settlement of EPS geofoam embankment is higher than the allowable value.

It should be noted that the design for external stability is primarily concerned only with the settlement and bearing capacity of the foundation soil underlying the EPS geofoam embankment. An analysis of the embankment slope stability and the effects of seismic loading are not included in this design guideline.

The details of each design step procedure, with the pertinent design charts are explained and provided in the following subsections.

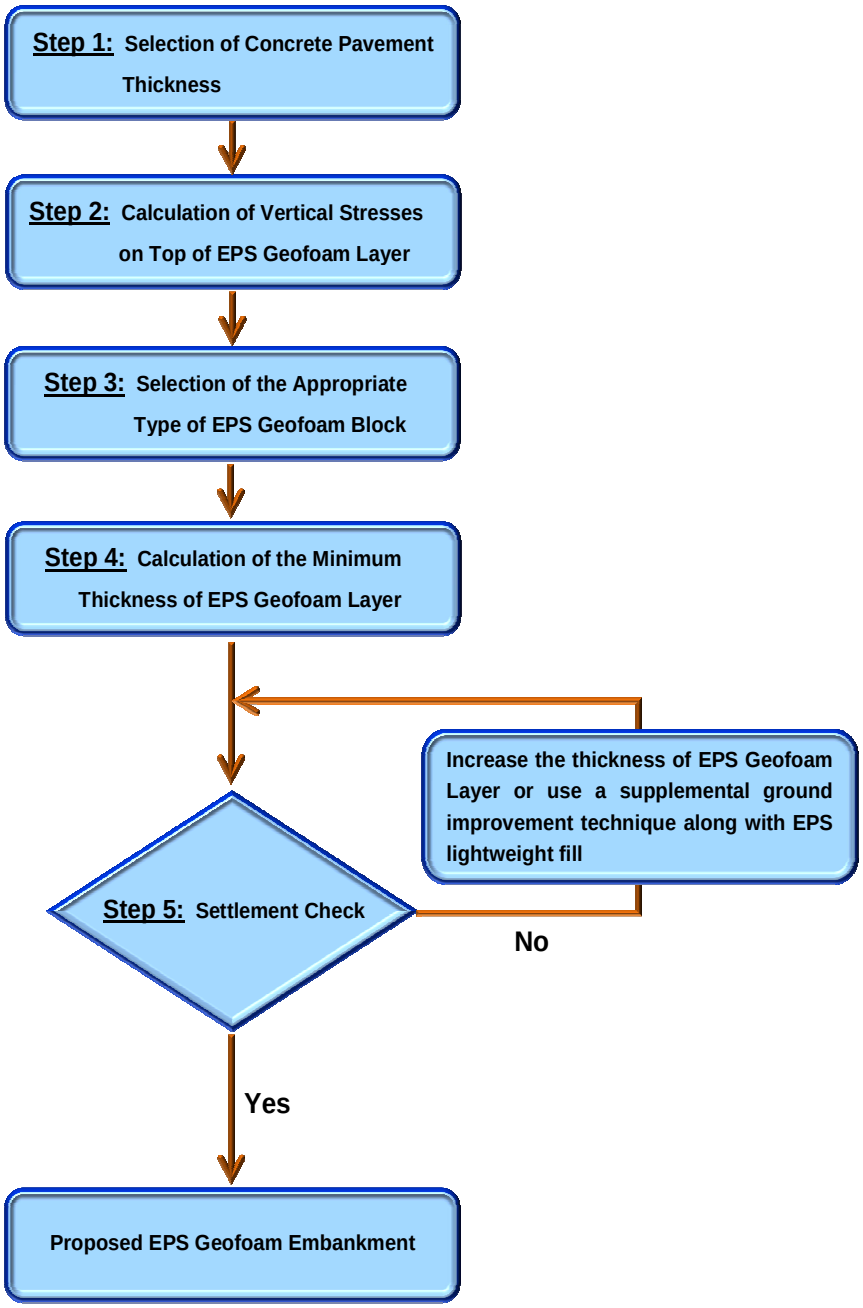

Figure 7.2 Flow chart of design procedure for EPS geofoam embankment

7.4.1 Step 1: Selection of Concrete Pavement Thickness

In this step, the design chart for obtaining the thickness of the concrete pavement corresponding to the ESALs value is provided, as presented in Figure 7.3. The pavement thicknesses were calculated in accordance with the AASHTO 1993 design procedure and the following assumptions:

- EPS geofoam blocks are considered to be the subgrade supporting the layers of subbase material and concrete pavement. The representative resilient modulus values of EPS subgrade used in the calculation are assumed to be equal to the initial tangent Young's modulus of the EPS block (Stark, et al., 2004), as presented in Table 7.1.

Table 7.1 Equivalent soil subgrade properties of EPS geofoam for the pavement design

Type of EPS geofoam (ASTM D6817)	Density, min., pcf (kg/m^3)	Initial Tangent Young's modulus, E_{ti}, psi (MPa)	Resilient Modulus, M_R, psi (MPa)
EPS22	1.35 (21.6)	725 (5)	725 (5)
EPS29	1.80 (28.8)	1,090 (7.5)	1,090 (7.5)
EPS39	2.40 (38.4)	1,500 (10.3)	1,500 (10.3)

- According to TxDOT (2008), the ESALs traffic levels are classified as follows:
    - Low traffic: ESALs $\leq$ 500,000
    - Moderate traffic: 500,000 $<$ ESALs $\leq$ 3,000,000
    - High traffic: ESALs $>$ 3,000,000
- The designs of pavement thickness are based on an 85 percent-level of reliability. This level covers all low-volume road design and interstate and other freeways design (Huang, 2004 after AASHTO, 1986).
- The properties of Portland Cement Concrete (PCC) used in the design are listed as following:

- Mean PCC elastic modulus (E_c): 5,000,000 psi (34.5 GPa)
- Mean PCC modulus of rupture (S_c'): 650 psi (4.5 MPa)

- The designs are based on the high quality subbase material with a thickness of 15 to 20 in. (380 to 500 mm) to minimize the PCC slab thickness used.
- Fair drainage condition with the drainage coefficient (C_d) of 1.0 is used in the designs.
- It is recommended that the minimum thickness of the pavement system (i.e., for both subbase and pavement layers) should be equal to or greater than 24 in. (610 mm) in order to minimize the effects of differential icing and solar heating (Stark, et al., 2004).

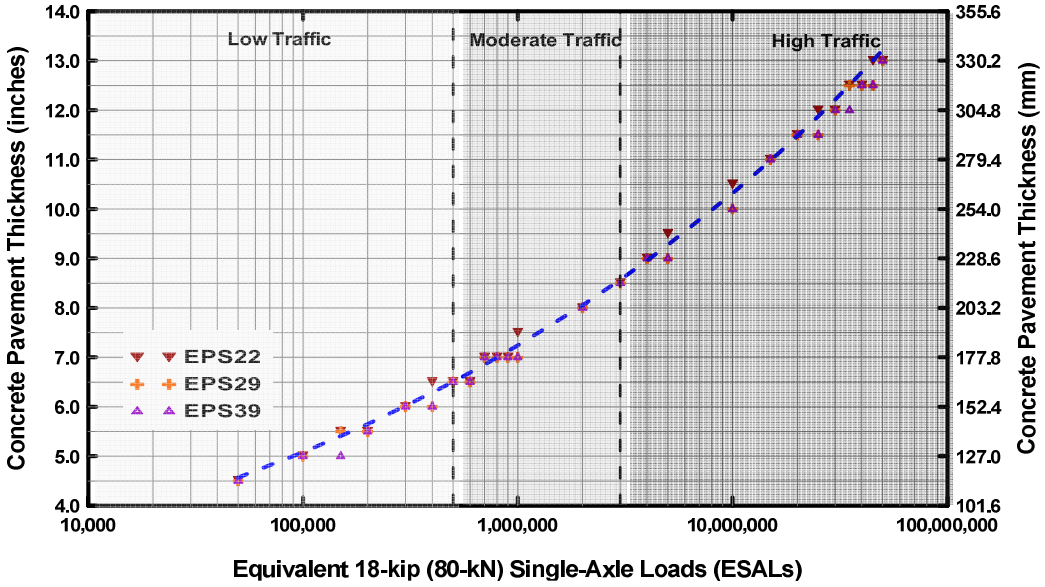

Figure 7.3 Design chart to obtain the thickness of concrete pavement

7.4.2 Step 2: Calculation of Vertical Stresses on Top of EPS Geofoam Layer

As discussed in Section 6.3.3, the vertical stresses on the top of EPS geofoam layer consist of the gravity stress from the weight of the pavement system and the traffic stresses, which can be estimated based on the following assumptions:

- The gravity stress from the weight of the pavement system is calculated as follows:

$$\sigma_{DL} = T_{Pavement} \times \gamma_{Pavement} \quad (7.1)$$

when σ_{DL} is gravity stress due to dead loads (i.e., weight of the pavement system); $T_{Pavement}$ is the pavement system thickness; and $\gamma_{Pavement}$ is the average unit weight of the pavement system (i.e., 140 pcf (22 kN/m^3)).

- The Burmister (1943) method is used to calculate the vertical stress from traffic load ($\sigma_{Traffic}$) distributed on the top of EPS geofoam layer. The detail of calculation was presented previously in Section 6.3.3.
- The effects of dynamic and vibratory from the traffic are considered in terms of an impact allowance. The impact coefficient (I) of 0.3 is used in the traffic stresses calculation.
- A design lane load of 0.64 k/ft. uniformly distributed in a longitudinal direction is the type of live load for the highway bridge design. However, the stress effects from this load should not be subjected to a dynamic load allowance. The magnitude of the stress due to the lane load can calculated as following:

$$\sigma_{Lane\ Load} = (0.64\ k/ft) \,/\, \text{Lane Width (ft)} \quad (7.2)$$

- The vertical stress from live loads (i.e., traffic loads and lane load) including the impact allowance can be estimated as follows:

$$\sigma_{LL} = [\sigma_{Traffic} \times (1 + I)] + \sigma_{Lane\ Load} = (\sigma_{Traffic} \times 1.3) + \sigma_{Lane\ Load} \quad (7.3)$$

7.4.3 Step 3: Selection of the Appropriate Type of EPS Geofoam Block

The appropriate EPS geofoam blocks selected for use as the backfill material of an embankment should have an allowable stress greater than or equal to the factored

vertical stresses on top of the EPS geofoam layer in order to limit the damage and long-term creep deformation of the geofoam embankment.

Currently, three different methods of evaluating the allowable stress in the EPS geofoam block and the factored stress on the top of EPS geofoam layer have been proposed in the design guidance from Japan, Europe, and the United States. In this study, the three different methods are briefly explained and compared by using the results from this present study.

7.4.3.1 Japanese Practice (Tsukamoto, 2011)

The EPS method Development Organization (EDO), Japan proposed that the allowable stress level in the EPS geofoam block is to 50 percent of the compressive strength at 10 percent axial strain, and the vertical stress on the top of EPS geofoam layer is equal to the sum of the gravity stress due to dead loads (σ_{DL}) and vertical stress from traffic loads (σ_{LL}), without any additional load factors. The relationship between the vertical stress on the top of EPS geofoam layer and allowable stress in the EPS geofoam block for this method can be written as the following equation:

$$\sigma_{DL} + \sigma_{LL} \leq 0.5\ (compressive\ strength\ of\ EPS\ block\ @\ 10\%\ strain) \qquad (7.4)$$

7.4.3.2 European Standard (EPS White Book, 2011)

The European product standard for EPS in Civil Engineering Application (EN 14933) adopted in March 2009 provided the design criteria to evaluate an allowable stress in the EPS geofoam block and a factored stress on the top of EPS geofoam layer for various load combinations. The three different cases of load combinations and allowable stresses are presented in the following.

Ultimate Limit State (STR) Short Term

The effects of both permanent loads (i.e., dead loads) and cyclic loads (i.e., traffic loads) were considered in this case. The relationship between factored vertical

stress on EPS geofoam layers and allowable stress in EPS geofoam blocks for this case is shown in following equation:

$$1.35\ (\sigma_{DL}) + 1.50\ (\sigma_{LL}) \leq\ (\sigma_{10})/\ 1.25 \tag{7.5}$$

when σ_{10} is the compressive strength of EPS geofoam at 10 percent axial strain.

Ultimate Limit State (STR) Permanent

Only the stress from permanent loads (i.e., dead loads) with the load factor of 1.35 was considered. Equation 7.6 below presents the relationship of the factored vertical stress on the EPS geofoam layer and allowable stress on the EPS geofoam block:

$$1.35\ (\sigma_{DL}) \leq\ (0.3\ \times\ \sigma_{10})/\ 1.25 \tag{7.6}$$

Ultimate Limit State (GEO) Cyclic Loads

As presented in Equation 7.7 below, only the stress from cyclic loads (i.e., traffic loads) was considered in this case. The load factor of 1.5 was used to multiply with the vertical stress from traffic loads to find the factored vertical stress on top of the EPS geofoam layer. The allowable stress in EPS geofoam block was calculated by dividing the multiple of 0.35 and the compressive resistance of EPS geofoam at 10 percent of strain with 1.25.

$$1.50\ (\sigma_{LL}) \leq\ (0.35\ \times\ \sigma_{10})/\ 1.25 \tag{7.7}$$

7.4.3.3 NCHRP 529 (Stark et al., 2004)

As presented in the previous sections, the allowable stress defined in the Japanese and European approaches are based on the compressive strength of EPS geofoam at 10 percent of axial strain. Contrary to those methods, the allowable stress, referred to as the allowable elastic stress limit in NCHRP 529, is based on the compressive resistance at 1 percent axial strain. In the NCHRP 529, the factored vertical stress on top of EPS geofoam layer is defined as the result of the combination of dead

and live loads multiplied by a factor of safety (FS) of 1.2, as presented in the left side of the following equation.

$$1.2 \times (\sigma_{DL} + \sigma_{LL}) \leq (compressive\ strength\ of\ EPS\ block\ @\ 1\%\ strain) \quad (7.8)$$

7.4.3.4 Appropriate EPS Geofoam Selection Criteria for this Design Guideline

In this section, the three methods explained previously are used to evaluate the allowable stress in the EPS geofoam block and factored stresses on the top of the EPS geofoam layer. The results from those methods are compared to receive the appropriate EPS geofoam selection criterion used in this design guideline. The data presented in Chapter 6, Section 6.3.3 and listed below is used in this study:

- The gravity stress from the weight of pavement system: σ_{DL} = 2.0 psi
- The vertical stress from traffic loads with the impact effect: σ_{LL} = 5.6 psi
- The properties of EPS22 geofoam are presented in Table 7.2.

Table 7.2 Properties of EPS22 Geofoam (source: ASTM D 6817)

Properties	EPS22 Geofoam
Density, min., kg/m^3 (pcf)	21.6 (1.35)
Compressive Resistance at 1%, min., kPa (psi)	50 (7.3)
Compressive Resistance at 5%, min., kPa (psi)	115 (16.7)
Compressive Resistance at 10%, min., kPa (psi)	135 (19.6)

Based on the provided data, the values of factored stresses on the top of the EPS geofoam layer and allowable stress in the EPS geofoam block are calculated in accordance with the design criteria proposed in the Japanese, European, and NCHRP 529 methods. The calculation results, along with the design criteria, are presented in Table 7.3.

Table 7.3 Factored Stresses and Allowable Stresses Calculated by Various Methods

Method	Factored stress, psi	Allowable stress, psi	Criteria satisfaction	
			Yes	No
1. Japanese method:				
$\sigma_{DL} + \sigma_{LL} \leq 0.5\ (\sigma_{10})$	7.6	9.8	✓	
2. European method:				
2.1 STR-short term:				
$1.35\ (\sigma_{DL}) + 1.50\ (\sigma_{LL}) \leq\ (\sigma_{10})/\ 1.25$	11.1	15.68	✓	
2.2 STR-permanent:				
$1.35\ (\sigma_{DL}) \leq\ (0.3\ \times\ \sigma_{10})/\ 1.25$	2.7	4.7	✓	
2.3 GEO-cyclic loads:				
$1.50\ (\sigma_{LL}) \leq\ (0.35\ \times\ \sigma_{10})/\ 1.25$	8.4	5.5		✓
3. NCHRP 529 method:				
$1.2\ \times (\sigma_{DL} +\ \sigma_{LL})\ \leq (\sigma_1)$	9.12	7.3		✓

The results summarized in the above table show that the design criteria for internal stability of EPS geofoam are satisfied for the Japanese method and European methods 2.1 and 2.2. However, it does not comply with the NCHRP 529 and European method 2.3 methods. This can be attributed to the more conservative design approaches of those methods.

Based on the results, the appropriate EPS geofoam selection criteria for this design guideline can be prepared using the factored stress on top of EPS geofoam layer from NCHRP 529 method compared to the allowable stress in EPS geofoam block from Japanese method, as presented in Equation 7.9. Using this criteria not only adopts a lesser conservative design but also provides reliable factor of safety.

$$1.2\ (\sigma_{DL} +\ \sigma_{LL})\ \leq 0.5\ (\sigma_{10}) \tag{7.9}$$

when σ_{10} is the compressive resistance of EPS geofoam at 10% axial strain.

7.4.4 Step 4: Calculation of the Minimum Thickness of EPS Geofoam Layer

The approach to determine minimum thickness of EPS geofoam layer provided in this design guideline was modified from an evaluation of external bearing capacity of an EPS-block geofoam embankment proposed by Stark et al. (2004) in the NCHRP 529 report. If an external bearing capacity failure occurs, the embankment can undergo excessive vertical settlement and hence can influence adjacent properties (Stark et al., 2004).

The general bearing capacity equation was suggested by Meyerhof (1963) as following:

$$q_{ult} = cN_cF_{cs}F_{cd}F_{ci} + qN_qF_{qs}F_{qd}F_{qi} + \frac{1}{2}\gamma BN_\gamma F_{\gamma s}F_{\gamma d}F_{\gamma i} \quad (7.10)$$

where c is cohesion of foundation soil (psf or kPa); $q = \gamma D_f$ is an effective stress at the level of the bottom of embankment (psf or kPa); D_f is depth of embedment (ft. or m); γ is unit weight of foundation soil (pcf or kN/m^3); B is bottom width of embankment (ft. or m); N_c, N_q, N_γ are bearing capacity factors; $F_{cs}, F_{qs}, F_{\gamma s}$ are shape factors; $F_{cd}, F_{qd}, F_{\gamma d}$ are depth factors; and $F_{ci}, F_{qi}, F_{\gamma i}$ are load inclination factors.

Based on the assumption that most EPS geofoam embankments will be constructed on the ground surface of saturated soft cohesive soil that allows c to equal the undrained shear strength, S_u, of the foundation soil as well as friction angle (ϕ) and D_f equal to zero. The general bearing capacity equation can be simplified as follows:

$$q_{ult} = S_uN_cF_{cs}F_{cd}F_{ci} + (0)N_qF_{qs}F_{qd}F_{qi} + \frac{1}{2}\gamma B(0)F_{\gamma s}F_{\gamma d}F_{\gamma i} \quad (7.11a)$$

$$q_{ult} = S_uN_cF_{cs}F_{cd}F_{ci} \quad (7.11b)$$

when, $F_{cs} = 1 + (\frac{B}{L})(\frac{N_q}{N_c})$; $F_{cd} = 1 + 0.4(\frac{D_f}{B})$; and $F_{ci} = \left[1 - \left(\frac{\beta^\circ}{90^\circ}\right)\right]^2$; β° = inclination of the load on the embankment with respect to the vertical (i.e., equal to zero for this case). Moreover, it should be noted that at ϕ = 0, N_c = 5.14, N_q = 1, and N_γ = 0.

According to Stark et al. (2004), the EPS geofoam embankment can be considered as a continuous or strip foundation that has the length significantly larger the width. This causes the term $\frac{B}{L}$ in above equations approach zero. By substituting all parameters into Equation 7.11b, the following results are obtained:

$$F_{cs} = 1 + \left(\frac{B}{L}\right)\left(\frac{N_q}{N_c}\right) = 1 + (0)\left(\frac{1}{5.14}\right) = 1$$

$$F_{cd} = 1 + 0.4\left(\frac{D_f}{B}\right) = 1 + \left(\frac{0}{B}\right) = 1$$

$$F_{ci} = \left[1 - \left(\frac{\beta^\circ}{90^\circ}\right)\right]^2 = \left[1 - \left(\frac{0}{90}\right)\right]^2 = 1$$

Finally, the Equation 7.11b can be rewritten as follows:

$$q_{ult} = 5.14\, S_u \tag{7.12}$$

Based on the allowable stress design (ASD) method, an allowable bearing capacity (q_{all}) can be calculated by dividing the ultimate bearing capacity (q_{ult}) by a factor of safety (FS), as presented in Equation 7.13.

$$q_{all} = \frac{q_{ult}}{FS} \qquad \text{or} \qquad q_{ult} = (FS)(q_{all}) \tag{7.13}$$

In the designing of EPS geofoam embankment, the stresses at the top surface of foundation soil are from three parts, including the normal stresses distributed from pavement system and traffic surcharges, as well as the normal stress applied by weight of fill materials. By substituting Equation 7.12 and the stresses on top of foundation soil into Equation 7.13, the following expression is obtained:

$$5.14\ S_u = (FS)[\Delta\sigma_{pavement} + \Delta\sigma_{traffic} + \Delta\sigma_{fill\ mass}] \quad (7.14a)$$

or $$S_u = \frac{(FS)}{5.14}[\Delta\sigma_{pavement} + \Delta\sigma_{traffic} + \Delta\sigma_{fill\ mass}] \quad (7.14b)$$

Based on the dimensions of an EPS geofoam embankment, as presented in Figure 7.4, the 2:1 method of determining the stress increase on top of foundation soil, the $\Delta\sigma_{pavement}$, $\Delta\sigma_{traffic}$, and $\Delta\sigma_{fill\ mass}$ can be expressed as follows:

$$\Delta\sigma_{pavement} = \frac{(\sigma_{o,\ pavement})(W)(L)}{(W+H_{Emb.})(L)} = \frac{(\sigma_{o,\ pavement})(W)}{(W+H_{Emb.})} \quad (7.15)$$

$$\Delta\sigma_{traffic} = \frac{(\sigma_{o,\ traffic})(W)(L)}{(W+H_{Emb.})(L)} = \frac{(\sigma_{o,\ traffic})(W)}{(W+H_{Emb.})} \quad (7.16)$$

$$\Delta\sigma_{fill\ mass} = \frac{[(\gamma_{EPS})(A_{EPS})(L)]+[(\gamma_{fill\ soil})(A_{fill\ soil})(L)]}{[W+2(Slope)(H_{Emb.})][L]}$$

$$= \frac{[(\gamma_{EPS})(A_{EPS})]+[(\gamma_{fill\ soil})(A_{fill\ soil})]}{[W+2(Slope)(H_{Emb.})]} \quad (7.17)$$

$$A_{EPS} = \frac{1}{2}\left[W + \left(W + 2(Slope)(H_{EPS})\right)\right][H_{EPS}]$$

$$= [W + (Slope)(H_{EPS})][H_{EPS}] \quad (7.18)$$

$$A_{whole\ emb.} = \left[\left(W + 2(Slope)\left(H_{pave.}\right)\right) + (Slope)(H_{Emb.})\right][H_{Emb.}] \quad (7.19)$$

$$A_{fill\ soil} = A_{whole\ emb.} - A_{EPS} \quad (7.20)$$

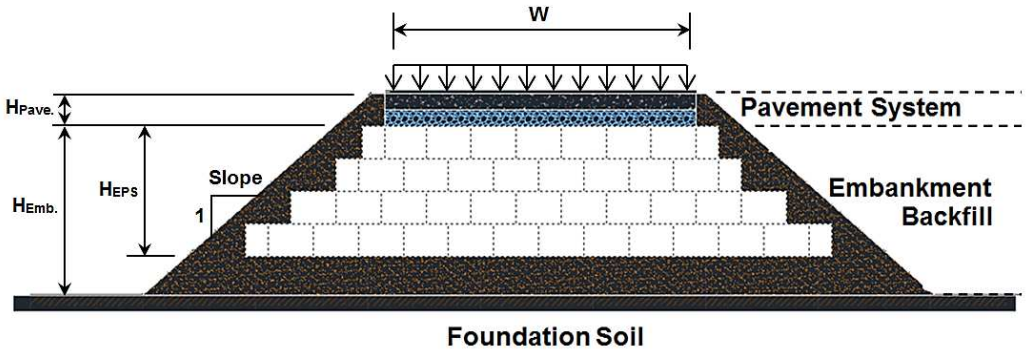

Figure 7.4 Typical cross section of an EPS geofoam embankment

In this guideline, the design charts for evaluating the required minimum thickness of EPS geofoam layer for undrained shear strength of foundation soil and desirable factor of safety are provided and presented in Figures 7.5 to 7.14. The charts were developed for designing the EPS geofoam embankments which have the side slope of 2H:1V; 3H:1V; and 4H:1V, based on the following assumptions:

- The thickness of pavement system is assumed to be 2 ft. (0.61 m).
- The pavement system is assumed to have an average unit weight of 140 pcf (22 kN/m^3).
- The normal stress induced on EPS geofoam layer ($\sigma_{o,\ traffic}$) due to the design truck HS-20 system on a 2-ft (0.61-m) thick pavement is calculated as 5.6 psi (38.61 kPa). This normal stress value was used in creating the design charts.
- The unit weight of the compacted backfill soil is assumed to be 120 pcf (18.85 kN/m^3).
- The unit weight of the EPS39 geofoam, which is 2.4 pcf (38.4 kg/m^3), was used in preparing the design charts. The selection of EPS39 geofoam was mainly based on the present conservative design approach.

The figure numbers of the design charts with their corresponding cases of EPS geofoam embankments are presented in Table 7.4.

Table 7.4 List of the Design Charts to find the Minimum Height of EPS Geofoam Layer

Figure	Design chart	Embankment height, $H_{Emb.}$, ft	Top width of embankment, W, ft
Figure 7.5	A	10	36 (2 Lanes)
Figure 7.6	B	10	76 (4 Lanes)
Figure 7.7	C	20	36 (2 Lanes)
Figure 7.8	D	20	76 (4 Lanes)
Figure 7.9	E	30	36 (2 Lanes)
Figure 7.10	F	30	76 (4 Lanes)
Figure 7.11	G	40	36 (2 Lanes)
Figure 7.12	H	40	76 (4 Lanes)
Figure 7.13	I	50	36 (2 Lanes)
Figure 7.14	J	50	76 (4 Lanes)

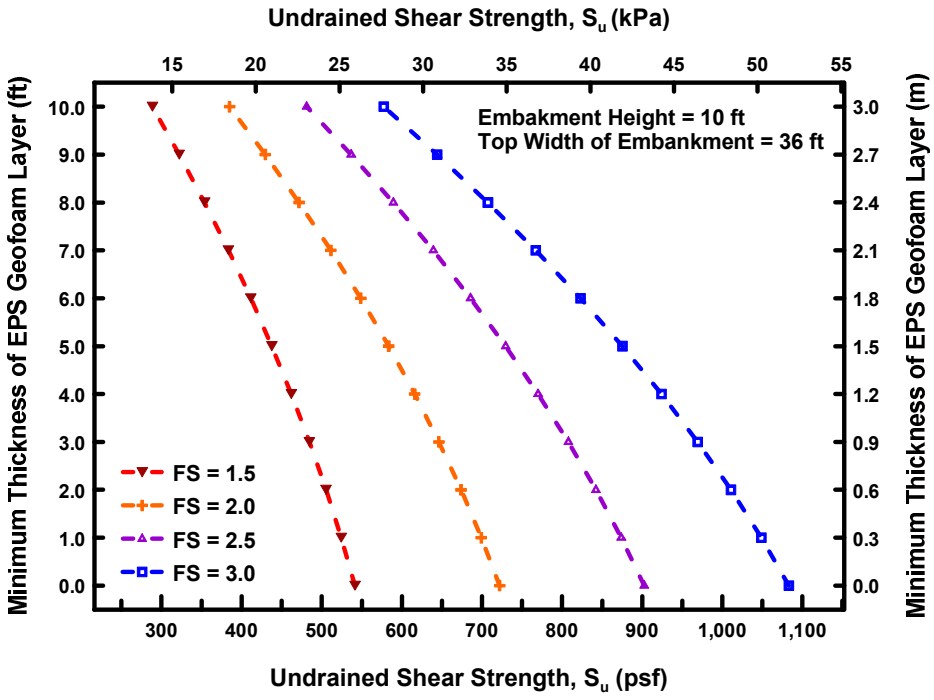

Figure 7.5 Design chart A: Embankment height = 10 ft. and Top width = 36 ft.

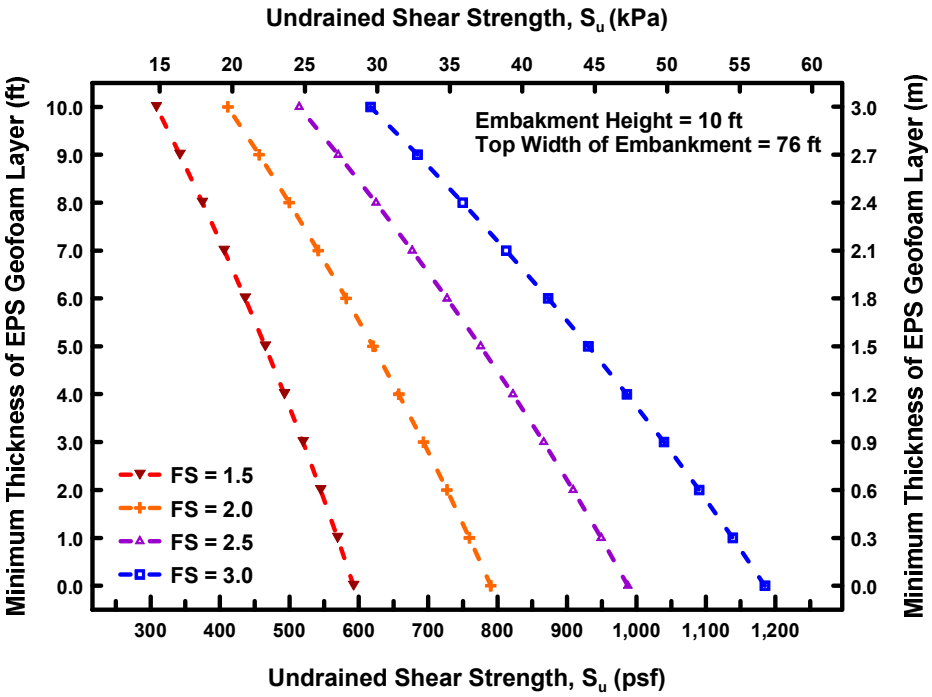

Figure 7.6 Design chart B: Embankment height = 10 ft. and Top width = 76 ft.

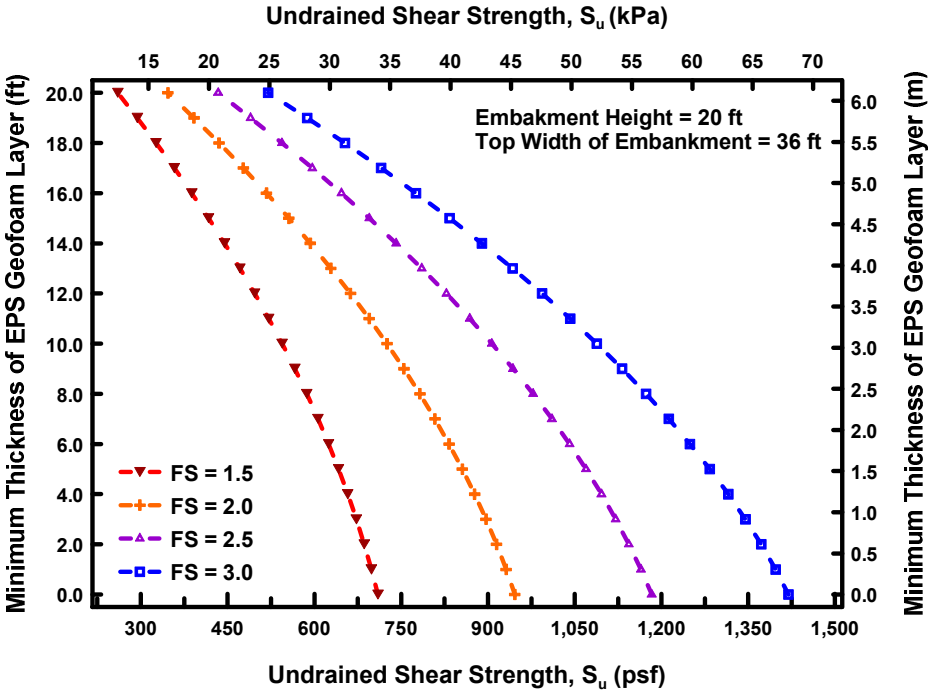

Figure 7.7 Design chart C: Embankment height = 20 ft. and Top width = 36 ft.

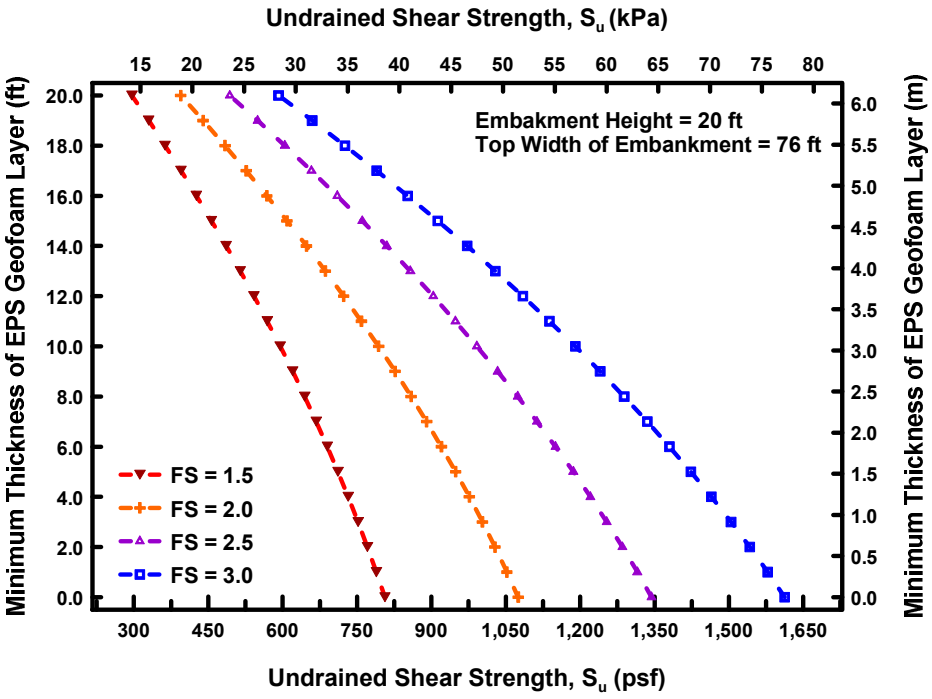

Figure 7.8 Design chart D: Embankment height = 20 ft. and Top width = 76 ft.

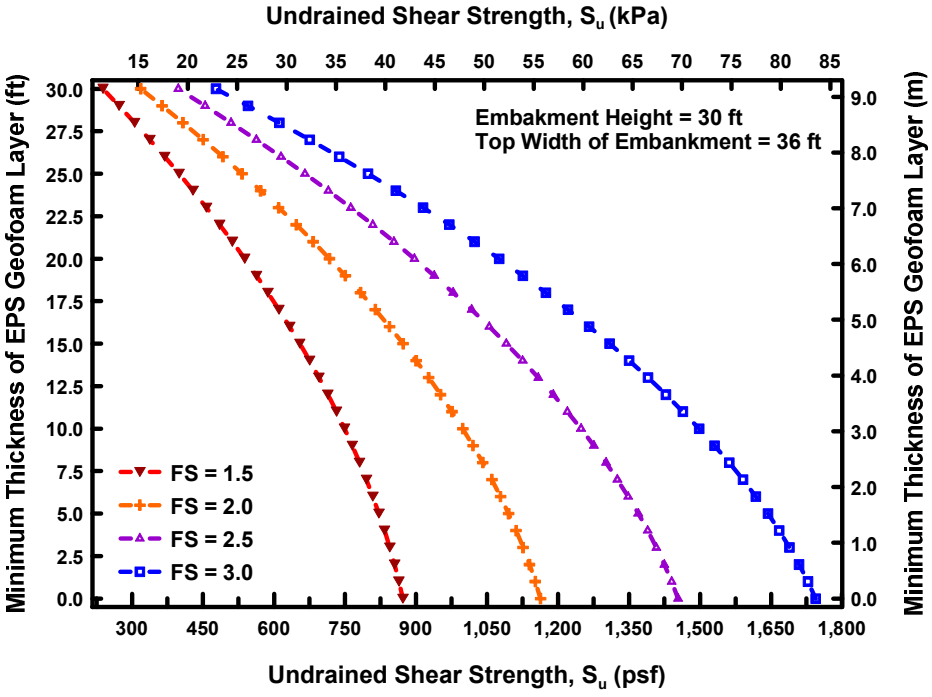

Figure 7.9 Design chart E: Embankment height = 30 ft. and Top width = 36 ft.

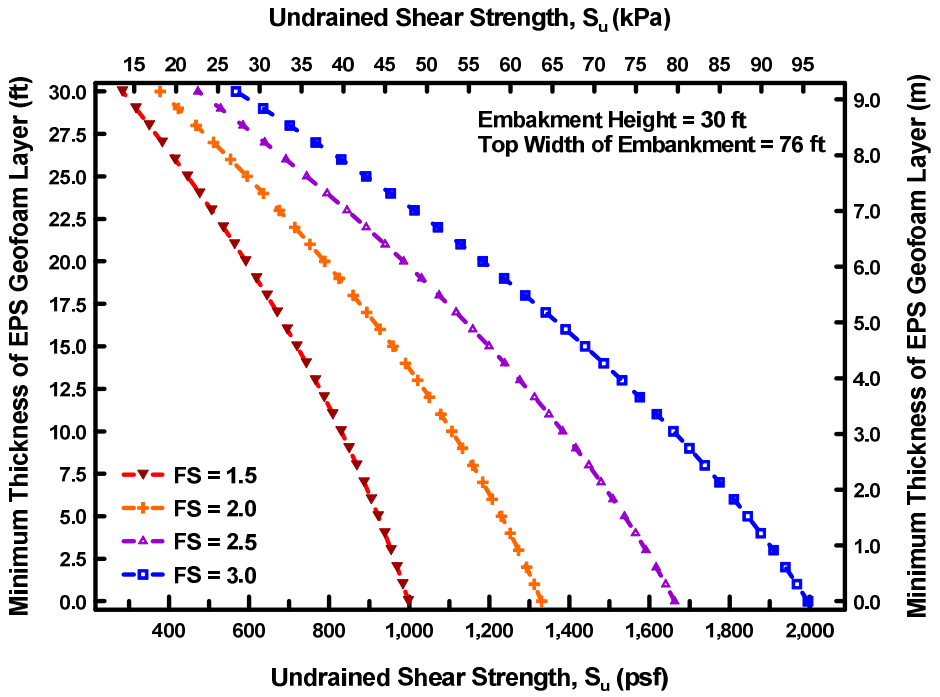

Figure 7.10 Design chart F: Embankment height = 30 ft. and Top width = 76 ft.

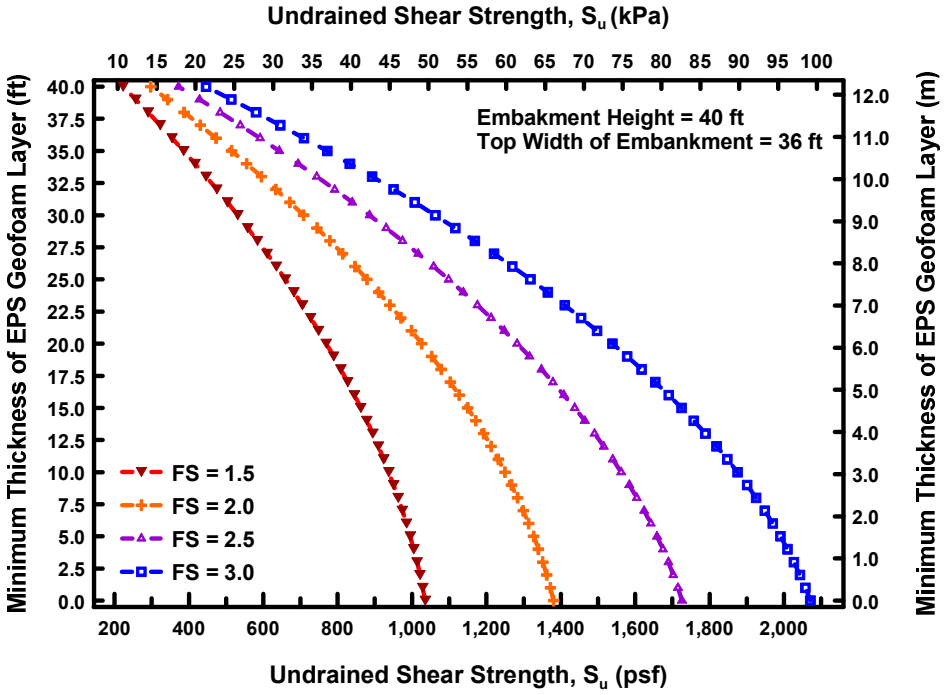

Figure 7.11 Design chart G: Embankment height = 40 ft. and Top width = 36 ft.

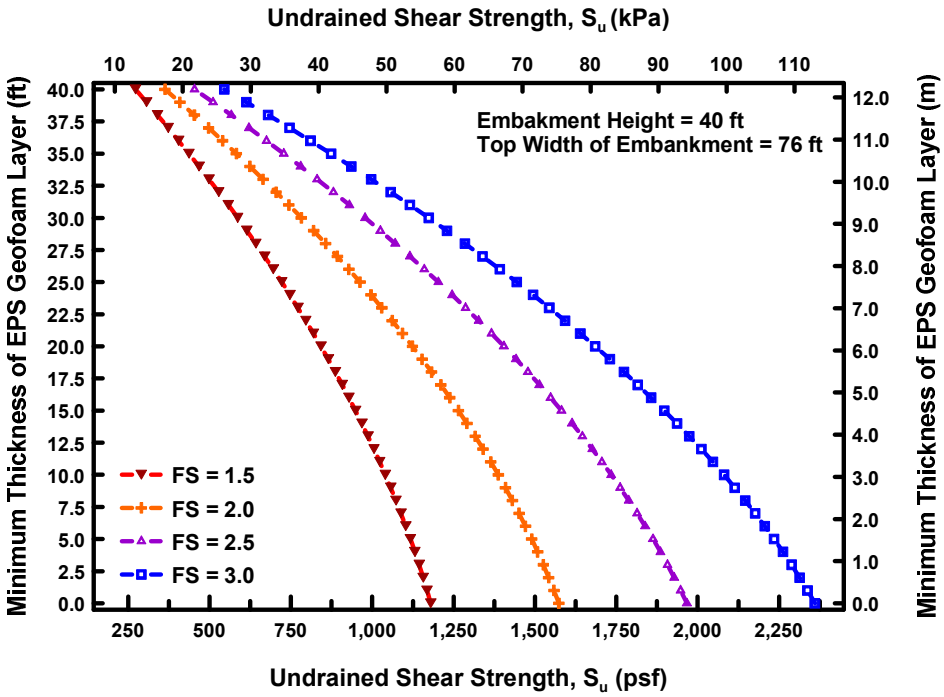

Figure 7.12 Design chart H: Embankment height = 40 ft. and Top width = 76 ft.

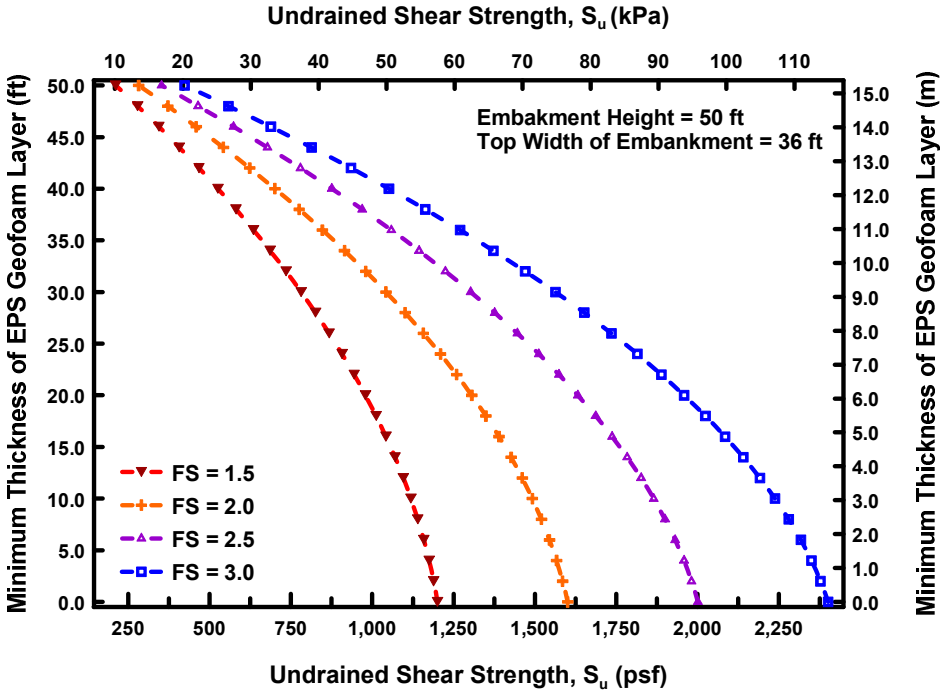

Figure 7.13 Design chart I: Embankment height = 50 ft. and Top width = 36 ft.

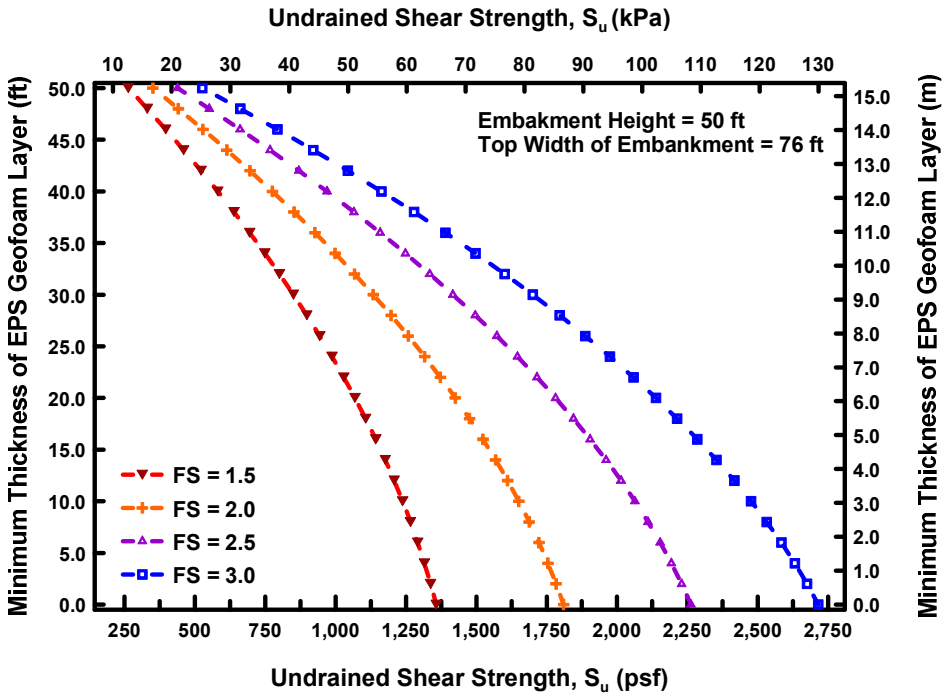

Figure 7.14 Design chart J: Embankment height = 50 ft. and Top width = 76 ft.

7.4.5 Step 5: Settlement Check

In general, the soil settlement caused by loads may be broadly divided into three categories, including elastic or immediate settlement; consolidation; and secondary compression (Holtz and Kovacs, 1981). However, in the NCHRP 529 report, Stark et al. (2004) subdivided the total settlement (S_{total}) which occurred on an embankment into five components, consisting of immediate settlement of fill mass (S_{if}); immediate settlement of foundation soil (S_i); primary consolidation of foundation soil (S_p); secondary consolidation of foundation soil (S_s); and long-term vertical deformation (creep) of the fill mass (S_{cf}), as expressed in Equation 7.21:

$$S_{total} = S_{if} + S_i + S_p + S_s + S_{cf} \tag{7.21}$$

According to Stark et al. (2004), the immediate settlement of both fill mass and foundation soils, as well as the long-term creep deformation of the fill mass, can be

disregarded in the calculation of the total settlement of an EPS-geofoam embankment. This is because the immediate settlements of the fill and foundation soil are completely occurred during the construction process and will not affect the condition of the final pavement system. Moreover, the value of long-term vertical deformation of the EPS geofoam block is expected to be less than 1.5 percent in accordance with its internal stability design (as mentioned in section 7.4.3). Hence, only primary and secondary consolidation settlements of soil foundation are focused on in the estimation of total settlement of the EPS geofoam embankment. Equation 7.21 can be rewritten as shown in the following:

$$S_{total} = S_p + S_s \tag{7.22}$$

Settlements of geofoam embankments can be estimated using either numerical models or analytical expressions. Once the settlements are estimated, they need to be compared with the allowable settlements.

According to FHWA (2012), there is little information available on the tolerable settlements of highway embankments. In this section, some of the accessible settlement criterions for a new highway embankment are provided, as presented in Table 7.5.

Table 7.5 Settlement Criteria for New Embankments

Source	Settlement Criteria
Stark et al. (2004); NCHRP 529, US	(a) Post-construction settlements of 12 to 24 in. (305 to 610 mm) during the economic life of a roadway are generally considered as the allowable settlement. (b) At the transition zone between geofoam and embankment soil, the calculated settlement gradient should not exceed 1:200 (vertical / horizontal).
FHWA (2012); US	Post-construction settlements of 12 to 24 in. (305 to 610 mm) over the lifetime of an embankment may be considered tolerable provided they are reasonably uniform, do not occur adjacent to a pile-support structure, and occur slowly over a long period of time.

Table 7.5 – *Continued*

Source	Settlement Criteria
SCDOT (2008); US	(a) Maximum vertical settlement along the profile grade over the design life of the embankment (minimum 100 years) should not exceed 8 to 16 in (203 to 406 mm). (b) Maximum vertical differential settlement between bridge end and end of approach slab should not exceed 0.075 to 0.125 of the approach slab length.
IowaDOT (2014); US	The total settlement of an embankment under the weight of the embankment itself and superimposed loading is frequently limited to a maximum of 3 in (76.2 mm).
Hsi and Martin (2005); Australia	The maximum settlement of between 4 to 6.3 in (100 to 160 mm) for over 40 years is considered as an allowable settlement for a new constructed embankment.
Balasubramaniam et al. (2010); Singapore	In Singapore, the post-construction settlement of 2 in (50 mm) is defined as an allowable settlement for a road embankment and the differential settlement should not more than 1:200 settlement gradient. However, ground improvement technique such as surcharge loads and vertical drain is required to improve the foundation soil before starting the embankment construction.
Long and O'Riordan (2001)	The maximum allowable residual settlement of 14 in (350 mm) is suggested and differential settlement should not exceed 2 in (50 mm) after the operation of 25 years design life.

It can be noticed from the above table that the allowable settlement for a new highway embankment has been defined in different ways. Most criteria assign the allowable settlement relatively high (i.e., from 8 to 24 in.). However, some criteria require very low allowable settlements with foundation soil improvement prior to the embankment construction. In this design guideline, the post-construction settlement of 8 to 16 in. (203 to 406 mm) is considered as the appropriate range to be used as the allowable settlement. The pertinent range is based on the lower and upper bounds established in different specifications as presented in table 7.5. It should be noted that the lower

allowable settlement and can be used only after applying appropriate ground improvement techniques such as, preloading or wick drains.

If the designed EPS geofoam embankment shows the calculated total settlement higher than the allowable settlement, redesigning of the EPS geofoam embankment by increasing the height of EPS geofoam layer or using a supplement ground improvement technique for subgrade foundation along with EPS lightweight fill is required.

7.5 An Example for the Design of EPS Geofoam Embankment

An example of a highway bridge approach embankment design is presented in this section to illustrate the present step-by-step design methodology.

A 30-ft high bridge approach embankment, with a side slope of 3H:1V is assumed to be constructed on US 67 in Cleburne, TX, to support a two-lane roadway with two 6-ft (1.8-m) shoulders. The ESALs traffic level used in the pavement thickness designing is assumed to be 4,000,000. Additionally, in this example, the properties of the foundation soil supporting the embankment, which are necessary for the designing, were assumed and are provided in each design step, as presented in following.

Step1: Designing of the Thickness of Concrete Pavement:

Based on the design chart provided in Figure 7.3 in section 7.4.1, the thickness of concrete pavement suitable for the ESALs value of 4,000,000 can be estimated and equal to 9.0 in. (228.6 mm). Thus, the 15-in. (381-mm) thickness of high quality subbase material with the elastic modulus of at least 40,000 psi (276 MPa) is required in order to increase the whole thickness of the pavement system to be 24 in. (610 mm). Figure 7.15 presents the dimension of the concrete pavement and subbase layer in the designed pavement system.

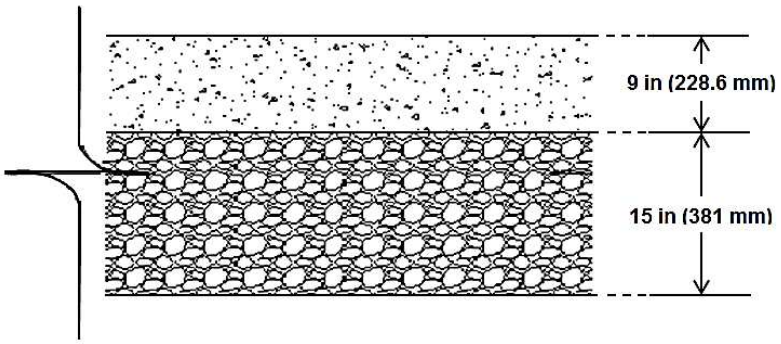

Figure 7.15 Dimension of the designed pavement system

Step2: Calculation of Vertical Stresses on Top of EPS geofoam layer:

In this step, the vertical stresses from both self-weight of the pavement system and the traffic loads are calculated. From Equation 7.1, and based on the assumption that the average unit weight of the pavement system is equal to 140 pcf (22 kN/m^3), the overburden stress from the weight of the designed pavement system can be calculated as per the following:

$$\sigma_{DL} = T_{Pavement} \times \gamma_{Pavement}$$

$$= \left(\frac{24}{12}\, ft\right) \times (140\, pcf) = 280\, psf = 1.94\, psi\ (13.4\, kPa)$$

The vertical stress on the EPS geofoam layer due to the traffic loads (σ_{LL}) is calculated based on the standard truck used in a bridge design. HS-20 has the wheel load of 16.0 kip on tire contact area of 200 square inches (20 in × 10 in). The Burmister (1943) method is used to calculate the vertical stress from the design wheel load on the pavement surface distributed to the top of EPS geofoam layer. The calculation details have been presented exhaustively in the Section 6.3.3.

$$\sigma_{Traffic} = 4.0\, psi = 576\, psf$$

$$\sigma_{Lane\ Load} = 0.64\, klf/(12\, ft) = 0.053\, ksf = 53\, psf = 0.37\, psi$$

$$\sigma_{LL} = (4.0 \times 1.3) + 0.37 = 5.57\, psi = 802\, psf$$

Step 3: Selection of the Appropriate Type of EPS Geofoam Block:

According to the modified criteria for selecting an appropriate type of EPS geofoam block, as presented in Equation 7.9, the required compressive resistance of EPS geofoam at 10% axial strain (σ_{10}) can be calculated as follows:

$$1.2\ [(1.94\ psi) + (5.57\ psi)]\ \leq 0.5\ (\sigma_{10})$$

$$\sigma_{10} \geq 18.02\ psi$$

Table 7.6 presents the minimum values of compressive resistance at 10% axial strain ($\sigma_{10,\ min}$) of EPS22, EPS29, and EPS39 geofoam, defined in ASTM D 6817. When compared with the required σ_{10} (i.e., 18.02 psi), the EPS22 geofoam type is selected to be used as the fill material for the designed embankment for economic reasons.

Table 7.6 Compressive Resistance of EPS Geofoam at 10% Axial Strain

EPS geofoam type	Compressive resistance at 10% axial strain, min, psi (kPa)
EPS22	19.6 (135)
EPS29	29.0 (200)
EPS39	40.0 (276)

Step 4: Calculation of the Minimum Thickness of EPS Geofoam Layer:

As stated previously, the embankment is assumed to be 30 ft. (9 m) height and designed to support a two-lane roadway; thus, the top width of the embankment is equal to 36 ft. (11 m) Based on this information, the design chart E, presented in Figure 7.9, is used to estimate the minimum height of EPS geofoam layer required for the designed embankment. In this example, the value of undrained shear strength (S_u) of the foundation soil is assumed to be 1,000 psf (47.88 kPa).

Based on the design chart E presented in Figure 7.9 and the given undrained shear strength, the required minimum thickness of EPS geofoam layer is 22 ft. (6.7 m) for the design factor of safety of three (FS = 3).

Step 5: Settlement Check:

In this step, the settlement of the embankment with 22-ft high EPS geofoam layer is calculated and compared with the allowable settlement mentioned previously in section 7.4.5. Figure 7.16 presents the dimensions of the designed EPS geofoam embankment, and the essential properties of foundation soil and backfill materials are listed in Table 7.7.

Table 7.7 Essential Materials Properties used in the Calculation

Properties	Foundation soil	Fill soil	EPS22 geofoam
Saturated unit weight, γ_{sat}, pcf	132.2	-	-
Unit weight, γ, pcf	-	120	1.35
Preconsolidation pressure, σ_p', psf	1,800	-	-
Void ratio, e_o	0.54	-	-
Compression index, C_c	0.27	-	-
Swell index, C_s	0.02	-	-

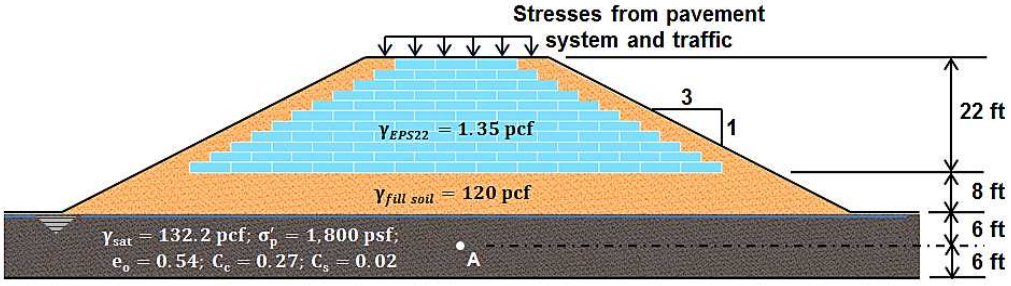

Figure 7.16 Dimensions of the designed EPS geofoam embankment

The calculation of the settlement which occurred on the designed EPS geofoam embankment is presented as follows:

- Determining overburden pressure at the midpoint of foundation soil layer (σ_o'):

$$\sigma_o' = \gamma' H = (132.2 - 62.4\, pcf) \times (6\, ft) = 418.8\, psf \quad \#$$

- Determining overconsolidation ratio (OCR) of the foundation soil:

$$OCR = \frac{\sigma_p'}{\sigma_o'} = \frac{(1{,}800\, psf)}{(418.8\, psf)} = 4.3 \quad \text{: OC clay} \quad \#$$

- Computing stresses increase at the midpoint of foundation soil layer ($\Delta\sigma_z'$):

1) The stresses increase due to the weight of concrete pavement system and traffic loads are evaluated using 2:1 stress distribution method:

$$\Delta\sigma_{z,\ pavement} = \frac{\sigma_{DL} \times W}{(W+Z)} = \frac{(280\, psf) \times (36\ ft)}{(36 + 30 + 6\ ft)} = 140\, psf \quad \#$$

$$\Delta\sigma_{z,\ traffic} = \frac{\sigma_{LL} \times W}{(W+Z)} = \frac{(802\, psf) \times (36\ ft)}{(36 + 30 + 6\ ft)} = 401\, psf \quad \#$$

2) The stress increase under an embankment can be calculated using the method and chart proposed by Osterberg (1957). The parameters for the calculation are presented in Figure 7.17, and the chart to find an influence value (I) for embankment loading is provided in Figure 7.18.

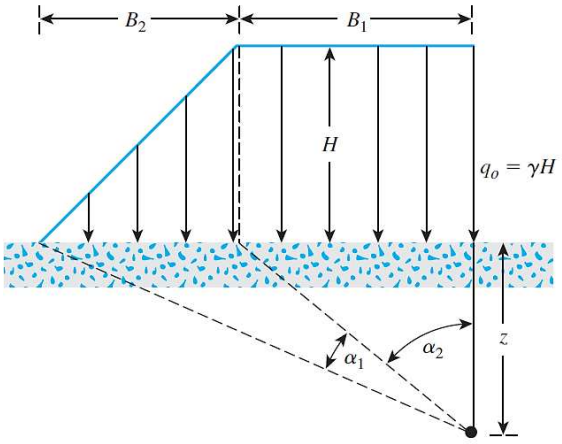

Figure 7.17 Embankment loading (after Das, 2010)

$$q_o = \sum(\gamma H)_{fill\ mass} = (\gamma H)_{EPS22} + (\gamma H)_{fill\ soil}$$

$$= [(1.35\ pcf)(22\ ft)] + [(120\ pcf)(8\ ft)]$$

$$= (29.7\ psf) + (960\ psf) = 989.7\ psf \quad \#$$

$$B_1 = \frac{W}{2} = \frac{(36\ ft)}{2} = 18\ ft$$

$$B_2 = \frac{H}{(1/Slope)} = (30\ ft)(3) = 90\ ft$$

$$Z = 6\ ft$$

$$\frac{B_1}{Z} = \frac{(18\ ft)}{(6\ ft)} = 3 \quad \#$$

$$\frac{B_2}{Z} = \frac{(90\ ft)}{(6\ ft)} = 15 \quad \#$$

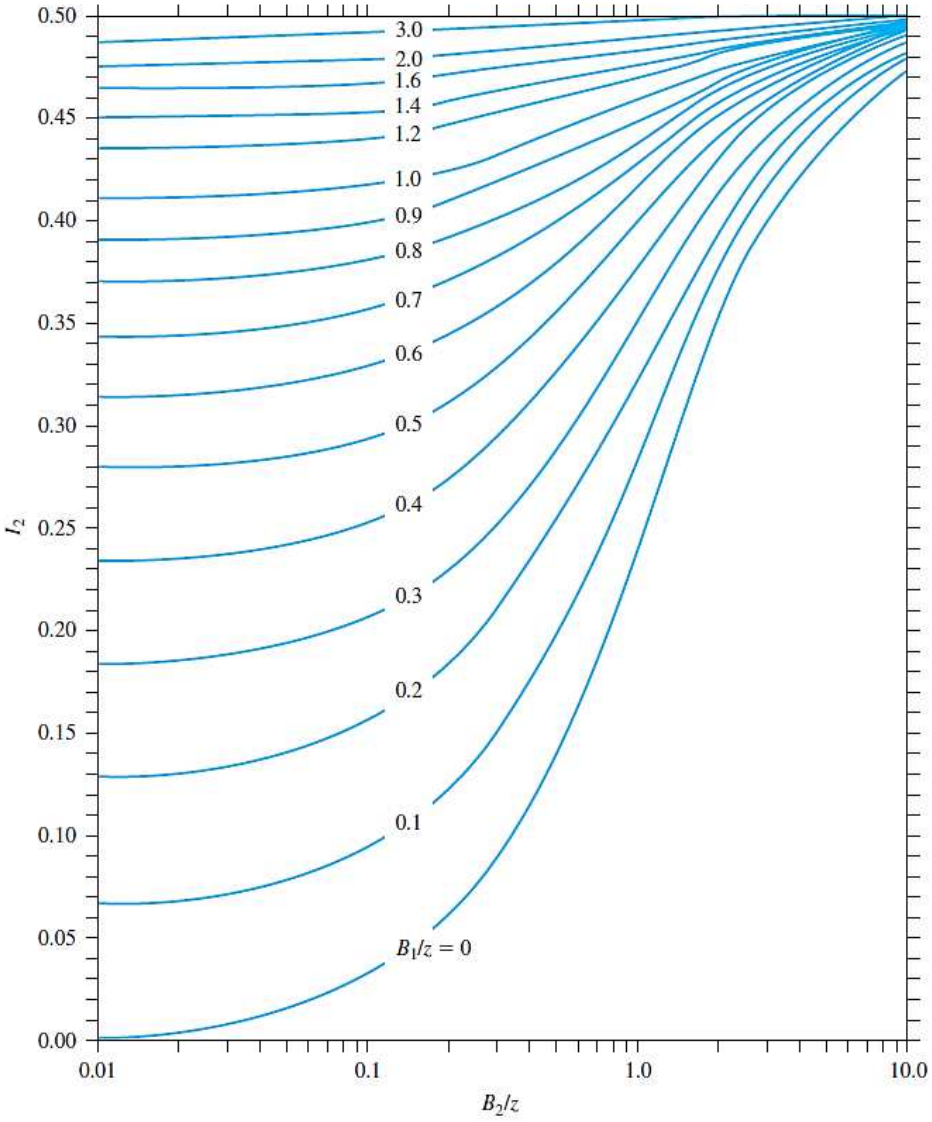

Figure 7.18 Chart of influence value (I) for embankment loading (After Osterberg, 1957)

By pointing $\frac{B_1}{Z}$ and $\frac{B_2}{Z}$ into the chart in Figure 7.18, the value of an influence value (I) of 0.5 can be obtained and this value will be the same for both left side and right side of the embankment. The stress increase at midpoint of foundation soil layer due to the embankment loading is calculated in the following steps:

$$\Delta\sigma_{z,\ fill\ mass} = \sum(q_o\ I) = q_o\ (I_{Left} + I_{Right})$$

$$= (989.7\ psf\ )\ (0.5 + 0.5) = 989.7\ psf \qquad \#$$

Thus, $\Delta\sigma_z' = \Delta\sigma_{z,\ pavement} + \Delta\sigma_{z,\ traffic} + \Delta\sigma_{z,\ fill\ mass}$

$$= (140\ psf) + (401\ psf) + (989.7\ psf) = 1{,}530.7\ psf \qquad \#$$

- Comparing the sum of σ_o' and $\Delta\sigma_z'$ to the value of σ_p' and calculating the settlement of the design EPS geofoam embankment:

$$\sigma_o' + \Delta\sigma_z' = (418.8\ psf) + (1{,}530.7\ psf)$$

$$= (1{,}949.5\ psf) > (1{,}800\ psf)$$

Thus, the primary consolidation settlement (S_p) of the foundation soil can be calculated:

$$S_p = \left[\frac{C_r\ H}{1+ e_o}\log\frac{\sigma_p'}{\sigma_o'}\right] + \left[\frac{C_c\ H}{1+ e_o}\log\left(\frac{\sigma_o' + \Delta\sigma_z'}{\sigma_p'}\right)\right]$$

$$= \left[\frac{(0.02)\times(12\ ft)}{1+ 0.54}\log\left(\frac{1{,}800\ psf}{418.8\ psf}\right)\right] + \left[\frac{(0.27)\times(12\ ft)}{1+ 0.54}\log\left(\frac{1{,}949.5\ psf}{1{,}800\ psf}\right)\right]$$

$$= (0.0987\ ft) + (0.0729\ ft) = 0.1716\ ft = 2.1\ in \qquad \#$$

In this example, the calculation of secondary consolidation settlement can be skipped because the magnitude of the primary consolidation settlement is very low. Even though the secondary consolidation settlement is added to primary consolidation, the total settlement is still less than the allowable settlement (i.e., 8 to 16 in.).

- Comparing the calculated settlement with the allowable settlement

As aforementioned, the predicted settlement of the designed EPS geofoam embankment is lower than the allowable settlement, which is 8 to 16 in. (203 to 406 mm). Therefore, the thickness of 22 ft. (6.7 m) of the EPS22 geofoam layer is acceptable for

the designed 30-ft. (9-m) high embankment. Table 7.8 presents the summary of the thickness of each component of the designed embankment.

Table 7.8 Thickness of Layers of the Designed Embankment

Component	Thickness
Concrete pavement	9 in. (228.6 mm)
Subbase	15 in. (381 mm)
EPS22 geofoam layer	22 ft. (6.7 m)
Fill soil	8 ft. (2.44 m)
Foundation soil	-

7.6 Recommendations for EPS Geofoam Embankment Construction

In this section, the recommendations for EPS geofoam application to bridge approach embankments are provided. The recommendations are summarized based on the lessons learned from failure involving geofoam roads and embankments compiled by Horvath (1999) and Frydenlund and Aaboe (2001) and the geofoam construction practices suggested by Stark et al. (2004).

7.6.1 An Appropriate Layout of EPS Geofoam Blocks

Horvath (1999) presented the case study of pavement failure due to insufficient thickness of EPS geofoam layer and the geofoam blocks shifting. Based on this, some suggestions involving the layout of an EPS-block geofoam lightweight fill have been provided. Moreover, the details of an appropriate layout of EPS geofoam blocks to obtain adequate interlocking in a vertical direction are exhaustively explained in NCHRP web document 65 by Stark et al. (2004). In this study, the recommendations for good practice in the layout of EPS geofoam blocks are summarized and briefly described as follows:

- EPS geofoam blocks should be placed with their smallest dimension oriented vertically and fit tightly against adjacent blocks on all sides.

- At least two layers of EPS blocks are required to be filled beneath roads to avoid the block shifting.
- In order to minimize the continuity of vertical joints between overlaying blocks, the EPS geofoam blocks should be placed in a running bond and rotating the pattern by 90 degrees in each successive layer (NYDOT 2008), as presented in Figure 7.19.

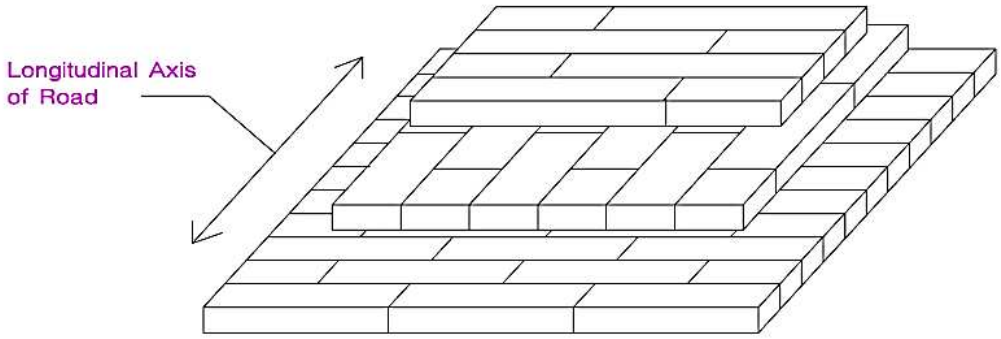

Figure 7.19 Isometric view of typical EPS blocks layout for a road embankment (Stark et al. 2004)

- At the transition zone between geofoam fill and soil fill embankments, the EPS geofoam blocks should be installed with the shape of steps, as illustrated in Figure 7.20, in order to avoid high differential settlement between geofoam and embankment soil.

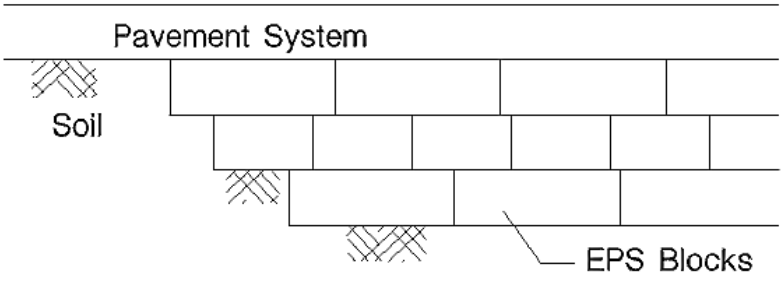

Figure 7.20 Layout of EPS geofoam blocks at the transition zone (Stark et al. 2004)

- If the EPS blocks need to be cut in irregular shapes, the precise cutting can be performed by using a portable hot-wire cutting device. Even though the hot-wire cutting devices made for cutting EPS geofoam typically do not cause the EPS to burn, a fire extinguisher should be available during cutting the EPS blocks. A wire saw and chain saw are sometimes used to cut the EPS blocks.

7.6.2 Site Preparation

The proper site preparation prior to placing the EPS geofoam blocks is considered an important factor affecting internal stability of the embankment and overall constructability (Stark et al. 2004). The details of site preparation are included in construction specifications, and some of them are briefly explained in the following:

- Ideally, the foundation subgrade soils supporting the EPS blocks should not have standing water or accumulated ice or snow. However, based on experience, an area that has some amount of standing water can be acceptable, but the potential for hydrostatic uplift of the blocks during construction needs to be considered (Stark et al. 2004).
- The drainage systems at the bottom of the EPS geofoam layer should be provided during and after construction to minimize water accumulation along the EPS embankment.
- Approximately 0.5 to 1.0 in. (12 to 25 mm.) thickness of sand bed layer should be provided over the existing soil surface on which the EPS geofoam blocks are to be placed. This sand bed layer serves both to prevent the damage caused by debris or large pieces of vegetation protruding from the subgrade to the EPS geofoam blocks, as well as to provide a smooth surface for the first layer of EPS blocks.

7.6.3 EPS Geofoam Blocks Storage during Construction Process

In case the EPS blocks need to be stockpiled during the construction process, a secure storage area should be provided for this purpose. The EPS blocks should be kept away from any source of heat and fire, such as construction activity that produces heat or flame. Tobacco smoking should also be prohibited in the storage area (Stark et al. 2004).

Frydenlund and Aaboe (2001) reported two cases of failure of EPS geofoam in Norway due to fires. Both fires were caused by the sparks coming from welding activities close to uncovered geofoam, during construction. Therefore, a fire extinguisher should be provided during any construction activity.

7.6.4 Minimum Soil Cover to Protect EPS Geofoam from Exposing to Petrol Agents

Polystyrene, the main raw material of EPS geofoam, is a stable chemical compound. However, it can be dissolved when exposed to petroleum agents (Frydenlund and Aaboe, 2001). Although there is very small possibility of a petroleum tanker overturning and spilling petrol on the road surface at the location of an EPS fill, the EPS geofoam blocks need to be protected from the exposure to the petroleum agents. Minimum soil cover over the EPS geofoam blocks of 2 ft. (0.6 m.) is required, and a loading distributing concrete slab on top of the EPS blocks layer or a high density polypropylene sheet can also help protect the EPS blocks from exposure to the petroleum agents.

7.6.5 Hydrostatic Uplift (Flotation)

Because the density of EPS geofoam block is much lower than water, it can float when submerged. Frydenlund and Aaboe (2001) reported two cases of EPS project failure due to water fluctuations and buoyancy forces. The first case occurred in Norway on the 16th of October 1987. The area of the first EPS fill in Oslo was exposed to major

floods, causing EPS blocks flotation and failure in an adjacent section of motorway. The other case happened in Thailand when an unexpected high water level caused a completed road fill to be washed away.

It is recommended that the EPS geofoam embankments be constructed in an area having a low potential for being submerged by water and enough overburden pressure against the upward vertical uplift caused by the buoyancy forces. The procedures of the design are exhaustively explained in NCHRP 529.

7.7 Summary

In this chapter, the design guideline for an EPS geofoam embankment is provided. The guideline is limited to trapezoidal shaped embankments with side slopes of 2H:1V; 3H:1V; or 4H:1V and top width of 36 ft. (11 m) and 76 ft. (23 m) for a two-lane and a four-lane roadway, respectively. The height of embankment varies from 10 ft. (3 m) to 50 ft. (15.24 m) with increments of 10 ft. (3 m). The design charts to obtain the thickness of concrete pavement, as well as the minimum height of the EPS geofoam layer, are created to provide a simple approach for the users. Moreover, the criteria for selecting an appropriate type of EPS geofoam is modified from NCHRP 529 and the Japanese methods to receive an appropriate design with a reliable factor of safety. To provide a clear understanding of using the proposed design guidelines, an example of a highway bridge approach embankment design is presented step-by-step. Finally, the recommendations for an appropriate layout of EPS geofoam blocks, site preparation, EPS blocks storage during construction, minimum soil cover to protect EPS blocks from exposing to the petrol agents, and Hydrostatic uplift are discussed.

Chapter 8

Summary, Conclusions and Recommendations

8.1 General

The bump or differential settlement occurs at the ends of the bridge due to the differences in elevation of approach pavements and bridge decks caused by an unequal settlement of the approach embankment and bridge abutment. The bump problem is considered as one of the main problems affecting the performance of the bridge structure.

The presence of the bump causes an inconvenience to travelling passengers and unsafe driving conditions. Moreover, this problem has been reported by many state highway agencies in the United States as one of the major maintenance problems. The agencies have been spending annually over $100 million on maintenance and repairs to the bridges and highways damaged by this bump problem. Several factors causing the formation of the bump have been studied, and solutions proposed. Among those, the effects of consolidation settlement of foundation soil, poor compaction and consolidation of backfill materials, and poor drainage system and soil erosion are considered as the main factors frequently causing the differential settlement or the bump problem between embankments and bridge decks.

Recently, several techniques have been utilized to mitigate the bridge approach settlement problem. These techniques can be classified into four categories, including (1) improvement of foundation soil, (2) improvement of approach embankment backfill materials, (3) water management and erosion control, and (4) use of lightweight materials. This research study is performed to evaluate the effectiveness of using the expanded polystyrene (EPS) geofoam as an alternative backfill material in alleviating the settlement of the bridge approach embankment. The EPS geofoam is a very lightweight

block made of rigid cellular foamed polymeric material. The weight of the EPS geofoam is approximately 1% of the weight of soil and less than 10% of the weight of other lightweight fill alternatives. With this advantage, the EPS geofoam is expected to reduce the stress increase on the underlying foundation soil and, consequently, reduce the differential settlement problem at the interface between the bridge abutment and the approach embankment.

EPS22 geofoam blocks were recommended to be used to replace the top 6-ft depth of the approach embankment fill on east end of the bridge situated on US 67 over SH 174 Cleburne in Johnson County, Texas. The embankment height is 40 ft. (12.2 m) and it was designed to support a two-lane roadway.

The approach slab on top of the embankment had experienced more than 16 in. (406 mm) of settlement in the 16 years since the initial construction. During that time, several treatment methods were attempted; however, they were not proven to be effective to reduce the settlements. This rehabilitated embankment was used as the test site for evaluating the effectiveness of EPS geofoam in mitigating the settlement problem. The site was instrumented with horizontal inclinometers and pressure cells for monitoring the settlement behavior of the embankment and pressure response of the geofoam, respectively.

The data collected from the field were used for the pressure distribution and settlement analysis study. Statistical analysis was performed on the post-construction vertical displacement data to verify that the displacement was less than 1.5 in. (38 mm). Moreover, the hyperbolic model formulated by Lin and Wong (1999) was used to analyze the observed field data and establish the time-settlement equation for predicting the long-term settlement of the test embankment.

Numerical analysis was also performed in this study. The test embankment was simulated to understand its settlement behavior by using the commercial geotechnical

finite element method (FEM) software, Plaxis. The input parameters used in the models were obtained from laboratory testing performed on the foundation and backfill soils collected from the field. The model analysis was validated by comparing the results with the data measured from the field. After validation, the model was used to predict the long-term settlement of the test embankment and to estimate the change in settlement with variations in heights and types of EPS geofoam used in the embankment.

Finally, the design guidelines and recommendations for possible future use in EPS geofoam embankment projects have been provided. The guidelines are also summarized based on three different standards, including NCHRP 529, European, and Japanese standards, along with the results obtained from field and the FEM models.

8.2 Summary and Conclusions

The main objective of this research is to comprehensively evaluate the effectiveness of using EPS geofoam as an alternative fill material in mitigating the settlements which occur in bridge approach embankments. The conclusions of this study are as follows:

8.2.1 Field Instrumentation and Monitoring Studies

- According to the results from field visual inspection, an insignificant difference in elevation was noticed on the pavement surface between the approach slab and bridge deck. However, more than 3 in. (76 mm) of differential settlement between the roadway section placed on EPS geofoam layer and the fill soil on embankment side slope was observed at the location where the HI #2 inclinometer casing had been installed. This seems to affirm the fact that the EPS geofoam was successful in mitigating the settlement underneath the bridge approach slab.

- The analysis of traffic-induced vertical stress distribution in the EPS geofoam layer was performed on the pressure response data recorded at the bottom of the geofoam blocks layer. The result obtained from the analysis showed that about 36.5% of the design live load (i.e., traffic loads) was distributed at the top of the backfill soil under the 6-ft. (1.83-m) depth EPS geofoam layer. This value is slightly different from those calculated by the Development Organization (EDO) Japan and 2V:1H distribution methods. This indicates that the load distribution mechanisms in EPS geofoam fills are complicated and not fully understood. However, the method of 2V:1H load distribution can be acceptable for evaluating the stress distributed in the EPS geofoam layer.
- The monitored data from the horizontal inclinometer showed that the maximum vertical displacement measured at the middle of the pavement on top of the EPS geofoam layer increased considerably at the beginning and then, gradually increased with time. The trend of the vertical movement became constant at the settlement of about 1.30 to 1.40 in. (33 to 35.5 mm); whereas, the maximum vertical displacement after embankment construction was estimated to be about 1.0 to 1.1 in. (25 to 28 mm). This indicates that the use of EPS geofoam blocks is effective in reducing the settlement of the test embankment.
- According to the statistical analysis performed on the settlement data from the test embankment, it can be concluded that the post-construction vertical displacement of the test embankment was greater than 1.0 in. (25 mm), but less than 1.5 in. (38 mm).
- The long-term settlements of the test embankment were predicted from the field data collected for about 30 months after its construction by using a hyperbolic model. The total settlement of 1.50 in. (38 mm) and post-

construction settlement of 1.30 in. (33 mm) were predicted to occur on the test embankment at 20-year time intervals. These settlements are considered low, and they can cause only a slight bump at the bridge deck-approach slab interface, which does not affect the riding quality.

8.2.2 Numerical Analysis Studies

- The numerical analysis was performed based on the data of soil properties obtained from laboratory tests conducted on the foundation and backfill soils collected from field and the EPS geofoam properties defined in ASTM D 6817-07. The analysis showed the agreement of the results with the field observations data in both long-term settlement prediction and pressure response in the embankment. However, due to the limitation of loads assignment in the numerical model, the numerical analysis showed shorter time intervals to reach the maximum settlement than that observed from the field monitored data.
- The validated numerical model was used to predict the settlement of the embankment by varying the height of EPS geofoam layer. Only 2.1 in. (53.3 mm) of the vertical displacement was predicted by the model which occurred in the embankment without the EPS geofoam. However, in the real conditions, not only the consolidation settlement of the foundation and backfill soil, but also other factors such as soil erosion affect the total vertical displacement under the approach slab. Thus, it can be expected that the realistic settlement should be greater than the predicted value.
- According to the numerical analysis results, it can be concluded that the vertical displacements occurring on the EPS geofoam embankments decrease in a hyperbolic shape when the height of the EPS blocks layer

increases and the type of EPS geofoam block is changed from EPS12 to EPS46. It should be noted that the increase of the suffix numbers in the name of EPS geofoam presents the increase of the EPS block density and its compressive strength.

8.2.3 Design Guideline and Recommendations for EPS Geofoam Embankment

- The design guideline for an EPS geofoam embankment is provided. The guideline is summarized and modified from three different standards, NCHRP 529, European, and Japanese method, along with the field-monitored data and numerical analysis. The guideline is limited to trapezoidal shaped embankments with side slopes of 2H:1V, 3H:1V, or 4H:1V. The design charts to obtain the minimum height of an EPS geofoam layer are created based on the bearing capacity of the foundation soil supporting the embankment. Moreover, the recommendations for an EPS geofoam embankment construction are also provided in order to advise the agencies and contractors what should be performed during the construction process.
- The external stabilities of the EPS geofoam embankment considered in this design guideline are the bearing capacity of the foundation soil and the settlement of the embankment. The slope stability of the embankment is not considered because the main focus of this study is on using EPS geofoam to mitigate the settlement problem. On the other hand, the EPS block is a rigid material which tends to produce settlements when subjected to vertical stresses rather than sliding.

8.2.4 Overall Conclusions

- According to the studies performed in this research, it can be concluded that using EPS geofoam blocks as an alternative embankment fill material is effective for alleviating the differential settlements near a bridge approach slab and, consequently, for reducing the problem of a bump at the end of the bridge.
- The EPS geofoam blocks not only reduce the stress increase, resulting in less settlement in foundation soil, but also mitigate the soil erosion problem in the embankment backfill.

8.3 Limitations and Recommendations

- The soils used in laboratory tests are disturbed soil samples. The results received from the tests may be different from those of the undisturbed soil samples.
- More techniques for measuring the embankment settlement, such as elevation surveys and rod extensometers, should be conducted in order to compare the results with those collected by horizontal inclinometers.
- During the installation process, the results of lateral pressure obtained from vertically installed pressure cells should be calibrated, and the pressure cells must be installed in proper contact with the EPS geofoam and abutment walls.
- Plaxis, a Finite Element Program used in the numerical analysis in this study, has limitations in dynamic load assignment and in modeling soil erosion behavior. Therefore, these complicated phenomena could not be simulated, and the results from the numerical analysis were not actually matched with realistic behavior of soil in the field.

- In this study, the design charts developed in the design guideline for EPS geofoam embankments are based on the assumption that the foundation soils are purely cohesive soil. In the future study, this can be extended in other soil conditions.

References

AASHTO (1986). “Guide for Design of Pavement Structures.” American Association of State Highway and Transportation Officials.

AASHTO (1993). “Guide for Design of Pavement Structures.” American Association of State Highway and Transportation Officials.

AASHTO (2012). “AASHTO LRFD Bridge Design Specifications.” American Association of Transportation Officials.

Abendroth, R. E., Greimann, L.F. and Laviolette, M. D. (2007). “An Integral Abutment Bridge With Precast Concrete Piles.” *Final Rep., IHRB Project TR-438, CTRE Project No. 99-48*, IOWA Department of Transportation, Center for Transportation Research and Education Report, Ames, Iowa.

Abu-Hejleh, N., Zornberg, J. G., Wang, T., McMullen, M., and Outcalt, W. (2001). “Performance of geosynthetic-reinforced walls supporting the founders/meadows bridge and approaching roadway structures.” Report No. CDOT-DTD-R-2001-12, Colorado Department of Transportation, CO.

Abu-Hejleh, N., Hanneman, D., White, D. J. and Ksouri, I. (2006). “Flowfill and MSE Bridge Approaches: Performance, Cost and Recommendations for Improvements.” *Report No. CDOT-DTD-R-2006-2.* Colorado Department of Transportation, Denver.

ACI 229R-99 (2005). “Controlled low-strength materials.” American Concrete Institute, US.

Adams, M., Nicks, J., Stabie, T., Wu, J., Schlatter, W., and Hartmann, J. (2011). “Geosynthetic reinforced soil integrated bridge system: synthesis report.” Report No. FHWA-HRT-11-027, Office of Infrastructure Research and Development, Federal Highway Administration, VA.

Archeewa, E. (2010). “Comprehensive Studies on Deep Soil Mixing and Lightweight Aggregates Application to Mitigate Approach Slab Settlements.” Dissertation submitted in partial fulfillment of the requirements for the degree of the Doctor of Philosophy, the University of Texas at Arlington, Arlington, Texas.

Ardani, A. (1987). “Bridge Approach Settlement.” *Rep. No. CDOT-DTP-R-87-06*, Colorado Dept. of Highways, Denver.

Arellano, D. Stark, T. D., Horvath, J. S., and Leshchinsky, D. (2011). “Guidelines for geofoam applications in slope stability projects.” Final report for Project No. 24-11(02), National Cooperative Highway Research Program (NCHRP), Transportation Research Board of the National Academies.

Arsoy, S., Barker, R. M. and Duncan, J. M. (1999). “The Behavior of Integral Abutment Bridges.” *Rep. No. VTRC 00-CR3*, Virginia Transportation Research Council, Charlottesville, VA.

ASTM Designation: C 165-07. “Standard Test Method for Measuring Compressive Properties of Thermal Insulations.” ASTM International, PA, US.

ASTM Designation: C 203-05. “Standard Test Methods for Breaking Load and Flexural Properties of Block-Type Thermal Insulation.” ASTM International, PA, US.

ASTM Designation: C 273-11. “Standard Test Method for Shear Properties of Sandwich Core Materials.” ASTM International, PA, US.

ASTM Designation: C 578. “Standard Specification for Rigid, Cellular Polystyrene Thermal Insulation.” ASTM International, PA, US.

ASTM Designation: C 1623. “Standard Specification for Manufactured Concrete Masonry Lintels.” ASTM International, PA, US.

ASTM Designation: D 422-63. “Standard Test Method for Particle-Size Analysis of Soils.” ASTM International, PA, US.

ASTM Designation: D 698-07. “Standard Test Methods for Laboratory Compaction Characteristics of Soil Using Standard Effort (12 400 ft-lbf/ft3 (600 kN-m/m3)).” ASTM International, PA, US.

ASTM Designation: D 854-14. “Standard Test Methods for Specific Gravity of Soil Solids by Water Pycnometer.” ASTM International, PA, US.

ASTM Designation: D 1621-00. “Standard Test Method for Compressive Properties of Rigid Cellular Plastics.” ASTM International, PA, US.

ASTM Designation: D 1622-08. “Standard Test Method for Apparent Density of Rigid Cellular Plastics.” ASTM International, PA, US.

ASTM Designation: D 2166-00. “Standard Test Method for Unconfined Compressive Strength of Cohesive Soil.” ASTM International, PA, US.

ASTM Designation: D 2216-98. “Standard Test Method for Laboratory Determination of Water (Moisture) Content of Soil and Rock by Mass.” ASTM International, PA, US.

ASTM Designation: D 2435-96. “Standard Test Method for One-Dimensional Consolidation Properties of Soils.” ASTM International, PA, US.

ASTM Designation: D 2850. “Standard Test Method for Unconsolidated-Undrained Triaxial Compression Test on Cohesive Soils.” ASTM International, PA, US.

ASTM Designation: D 2937-00. “Standard Test Method for Density of Soil in Place by the Drive-Cylinder Method.” ASTM International, PA, US.

ASTM Designation: D 3080-98. “Standard Test Method for Direct Shear Test of Soils Under Consolidated Drained Conditions.” ASTM International, PA, US.

ASTM Designation: D 4318-10. “Standard Test Method for Liquid Limit, Plastic Limit, and Plasticity Index of Soils.” ASTM International, PA, US.

ASTM Designation: D 5321-14. “Standard Test Method for Determining the Shear Strength of Soil-Geosynthetic and Geosynthetic-Geosynthetic Interfaces by Direct Shear.” ASTM International, PA, US.

ASTM Designation: D 6817-07. “Standard specification for rigid cellular polystyrene geofoam.” ASTM International, PA, US.

Bakeer, M., Shutt, M., Zhong, J., Das, S. and Morvant, M. (2005). Performance of Pile-Supported Bridge Approach Slabs.” *Journal of Bridge Engineering*, ASCE.

Balasubramaniam, A. S., Cai, H., Zhu, D., Surarak, C., and Oh, E. Y. N. (2010). “Settlement of Embankments in Soft Soils.” *Geotechnical Engineering Journal of the SEAGS & AGSSEA,* Vol. 41, No. 2, June 2010.

Barksdale, R.D., and Bachus, R.C. (1983) “Design and Construction of Stone Columns, Vol. 1” *Rep. No. FHWA/RD-83/026*, Federal Highway Administration, Washington, D.C.

Barron, R. F., Wright, J., Kramer, C., Andrew, W. H, Fung, H. and Liu, C. (2006), “Cement Deep Soil Mixing Remediation of Sunset North Basin Dam” *Dam Safety 2006*, Association of Dam Safety Officials.

Bartlett, S. F., Lawton, E. C., Farnsworth, C. B., and Newman, M. P. (2012). “Design and evaluation of expanded polystyrene geofoam embankments for the I-15 reconstruction project, Salt Lake City, Utah.” Report No. UT-1X.XX, Utah Department of Transportation, UT.

Bathe, K. J. (2003). Finite Element Procedures, Prentice-Hall of India, New Delhi.

Bergado, D.T., Anderson, T.R, Miura, N, and Balasubramaniam, A.S. (1996). “Soft Ground Improvement in lowland and other environments.” ASCE, New York.

Biot, M. A. (1941). “General Theory of Three Dimensional Consolidation.” *Journal of Applied Physics,* Vol. 12, 155-164.

Booker, J. R., Carter, J. P., Small, J. C., Brown, P. T., and Poulos, H. G. (1989). “Some Recent Applications of Numerical Methods to Geotechnical Analysis.” *Computers and Structures,* Vol. 31, No. 1, 81-92.

Bowles, J. E. (1988). *Foundation Analysis and Design*, McGraw-Hill, New York.

Briaud, J. L., James, R. W., and Hoffman, S. B. (1997). NCHRP synthesis 234: Settlement of Bridge Approaches (the bump at the end of the bridge), Transportation Research Board, National Research Council, Washington, D.C. pp.75.

Bruce, D. (2001). “An Introduction to the Deep Mixing Methods as Used in Geotechnical Applications. Volume III. The Verification and Properties of Treated Ground.” Report No. FHWA-RD-99-167, US Department of Transportation, Federal Highway Administration, 2001.

Budhu, M. (2000). “Numerical and Visualization Techniques in Geotechnical Engineering Education.” *Educational Issue in Geotechnical Engineering,* 39-47.

Burke, M.P. (1987). “Bridge Approach Pavements, Integral Bridges, and Cycle-Control Joints.” *Transportation Research Record 1113*, TRB, National Research Council, Washington D.C., 54-65.

Burke, G. (2001) “Current Methods of Sampling and Testing of Soil Cement and Their Limitations.” Proceedings of International Workshop on Deep Mixing Technology, Vol. 2, National Deep Mixing Program, Oakland, CA. 2001.

Burmister, D. M. (1943). “The Theory of Stresses and Displacements in Layered Systems and Applications to the Design of Airport Runways.” Proceedings, Highway Research Board, Vol. 23 (1943), 126-144.

Bush, D.I., Jenner, C.G., and Bassett, R.H., 1990. The design and construction of geocell foundation mattress supporting embankments over soft ground. Geotextiles and Geomembranes, 9: 83-98.

Casagrande, A. (1936). “Determination of Preconsolidation Load and Its Practical Significance.” Proceedings 1st International Conference on Soil Mechanics and Foundation Engineering, Cambridge, Mass., Vol. 3, 60-64.

Cecich, V., Gonzales, L., Hoisaeter, A., Williams, J., and Reddy, K. (1996). “Use of shredded tires as lightweight backfill material for retaining structures.” *Waste Management & Research, Vol. 14*, 433-451.

Chen, D. H., Nazarian, S., and Bilyen, J. (2007). “Failure analysis of a bridge embankment with cracked approach slabs & leaking sand.” *Journal of Performance of Constructed Facilities, Vol. 21, Issue 5*, 375-381.

Chen, Y. and Chai, Y. H. (2011). “Experimental Study on the Performance of Approach Slabs under Deteriorating Soil Washout Conditions.” *Journal of Bridge Engineering*, September/October 2011(16), 624-632.

Cooper, M.R. and Rose, A.N. (1999). “Stone column support for an embankment on deep alluvial soils.” *Proc. of the Institution of Civil Enginee*rs, Geotechnical Engineering, 137(1),15-25.

Cotton, D. M., Kilian, A. P., and Allen, T. (1987). “Westbound Embankment Preload on Rainier Avenue, Seattle, Washington.” *Transportation Research Record No. 1119*, Transportation Research Board, Washington D.C., 61-75.

Cowland. J.W., and Wong, S.C.K. (1993). “Performance of a road embankment on soft clay supported on a geocell mattress foundation.” *Geotextiles and Geomembranes*, 12, 687-705.

Das, S. C., Bakeer, R., Zhong, J., and Schutt, M. (1990). “Assessment of mitigation embankment settlement with pile supported approach slabs.” Louisiana Transportation and Research Center, Baton Rouge, La.

Das. B. M. (2009). Soil Mechanics Laboratory Manual: 7th Edition, Oxford University Press, US.

Das, B. M. (2010). “Principles of foundation engineering: 7th edition.” Cengage Learning, CT, USA.

Dolton, B. and Hannah, C. (2006). “Cellular concrete: engineering and technological advancement for construction in cold climates.” The 2006 Annual General Conference of the Canadian Society for Civil Engineering, Canada.

Dunn, K. H. Anderson, G.H. Rodes, T.H., and Zieher, J.J. (1983). “ Performance Evaluation of Bridge Approaches.” Wisconsin Department of Transportation.

Dupont, B. and Allen, D. (2002). “Movements and Settlements of Highway Bridge Approaches.” *Rep. No. KTC-02-18/SPR-220-00-1F*, Kentucky Transportation Center Report, Lexington, KY.

Dusenberry, K. and Bygness, R. (2006). “Geofoam provides lightweight fill for York Bridge in Washington.” *Geosynthetics Magazine, Vol. 24, No. 4,* 2-7.

Edgar, T. V., Puckett, J. A., and D’Spain, R. B. (1989). “Effect of Geotextile on Lateral Pressure and Deformation in Highway Embankments.” *Geotextiles and Geomembranes*, 8(4), 275-306.

Elias, V., Welsh, J., Warren, J., and Lukas, R. (1998). “Ground improvement technical summaries.” Earth Engineering and Sciences, Inc., U.S. Department of Transportation, Federal Highway Administration.

Elias, V., Christopher, E. R., and Berg, R. R. (2001). “Mechanically stabilized earth walls and reinforced soil slopes: design and construction guidelines.” Federal Highway Administration, FHWA NHI-00-043, Washington, DC.

Elragi, A. F., Negussey, D., Kyanka, G. (2000). “Sample size effects on the behavior of EPS geofoam.” Proceeding of the Soft Ground Technology Conference, ASCE Geotechnical Publication 112, the Netherlands, 2000.

Elragi, A. F. (2006). “Selected engineering properties and applications of EPS geofoam.” Copyright © Softoria 2006.

Engstrom, G. M. and Lamb, R. (1994). “Using shredded tires as a lightweight fill material for road subgrades.” Summary Report: Report No. MN/RD – 94/10, Minnesota Department of Transportation, MN.

EPS White Book (2011). “EUMEPS Background Information on Standardization of EPS.” Issued by EUMEPS in 2011, Version 03/31/11.

Eriksson, L. and Trank, R. (1991). “Properties of expanded polystyrene-laboratory experiments.” *Expanded Polystyrene as Light Fill material; Technical Visit around Stockholm, 1991,* Stockholm.

Federal Highway Administration (2000). “Priority, Market-Ready Technologies and Innovations”, *Rep. No. FHWA-HRT-04-053*.

Federal Highway Administration (2012). “User Guidelines for Waste and Byproduct Materials in Pavement Construction.” User Guideline: Embankment of Fill, Publication No. FHWA-RD-97-148, US.

Frydenlund, T. E. and Aaboe, R. (2001). “Long term performance and durability of EPS as a lightweight fill material.” EPS Geofoam 2001, 3rd International Conference, UT.

Gan, C. H. and Tan, S. M. (2003). “Some construction experiences on soft soil using lightweight materials.” 2nd International Conference on Advances in Soft Soil Engineering and Technology, Malaysia.

Goughnour, R. R. and Bayuk, A.A. (1979). “A Field Study of Long-term Settlement of Loads Supported by Stone Column in Soft Ground.” *Proc. of International Conference on Soil Reinforcement: Reinforced Earth and Other Techniques*, Vol. 1, Paris, 279-286.

Greimann, L. F., Abendroth, R.E., Johnson, D.E. and Ebner, P.B. (1987). “Pile Design and Tests for Integral Abutment Bridges.” *Final Rep. Iowa DOT Project HR 273, ERI Project 1780, ISU-ERI-Ames-88060*, Ames, Iowa.

Ha, H. S., Seo, J., and Briaud, J. (2002). “Investigation of settlement at bridge approach slab expansion joint: survey and site investigations.” Report No. FHWA/TX-03/4147-1, Texas Department of Transportation.

Hamidi, B., Nikraz, H. and Varaksin, S. (2011). “Advances in dynamic compaction.” *Proceeding of Indian Geotechnical Conference: Paper No. H-146*, India, 433-436.

Hausmann, M. R. (1990). “Engineering Principles of Ground Modification”, McGraw-Hill Publishing Company, New York.

Helwany, S. (2007). “Evaluation of bridge approach settlement mitigation methods.” Final: Final Report.” The University of Wisconsin-Milwaukee, Wisconsin Highway Research Program.

Helwany, S., Koutnik, T. E., and Ghorbanpoor, A. (2007). “Evaluation of Bridge Approach Settlement Mitigation Methods: Final Report.” Wisconsin Highway Research Program, The University of Wisconsin-Milwaukee, Milwaukee, WI.

Holtz, R.D. and Kovacs, W.D. (1981). “An Introduction to Geotechnical Engineering.” Prentice Hall Hall, Inc., Englewoods Cliffs, New Jersey.

Hopkins, T.C. (1969). “Settlement of Highway Bridge Approaches and Embankment Foundations.” *Rep. No. KYHPR-64-17; HPR-1(4)*, Kentucky Transportation Center, Lexington, Kentucky.

Hopkins, T. C. and Deen, R.C. (1969). “The Bump at the End of the Bridge.” *Rep. No. KYHPR-64-17; HPR-1(4)*, Kentucky Transportation Center, Lexington, Kentucky.

Hopkins, T. C. (1973). “Settlement of Highway Bridge Approaches and Embankment Foundations.” *Rep. No. KYHPR-64-17; HPR-1(8)*, Kentucky Transportation Center, Lexington, Kentucky, 40.

Hoppe, E. J. and Gomez, J. P. (1996). “Field study of an integral backwall bridge.” *Rep. No. VTRC 97-R7*, Virginia Transportation Research Council, Charlottesville, VA.

Hoppe, E. J. (1999). Guidelines for the Use, Design, and Construction of Bridge Approach Slabs: Final Report, Virginia Transportation Research Council, Charlottesville, Virginia.

Horvath, J. S. (1991). “Using Geosynthetics to Reduce Surcharge-Induced Stresses on Rigid Earth Retaining Structures.” *Transportation Research Record 1330*, 47-53.

Horvath, J. S. (1992). “Lite products come of age; new developments in geosynthetics.” ASTM Standardization News, American Society for Testing and Material, USA, Vol. 20, No. 9, 50-53.

Horvath, J. S. (1995). “Geofoam geosynthetic.” Horvath Engineering, P.C. Publisher, Scarsdale, NY.

Horvath, J. S. (1999). “Geofoam and geocomb: lessons from the second millennium A.D. as insight for the future.” Manhattan College Research Report No. CE/GE-99-2, Manhattan College, NY, USA.

Horvath, J. S. (1999). “Lessons Learned from Failures Involving Geofoam in Roads and Embankments.” Manhattan College Research Report No. CE/GE-99-1, Manhattan College, NY.

Horvath, J. S. (2000). “Integral abutment bridges: Problems and innovative solutions using EPS geofoam and other geosynthetics.” Manhattan College Research Report No. CE/GE-00-2, Manhattan College, New York.

Horvath, J. S. (2005). “Integral-Abutment Bridges: Geotechnical Problems and Solutions Using Geosynthetics and Ground Improvement.” *IAJB 2005 - The 2005 FHWA Conference on Integral Abutment and Jointless Bridges*. 16-18 March, Baltimore, Maryland, USA.

Hsi, J. P. and Martin, J. (2005). “Soft Ground Treatment and Performance, Yengun to Chinderah Freeway, NSW, Australia.” Ground Improvement, Elsevier Geo-Engineering Book Series, Elsevier 2005.

Hsi, J. P. (2007). “Managing Difficult Ground-Case Studies.” Proceedings of First Sri Lankan Geotechnical Society International Conference on soil and Rock Engineering, Colombo.

Hsi, J. P. (2008). “Bridge Approach Embankments Supported on Concrete Injected Columns.” *Proceedings of The Challenge of Sustainability in the Geoenvironment*, ASCE, Geocongress 08, New Orleans, Louisiana.

Huang, Y. H. (2004). Pavement Analysis and Design: 2nd edition, Pearson Prentice Hall, NJ, US.

IowaDOT (2014). “Intermediate Foundation Improvements (IFIs).” Geotechnical Design Manual, Iowa Department of Transportation, US.

James, R.W., Zhang, H. and Zollinger, D.G. (1991). “Observations of severe abutment backwall damage.” *Transportation Research Record 1319*, Transportation Research Board, 55-61.

Jayawickrama, P., Nash, P., Leaverton, M. and Mishra, D. (2005). “Water Intrusion in Base/Subgrade Materials at Bridge Ends.” *TxDOT Report, FHWA/TX-06/0-5096-1*, Texas Tech University, Lubbock, Texas.

Jones, C. A., Stewart, D. I., and Danilewicz, C. J. (2008). “Bridge distress caused by approach settlement.” *Geotechnical Engineering 161, Issue GE2,* 63-74.

Kalla, S. (2010). “Modeling Studies to Assess Long Term Settlement of Light Weight Aggregate Embankment.” Thesis submitted to the Faculty of the Graduate School of the University of Texas at Arlington, Arlington, TX.

Koerner, R. M. (2005). “Designing with Geosynthetics.” Pearson Prentice Hall, Pearson Education , Inc. Upper Saddle River, New Jersey, US.

Kramer, S. L. and Sajer, P. (1991) “Bridge Approach Slab Effectiveness.” *Final Report*, Washington State Department of Transportation, Olympia, Washington.

Krishnaswamy, N.R., Rajagopal, K.**,** and Madhavi Latha, G. **(**2000). "Model studies on geocell supported embankments constructed over soft clay foundation." *Geotechnical Testing Journal*, ASTM, 23: 45-54.

Krishnamoorthy (2008). "Consolidation Analysis Using Finite Element Method." The 12th International Conference of International Association for Computer Methods and Advances in Geomechanics (IACMAG), Goa, India.

Laguros, J. G., Zaman, M. M., and Mahmood, I. U. (1990). "Evaluation of Causes of Excessive Settlements of Pavements Behind Bridge Abutments and their Remedies; Phase II. (Executive Summary)." *Rep. No. FHWA/OK 89 (07)*, Oklahoma Department of Transportation.

Lawton, E.C., and Fox, N.S. (1994). "Settlement of Structures Supported on Marginal or Inadequate Soils Stiffened with Short Aggregate Piers." *ASCE GSP No. 40,* Vertical and Horizontal Deformations of Foundations and Embankments, ASCE, Vol. 2, 962-974.

Lenke, L. R. (2006). "Settlement Issues-Bridge Approach Slabs." *Rep. No. NM04MNT-02*, New Mexico Department of Transportation.

Lien, B. H. and Fox, N. S. (2001) "Case Histories of Geopier® Soil Reinforcement for Transportation Applications." Proc. of Asian Institute of Technology Conference, Bangkok, Thailand.

Lin, Q.L., Wong, I.H. (1999). "Use of Deep Cement Mixing to Reduce Settlements at Bridge Approaches." Journal of Geotechnical and Geoenvironmental Engineering, ASCE, Vol. 125(4),309.

Liu, H.L., Ng, C.W.W., and Fei, K. (2007). "Performance of a Geogrid-Reinforced and Pile-Supported Highway Embankment over Soft Clay: Case Study." *Journal of Geotechnical and Geoenvironmental Engineering*, ASCE, 133(12),1483-1493.

Long, J. H., Olson, S. M., Stark, T. D., and Samara, E. A. (1998). “Differential movement at Embankment-bridge structure interface in Illinois.” *Transportation Research Record 1633*, Transportation Research Board, Washington, DC, 53-60.

Long M. M. and O’Riordan, N. J. (2001). “Field Behavior of Very Soft Clays at the Athlone Embankments.” Geotechnique Vol. 51, No. 4, 293-309.

Lukas, R.G. (1986) “Dynamic Compaction for Highway Construction, Vol. 1, Design and construction Guidelines.” *Rep. No. FHWA/RD-86/133* , Federal Highway Administration, National Technical Information Service, Washington, D.C.

Lukas, R.G. (1995) “Dynamic Compaction, Geotechnical Engineering Circular No. 1” *Rep. No. FHWA-SA-95-037*, Federal Highway Administration, Washington, D.C.

Luna R., Jonathan L. R., and Andrew, J. W. (2004). “Evaluation of Bridge Approach Slabs, Performance and Design.” *Rep. No. RDT 04-010*, Department of Civil, Architectural and Environmental Engineering, University of Missouri, Rolla.

Lund, H. F. (1993). Recycling Handbook. New York, U.S.A., McGraw Hill, Inc., U.S.A.

Lutenegger, A. J. and Ciufetti, M. (2009). “Full-scale pilot study to reduce lateral stresses in retaining structures using geofoam.” Final Report for Project No. RSCH010-983, Vermont Department of Transportation.

Mahmood, I. U. (1990). “Evaluation of causes of bridge approach settlement and development of settlement prediction models.” PhD Thesis, University of Oklahoma, Norman, Okla.

Mekkawy, M., White, D.J., Souleiman, M.T. and Sritharan, S. (2005). “Simple Design Alternatives to Improve Drainage and Reduce Erosion at Bridge Abutments.” *Proceedings of the 2005 Mid-Continent Transportation Research Symposium*, Ames, Iowa.

Meyerhof, G. G. (1963). “Some Recent Research on the Bearing Capacity of Foundations.” *Canadian Geotechnical Journal,* Vol. 1, No. 1, 16-26.

Michell, J. K., and Huber, T.R (1985) “Performance of a Stone Column Foundation.” *Journal of Geotechnical Engineering*, ASCE, 111(2), 205-223.

Minks, A.G., Wissmann, K.J., Caskey, J.M., and Pando, M.A. (2001). “Distribution of Stresses and Settlements below Floor Slabs Supported by Rammed Aggregate Piers.” Proceedings of 54th Canadian Geotechnical Conference, Calgary, Alberta, Canada, 16-19.

Mishra, D., Jayawickrama, P. W., and Nash, P. T. (2010). “Development of maintenance strategies to mitigate bridge end damage form water intrusion.” *Transportation Research Record: Journal of the Transportation Research Board, No. 2170*, Transportation Research Board of the National Academies, Washington, D.C., 56-63.

Mistry, V. C. (2005). “Integral abutment and jointless bridges.” The 2005-FHWA Conference, 3-11.

Montgomery, D. C. (2013). Design and Analysis of Experiments, 8th edition, John Wiley & Sons, Inc. Singapore.

Munoz, A. and Mattox, M. (1977) “Vibroreplacement and Reinforced Earth Unite to Strengthen a Weak Foundation.” Civil Engineering, ASCE, 58-62.

Nassif, H. (2002). “Finite Element Modeling of Bridge Approach and Transition Slabs.” *Rep. No. FHWA-NJ-2002-007*, Department of Civil and Environmental Engineering, Center for Advanced Infrastructure & Transportation (CAIT), Rutgers, New Jersey.

Negussey, D. and Sun, M. C. (1996). “Reducing lateral pressure by geofoam substitution.” Report to Society of the Plastics Industry, Syracuse University, NY.

Negussey, D. (1997). “Properties and applications of geofoam,” Society of Plastic Engineers.

Negussey, D. and Stuedlein, A. (2003). “Geofoam fill performance monitoring.” Utah Department of Transportation Research Division Report No. UT-03.17, UT.

Nicholson D.P. and Jardine R.J. (1982). “Performance of vertical drains at Queenborough bypass.” Vertical Drains, the Institution of Civil Engineers: London, 67-90.

NYDOT (2008). “Guidelines for Design and Construction of Expanded Polystyrene Fill as a Lightweight Soil Replacement.” Geotechnical Engineering Manual, New York State Department of Transportation, NY.

NYDOT (2013). “Highway design manual.” New York State Department of Transportation, NY.

NYSDOT (2002). Standard Specifications, New York State Department of Transportation.

Osterberg, J. O. (1957). “Influence Value for Vertical Stresses in Semi-Infinite Mass Due to Embankment Loading,” Proceedings, Fourth International Conference on Soil Mechanics and Foundation Engineering, London, Vol. 1, 393-396.

Pedarla, A. (2009). “Durability studies on stabilization effectiveness of soils containing different fractions of montmorillonite.” Thesis submitted to the department of civil engineering, The University of Texas at Arlington, Texas in partial fulfillment of the master degree.

Porbaha, A. (1998). “State of the Art in Deep Mixing Technology, Part I: Basic Concepts and Overview of Technology.” *Ground Improvement*, 2(2), 81-92.

Porbaha, A. (2000). “State of the Art in Deep Mixing Technology: Design Considerations.” *Ground Improvement*, 4(3), 111-125.

Puppala, A. J. (2003). “Evaluation of in-situ method for quality assessment of deep mixing.” Final Report, Project NDM 101a, National deep mixing program.

Puppala, A. J., Madhyannapu, R. S., Nazarian, S., Yuan, D., and Hoyos, L. (2008). “Deep soil mixing technology for mitigation of pavement roughness.” Report No. FHWA/TX-08/0-5179-1, Texas Department of Transportation, TX.

Puppala, A. J., Saride, S., Archeewa, E., Hoyos, L. R., and Nazarian, S. (2009). "Recommendations for Design, Construction, and Maintenance of Bridge Approach Slabs: Synthesis Report." Rep. No. FHWA/TX-09/0-6022-1, the University of Texas at Arlington, Arlington, Texas.

Puppala A. J., Archeewa, E., Saride, S., Nazarian, S., and Hoyos, L. (2012). "Recommendations for design, construction, and maintenance of bridge approach slabs." Report No. FHWA/TX-11/0-6022-2, Texas Department of Transportation, TX.

Puppala, A. J. and Chittoori, C. S. (2012). "Transportation infrastructure settlement and heave distress challenge and solutions." *Journal of Zhejiang University-Science A (Applied Physics & Engineering): 13(11),* 850-857.

Ranjan, G. and Rao, A. (1993). "Basic and applied soil mechanics." Wiley Eastern Limited, New Delhi, India.

Rathmayer, H. (1996). "Deep Mixing Methods for Soft Subsoil Improvement in the Nordic Countries." *Proceedings of IS-Tokyo '96*, The 2nd International Conference on Ground Improvement Geosystems, 14-17 May 1996, Tokyo, 869-878.

Rixner, J.J., Kraemer, S.R., and Smith, A.D. (1986). "Prefabricated Vertical Drains, Vol. 1." *Rep. No. FHWA-RD-86/168*, Federal Highway Administration, Washington, D.C.

Rowe, R.K., Gnanendran, C.T., Landva, A.O. and Valsangkar, A.J. (1995). "Construction and performance of a full-scale geotextile reinforced test embankment." *Canadian Geotechnical Journal*, 32(3), 512–534.

Salarashayeri, A.F. and Siosemarde, M. (2012). "Prediction of Soil Hydraulic Conductivity from Particle-Size Distribution." *World Academy Science, Engineering and Technology*, 61, 454-458.

Saride, S., Sirigiripet, S. K., Puppala, A. J., and Williammee, R. (2008). “Performance of expanded clay shale (ECS) as an embankment backfill.” GeoCongress Conference 2008: Geosustainability and Geohazard Mitigation; Copyright ASCE 2008.

Saride, S., Puppala, A. J., Williammee, R., and Sirigiripet, S. K. (2010). “Use of lightweight ECS as a fill material to control approach embankment settlements.” *Journal of Materials in Civil Engineering*, ASCE, 607-617.

SCDOT (2008). “Geotechnical Performance Limits.” Geotechnical Design Manual, South Carolina Department of Transportation, SC, US.

SCDOT (2010). “SCDOT Geotechnical design manual.” South Carolina Department of Transportation, SC.

Schaefer, V.R, Koch, J.C. (1992). “Void Development under Bridge Approaches,” *Rep. No. SD90-03*, South Dakota Department of Transportation.

Seo, J. (2003). “The Bump at the End of the Bridge: An Investigation.” Dissertation submitted in partial fulfillment of the requirements for the degree of the Doctor of Philosophy, Texas, A&M University, College Station, Texas.

Serridge, C.J. and Synac, O. (2007). “Ground Improvement Solutions for Motorway Widening Schemes and New Highway Embankment Construction Over Soft Ground.” *Ground Improvement Journal*, 11(4), 219-228.

Slocombe, B. C. (2004). “Dynamic compaction.” *2nd edition Ground Improvement edited by Moseley, M. P. and Kirsch, K.*, Spon Press: Taylor & Francis Group, NY.

Slope Indicator (2004). VW Total Pressure Cell, Slope Indicator Company, Washington, US.

Slope Indicator (2006). Horizontal Digitilt Inclinometer Probe, Slope Indicator Company, Washington, US.

Slope Indicator (2011). Horizontal Digitilt Inclinometer Probe, Slope Indicator Company, Washington, US.

Stapelfeldt, T. (2006). “Preloading and vertical drains.” Helsinki University of Technology.

Stark, T. D., Arellano, D., Horvath, J. S., and Leshchinsky, D. (2004). “Geofoam applications in the design and construction of highway embankments.” NCHRP Web Document 65, Project 24-11, National Cooperative Highway Research Program, Transportation Research Board.

Stark, T. D., Horvath, J. S., and Leshchinsky, D. (2004). “Guideline and recommended standard for geofoam applications in highway embankments.” NCHRP Report 529, National Cooperative Highway Research Program, Transportation Research Board.

Stewart, C. F. (1985). “Highway Structure Approaches.” California Department of Transportation, Sacramento, CA.

Sura, J. M. and Othman, M. A. (2011). “Case history of roadway embankment construction over very weak clay.” Geo-Frontier 2011, ASCE.

Suzuki, Y., Nishimura, A., and Kuno, T. (1996). “Design and construction of road embankment on steep hillside by EPS.” Proceeding of the International Symposium on EPS Construction Method, Tokyo, Japan, 265-273.

Tadros, M. K. and Benak, J. V. (1989). “Bridge Abutment and Bridge Approach Slab Settlement, phase I.” *Final Rep.*, Nebraska Dept. of Roads, Lincoln, Nebraska.

Tarawneh, B. and Siddiqi, J. (2014). “Performance issues of mechanically stabilized earth wall supporting bridge abutment.” *Proceeding of 8th International Conference on Engineering and Technology Research*, Dubai.

The EPS Industry Alliance. “Expanded Polystyrene (EPS) geofoam applications & technical data.” The EPS Industry Alliance, MD. (www.epsmolders.org).

Thompsett, D. J., Walker, A., Radley, R. J., and Grieveson, B. M. (1995). "Design and construction of expanded polystyrene embankments." *Construction and Building Materials*, Vol. 9, No. 6, pp. 40341.

Tjie-Liong, G., Irsyam, M., and Gunawan, A. (2013). "The application of ground improvement techniques in Indonesia." *Advances in Geotechnical Infrastructure*, Geotechnical Society of Singapore (GeoSS).

Tsukamoto, H., 2011, "History of R&D and Design Code for EDO-EPS Method in Japan." EPS 2011, Oslo, Norway.

TxDOT (2001). Bridge Design Manual, Texas Department of Transportation, TX.

TxDOT (2008). Flexible Base Selection Guide, Texas Department of Transportation, TX.

Wahls, H. E. (1990). *NCHRP Synthesis of Highway Practice No. 159: Design and Construction of Bridge Approaches*. Transportation Research Board, National Research Council, Washington, D.C.

Walkinshaw, J. L. (1978). "Survey of Bridge Movements in the Western United States." *Transportation Research Record 678: Tolerable Movements of Bridge Foundations, Sand Drains, K-Test, Slopes, and Culverts*, Transportation Research Board, National Research Council, Washington, D.C., 6–12.

White, D.J., Wissman, K., Barnes, A.G. and Gaul, A.J. (2002). "Embankment Support: A Comparison of Stone Column and Rammed Aggregate Pier Soil Reinforcement." *Proc. 81st Annual TRB Meeting*, Washington, D. C.

White, D. J. and Suleiman, M.T. (2004). "Design of Short Aggregate Piers to Support Highway Embankments." 83rd Annual Meeting Transportation Research Board, Washington, D.C.

White, D., Sritharan, S., Suleiman, M., Mohamed M. and Sudhar, C. (2005). "Identification of the Best Practices for Design, Construction, and Repair of Bridge Approaches." *CTRE. Project 02-118*, Iowa State University. Ames, Iowa.

White, D. J., Mekkawy, M. M., Sritharan, S., and Suleiman, M. T. (2007). “Underlying Causes for Settlement of Bridge Approach Pavement Systems.” *Journal of Performance of Constructed Facilities*, 21(4), 273-282.

Williammee, R. (2008) Personal communication, Fort Worth District Materials Engineer, Texas Department of Transportation.

Wilson, J. (1999). “Flowable fill as backfill for bridge abutments.” Report No. WI-16-99, Wisconsin Department of Transportation, WI.

WisDOT (2014). WisDOT Bridge Manual, Wisconsin Department of Transportation, WI.

Wolde-Tinsae, A.M, Aggour, S.M. and Chini, S.A. (1987). “Structural and Soil Provisions for Approaches to Bridges.” *Interim Report AW087-321-046*, Maryland Department of Transportation.

Wong, H. K. W, and Small, J. C. (1994). “Effect of Orientation of Bridge Slabs on Pavement Deformation.” *Journal of Transportation Engineering*, 120(4), 590-602.

WSDOT (2014). Geotechnical Design Manual: M 46-03.10, Environmental and Engineering Programs, Geotechnical office, Washington State Department of Transportation.

Wu, J.T.H., Lee, K.Z.Z. and Ketchart, K. (2003). “A Review of Case Histories on GRS Bridge-Supporting Structures with Flexible Facing.” Proc. 82nd Annual TRB Meeting.

Yenigalla, R. V. (2011). “An overview of mitigation strategies for settlements under bridge approach slabs.” Master Degree Thesis submitted the Faculty of the Graduate School of the University of Texas at Arlington, TX.

Zdravkovic, L. and Potts, D. M. (2010). “Application of Numerical Analysis in Geotechnical Engineering Practice.” GeoFlorida 2010: Advances in Analysis, Modeling and Design, ASCE.

Biographical Information

Pinit Ruttanaporamakul was born on 12th October 1979 in Narathiwas province, Thailand. He completed his schooling and secondary education from Dechapattanaya-nukul School and the Armed Forces Academies Preparatory School, Thailand in 1996 and 1998, respectively. Then, he joined the Royal Thai Air Force Academy in 1999 and received the bachelor's degree in Civil Engineering in 2003. After graduation, he started working for the Royal Thai Air Force in the position of an instructor in the Civil Engineering Department of the Royal Thai Air Force Academy. In 2004, he joined the Asian Institute of Technology (AIT), Thailand to pursue his Master in Civil Engineering in the field of Structural Engineering and graduated in 2006. He received a scholarship from the Royal Thai Air Force to pursue another Master degree in Civil Engineering with a major concentration in Geotechnical Engineering at the University of Texas at Arlington (UTA) in 2010 and graduated in summer 2012. He continued pursuing his doctoral degree in the geotechnical engineering field at UTA in fall 2012. During the course of his study, he worked as a graduate research assistant and teaching assistant under Dr. Anand J. Puppala and had an opportunity to work on various research projects.